Synthesis, biological evaluation, and screening of 2,5-anhydro-D-mannitol derivatives towards selective targeting and imaging of GLUT5 transporter protein

by

Natasha Rana

A thesis submitted in partial fulfillment of the requirements for the degree of

Doctor of Philosophy

Department of Chemistry
University of Alberta

Abstract

The solute carrier (SLC) family of membrane proteins is responsible for the internalization of a variety of essential small molecule compounds such as amino acids, monosaccharides, neurotransmitters, vitamins, as well as many inorganic ions. In recent years, these proteins have been recognized as potential therapeutic targets. Hexoses like glucose and fructose are energy sources and fuels for various metabolic processes inside the cell. Transport of hexoses through the cell membrane is facilitated through two distinct gene families (1) sodium-glucose transporters (SGLTs) and glucose transporters (GLUTs). GLUTs are passive transporters that use concentration and chemical gradient for the movement of hexoses across the cell membrane. To date, there are fourteen members (isoforms) of GLUTs, encoded by the human SLC2A genome family. Each GLUT varies in terms of which tissues it is found in, its substrate affinity and transport kinetics, and its sequence. In recent years, deregulation and alteration of energy metabolism have gained great attention due to their relation to various metabolic disorders, cancer, and diabetes. Overexpression of GLUTs in various cancers makes them an interesting and important biomarker to develop diagnostic and therapeutic probes for early detection and treatment. GLUT1 is a ubiquitous transporter that mediates the passage of D-glucose with high affinity. However, some cancers do not display overexpression of GLUT1, suggesting that D-glucose might not be the common energy source for all types of cancer or cancer cells switch their metabolic needs to other sugars like fructose, in glucose deficient environment. The principal fructose transporter, GLUT5, is responsible for absorbing dietary fructose and shows no facility for transporting D-glucose and other sugars. In addition, while normal breast tissues display limited expression of GLUT5, a significant percentage of breast tumor shows overexpression of this protein, making GLUT5 an intriguing target for imaging and detection. Fructose transport through GLUT5 occurs at an affinity (K_i) of 15mM. Interestingly, the C-2 deoxy analog of D-fructose (2,5-anhydro-D-mannitol; 2,5-AM) also displayed a similar affinity (K_i = 12.6 mM) to that of D-fructose. These observations inspired our decision to develop, evaluate and screen a library of 2,5-AM

derivatives with the goal of developing diagnostic and therapeutic probes targeting GLUT5.

Chapter 2 describes the preparation of a small library of 2,5-AM derivatives that were screened for inhibition of a previously reported PET tracer and potent GLUT5 substrate, 6-deoxy-6-[18F]fluoro-D-fructose ([^{18}F]-6-FDF). Several of these derivatives were subjected to computational analysis involving docking and molecular dynamics simulations using the published GLUT5 three-dimensional structure. These calculations helped to identify the key interactions likely to be involved in the binding of 2,5-AM derivatives to GLUT5 and will inform the design of further generations of inhibitor libraries en route to potent molecular imaging probes targeting GLUT5.

The most promising compounds from Chapter 2 were then used as a starting point for the design and synthesis of [18F]-containing PET radiotracers for potential use in medical imaging, and fluorescent probes applicable to confocal microscopy study or in situ optical detection of tumors (Chapter 3).

Chapter 4 describes attempts to apply the fluorescent probe molecule 6-NBDF in a fluorescence-based assay to assess 2,5-AM derivatives for inhibition of its uptake by GLUT5. Importantly, this assay would avoid the need for a radioactive reporter molecule, as was used in Chapter 2. Conditions were developed for a robust assay that will be suitable for automation in order to screen large libraries of drug-like compounds or natural product extracts.

Finally, Chapter 5 details possible future directions of this research, including different methods of forming GLUT5 targeting small molecules as NIR dye conjugates, drug conjugates, and dual probes.

Preface

Chapter 2 of this thesis has been published as Rana, N.; Aziz, M.A.; Oraby, A.K.; Wuest, M.; Dufour, J.; Abouzid, K.A.; Wuest, F.; West, F. G. Towards Selective Binding to the GLUT5 Transporter: Synthesis, Molecular Dynamics and In Vitro Evaluation of Novel C-3-Modified 2,5-Anhydro-D-mannitol Analogs. *Pharmaceutics*, **2022,** *14*, 828. The project was conceived by F.W. and F.G.W.; F.W. and M.W. supervised J.D.; F.G.W. supervised me and A.K.O.; F.G.W. and K.A.M.A. supervised M.A.A. M.A.A. and I were responsible for the synthesis and characterization of all compounds. Experiments were designed and performed by me, M.A.A., M.W. and J.D. Computational work was carried out by A.K.O. I was responsible for writing the manuscript, with input from M.A.A., A.K.O., M.W. and K.A.M.A. The manuscript was edited by F.W. and F.G.W., with input from all authors. All authors have read and agreed to the published version of the manuscript.

Chapter 3 of this thesis will be published as Rana, N., Wuest, M., Yuen, R., Bergman, C. B., Woodfield, J. D., Verona, M., Dufour, J., Wuest, F., West, F. G. Imaging breast cancer cells and tumors with 2,5-anhydromannitol derivatives. The project was conceived by F.W. and F.G.W.; F.W. and M.W. supervised J.D., J.D.W., C.B. and M.V.; F.G.W. supervised me and R.Y. I was responsible for the synthesis and characterization of all compounds. Radiosynthesis was designed and performed by M.V. and C.B. In vitro and in vivo experiments were designed and performed by M.W. J.D.W. and J.D. R.Y. and I were responsible for designing and performing confocal microscopy experiments. M.W. and I participated in data analysis and writing of the manuscript.

Chapter 4 of this thesis will be published as Rana, N.; Aziz, M.A.; Serya, R.A.T.; Lasheen, D. S.; Samir, N; Abouzid, K.A.M., West, F.G. A novel fluorescence-based assay for the identification of GLUT5 inhibitors through systematic screening of 2,5-anhydro D-mannitol derivatives. The project was conceived by F.W. and F.G.W.; F.G.W. supervised me; F.G.W., K.A.M.A., R.A.T.L., N.S. supervised M.A.A. M.A.A. and I was responsible for the synthesis and characterization of all compounds. I was

responsible in designing and performing in vitro experiments followed by data analysis. M.A.A. and I were responsible for writing the manuscript, with input from F.G.W., K.A.M.A., R.A.T.L., N.S.

Dedication

This thesis is dedicated to my parents and the people who have supported me throughout my education. Thanks for making me see this adventure through to the end.

Acknowledgements

I would like to express my deepest gratitude, my debt of thanks to my Ph.D. supervisor Prof. F. G. West for his advice, encouragement, care, and commitment to student learning. This work and journey would not have been possible without your immense support and guidance. I am very thankful to you for welcoming me into your group and accommodating me in your laboratory and providing the appropriate learning and working atmosphere to manage my Ph.D. project flexibly and successfully. I am incredibly grateful for your mentoring, help, and encouragement to engage in a multidisciplinary project to reach this point in my project and learn valuable skills. I would not be able to defend my thesis and achieve such a milestone without your support and thoughtful advice. Thanks for this amazing journey and for being always here for me.

Words cannot express how grateful and thankful I am to my amazing collaborators, Dr. Frank Wuest and Dr. Melinda Wuest for providing me with unlimited guidance and confidence to work in a multi-disciplinary environment. My thesis story would not be significant without your navigation and help. I would like to express my deepest sincere appreciation to them for enriching my knowledge in my discipline.

I am also profoundly grateful to my Supervisory Committee Members, Dr. Frank Wuest, Dr. Todd Lowary and Dr. Mathew Macauley for their support and dedication to help aid my research with their valuable ideas and expertise during my graduate studies.

I am also truly thankful to all examiners for the Ph.D. defense exam. I am o very thankful to my arm's length examiner, Dr. Juli Gibbs and external examiner, Dr. Marina Tanasova for your time and effort to attend my defense.

I would like to thank the past and current members of the West group for creating such an amazing environment to conduct research. I have acquired inevitable research skills from the West group, which broadened my knowledge to reach such a stage. I would like to express my deepest gratitude to Dr. Olivier Soueidan and Dr. Marius Constantin from whom I learnt several things in my lab and life. Both of you were amazing mentors for me throughout my graduate studies. Also, I am thankful to

a bountiful of past group members, Dr. Pavan Kondapi, Dr. Shorena Gelozia, Dr. Yury Karpov, Dr. Ahmed Elmenoufy, and Yaseen Almehmadi for always inspiring me and supporting me to go through this rewarding journey. I am deeply grateful to my friends, Marwa Morsy, Ismat Luna, Jenny Lin, Richard Yuen, Maxwell Boetang, and Ahmed Oraby for their presence beside me during my studies and for making my Ph.D. life valuable, fun, and memorable. I am also extremely thankful to the staff members of the NMR, IR, Mass Spectroscopy facility labs, and X-ray services. Research would not have been possible without the support you provide. Thank you very much to every single one of you for being so approachable. I am grateful and thankful to my friend, Tejal Aslesh for your constant motivation and support during my Ph.D. journey.

Finally, words cannot express how grateful and thankful I am to my family and relatives, especially to my late father Raj Kumar Rana and my mother Kamlesh Rana, my beloved sibling Dr. Tarun Rana, and my in-laws, as well as my beloved husband and best friend Kapil Khatri. I would like to thank them for their endless prayers and support to pass stressful moments throughout my studies. Indeed, I cannot thank you enough for the never-ending support, unlimited love, and care. Love you all immensely.

Table of Contents

List of figures

Chapter 1

Chapter 2

Chapter 3

List of Tables

List of Schemes

Abbreviations

OAc	acetate
Ac_2O	acetic anhydride
Ac	acetyl
AcCl	acetyl chloride
^{14}C	an isotope of carbon
^{18}F	an isotope of fluorine (also known as positron emitter)
^{18}O	an isotope of oxygen
app	apparent (spectral)
Ar	aryl
2,5-AM	2,5-anhydro-D-mannitol
Bn	benzyl
SN_2	bimolecular nucleophilic substitution
brbroad	(spectral)
calcd	calculated
cal.	calories (units of energy)
^{13}C NMR	carbon 13 nuclear magnetic resonance
CsF	cesium fluoride
δ	chemical shift in parts per million downfield from tetramethylsilane
CHO (cells)	Chinese hamster ovary cells
in silico	computer simulation in reference to biological experiments
IC_{50}	concentration of the inhibitor required to achieve half maximal inhibition
J	coupling constant (in NMR)
CB	cytochalasin B
dr	diastereomeric ratio

°C	degrees Celsius
2-FDG	2-deoxy-2-fluoro-D-glucose
1-FDF	1-deoxy-1-fluoro-D-fructose
6-FDF	6-deoxy-6-fluoro-D-fructose
DAST	diethylaminosulfur trifluoride
DEAD	diethyl azodicarboxylate
DIPEA	N,N-diisopropylethylamine
DCM	dichloromethane
Et_2O	diethyl ether
DIAD	diisopropyl azodicarboxylate
DMAP	4-dimethylaminopyridine
DMSO	dimethyl sulfoxide
d	doublet (spectral)
dd	doublet of doublets
dt	doublet of triplets (spectral)
dq	doublet of quartets (spectral)
DMEM	Dulbecco's Modified Eagle's Medium
EMT6	Epithelial-mesenchymal transition
EtOH	ethanol
Et	ethyl
EtOAc	ethylacetate
ESI	electrospray ionization (mass spectrometry)
ee	enantiomeric excess
equiv	equivalent
FBS	fetal bovine serum
FPR	fluorescence plate reader
R	generalized alkyl group of substituents
X	generalized heteroatom
g	gram
Hz	hertz

h	hour
HK	hexokinase
HBA	hydrogen bond acceptor
HBD	hydrogen bond donor
i-Pr	isopropyl
KHK	ketohexokinase (often referred as fructokinase)
k	kilo
L	litre(s)
MHz	megahertz
m.p.	melting point
GLUT	membrane hexose transporter
M	metal atom; moles per litre
MeOH	methanol
tert-AmOH	2-methyl-2-butanol
Me	methyl
Km	Michaelis constant
µ	micro
mg	milligram
mL	millilitre
min	minute
MD	molecular dynamics
m	multiplet (spectral); milli
N	normality
DMF	N,N-dimethylformamide
NBD	7-nitrobenz-2-oxa-1,3-diazole
NMR	nuclear magnetic resonance
Nu	nucleophile
S_NAr	Nucleophilic aromatic substitution
mol	number of moles
OMe	methoxy

Ph	phenyl
PBS	phosphate buffer saline
Piv	pivaloyl
PET	positron emission tomography
KHF_2	potassium bifluoride
KF	potassium fluoride
PDB	protein data bank
H^+	proton
^1H NMR	proton nuclear magnetic resonance
Py	pyridine
quant.	Quantitative
q	quartet (spectral)
in vivo	referring to the studies performed in living organisms
in vitro	referring to the studies performed in cell culture or processed
Rf	retention factor (chromatography)
RNA	ribonucleic acid
rt	room temperature
RMSD	root-mean-square deviation of atomic positions
RMSF	root-mean square fluctuation of individual residue flexibility
s	singlet (spectral); second
SD	standard deviation
SAR	structure activity relationship
T	temperature
TBAF	tetra-N-butylammonium fluoride
TBS	tert-butyldimethylsilyl
TBDPS	tert-butyldiphenylsilyl
THF	tetrahydrofuran

^{19}F	the only stable isotope of fluorine
TLC	thin layer chromatography
Ts	p-toluenesulfonyl; tosyl
TM	trans-membrane (protein)
TEA	triethylamine (also referred as Et_3N)
TFA	trifluoroacetic acid
Tf	trifluoromethanesulfonyl; triflate
TMS	trimethylsilyl
t	triplet (spectral)
Tr	trityl
SN_1	unimolecular nucleophilic substitution
UV	ultra-violet
cm^{-1}	wave numbers

Chapter 1

Introduction

1.1. Hexose Transporters

Hexoses such as glucose and fructose are elemental sources of energy in eukaryotic organisms functioning as fuels for various metabolic processes and cellular homeostasis.[1] Glucose homeostasis is regulated through three processes, (1) glucose production (liver) (2) glucose absorption (intestine), and (3) glucose consumption (all tissues).[2] Most mammalian cells rely on a constant supply of glucose, a key component in the cellular production of the energy molecule adenosine 5'-triphosphate (ATP).[3,4] Low glucose levels in the brain can result in loss of consciousness, seizures, and other serious effects. Contrarily, excess glucose levels (glucotoxicity) can cause neuropathy, renal failure, and blindness.[5,6] Hydrophilicity of these monosaccharides blocks their transport through the hydrophobic lipid bilayer membrane via simple diffusion process. The solute carrier (SLC) gene family of integral membrane proteins (IMPs), containing 43 families (SLC1 – SLC43) with 298 genes, plays an essential role in the internalization of nutrients such as monosaccharides, vitamins, amino acids, inorganic ions as well as short chain fatty acids.[7] Transport of glucose and other sugars is mediated through two different types of transporter proteins, (1) sodium-glucose transporters (SGLTs) and (2) glucose transporters (GLUTs). SGLTs, Na^+-coupled carrier systems (gene name SLC5A) are also known as symporters or co-transporters and use sodium ion gradient for the transport of glucose and galactose (with low affinity). On the other hand, GLUTs (gene name SLC2A), known as uniporters, are passive transporters where energetically favored movement of hexoses (Figure 1.1) is driven by concentration and electrochemical gradient.[8,9,10,11,12,13] In 1985, Mueckler and coworkers proposed a structure model of GLUT1 protein containing 492 amino acid residues.[14] In 2014, Deng et al reported the crystal structure of human GLUT1 expressed in insect cells.[15]

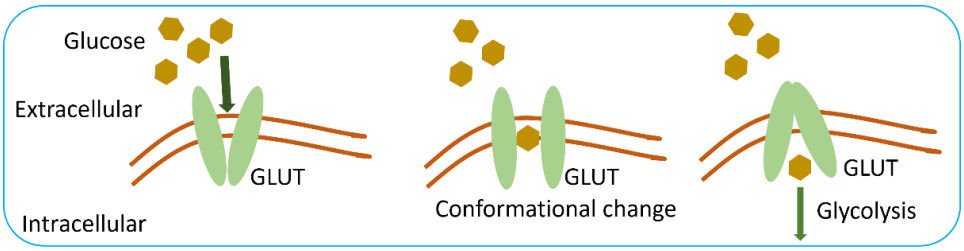

Figure 1.1. Transport of hexoses through the plasma membrane by GLUTs

1.2. The GLUT family - Classification

The human SLC2A genome family consists of 14 members (isoforms) of GLUTs (GLUT1-GLUT14). Each GLUT is categorized into three subfamilies based on the degree of evolutionary divergence, tissue specific expression and amino acid sequence differences (Figure 1.2.).[16] These isoforms differ from the rest in their functional characteristics (such as Km values, substrate specificity, and binding affinities), structure elements, and tissue specific expression.[17]

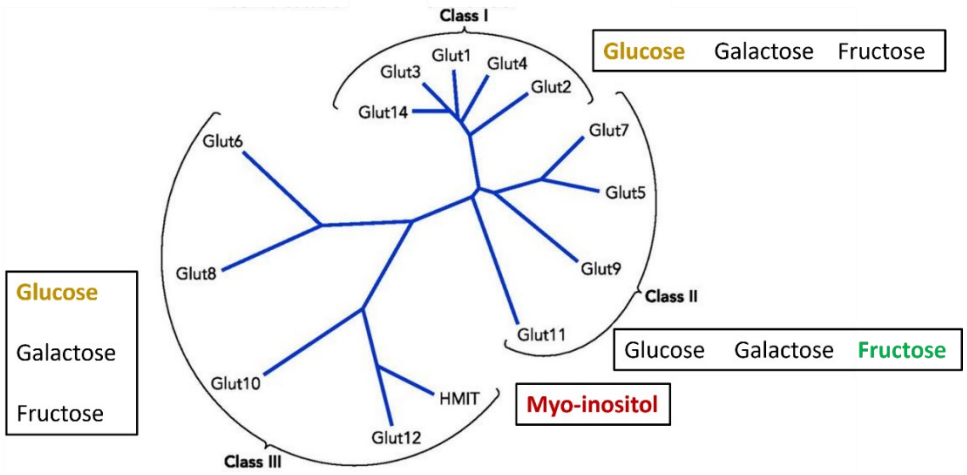

Figure 1.2. Classification of GLUTs and relationship between the SLC2A gene family members. Distance between branches and length of the lines represent the degree of evolutionary divergence. (Figure copied with permission from Manolescu et al.[9])

1.2.1. Substrate specificity of different GLUTs

Class-I facilitated hexose transporters consists of GLUTs 1-4 and GLUT14. GLUT1, the ubiquitous glucose transporter, is responsible for the basic supply of D-glucose to the cells (Table 1.1).[14] GLUT2 transports D-glucose with high affinity and D-fructose with lower affinity.[18] GLUT3, 4 is able to transport D-glucose with high affinity [8]; in

addition, GLUT4 also mediates the transport of D-galactose. However, translocation of GLUT4 from intracellular membrane to plasma membrane is stimulated in presence of insulin causing a 10-20-fold increase in D-glucose transport.[5,19,20] Recently identified, GLUT14 is responsible for the transport of D-glucose. GLUT 1, 3, and 4 have also been discovered to mediate the transport of dehydroascorbic acid (DHAA).[21]

Class-II facilitated hexose transporters comprise GLUT5, 7, 9, and 11, which are primarily D-fructose transporters. GLUT5 mediates the uptake of D-fructose with high affinity and very limited or no affinity to D-glucose transport. GLUT7 facilitates the uptake of D-glucose and D-fructose with high affinity. GLUT9 is also observed to transport D-glucose. GLUT14 is a low affinity D-glucose transporter.[8-13]

Class-III facilitated hexose transporters include GLUT6, 8, 10, 12, and 13. GLUT6 is observed to be a low affinity D-glucose transporter. GLUT8 facilitates the uptake of D-glucose with high affinity and can be inhibited by galactose and fructose acting as a multifunctional transporter.[8-13] GLUT8 and 10 can also mediate the transport of D-galactose. GLUT12 tends to facilitate D-glucose transport but is found to be inhibited by D-galactose and D-fructose. GLUT13 also known as H^+-coupled myo-inositol transporter (HMIT) is specifically responsible for the transport of myo-inositol, polyhydroxycyclohexane employed in cell signaling pathways. HMIT can also transport myo-inositol related stereoisomers but has no activity for the transport of hexose sugars.[22]

Table 1.1. Classification and substrate specificity of GLUTs

Class	Member	Substrate(s)
I	GLUT1	D-glucose and D-galactose
	GLUT2	D-glucose, D-galactose, and D-fructose
	GLUT3	D-glucose and D-galactose
	GLUT4	D-glucose
	GLUT14	D-glucose and D-galactose
II	GLUT5	D-fructose (low affinity for D-glucose)
	GLUT7	D-glucose and D-fructose
	GLUT9	D-glucose and D-fructose
	GLUT11	D-glucose and D-fructose
III	GLUT6	D-glucose (not well understood)
	GLUT8	D-glucose (low affinity for D-fructose)
	GLUT10	D-glucose and D-fructose
	GLUT12	D-glucose, D-galactose, and D-fructose
	GLUT13 (HMIT)	Myo-inositol

1.2.2. Tissue expression

Class-I GLUTs: GLUT1 is expressed ubiquitously in most of the mammalian cells with the highest expression levels, particularly in blood brain barrier, erythrocytes, and brain (Figure 1.3).[23,24,25] GLUT2 is observed to be predominantly expressed in pancreatic β-cells, small intestine, kidney, and liver.[26,27] GLUT3 is found to be expressed in the brain.[28] GLUT4 is observed to be expressed in insulin-sensitive tissues like the heart, adipose tissue, and skeletal muscle.[29] GLUT 14 is reported to be 95% identical with GLUT3 and is observed to be exclusively expressed in testes.

Class-II GLUTs: The fructose-specific transporter GLUT5 is found to be predominantly expressed in the kidney, small intestine, and testes.[30] GLUT7 was

characterized in enterocytes brush border membrane.[31,32] Expression of GLUT9 is located in the kidney with little expression in the small intestine, placenta, lung, and leukocytes.[31,33] GLUT11 exhibits high expression levels in the pancreas, kidney, and placenta with moderate expression in the heart and skeletal muscle.[31]

Class-III GLUTs: GLUT6, a low affinity glucose transporter, was found to be expressed in the brain, spleen, and peripheral leukocytes. GLUT8 was found to be expressed in testes, insulin sensitive tissues (adipose tissue, heart, and skeletal muscle), and preimplantation embryos.[31] GLUT10 is found to be located in the liver and pancreas. Expression of GLUT12 is found in the heart and prostate. HMIT is observed to be expressed in the brain.[31]

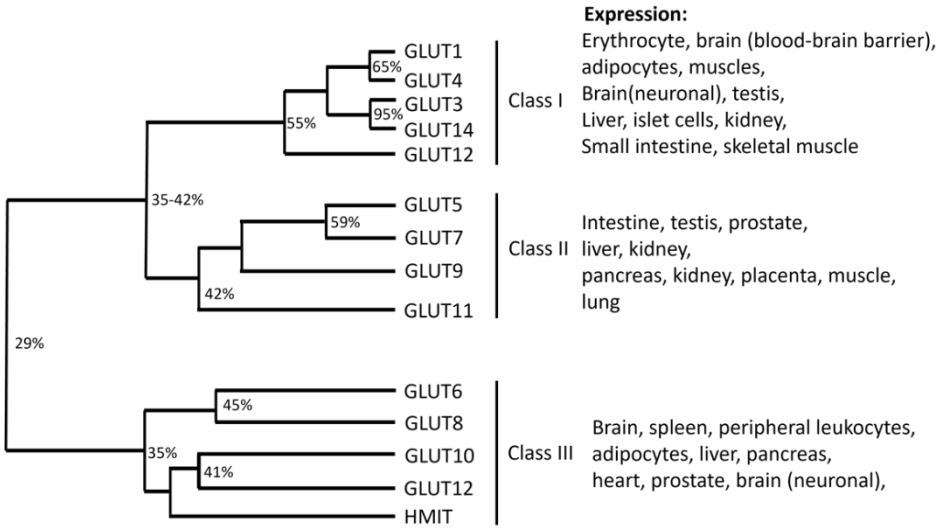

Figure 1.3. Classification and tissue expression of GLUTs1-1 (Figure adapted from Scheepers et al.[7])

1.3. Variations in GLUT structure and mechanism of carbohydrate uptake

Through hydropathy analysis, it was revealed that GLUTs have 12 transmembrane domains (TMs) having N-terminus and C-terminus (Figure 1.4) with TM6 and TM7 connected through a long loop present on the cytosolic side of the membrane.[8-13,15,34.35]

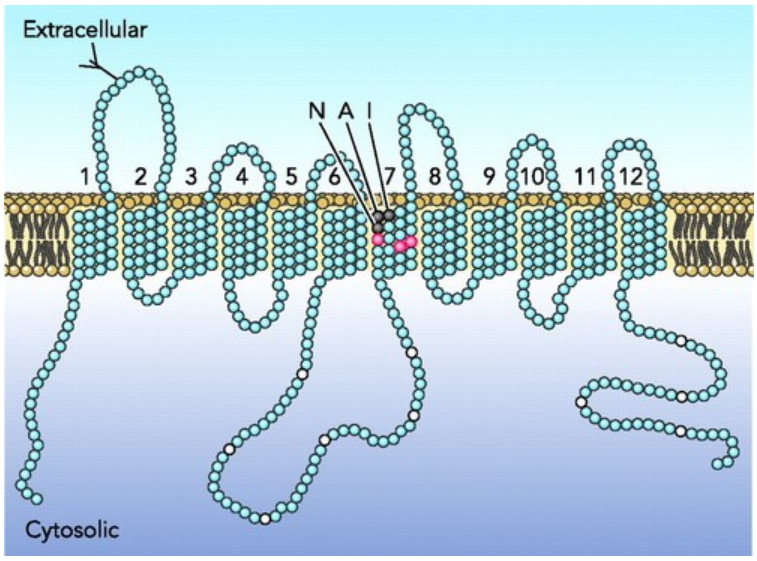

Figure 1.4. Structure of GLUT protein (Figure copied with permission from Manolescu et al.[9])

1.3.1. Structure

Class-I GLUTs – GLUT1-4 are reported to have a similar topology with a conservation of 38% of all the amino acids.[36] The glutamine residue, present in TM5 is common among class-I GLUTs suggesting its importance in glucose recognition.[37] Moreover, QLS (putative recognition motif) motif in TM7 is found to be present in GLUT1, 3, and 4 responsible for glucose transport but not in fructose transporting GLUTs including GLUT2 suggesting the involvement of this motif in glucose/fructose selectivity.[35]

Class-II GLUTs – These transporter proteins also have a similar topology with 12 TMs and a single N-linked glycosylation site between TM1 and TM2. A major difference is that all class-II GLUTs have isoleucine as the only hydrophobic residue in TM7 interacting with neighboring TMs regulating glucose/fructose selectivity.[38] Another striking difference between class-I and class-II GLUTs is the lack of a QLS motif.[35]

Class-III GLUTs – These proteins also have 12 TMs like class-I and class-II GLUTs. However, class-III GLUTs do not have N-linked glycosylation between TM1 and TM2.[12] It is also predicted that HMIT, within the same loop, has more than one N-linked glycosylation site. Additionally, class-III GLUTs don't have a QLS motif, making this motif unique to class-I GLUTs.[22]

1.3.2. Mechanism

Study of kinetics of transport of glucose has been extensively studied in GLUT1. In the initial experiments, it was predicted that the transport of hexoses is influenced by the initial hexose concentration (outside and inside the cell) and binding affinity of protein and the ligand causes the saturation on the rate of transfer.[39,40] These studies have proposed several models in which the earliest theory was proposed by Widdas and called the "simple carrier model", shown as a general representation in Figure 1.5.[41] It was assumed to carry out the process in 4 stages, the opening of GLUT to one side of the membrane (cis side) allowing the binding of the substrate, translocation of substrate binding GLUT from cis side to trans side (another side of the membrane), the release of the substrate on the trans side, switching of GLUT back to cis side for substrate binding.[41]

Nowadays, there are two popular models other than the "simple carrier model" which are still under consideration. One of them is a "two site/fixed site transporter" having both binding sites concurrently available from either side of the membrane, supporting the antiporter properties of some GLUT proteins.[42,43,44]

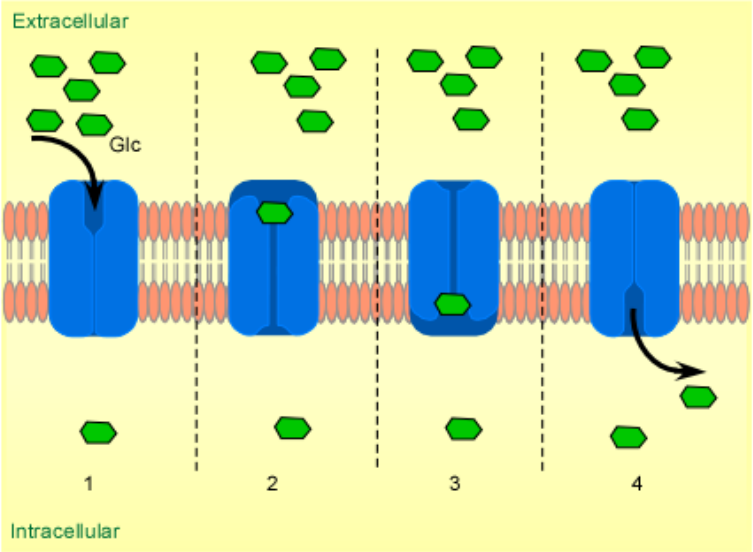

Figure 1.5. A general representation of the hexose transport mechanism by GLUTs (Figure copied with permission from Augustin et al.[41])

The other proposed mechanism is the "alternating access model", involving the flux of hexoses through a conformational change in the protein explaining the presumption of GLUT1 being a uniporter. Recent crystal structures of GLUTs 1, 3, and 5 also align with the alternating access mechanism predicting 4 conformational states through the whole hexose transport cycle: outward open, outward occluded, inward occluded, and inward open state (Figure 1.6).[15,34,45] It was also reported that inter transmembrane (ITM)-helix salt bridges stabilize the outward open conformation. The binding of hexoses also generates the translocation of N- and C- domains of the proteins, forcing the hexose out of the transporter. After the release of the hexose, the transporter switches back to outward open conformation prepared for another hexose binding to continue the cycle of uptake process.[45]

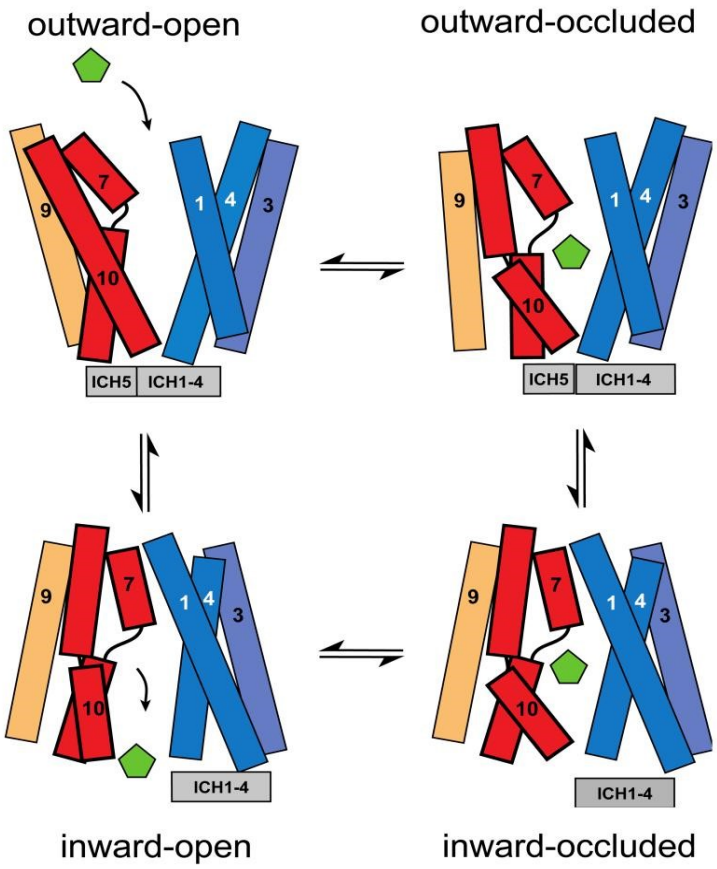

Figure 1.6. Mechanism of transport of hexose through "alternating access model (Figure copied with permission from Nomura et al.[45])

Since GLUTs function as passive transporters, hexoses can move out of the cell through the same pathway. However, in the presence of kinase enzymes within the cells, hexoses can undergo phosphorylation and due to this charge difference (Figure1.7), as they become metabolically trapped thus preventing their efflux from the cell.[46]

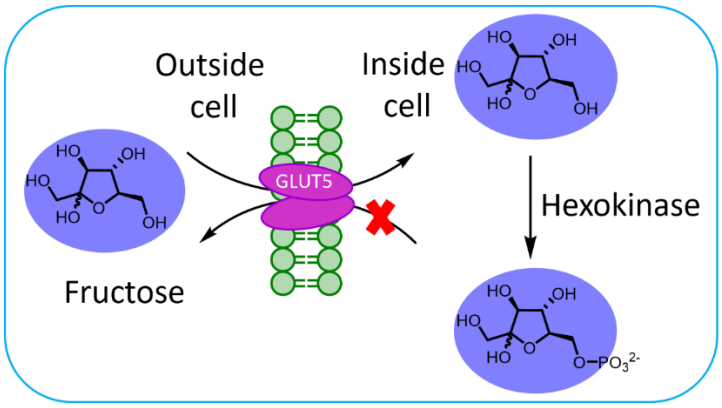

Figure 1.7. Enzymatic phosphorylation – A metabolic trap for hexoses

1.4. GLUT binding studies and structural requirements for hexose binding

Hexoses tend to exist as a mixture of different forms (open, pyranose, furanose.) in solution.[47] Other physiological factors such as ions (Mg^{2+} and Ca^{2+}), water molecules, and pH can change the conformation of the hexoses (Figures 1.8 and 1.9).[48] Due to the presence of multiple interconverting forms and their differential recognition and transport, the overall uptake measurements for a particular GLUT should not be confused as the transporter's affinity for any one of the forms, but rather thought of as a conglomerate number made up of several different rates for different hexose forms.

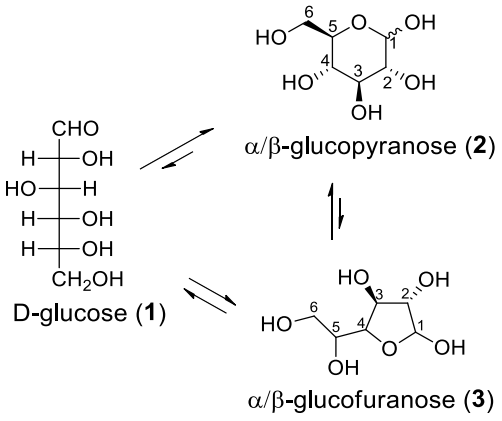

Figure 1.8. Various forms of D-glucose

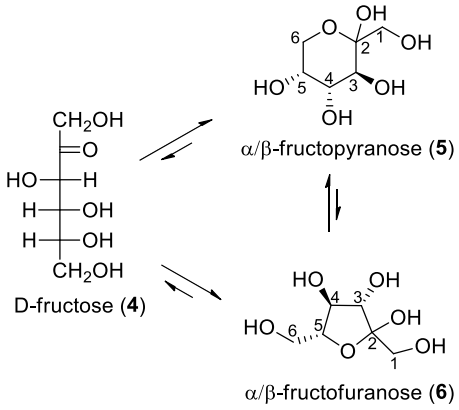

Figure 1.9. Various forms of D-fructose

In addition, stereochemistry of carbon linked to hydroxyl groups and presence of hydroxyl groups, also known as "essential hydroxyl groups" play a very crucial role in GLUT recognition.[8-13] Modification of such hydroxyl groups can result in loss of recognition by GLUTs. In addition, there are specific amino acids that are essential for GLUT-hexose binding.[15,45] Mutation of some amino acids can alter the binding process. It has been reported that single point mutation from isoleucine to valine/alanine in human GLUT5 can transform substrate preference from D-fructose to D-glucose.[45] Crystallization of protein-ligand and docking analysis can also provide clear insights into the binding interactions. Therefore, various modifications of the substrate, mutations in the GLUT, and kinetic analysis can help to provide an overview of

structural requirements and molecular interactions of various substrates with different GLUTs.

1.4.1. GLUT binding studies for glucose transport

In the class-I hexose transporter family, GLUTs1-4 are primarily D-glucose transporters. In the initial stages of substrate selectivity, it was observed that GLUT1 favors D-glucose but not L-glucose.[49] Studies carried out independently by Barnett[50] and Kahlenberg[51] demonstrated structural requirements of glucose by measuring the affinity of modified D-glucose derivatives (tested in human erythrocytes) with GLUT1 and GLUT4 respectively. Rees and coworkers also demonstrated the importance of the ring/C-5 oxygen atom.[52] These binding experiments explained the sensitivity of hexose-GLUT interactions to stereochemical configuration and substitution-induced steric encumbrance at various positions. The binding affinity of these derivatives was inferred from their ability to inhibit the update of [^{3}H]-D-glucose.

In solution, D-glucose exists majorly (>99%) in D-glucopyranose form as a mixture of α and β anomers. In GLUT1 binding experiments, it was observed that this transporter can transport both the anomers but with different binding affinities.[53] Removal of C-1 hydroxyl group (Figure 1.10), 1-deoxyglucose (**8**) (lacking both hydrogen bond donor and hydrogen bond acceptor) displayed 10-fold lower affinity (K_i = 76 mM) than D-glucose (**7**) (K_i = 6.3 mM), signifying the importance of polar substituent at this position.[50] Additionally, an apparent difference was observed in GLUT1 affinities for α-D-glucopyranosyl fluoride (**9**) (K_i = 72 mM) and β-D-glucopyranosyl fluoride (**10**) (K_i = 15 mM), indicating the significance of the orientation of the anomeric substituent for effective GLUT-substrate binding.[50] However, for methyl α-D-glucopyranoside (**11**) and methyl β-D-glucopyranoside (**12**), no affinity was observed. This indicates that GLUT1 can tolerate modifications at the C-1 position of D-glucose, depending strongly on the C-1 site as a hydrogen bond acceptor and favoring β-anomer over α-anomer.

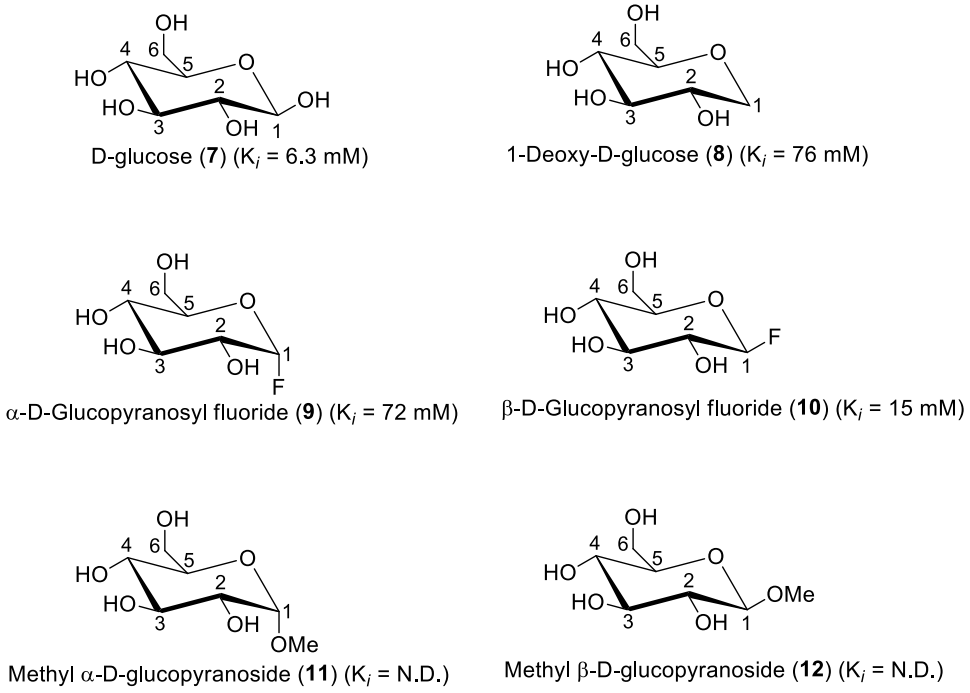

Figure 1.10. Structure of various C-1 modified D-glucose derivatives as GLUT1 ligands

In the case of modifications at the C-2 position (**7-17)** (Figure 1.11), it was observed that the C-2 site plays an insignificant role in GLUT-substrate interactions. For analogs like D-mannose (**16**) and 2-chloro-2-deoxy-D-glucose (**14**), little change in affinities was observed for GLUT1. Interestingly, in the case of 2-deoxy-D-glucose (**13**), lacking both hydrogen bond donor and hydrogen bond acceptor properties, higher affinity (Ki = 3.2 mM) for GLUT1 was observed, showing this to be a favorable position for substitution and stereochemical alterations.[50] However, methoxy analog (**15)** and glycal form of glucose **(17)** resulted in decrease in affinity.

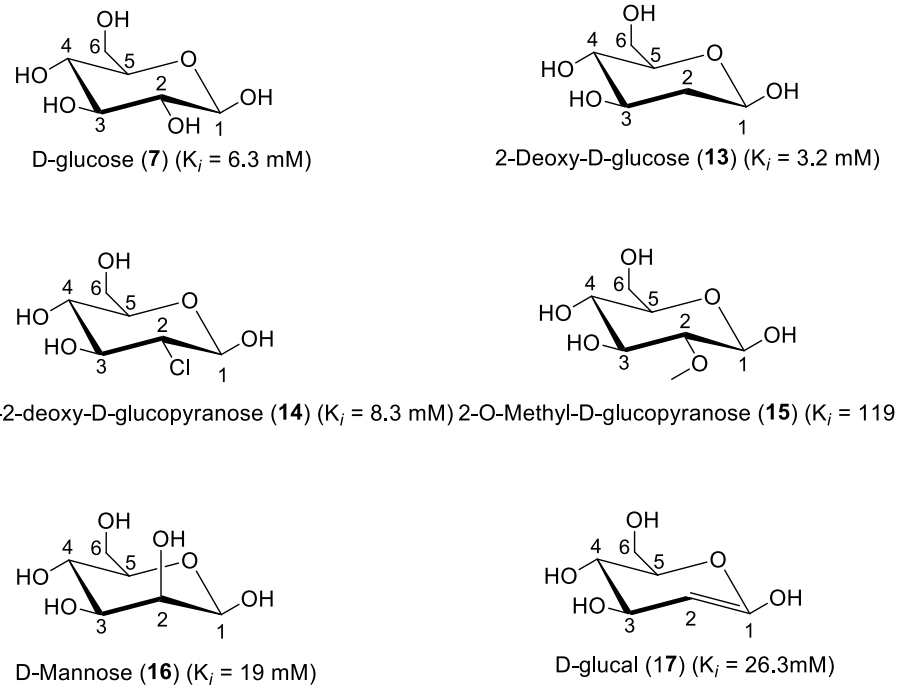

Figure 1.11. Structures of various C-2 modified D-glucose derivatives and their Ki values for transport of radiolabeled glucose by GLUT1

Modifications at the C-3 position (**18-22)** (Figure 1.12) with methoxy (**20**) and propoxy (**21**) groups led to a significant decrease in affinity suggesting the low tolerance of GLUTs towards the steric congestion. Removal of the C-3 hydroxyl group (3-deoxy-D-glucose **18**) caused decrease in affinity, indicating poor tolerance by GLUT1 towards modification at this site. However, substitution with hydrogen bond acceptor, 3-deoxy-3-fluoro-D-glucose **19** resulted in similar affinity to that of D-glucose. Similarly, modification at C-4 (D-galactose, **22**) was observed to be tolerated better.[50] This indicates the tolerance of equatorial C3-OH for efficient GLUT1-substrate binding.

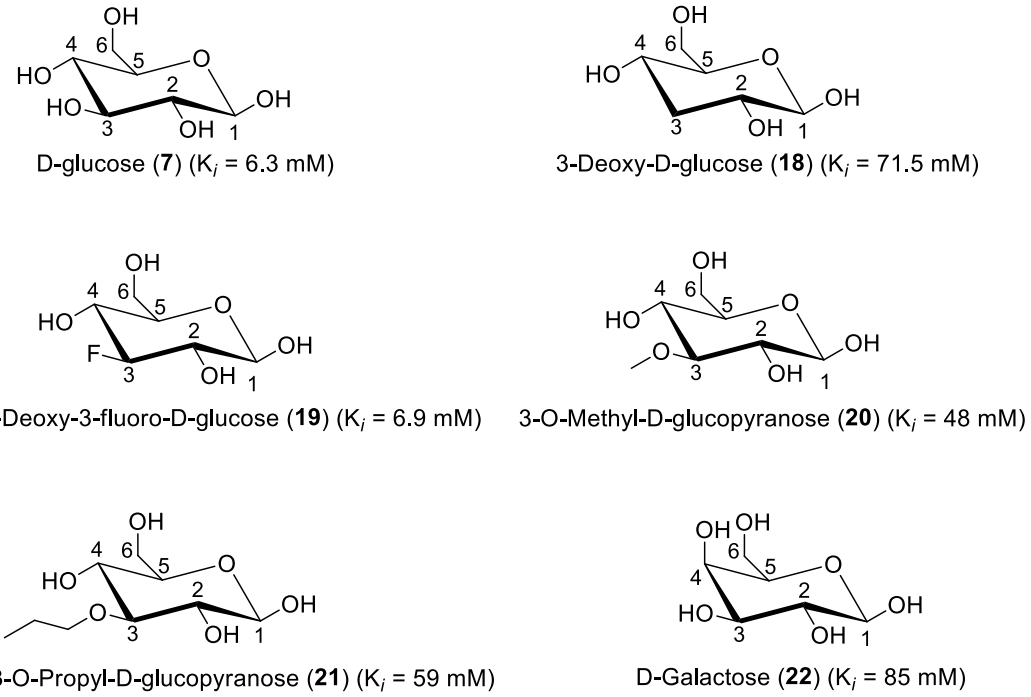

Figure 1.12. Structure of various C-3 and C-4 modified D-glucose derivatives as GLUT1 ligands and their Ki values for transport of radiolabeled glucose by GLUT1

In the case of modifications at the C-6 position (Figure 1.13), removal of the C6-OH group, 6-deoxy-D-glucose (**23**), comparable affinity to D-glucose were observed.[50] Interestingly, the substitution of C6-OH with fluoride (**24**) resulted in better affinity than D-glucose.

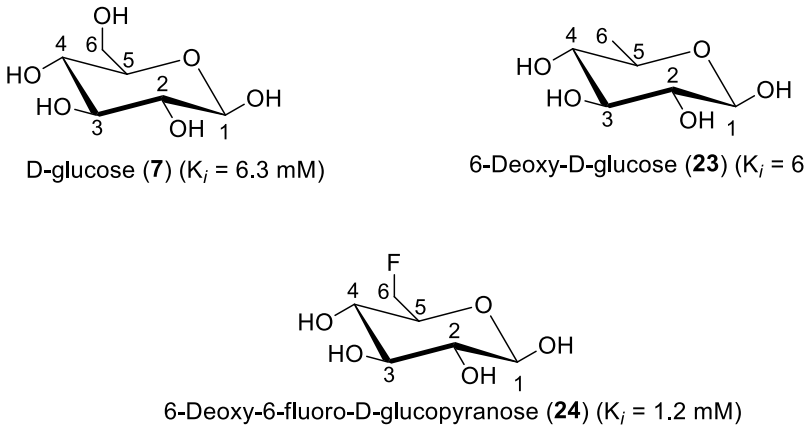

Figure 1.13. Structure of various C-6 modified D-glucose derivatives as GLUT1 ligands and their Ki values for transport of radiolabeled glucose by GLUT1

These structure activity relationship studies demonstrate the sensitivity of glucose transporter interaction to position modifications at several sites on the D-glucose scaffold (Figure 1.14).

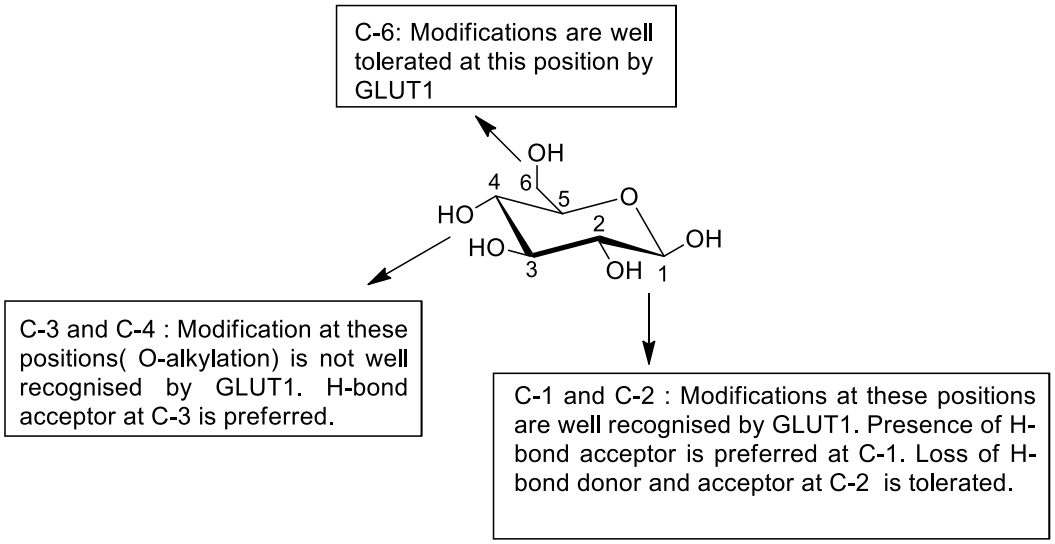

Figure 1.14. Summary of GLUT1 recognition for modified D-glucose

1.4.2. GLUT binding studies for fructose transport.

Among the 14 GLUTs, GLUT2 and 5 are considered to be the main fructose transporters. Other GLUTs (7, 9, 11, and 12) are reported to transport fructose along with glucose and other sugars with different affinities.[8-13] GLUT2 is known to transport fructose with low affinity and glucose with high affinity. Little is known about the interactions of GLUT2 with fructose and related substrates, so the discussion here will be limited to GLUT5, whose sole substrate is fructose. GLUT5 has gained more scientific attention due to its unique substrate specificity and its potential role as a biomarker for various types of cancers and diseases.[10]

1.4.3. GLUT5 binding studies for fructose transport.

The Holman Group has done extensive studies on the binding of fructose analogs to GLUT5. These structure activity relationship studies were conducted using Chinese hamster ovary (CHO) cells engineered to overexpress GLUT5.[54,55,56,57]

Aqueous D-fructose equilibrates between three interconverting forms with β-fructopyranose as the major form (75%) followed by β-fructofuranose (21%) and α-

fructofuranose (4%).[8-13] In measurements of inhibition of uptake of radiolabeled D-fructose, the Ki of D-fructose was found to be 15 mM.[54] It appears that the stereochemical configuration of the carbon with secondary alcohol plays a crucial role in GLUT5 binding as observed from K_i values of, D-psicose (C-3 epimer, **26**), D-tagatose (C-4 epimer, **27**), and L-sorbose (C-5 epimer, **28**), where **27** and **28** exhibited a 4 to10-fold weaker inhibition than fructose (Figure 1.15).[54]

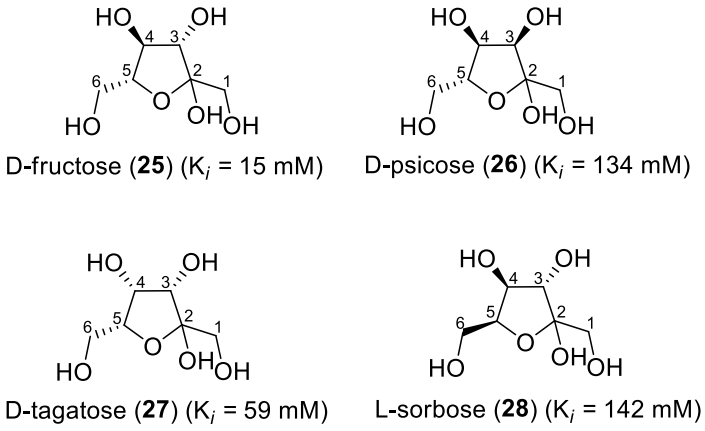

Figure 1.15. C-3, C-4, and C-5 diastereoisomers of D-fructose

This can also be explained due to changes in different forms (change in equilibrium ratio) due to epimerization. For example, L-sorbose exists majorly in β-furanose forms and D-psicose exists in an equal mixture of four possible isomers.

In earlier studies of glucose transport, it was observed that glucose is recognized in its pyranose form. In these studies, it appears that GLUT5 displays a similar affinity for both D-fructofuranose and D-fructopyranose forms (Figure 1.16). This conclusion was reached based on the Ki measurements for several methyl fructosides unable to undergo equilibration with other forms. For example, methyl-β-D-fructopyranoside **30** and methyl-β-D-fructofuranoside **32** both displayed Ki values similar to that of fructose itself. However, the Ki of methyl-α-fructofuranoside **31** was found to be roughly twice that of fructose, indicating the importance of the anomeric configuration. In addition, the Ki of methyl-α-D-fructopyranoside **29** could not be determined.

Along with stereochemical alteration, different substituents also gave some interesting results in affinity towards GLUT5. It was observed that GLUT5 exhibits a

higher affinity for methyl-β-D-fructofuranoside (**32**) as compared to the bulkier allyl furanoside **34**. Interestingly, removal of the anomeric C-2 hydroxyl group entirely (2,5-anydromannitol **33**) afforded a Ki similar to that of fructose, indicating that the presence of any sort of polar substituent at C-2 is not required for effective GLUT5 binding process.[54]

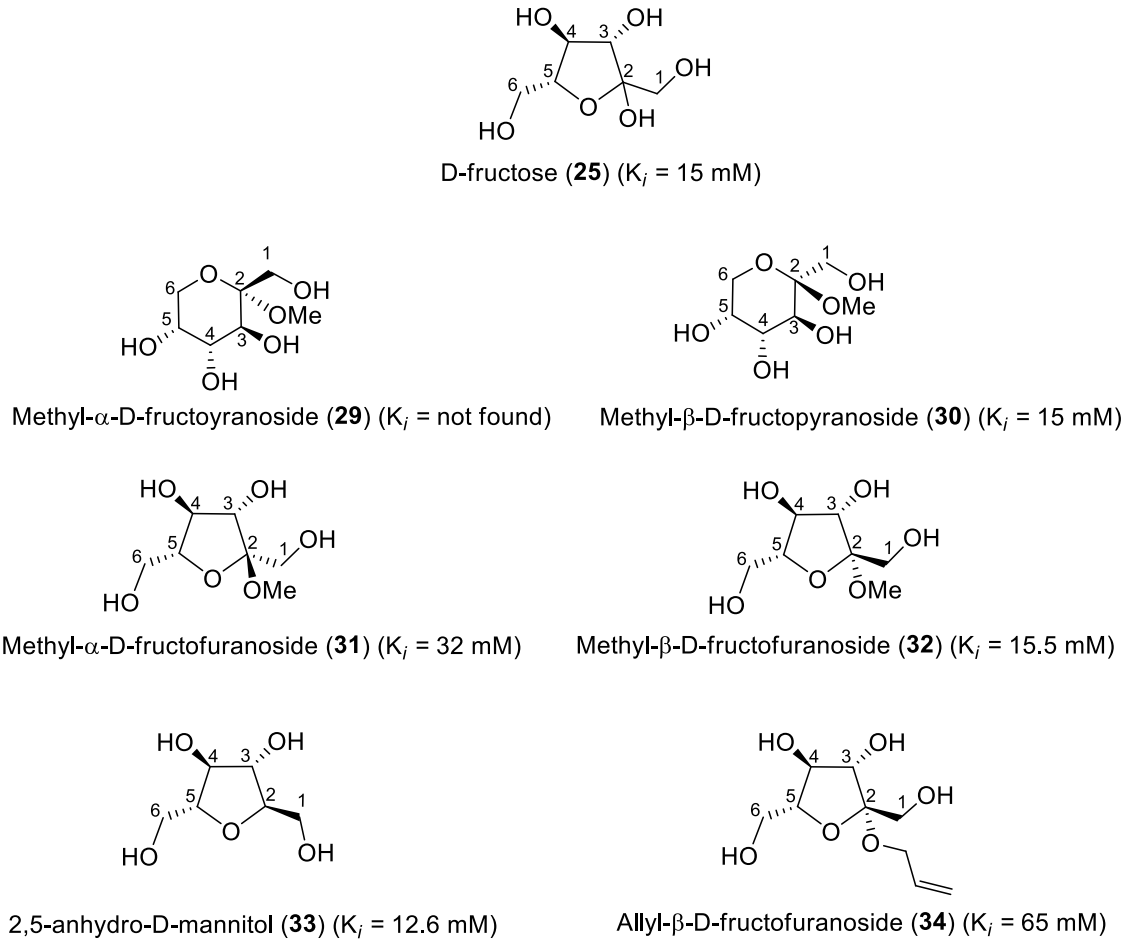

Figure 1.16. Comparison of GLUT5 affinity for fructopyranose, fructofuranose, and C-2 modified derivatives

However as mentioned before, epimerization at C-2 does influence binding affinity. For other secondary alcohol positions (C-3, C-4, and C-5), substitution with the allyl group was evaluated (Figure 1.17). All three allylated analogs (**35-37)** were

poorly tolerated suggesting that the presence of the hydroxyl group plays an important role in binding and causes unfavorable interaction on substitution.[54]

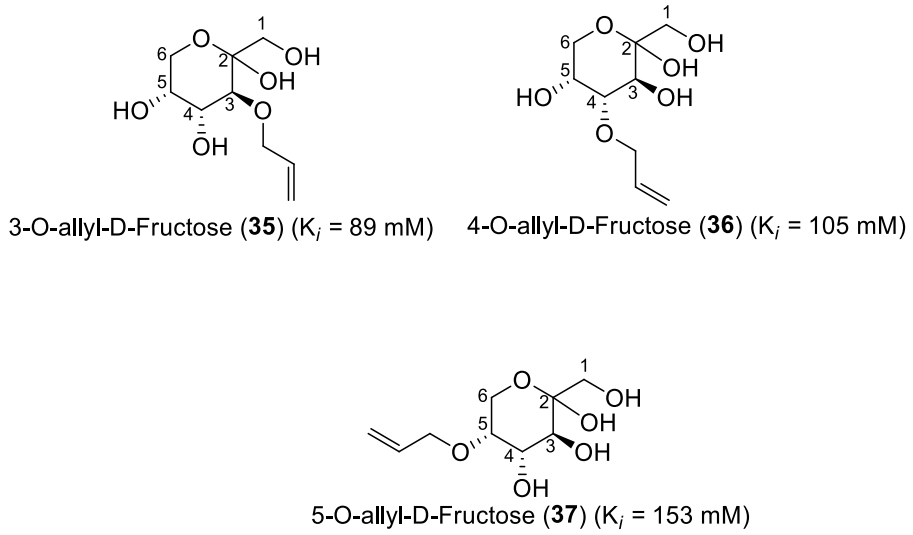

Figure 1.17. Position C-3, C-4, and C-5 D-fructose modified derivatives

In the evaluation of C-1 modified D-fructose derivatives (**38, 39**) (Figure 1.18), it was observed that on substituting hydroxyl group with allyloxy group (**38),** very poor or no affinity was observed. However, in presence of hydrogen bond acceptor at C-1 (**39**), no affinity was reported.[54] Further studies are required to understand the tolerance and affinity of C-1 modified derivatives towards GLUT5.

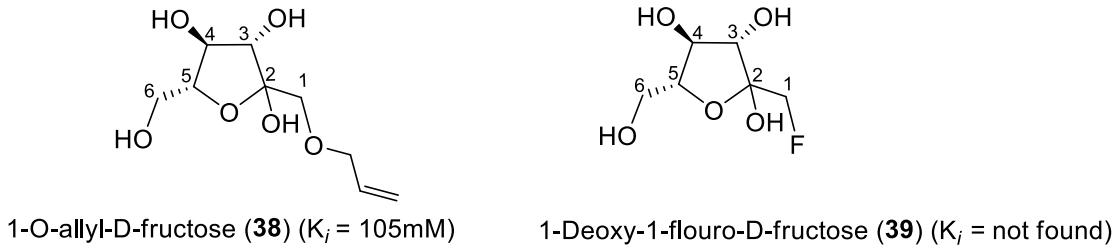

Figure 1.18. Position C-1 modified D-fructose derivatives

Furthermore, modification at the C-6 position with the allyl group **(41)** was observed to be moderately tolerated by GLUT5 (Figure 1.19). Deoxy analog, 6-deoxy-

6-fluoro-D-fructose (**40**) displayed a higher affinity for GLUT5 than D-fructose indicating the tolerance of GLUT5 for loss of a hydrogen bond donor at C-6.[55]

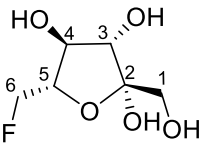

6-Deoxy-6-flouro-D-fructose (**40**) (K_i = 0.15 mM)

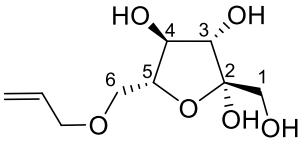

6-O-allyl-D-fructose (**41**) (K_i = 20.6 mM)

Figure 1.19. Position C-6 modified D-fructose derivatives

As mentioned above, C-2 deoxy analog of D-fructose also known as 2,5-anhydro-D-mannitol (2,5-AM), **33**, exhibited a similar affinity to that of both β-D-fructopyranoside (**30**) and β-D-fructofuranoside (**32**).[54,56] 1-Amino analogs of **33** (e.g., **42**, **44**, and **45**) displayed significantly higher affinity for GLUT5 than 1-aminoallyl-D-fructose **43**. A 28-fold increase in affinity relative to D-fructose was observed in **44** and **45** by attaching aromatic groups to nitrogen.[57] Alternatively, in presence of electron withdrawing nitro aromatic groups, the hydrogen bond donor character of the aryl N-H bond is also greater than that of allylated amine.

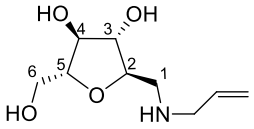

1-Aminoallyl-2,5-anhydro-D-mannitol (**42**) (K_i = 2.6 mM)

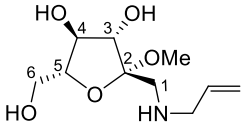

1-Aminoallyl-D-fructose (**43**) (K_i = 27 mM)

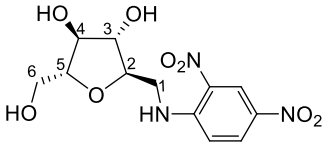

1-(N-(2,4-dinitrophenyl))-2,5-anhydro-D-mannitol (**44**) (K_i = 0.56 mM)

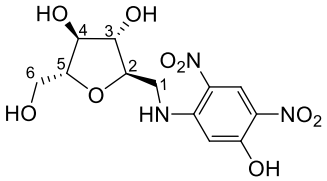

1-(N-(2,4-dinitro-5-ol-phenyl))-2,5-anhydro-D-mannitol (**45**) (K_i = 0.63 mM)

Figure 1.20. 2,5-AM based high affinity GLUT5 ligands

To investigate more on locked conformations, glycol-1,3-oxazolidin-2-thiones (**46-49**, Figure 1.21) were prepared yielding bicyclic structures. It was revealed that this class of compounds are weak binders with a low affinity towards GLUT5.[55]

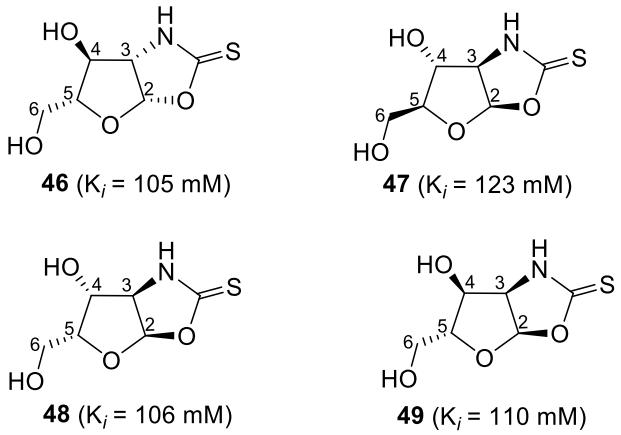

Figure 1.21. Inhibition constants of glycol-1,3-oxazolidin-2-thiones

Following these observations, synthesis of fructose analogs (**50-54**) containing hydroxymethyl groups at the anomeric carbon (corresponding to the fructose C-1 substituent) was carried out and their ability to compete with the natural ligand (D-fructose) was tested in GLUT5 overexpressing CHO cells (Figure 1.22). Some of these compounds were observed to be strong GLUT5 binders. Modification of oxazolidinethione to oxazolidinone (i.e., C=S to C=O, compounds **51** and **53**) resulted in improved binding affinity. On the other hand, the installation of an alkyl group on the C-1 oxygen atom had a relatively minor effect.[55]

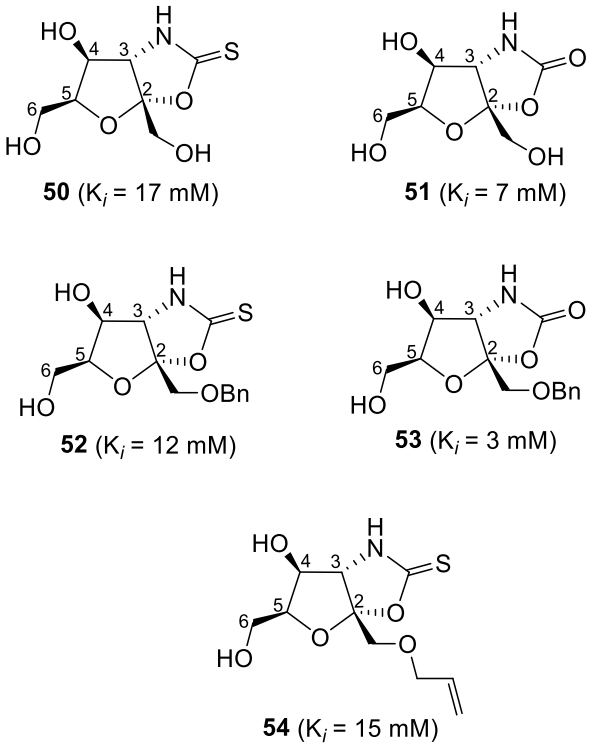

Figure 1.22. Inhibition constants of glycol-1,3-oxazolidinthiones and oxazolidinones

Recently, an evaluation of C-3 modified 2,5-AM derivatives **(55-60)** was carried out in EMT6, murine breast cancer cells (Figure 1.23). Strong inhibition was observed with analogs having hydrogen bond donor character as compared to fructose itself **(58-60)**. No inhibition or weaker inhibition was observed in the case of hydrogen bond acceptor groups at the C-3 site **(55-57)**.[58] More elaborative studies will be presented in the next chapter.

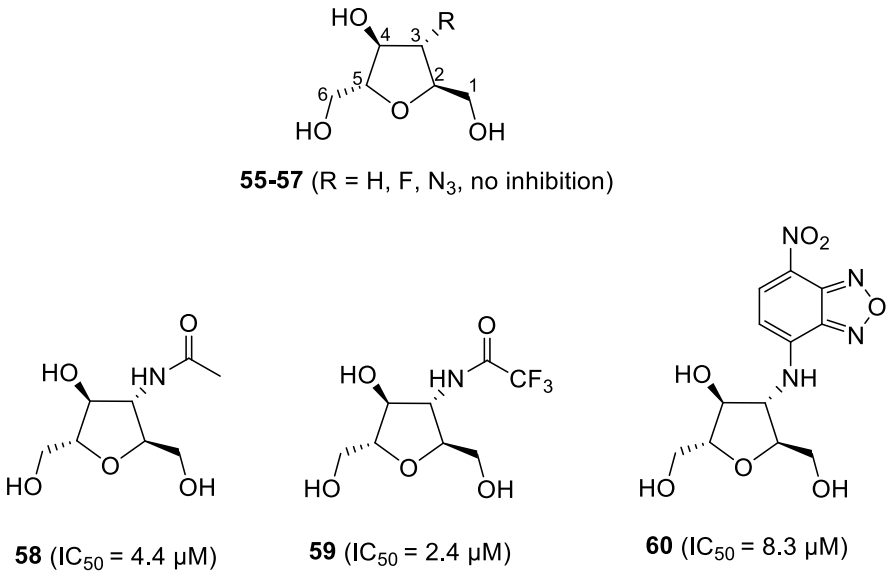

Figure 1.23. Inhibition concentration (IC_{50}) of C-3 modified 2,5-AM derivatives

Such observations (Figure 1.24) illustrate that both furanose and pyranose forms of D-fructose are recognized by GLUT5 with similar affinity. Stereochemistry of carbon centers attached to hydroxyl groups and substitution groups at C-1, C-3, and C-4 are very crucial for binding interactions. C-2 and C-6 position was observed to be tolerant of modification to develop diagnostic and therapeutic probes. In the case of 2,5-AM, modification at C-3 is also flexible as long as the hydrogen bond donor character is retained.

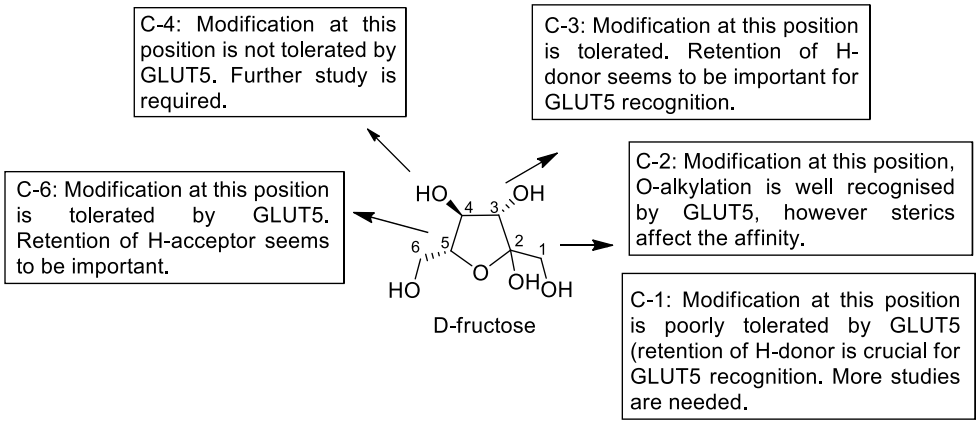

Figure 1.24. Summary of GLUT5 recognition for modified D-fructose

1.5. Role of fructose and its correlation to GLUT5 in promoting cancer and other diseases

In 1924, Otto Warburg described that cancer cells, in contrast to normal cells demonstrate a property of fermenting glucose into lactate even in a sufficient supply of oxygen.[59] This glycolytic pathway acts as a key energy source for cancer cells and this phenomenon is known as "Warburg Effect". The mechanism of the glycolytic pathway can provide some key insights to understand metabolic disorders. D-glucose not only acts as an energy source but also as a crucial substrate for the production of metabolites including fatty acids and nucleotides, and for redox regulation.[60] However, monitoring D-glucose metabolism by detecting GLUT1 through positron emission tomography (PET) with [^{18}F]-2-deoxy-2-fluorodeoxy-D-glucose ([^{18}F]-2-FDG), failed to detect some types of cancer as GLUT1 was detected only in 87 out of 154 types of cancerous tissues.[61] One of the reasons for this observation could be that D-glucose might not be the common energy source for all types of cancer.

Recently, fructose has been recognized as a significant driving force in metabolism-induced cancer.[62-70] It is known that fructose metabolism suppresses mitochondrial function stimulating the glycolysis pathway.[62] GLUT5, a transporter of fructose with no facility for transporting D-galactose and D-glucose, is predominantly present in the small intestine and is responsible for absorbing dietary D-fructose from the gut and into the bloodstream.[63] Skeletal muscle tissue is also observed to produce some energy using fructose. Fructose is mainly metabolized in the liver, where it is transported across its membrane through GLUT2. Evidence correlating human health and fructose consumption has generated increased interest in fructose-transporting GLUTs.

Notably, while normal breast tissues show no or limited expression of GLUT5, a significant percentage of breast tumors display overexpression of this protein.[64] In addition to breast cancer, GLUT5 is correlated with other cancers including lung adenocarcinoma, pancreatic cancer, acute myeloid lymphoma, and other cancers.[60] Exposure to high fructose levels has been found to be correlated with increased expression of GLUT5 in the intestine.[65] Moreover, in recent years, it was also reported that increased expression of GLUT5 in the intestine and increased fructose

consumption plays a major role in non-alcoholic fatty liver disease (NAFLD) and the more advanced, life-threatening non-alcoholic steatohepatitis (NASH).[66,67]

Other recent findings support the notion that fructose transporters could be valuable targets for small molecule therapeutic drugs and imaging probes. For example, diets containing high fructose content correlate with increased rates of tumor growth, in addition to obesity, diabetes, and heart and kidney diseases.[10] Exposure to high fructose concentrations can result in the transformation of tumor cells into more aggressive phenotypes.[70]

Obesity, exceeding body mass index by 30 kg/m^2, has become an epidemic around the world. It is suspected that fructose used in high fructose corn syrup (HFCS) plays a key role in rising levels of obesity in North America. Peptide hormones such as insulin and leptin modulate food intake.[10] Generally, glucose consumption stimulates insulin secretion which in turn increases the concentration of leptin causing satiety. However, fructose consumption and metabolism are different than glucose resulting in lower insulin secretion leading to low levels of satiety, more likely to cause obesity. In addition, fructose consumption has been also shown to increase the onset of type 2 diabetes due to low levels of insulin secretion.[10] Furthermore, gout, the most common inflammatory arthritis in men is also reported to be linked to an increase in fructose consumption. In that report, a survey was conducted on more than 50,000 male doctors (40-75 years) regarding their diet, medical, and drug history. It was found that men having high levels of fructose (in soft drinks, and daily food) were prone to show a much greater risk of Gout.[10] In renal cell carcinoma, a strong correlation between GLUT5 with clear cell RCC subtype was observed in a panel of 80 samples.[68] In another study, in tumor cells from patients with acute myeloid leukemia, high levels of GLUT5 were identified and the severity of pathological progression was also linked to increased GLUT5 expression. Also, in lung adenocarcinoma, it was observed that fructose promotes tumor cell growth and survival through GLUT5, as it was observed that by inhibiting or increasing the expression of the SLCA2A5 gene (GLUT5), a corresponding change in fructose uptake was observed.[69] In a work published by

Alejandro et al., it was observed that expression of GLUT5 was detected in 27% of colon, breast adenocarcinoma, liver carcinoma, and lymphomas.[65]

Given these observations, there is clear value in seeking greater insight into the mechanisms of fructose uptake and metabolism concerning the diseases mentioned, and biomarkers based on fructose uptake and consumption could be valuable for both diagnosis and therapeutic treatment. Since it is so critical for the cellular utilization of fructose, GLUT5 could function as a biomarker for a variety of cancers and metabolic diseases.

1.5.1. Overexpression of GLUT5 and increased utilization of fructose promotes the development of breast cancer

Evidence of overexpression of GLUT5 transporter in breast cancer cells was reported in 1996.[64] Interestingly, it was observed that contrary to other cell types, only 42% of breast cancer cells were observed to express very low levels of GLUT1. (Figure 1.25) These observations suggested that there might be other nutrients that could be potentially used by breast cancer cells. In recent studies, it was found that fructose among other nutrients tested (ribose, pyruvates, and amino acids) could substitute for glucose to support proliferation and colony formation of breast cancer cells in a dose-dependent manner even in conditions of glucose deprivation.[70]

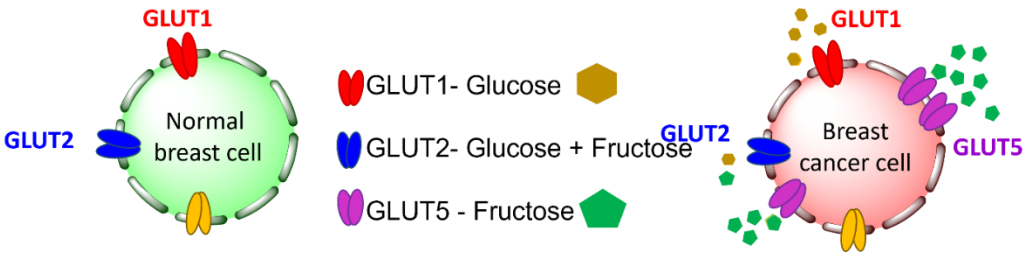

Figure 1.25. Comparison between normal breast cancer and breast cancer cell along with their GLUT expression and substrate specificity

Work conducted by Fan et al demonstrated that GLUT5 knockdown blocked the utilization of fructose by breast cancer cells.[70] Interestingly, along with GLUT5, breast cancer cells were observed to overexpress another transporter GLUT2. These results were also further confirmed when both GLUT2 and GLUT5 were observed to

be regulated through transcription factor HIFα in breast cancer cells and tissues under hypoxic conditions.[71] It was also reported that triple negative breast cancer (TNBC) cells show higher expression of GLUT5 than estrogen receptor positive (ER+) breast cancer cells.

These findings explain the relationship between increased dietary fructose and breast cancer providing insights into potential therapeutic strategies aiding to eliminate fructose mediated breast cancer. As a result, GLUT5 could be potentially used as a portal for the delivery of tracer molecules and cytotoxic drugs for breast cancer prognosis and treatment.

1.6. Molecular imaging and techniques

Molecular imaging is defined as in vivo visualization, characterization, and quantitative measurement of biological processes at molecular and cellular levels.[72,73] Molecular imaging has a great potential to detect diseases in their early stages, characterizing pathologies of affected tissues without invasive biopsies and surgery. As a result, personalized medicine and patient specific therapeutic regimens can be applied.[74]

There are various strategies (Figure 1.26) that are currently used in clinical practices such as positron emission tomography (PET), single photo emission tomography (SPECT), magnetic resonance imaging (MRI), magnetic resonance spectroscopy (MRS), ultrasound (US), computed tomography (CT), and some emerging preclinical ones (for example, contrast-enhanced ultrasound, photoacoustic imaging, and other methods) to be further translated into clinical use in the near future.[72,74]

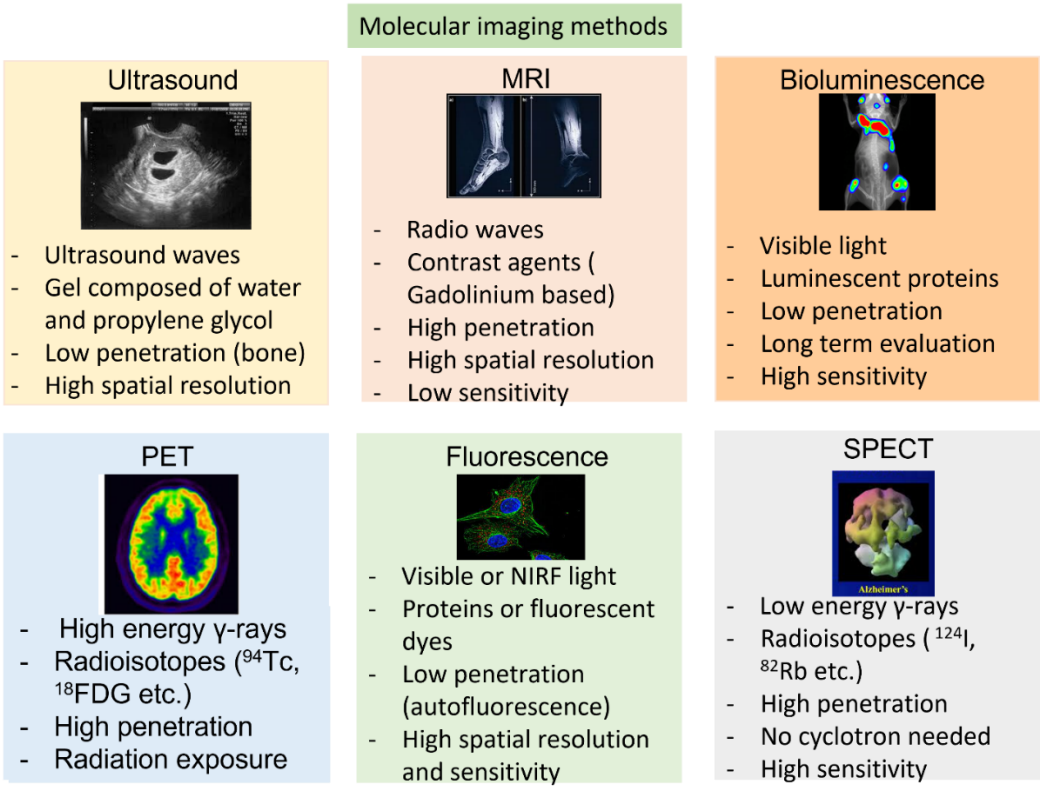

Figure 1.26. Various strategies currently used in molecular imaging

Current molecular imaging methods primarily use PET based techniques which will be discussed in detail in the next section. Ongoing preclinical research is focusing on developing novel molecular probes for different diseases followed by developing multifunctional contrast agents to image these molecular targets with new instruments and technologies. Optical imaging using fluorescent probes and ultrasound imaging with molecular microbubbles have gained recent attention as they provide real time imaging, producing high spatial resolution images, and don't need ionizing irradiation. Photoacoustic imaging is a hybrid of ultrasound and optical techniques involving the excitation of an optically-excitable molecular probe followed by detecting the observed oscillatory signal from the movement of the molecular probe through ultrasound.[74]

Currently available real-time in vivo optical imaging techniques are limited to the surface and ocular due to limited in-depth tissue penetration,[74] although, there are recent advancements in endoscopic and catheter devices for optical coherence tomography (OCT). The majority of the imaging methods mentioned above function

by exciting photons and measuring reflected light. Alternatively, Raman spectroscopy is an emerging technique that works via the Raman effect (detection of signal formed through light scattering effects). However, this method is limited as it only includes near infrared fluorescent dyes, quantum dots, and nanoparticles.[73,74]

As a result, molecular imaging can be approached in several directions of medical imaging, for example, early screening/detection, monitoring, diagnosis, treatment, and follow-up. Current techniques and trends give the hope that these new strategies will improve the success rate for curing diseases such as cancer, cardiovascular diseases, and finding more specific treatments for diseases like Parkinson's, and Alzheimer's.

1.6.1. Positron Emission Tomography (PET)

PET is an imaging technique that helps to visualize metabolic or biochemical functions taking place in the body such as blood flow or metabolism.[74] This technique is a combination of nuclear medicine and biochemical analysis evaluating the physiology and anatomy of organs or tissues.[72] A PET scan uses tiny amounts (well below the toxic limit) of the radioactive substance, known as a radiopharmaceutical (radioactive drug or tracer) to demonstrate normal and abnormal metabolic activity. PET offers quantitative analysis, permitting relative changes to be monitored over time as a disease responds to a specific treatment. Conjugation of PET with other diagnostic tests (CT and MRI) called PET/CT or PET/MRI helps to provide more definitive information about cancerous tissues, epilepsy, Alzheimer's, and heart diseases.[74]

A PET scan is based on the detection of radioactivity emitted when a small amount of radiotracer is injected into a vein. As the name of the method states, this technique operates through a positron emitter tracer molecule.[75,76,77] Positron emitting isotopes such as carbon-11, oxygen-15, nitrogen-13, and fluorine-18 are generally used in the labeling of amino acids, carbohydrates, and nucleosides.[78] After the tracer is administered to the patient's body, positrons emitted from the radiotracer collide with the electrons of the tissue, resulting in the generation of two high energy gamma rays, a phenomenon known as the annihilation process (Figure 1.27).[79]

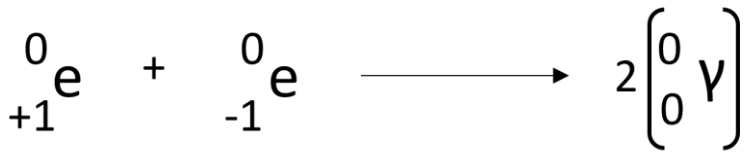

Figure 1.27. Schematic representation of the annihilation process

As a result, two gamma rays emitted, easily pass through human tissue, allowing them to be detected and their origin to be located by radiation detectors. In order to decide which positron emitting isotope should be used in making radiolabeled tracer, the half-life of the isotope and the kinetic energy of the emitted positron are two important factors to determine its usage in PET (Table 1.2).[80,81] For the radiolabeling process to occur during the first half-life of a radionuclide, a radionuclide with a longer half-life is desired to provide sufficient time to run diagnostic imaging before most of the activity has been lost Secondly, to get PET images with high spatial resolution, it is desired that the range of emitted positron (distance positron travel from the nucleus of emission) to be shorter or kinetic energy to be lower for better images.[81]

Table 1.2. List of radioisotopes that decay by positron emission and their properties

Isotope	Half Life/ $t_{1/2}$ (min)	Positron energy /E_{max} (MeV)	Positron Range (mm)
^{82}Rb	1.26	3.15	1.7
^{15}O	2.03	1.70	1.5
^{13}N	9.97	1.19	1.4
^{11}C	20.3	0.96	1.1
^{18}F	109.8	0.64	1.0
^{124}I	6000	2.13	2.6
^{64}Cu	768	0.66	N/A
^{68}Ga	67.72	1.90	2.9

In the annihilation process, the positron emitted by the radiotracer starts losing its kinetic energy upon inelastic collision with the electrons of the tissue. As the positron loses the kinetic energy, it forms a positronium state on combing with the electron, which lasts about 10^{-10} seconds (Figure 1.28). Therefore, the reaction of positronium and electron results in the ejection of two gamma rays. The emitted gamma rays travel at an angle of 180˚to each other.[75,77,79,81]

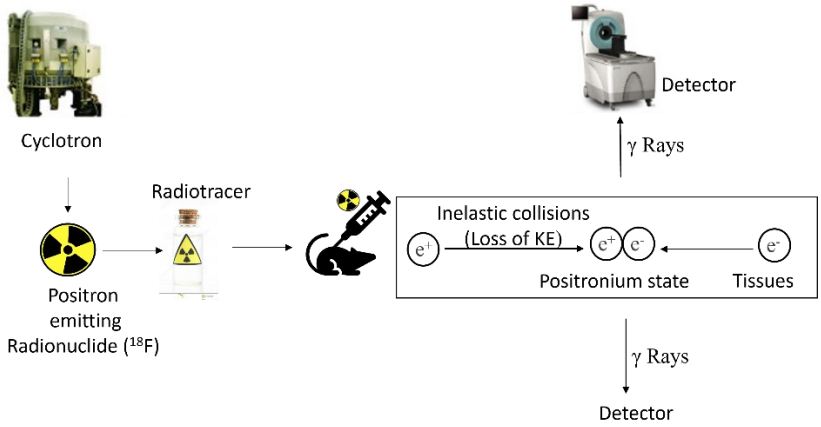

Figure 1.28. Working principle of PET

Fluorine-18 (^{18}F) is one of the most important radionuclides for PET. It exhibits a great position within the steadily growing portfolio of applicable radioisotopes for in vitro and in vivo imaging. It is mainly due to its interesting physical properties such as low energy of positron (~49 keV) to produce high resolution diagnostic images and a half-life of 109.9 minutes rendering multistep synthesis possible.[82] Employment of isotopes ^{68}Ga, ^{11}C, ^{94}Tc.. for the radiolabeling of PET tracer is also very common and widely used.[83] As mentioned in the previous section, glucose transporters like GLUT1 and GLUT5 are observed to be overexpressed in many tumor cell types and hexoses like glucose or fructose are absorbed at a much faster rate in tumor cells in comparison to normal cells.[59-71] Such hexoses upon labeling with radionuclides followed by accumulation in tumor cells can help in imaging the location and size of the tumor.

In order to act as an optimal tracer for tumor imaging, the radiolabeled hexose should have the 1) property of being transported via a specific GLUT to avoid off target

detection, and 2) capacity of undergoing enzymatic phosphorylation for metabolic trapping of tracer inside the tracer cells.[75,77] Development of ^{18}F containing PET tracers will be discussed in more detail in the next section.

In summary, a PET scan can be an effective way to identify the variety of conditions, including heart diseases, brain disorders, and cancer. Since cancer cells have higher metabolic rates than normal cells, solid tumors show up as bright spots in a PET scan. It is crucial to interpret these scans carefully, as many non-cancerous conditions can also look like cancer. Regarding the risks of PET scan, the amount of radiation a patient is exposed to is very low; however, there are risks of radiation exposure to unborn babies and through breastfeeding, and an allergic reaction is sometimes observed.[74]

1.7. Production of [^{18}F] and specific activity

1.7.1. Production of [^{18}F]

Fluorine-19 (^{19}F, the naturally occurring nonradioactive isotope) belongs to group 17 and is a p-block element with the natural abundance of 100%. In its gaseous state (F_2), elemental fluorine can react with almost every element or compound.[84] Requiring only a single electron to complete its valence shell, fluorine is the most electronegative element, with an electronegativity of 4.0.

The radioactive isotope ^{18}F consists of 9 protons and 9 neutrons with a half-life of 110 min. Other isotopes of fluorine which are radioactive and positron emitters have exceedingly short half-lives (e.g., ^{17}F, $t_{1/2}$ = 64.8 s) and are unsuitable for *in vivo* imaging purposes.[83,84]

Nuclides which undergo positron decay for stabilization are proton rich or neutron deficient. The development of such unstable nuclides can be achieved by bombarding a stable isotope (having a proton/neutron ratio of 0.8-1) with protons, generating a positron emitter.

As a result, for the generation of ^{18}F, the most common method used is by bombarding oxygen-18 enriched material with a proton beam (Figure 1.29). Oxygen-18 is a stable isotope naturally occurring in about 0.205% abundance along with other

isotopes i.e., oxygen-16 (99.752%) and oxygen-17 (0.038%). The ^{16}O (p, α) reaction yields nitrogen-13 having a small half-life of 9.96 min. The production of ^{18}F through ^{18}O bombardment is dependent on many factors such as proton energy, bombardment time, and current target volume. With 60 min bombardment time, the usual yield ranges between 37-74 GBq of ^{18}F.[83] The generated ^{18}F is present as [^{18}F]HF in target water and is generally extracted by using ion exchange cartridges. The material used for this nuclear reaction commonly consists of silver, copper, and titanium resistant enough to withstand high heat and pressure during irradiation.[83,84]

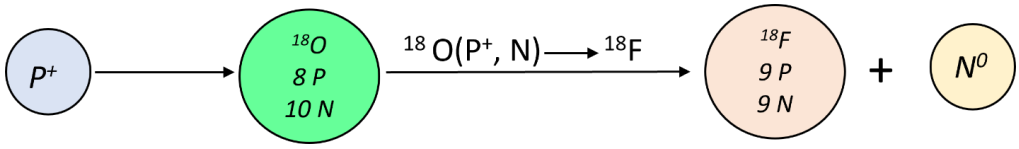

Figure 1.29. Production of ^{18}F through the bombardment of ^{18}O with protons

Another possibility to produce ^{18}F is by targeting neon gas by deuteron bombardment (^{20} Ne(d, α) ^{18}F). In this method, stable ^{19}F gas (0.1-2%) is added to neon gas before the irradiation process resulting in a generation of ^{18}F-[F_2] gas with low specific activity.[83]

In another method, fluorine gas is generated by using ^{18}O gas as the target undergoing the same ^{18}O (p, n) ^{18}F reaction yielding [^{18}F]HF which in turn is converted to [^{18}F]F_2 gas again with low specific activity.[84]

In order to obtain electrophilic [^{18}F]F_2 with high specific activity, the optimal method would be to start with ^{18}O enriched water as a target followed by converting the obtained ^{18}F with high SA to [^{18}F]F_2. This is achieved by reacting fluoride with methyl iodide followed by discharging it in a chamber containing small amounts of F_2 yielding [^{18}F]F_2.[83]

1.7.2. Specific Activity (SA)

Specific activity is defined as the proportion of the radiotracers in question to the total amount of compound (both labeled and unlabeled together) and is expressed in GBq (gigabecquerel)/μmol or mCi(millicurie)/mmol. Specific activity (SA)of the [^{18}F]F_2 gas would be the radioactivity of the gas (GBq/mCi) to the total amount or concentration

of ^{18}F, ^{19}F, and other isotopes of fluorine. This in turn means how much radioactive substance is diluted/ contaminated with non-radioactive isotopes.[83] If the SA is low, a high dose of the tracer compound would be administered for a PET scan with a risk of side effects to occur. As a result, it is important to determine the SA of the final radiopharmaceutical and study the pharmacology of the applied compound. SA can be determined by HPLC, gas chromatography, and conduction detectors.[83]

1.8. Fluorination reactions using ^{19}F and ^{18}F

Before the development of radiotracer containing ^{18}F, studies started first with the labeling of hexose with non-radioactive isotope ^{19}F followed by determining the recognition of GLUT for modified hexose. In the following section, we will discuss both electrophilic and nucleophilic fluorination methods which can be used in the labeling of hexose.

1.8.1. Electrophilic fluorination

In electrophilic fluorination, electrophilic fluorine sources react with electron rich organic molecules yielding organofluorine compounds. Initially, fluorine gas was used as the most common fluorination agent, but due to its high reactivity and low selectivity, secondary electrophilic labeling sources were explored.[85] XeF_2 is an alternative electrophilic source but exhibits poor functional group tolerance.[86]

Electrophilic reagents (Figure 1.30) used in modern organic synthesis consist of relatively more stable N-fluoro compounds such as fluorobis(phenyl)sulfonamide (NFSI) (**61**), N-fluoropyridinium salts (NFPy) (**62**), and acufluor (**63**).[87,88,89,90,91,92] In these reactions, the nucleophile interacts with the σ^* N-F bond from the fluorine side as the nitrogen side is sterically inaccessible. To generate asymmetric organic molecules with high stereoselectivity, chiral NFSI (**65**) and selectfluor (**66**) deliver electrophilic fluorine in an enantioselective fashion (Figure 1.31).[93]

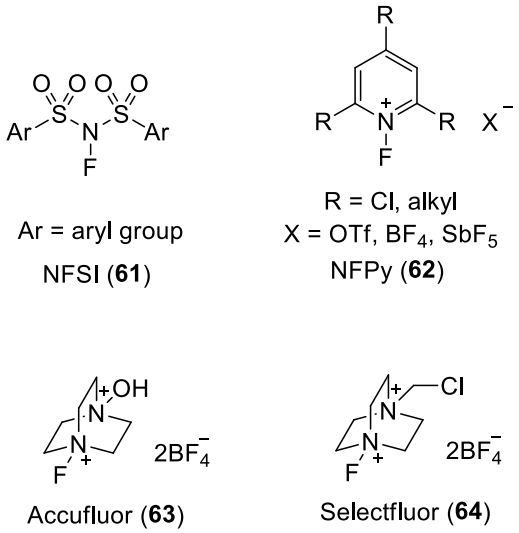

Figure 1.30. Electrophilic fluorination reagents

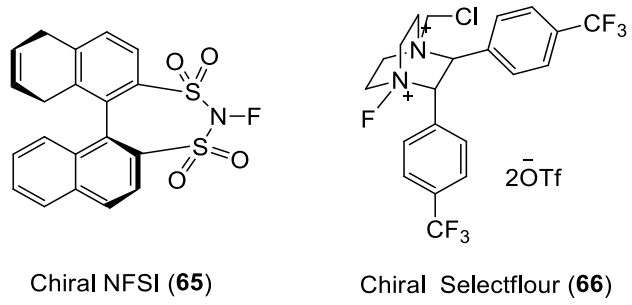

Figure 1.31. Chiral electrophilic fluorination reagents

Fluorination using [^{18}F]F_2 gas, and acetyl [^{18}F] hypofluoride reacts well with aromatic systems, but due to low regioselectivity, a mixture of the fluorinated aromatic system is obtained.[83] One of the most important electrophilic reactions using these reagents is the synthesis of [^{18}F]fluoro-DOPA, **70,** (Scheme 1.1), a neurotransmitter used in their investigation of presynaptic dopamine neurotransmission.[83] Scheme 1.1 represents the optimization studies that were performed to obtain **70** with higher purity.

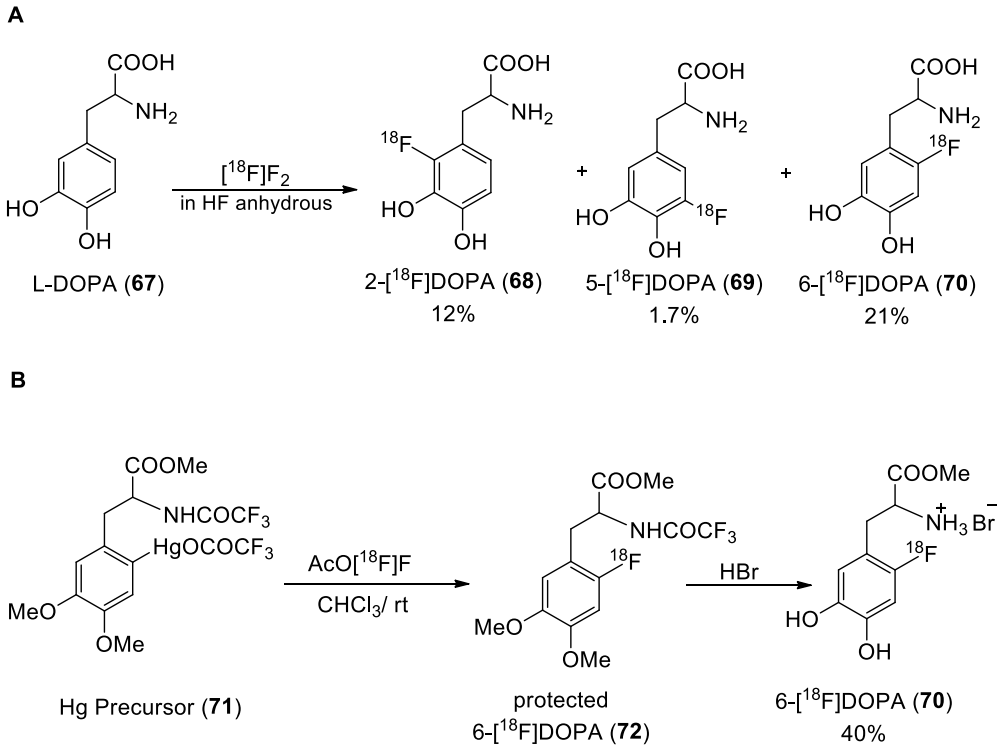

Scheme 1.1. Different methods for the synthesis of [^{18}F]fluoro-DOPA

1.8.2. Nucleophilic fluorination

In nucleophilic fluorination reactions, alkali metal fluorides like CsF, KF, and KHF_2 are the most often used reagents to fluorinate organic molecules.[94,95] Also, it is important to note that fluoride ions are more basic and less nucleophilic in nature. Primarily, these reactions are carried out in polar aprotic solvents (acetonitrile, dimethylformamide, dimethyl sulfoxide). However, alkali metal fluorides exhibit poor solubility in aprotic organic solvents. As a result, these reactions are often carried out in the presence of chelators such as Kryptofix 2.2.2. resulting in the formation of a complex between K^+ and cryptand and thus causing ionic dissociation and enhancing the fluorine nucleophilicity.[96]

KHF_2 is often used to incorporate fluorine in organic molecules in the nucleophilic ring opening of epoxides. Other metal fluorides like KF and CsF incorporate fluorine by SN_2 displacement reactions.[97]

The introduction of ^{18}F by nucleophilic substitution is directly related to the nature of leaving group (triflate, tosylate, mesylate).[98] Apart from high reactivity,

sulfonate esters (triflate>nosylate>tosylate>mesylate) are more valuable than halides, because they can be synthesized from their corresponding alcohols (especially hexoses).[83] However, due to the basic nature of fluoride ion, SN_2 reaction with a good leaving group can also produce unwanted elimination products. Other nucleophilic agents such as organic sulfur fluorides (Figure 1.32) can convert free hydroxyl groups directly to organic fluorides.[89,99,100]

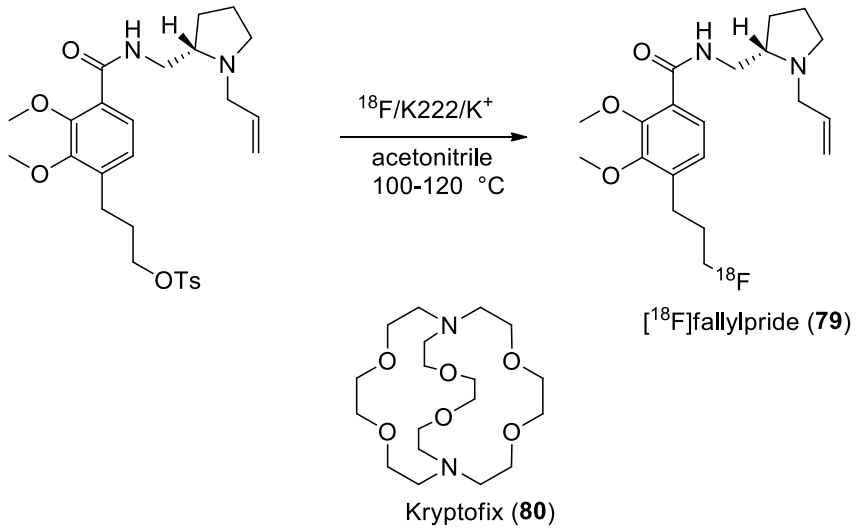

Scheme 1.2. Synthesis of [^{18}F]fallylpride by nucleophilic ^{18}F-fluorination of the corresponding tosylate precursor

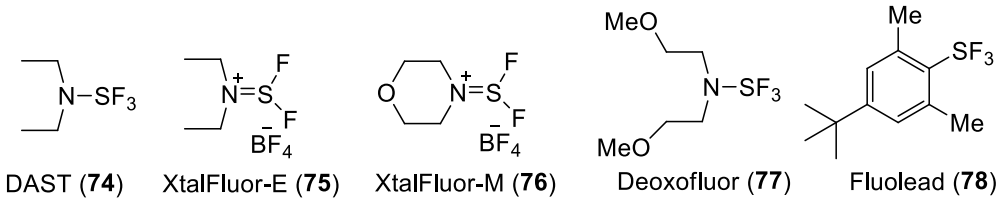

Figure 1.32. Nucleophilic fluorination reagents

1.8.3. Prosthetic group precursors for ^{18}F labeling

In the case of complex molecules bearing more than one reactive site (acidic protons or nucleophilic moieties), prosthetic groups or secondary labeling precursors are used (Figure 1.33). Precursors such as 2-[^{18}F]fluoroethyl-4-methylbenzene sulfonate (**81**),

1-bromo-2-[^{18}F]fluoroethane (**82**), and N-succinimidyl-4-[^{18}F]fluorobenzoate (**83**) are generally used in labeling NH_2, OH, or other nucleophilic moieties (Scheme 1.3).

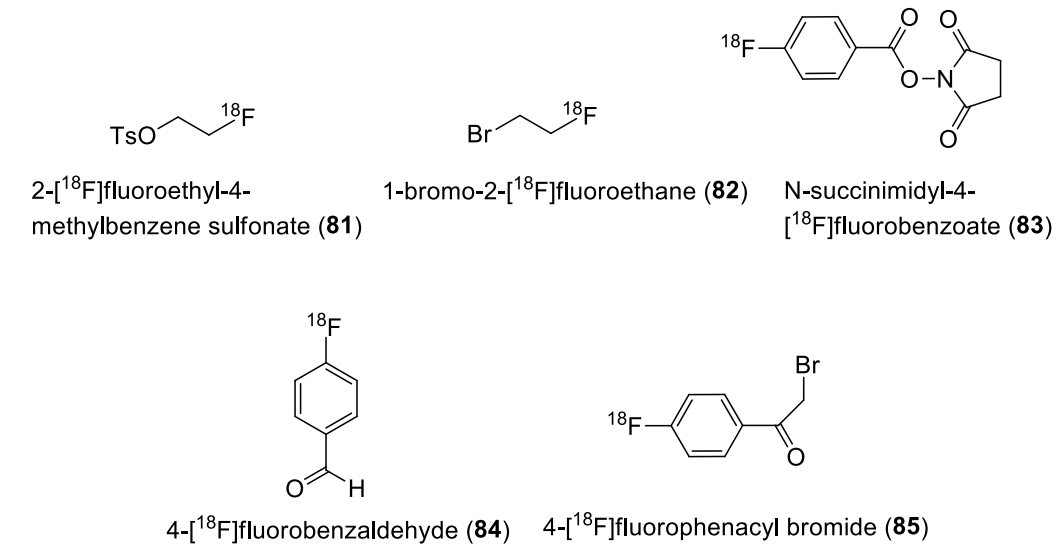

Figure 1.33. Prosthetic groups (secondary labeling precursor) used in ^{18}F labeling

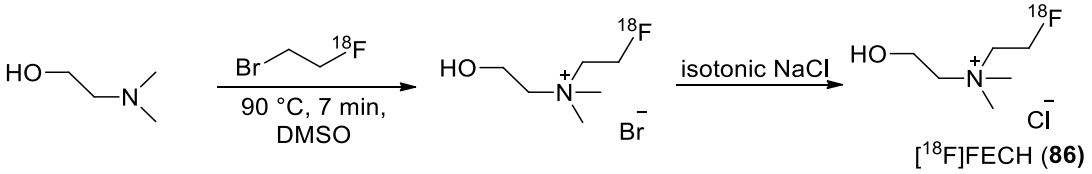

Scheme 1.3. Synthesis of [^{18}F]FECH (**86**)

After synthesizing compounds with ^{19}F, in vitro experiments are performed to evaluate their affinity toward their protein targets. In the case of GLUTs, these studies are performed through competitive inhibition experiments using a reference standard ([^{14}C]-D glucose, and [^{14}C]-D fructose along with synthesized compounds. Such studies are performed in cell lines expressing GLUTs of interest. After performing competitive inhibition experiments, cellular uptake of "hot" or ^{18}F-labeled compounds is measured in a concentration and time dependent manner.

Once synthesis and in vitro experiments are accomplished, in vivo evaluation of [^{18}F]-hexose is performed using small animal PET equipment. In this experiment,

[^{18}F]-hexose is injected into tumor bearing mice, and PET scanning is performed for a specific time period revealing the diagnostic efficiency of the tracer. Upon successful imaging, the tracer is sent for toxicology studies followed by clinical trials.

1.9. GLUT ligands used in molecular imaging and biomedical applications

Accelerated carbohydrate metabolism/uptake in a significant number of diseases and cancers has triggered interest in GLUT targeting probes. Such molecular interactions that operate through uptake of glucose and fructose via different GLUTs have created the basis for the development of biochemical and biomedical GLUT agents targeting metabolically compromised cells. The following section will be providing a brief overview of different types of agents (fluorescent probes, PET probes, GLUT inhibitors) that were investigated and developed to be used in imaging and medicinal applications.

1.9.1. GLUTs targeting imaging probes

To study real-time monitoring of carbohydrate uptake and to quantify expression levels of membrane transporters, the development of GLUT targeting probes was initiated. Holman and coworkers initiated experiments by quantifying glucose transport with biotin, mono- and bis- saccharide diazirine conjugates (Figure 1.34) and observed an increase in affinities by conjugating carbohydrate moieties to the linker.[101,102,103,56] Glucose conjugates displayed the highest affinity among other hexoses. Also, 1-amino 2,5-anhydro-D-mannitol as a carbohydrate moiety showed a higher affinity towards GLUT5.[56]

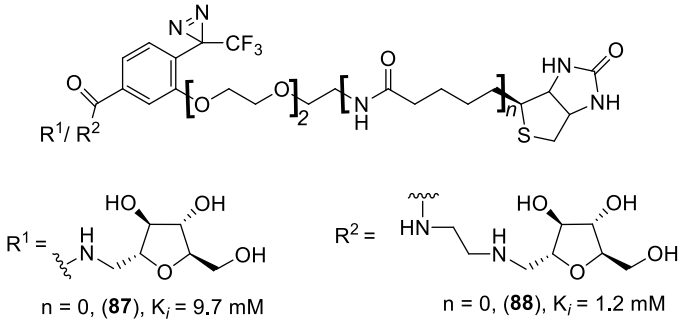

Figure 1.34. Examples of affinity labels for glucose and fructose transporters at plasma surfaces

Targeting GLUTs with fluorescent probes have also been investigated with a limited choice of fluorophore, 4-Chloro-7-nitrobenzofurazan (NBD) exhibiting green fluorescence.

Conjugates of amino sugars (Figure 1.35) such as 2-amino-2-deoxy-D-glucose **89** (G)[104], 1-amino-1-deoxy-D-fructose **90** (F)[105], and 1-amino-2,5-anhydro-D-mannitol **91** (M)[106] with NBD (**98**) generated probes that were observed to be effectively taken up tumor cells through GLUTs. 1-NBDF (**91**) was observed to be glucose and fructose dependent whereas in the case of 1-NBDAM (**90**), fructose dependent uptake was observed, indicating the participation of fructose specific GLUT5. It was observed that all the three probes were taken up by the cell due to significant increase in the fluorescence signal. Upon labeling of hexoses with a red fluorescent dye (cyanine 5), the disappearance of GLUT-mediated uptake was observed.[105] Interestingly, stereochemical alterations in fructose followed by in vitro evaluation displayed some compelling results. In work done by the West and Cheeseman team, it was observed that by alteration of the C-3, C-4, or C-5 stereocenter of fructose (**92-95**), affinity towards GLUT1 instead of GLUT5 was observed.[107] In contrast, C-1 analog 6-NBDF (**92**) was observed to be transported specifically through GLUT5. These results indicate that specificity of GLUTs is dependent on substrate stereochemistry.

Recently, it was found that 2,5-AM labeled with NBD at C-3 (**96**) efficiently inhibited the uptake of [^{14}C]fructose, operating selectively via the GLUT5 transporter.[58] Tanasova and coworkers also prepared a list of fluorescent probes (**97**) (ranging from blue to red visible region) containing fluorophores conjugated to 2,5-AM at the C-1 position.[108] Different probes displayed different uptake properties through GLUT5 indicating the specificity of GLUT5 for fluorophores bearing different sizes and charges.

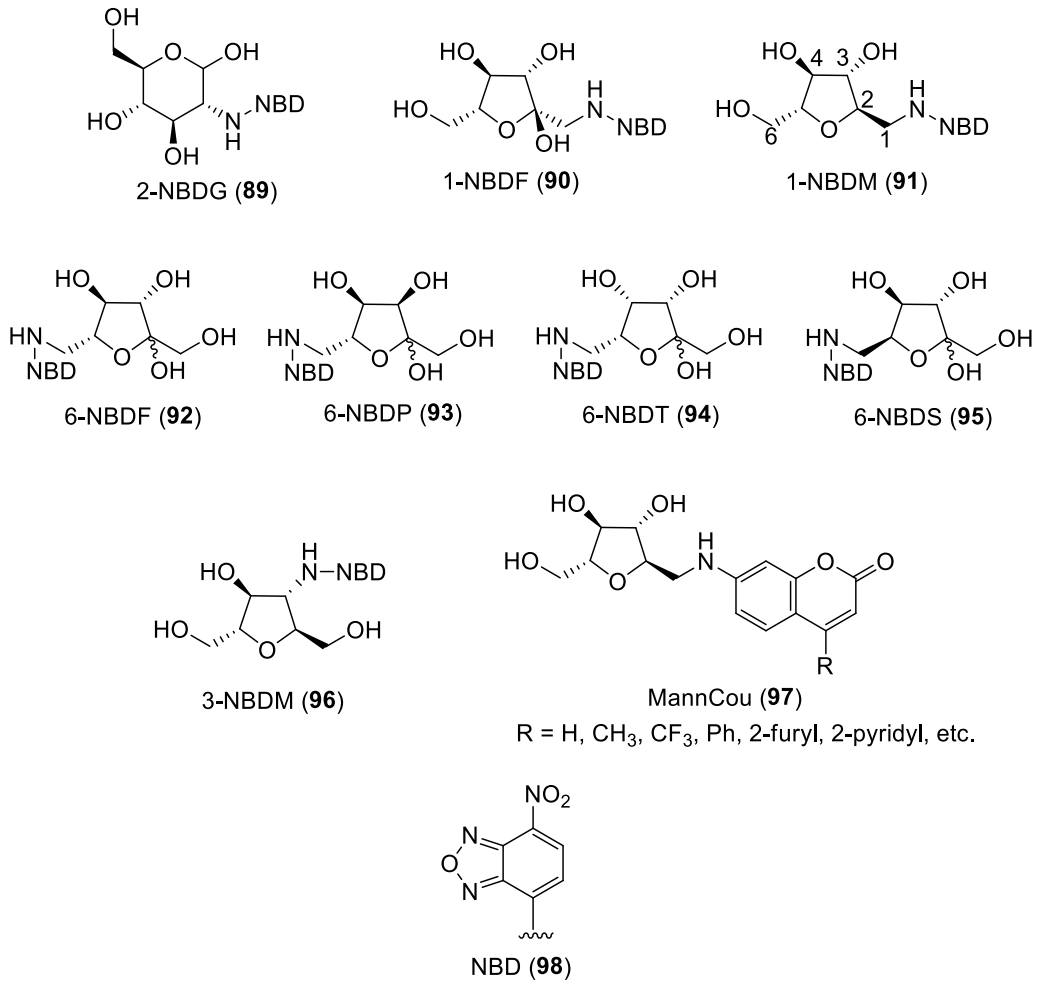

Figure 1.35. Fluorescent GLUT-targeting probes and fluorophore used in labeling

1.9.2. Diagnostic GLUT probes

The relationship between high nutrient uptake and metabolically compromised cells, particularly cancers, triggered interest in the development of GLUT targeting diagnostic probes (Figure 1.36). Results observed from kinetic analysis of fructose and glucose uptake provided the basis for the development of carbohydrate derived radioactive diagnostic probes. The first and most commonly used radiotracer for cancer diagnosis, 2-deoxy-2-fluoro-D-glucose (2-[^{18}F]FDG, **99**) was developed in 1978 at Brookhaven National Laboratory.[109] After cellular uptake, 2-[^{18}F]FDG undergoes enzymatic phosphorylation but doesn't get metabolized. As a result, 2-[^{18}F]FDG gets metabolically trapped inside the tumor cells and allows monitoring of both enhanced glucose transport and phosphorylation. In addition, after positron emission, 2-

[^{18}F]FDG-phosphate transforms into [^{18}O]-D-glucose and gets easily washed out from the patient's body.[110] However, 2-[^{18}F]FDG tends to be ineffective in cases of cancer with low glucose uptake capacity and also provides false positive results observed due to accumulation of glucose in immune cells during inflammatory processes.[111,110] Taking into consideration the significance and limitation of 2-[^{18}F]FDG, numerous efforts have been made to develop radiotracers that would reflect the carbohydrate content and their uptake inside cells independent of phosphorylation. Wassenaar and coworkers developed [^{123}I]-6-deoxy-6-iodo-D-glucose ([^{123}I]-6-DIG, **102**) to assess insulin resistance in adipocytes and cardiac cells, indicating preferential uptake of 6-DIG through the action of GLUT4.[110] Due to unique connection between the expression of fructose transporters GLUT5 and various types of cancers, fructose transporter targeting probes have gained special attention. Maeda and coworkers designed the first fructose derivative, 1-[^{18}F] fluoro-1-deoxy-D-fructose (1-[^{18}F]FDF, **101**) to be tested as a tracer for GLUT5 in cancer cells.[112] It was tested in mouse and rat tumor xenografts and displayed fast clearance through the liver and kidney. Extensive studies have been performed on another fructose based radiotracer, 6-[^{18}F]fluoro-6-deoxy-D-fructose (6-[^{18}F]FDF, **102**), developed by West and coworkers.[113,96,114] 6-[^{18}F]FDF was observed to be effectively taken up murine EMT6 and human breast cancer MCF7 cells. However, due to the absence of the C6-OH group, it was not a substrate for phosphorylation by hexokinase, and as a result, rapid efflux of the tracer was observed following the initial accumulation. Additionally, regarding optimization of fructose analogs, Cheeseman et al developed another tracer [^{14}C]-3-fluoro-3-deoxy-D-fructose (3-FDF, **103**), and results obtained by a series of competitive uptake and inhibition studies displayed stronger fructose-dependent uptake.[98]

Also, due to the high affinity of GLUT5 for 2,5-AM, another generation of radiotracer probes were developed. Sun and coworkers tested 1-[^{18}F]fluoro-1-deoxy-2,5-anhydro-D-mannitol (**104**), (1-[^{18}F]FDAM) for PET imaging of breast cancer.[114] The results displayed avid uptake of the probe by the tumor cells in comparison to normal cells; however, it was observed to be rapidly excreted. Overall, the above-

mentioned results have called for further development of fructose and fructose mimic-based radiotracers exhibiting longer retention and metabolically stable compounds.

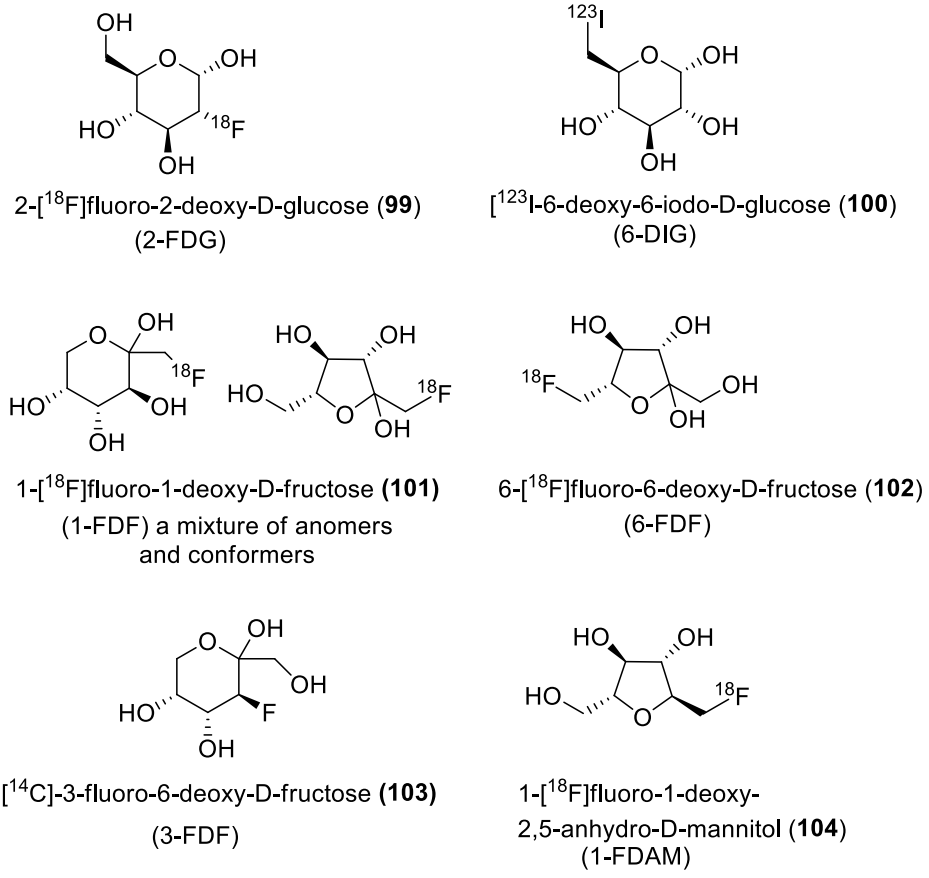

Figure 1.36. Glucose and fructose-based PET imaging probes

1.9.3. Chemotherapy drugs for GLUTs

The dependence on hexoses and its transport in a significant number of cancers resulted in strategies to improve the selective targeting of cancers via glycoconjugation.[115] Glufosamide, the first glucose-conjugated drug to reach human clinical trials, reacted by cleaving off glucose upon entering the cells to release the active drug.[114] Following this, several anticancer agents such as paclitaxel, clioquinol, and chlorambucil used a similar strategy of glycoconjugation by using different sugars in order to improve the cytotoxic properties of drugs.[115] This approach of glucose conjugation got extended to palladium and platinum complexes (Figure 1.37).[116] In an extensive study done by

Lippard and coworkers, C6-Pt conjugates of glucose (**105-107)** displayed greater cytotoxicity than cisplatin and nonconjugated drug, aglycone.[117]

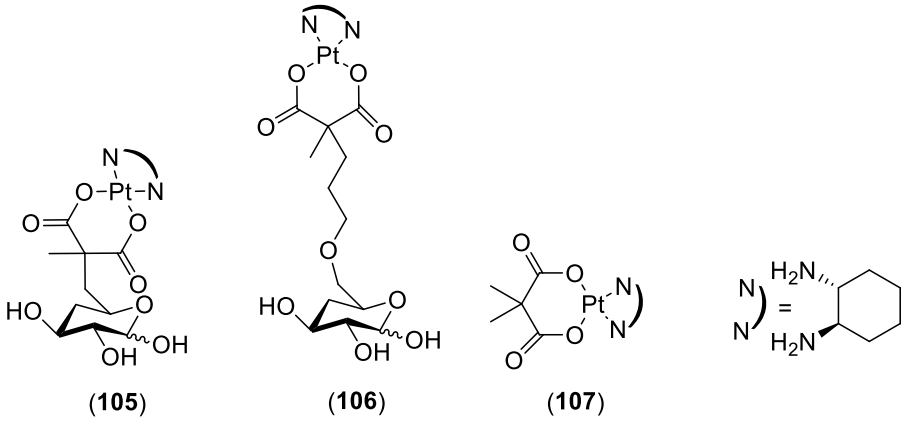

Figure 1.37. Glucose based platinum compounds as chemotherapy probes

Glycoconjugation combined with other delivery systems to achieve greater selectivity has also gained attention, as exemplified by the use of nanoparticles (NPs) as delivery systems for nonspecific and cytotoxic therapeutic drugs.[118] In work done by Li and coworkers, it was observed that glucose-conjugated chitosan nanoparticles encapsulating doxorubicin displayed 4-fold greater cytotoxicity towards cancer cells than the corresponding aglycons. To deliver drugs to the brain, glycoconjugation has also been used due to the high concentration of GLUT1 at the blood brain barrier.[119]

1.9.4. Natural products and carbohydrates –development of GLUT inhibitors

The development of therapeutic drugs or inhibitors was approached to reduce nutrient uptake in cancers. Reduction of nutrient uptake or starvation of cells has been used as a strategy to decrease the viability of cells. In addition, it has been observed that normal cells have the ability to endure harsh, nutrient scarce conditions whereas cancerous cells lack this ability.[120]

To date, there are many compounds that interact with GLUTs by not passing through the protein but by exerting an inhibitory effect upon binding the endofacial and exofacial site of the transporter protein. Out of the sugar molecules tested, it has been reported that C-6 analogs of glucose and galactose such as 6-O-benzyl, 6-O-propyl,

and 6-O-pentyl act as a specific noncompetitive unidirectional glucose uptake inhibitor and block glucose transport when outside the cell.[121]

For non-sugar small molecule compounds, cytochalasin B (**108**) is reported in multiple studies to act as a competitive and noncompetitive inhibitor of GLUTs (Figure 1.38).[122] Cytochalasin B is observed to be an inhibitor of Class I GLUTs as it is reported to show hydrogen bonding and hydrophobic interactions with the residues that are conserved in GLUT4. Tripeptides such as phenylalanine derivatives GLUTi1 (**109**) and GLUTi2 (**110**) also displayed strong inhibitory activity against GLUT1.[123,110]

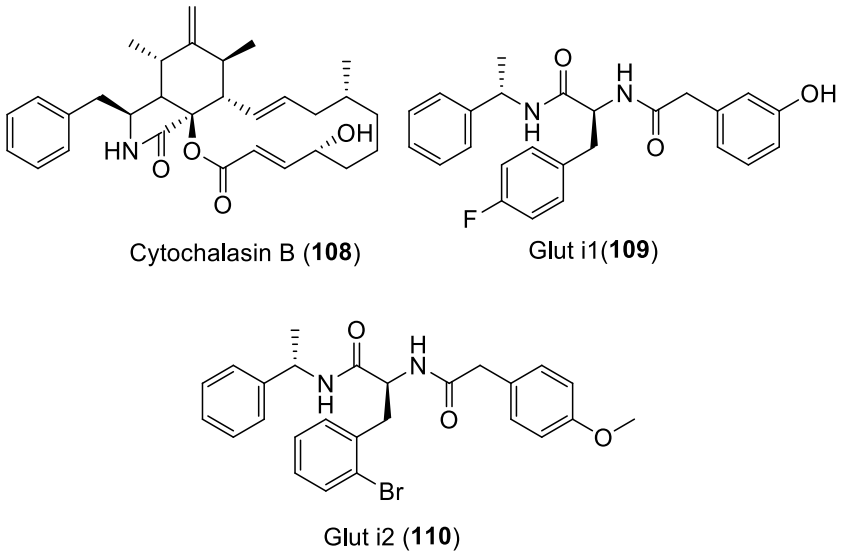

Figure 1.38. GLUT targeting inhibitors

In addition, natural flavonoids and some synthetic tyrosine kinase inhibitors (Figure 1.39) are reported to block the activity of class I GLUTs. Flavonoids such as catechin gallate (**112**) and quercetin (**111**) were also described to block GLUT4 in adipocytes and inhibit insulin stimulated translocation of GLUT4 to the cellular membrane.[124-125]

Reyes and coworkers, through a kinetic assay, showed that kinase inhibitor tyrphostin B46 acts as a competitive inhibitor of glucose uptake.[126] Recently, screening of a small library of natural products revealed astragalin-6-glucoside(Ast6G, **113**) and rubusoside (Rub, **114**) as millimolar inhibitors of human GLUT1 and GLUT5 through

a counterflow hexose transporter assay.[110] In addition, it was reported that Ast6 inhibits GLUT5 whereas Rub impacts both the transporters.

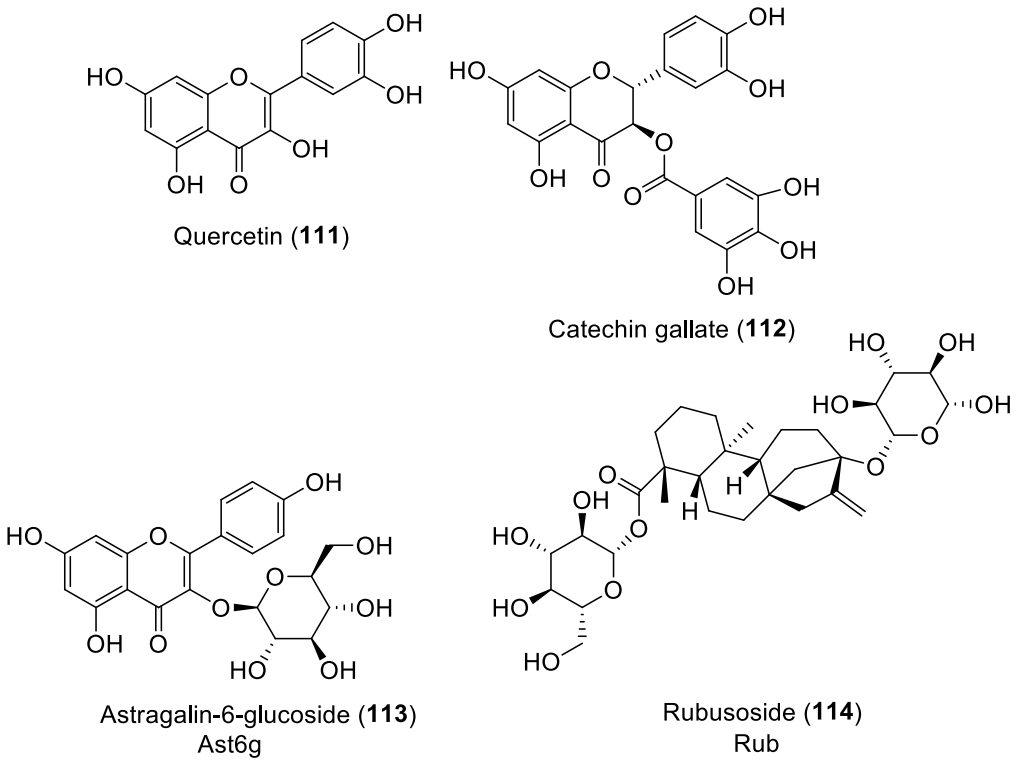

Figure 1.39. GLUT inhibitors

Both virtual and experimental screening of compound libraries also helps in identifying several substrates as potential GLUT inhibitors. In 2016, Buchman and coworkers screened about three million compounds in a cell-based assay, out of which, 285 hits were identified that inhibited GLUT1. Some compounds even showed good selectivity against GLUT2 and GLUT3.[127]

Regarding virtual screening, fragment library from NCI-2007 and ZINC was screened against GLUT1 by the Chen and Schlessinger team (Figure 1.40).[128] Several compounds were identified as micromolar inhibitors through experimental testing in transfected CHO cells. Major inhibitory effects of these compounds were revealed through binding analysis, and it was found that these inhibitors function by locking the transporter in an inward-facing state through hydrophobic and hydrogen bonding interactions.

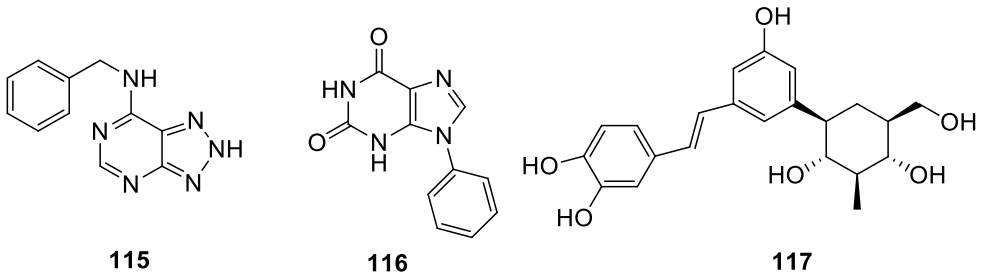

115 116 117

Figure 1.40. Examples of GLUT1 inhibitors from NCI-2007 and ZINC libraries

In work done by Shanmugam's team,[110] an 18 million compound ZINC library was subjected to in silico screening with a GLUT4 homology model and some potential inhibitors were identified (Figure 1.41.). Several hits were tested with myeloma L363 cells and only 2 compounds were observed to exert antiproliferative effects with micromolar efficiency.

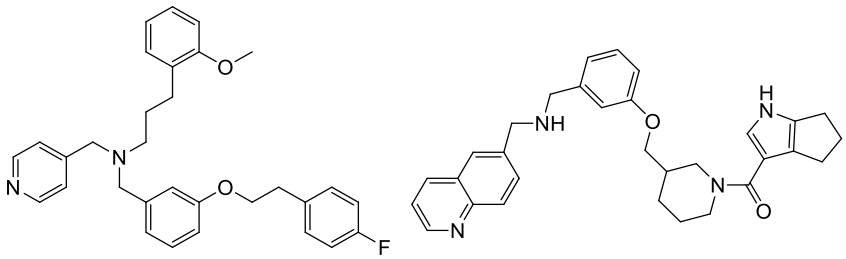

118 119

Figure 1.41. Examples of GLUT4 inhibitors from ZINC libraries

Another example of virtual screening studies on six million compound libraries performed by Choe and coworkers (Figure 1.42) recognized N-[4-(methyl sulfonyl)-2-nitro phenyl] benzo-1,3-dioxol-5-amine (MSNBA, **120**) as a GLUT5 inhibitor in the micromolar range.[129] Interestingly, MSNBA displayed a lack of inhibition for other GLUTs including nonspecific fructose transporter GLUT2.

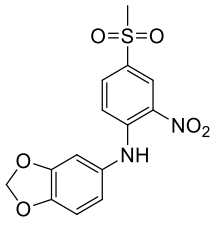

MSNBA (**120**)

Figure 1.42. Glut5 inhibitor

As a result, the development of GLUT inhibitors is crucial to understand the connection between nutrient uptake and disease development and progression. The identified inhibitors and their general scaffold ranging over different types of compounds include sugars, phenols, oximes, sulfones, and pyrrolidines. However, it is unclear how some of these substrates inhibit sugar uptake. With further advancements in molecular interactions and docking studies, designing, and developing GLUT-sensitive specific inhibitors is becoming an attractive arena.

1.10. Conclusion

Facilitative hexose transporter proteins (GLUTs) are associated with the transport of hexoses from intracellular space to extracellular space and vice versa. However, hexose phosphates cannot be transported through GLUTs. There are 14 types of GLUTs classified based on their amino acid sequence, substrate preference, and distribution within the body. The ubiquitous glucose transporter, GLUT1 somehow tolerates the modification of both primary and secondary hydroxyl groups of D-glucose, whereas GLUT5 is a fructose transporter doesn't easily tolerate the alteration of hydroxyl groups.

Breast cancer is one of the leading cause of cancer deaths in women. Early detection of breast cancer leads to a much higher survival rate as compared with later stage diagnosis. However, due to low-to-negative GLUT1 expression in breast cancer cells and false positive diagnosis observed in inflamed tissues, the development of other diagnostic probes was needed. Notably, while normal breast tissue shows limited or no expression of GLUT5, a significant percentage of breast tumors display overexpression of this protein. It should also be noted that in addition to breast cancer, GLUT5 is also

correlated with other cancers, including lung adenocarcinoma and acute lymphoblastic leukemia. We postulate that GLUT5 can serve as a biomarker for several cancers and for fructose-mediated metabolic diseases.

It is also reported that apart from fructose, GLUT5 also shows the internalization of fructose mimics based upon the related scaffold, 2,5-anhydromannitol (2,5-AM). These results laid the foundation for this project, the development of 2,5-AM based PET tracers and also fluorescent tracers displaying rapid uptake and low efflux rates in breast tumors.

In Chapter 2, synthesis, evaluation and docking studies of C-3 derived 2,5-AM derivates are described to study the inhibition effect exerted by these derivatives in GLUT5 expressing cell line. Chapter 3 presents the development and biological evaluation of the radiotracer and fluorescent tracer in breast cancer cells. In addition, Chapter 3 also demonstrates the uptake and biodistribution of the radiolabeled probe in animal tumor models, a necessary preclinical step to move the compounds towards evaluation in humans. Chapter 4 deals with the development of a novel fluorescence-based assay to study the structure activity relationship between GLUT5 and C-3 modified 2,5-AM derivatives. This chapter will describe the optimization studies performed using 6-NBDF as the reference compound whose uptake will be measured through plate reader experiments. Chapter 5 addresses the future direction and ideas that can be applied to identify GLUT5 inhibitors, how the current findings can be explored to develop better diagnostic and therapeutic probes and also some ideas to obtain mechanistic insight into the activation mechanism of GLUT5.

1.11. References

1. Dashty, M. A Quick Look at Biochemistry: Carbohydrate Metabolism.*Clin.Biochem.* **2013**, *46*, 1339–1352.

2. Kahn, B. B. Facilitative Glucose Transporters: Regulatory Mechanisms and Dysregulation in Diabetes. *J. Clin. Invest.* **1992**, *89*, 1367–1374.

3. Joost, H.-G.; Wandel, S.; Schürmann, A. Structure-Function Relationship of Glucosetransporters Catalyzing Facilitated Diffusion. *Exp. Clin. Endocrinol.* **1994**, *102*, 434–438.

4. Gould, G. W.; Holman, G. D. The Glucose Transporter Family: Structure, Function and Tissue-Specific Expression. *Biochem. J.* **1993**, *295*, 329–341.

5. Kahn, B. B.; Sheperd, P. R. Glucose Transporters and Insulin Action: Implications for Insulin Resistance and Diabetes Mellitus. *N. Engl. J. Med.* **1999**, *341*, 248– 257.

6. Kaiser, N.; Leibowitz, G.; Nesher, R. Glucotoxicity and Beta-Cell Failure in Type 2 Diabetes Mellitus. *J. Pediatr. Endocrinol. Metab.* **2003**, *16*, 5–22.

7. Scheepers, A.; Joost, H.-G.; Schu¨rmann, A. The Glucose Transporter Families SGLT and GLUT: Molecular Basis of Normal and Aberrant Function. *J. Parenter. Enter. Nutr.* **2004**, *28*, 364–371.

8. Thorens, B.; Mueckler, M. Glucose Transporters in the 21st Century. *Am. J. Physiol. Endocrino.l Metab.* **2010**, *298*, E141–E145; Bryant, N.J.; Govers, R.; James, D.E. Regulated transport of the glucose transporter GLUT4. *Nat. Rev.Mol.* **2002,** *3*, 267-277.

9. Manolescu, A. R.; Witkowska, K.; Kinnaird, A.; Cessford, T.; Cheeseman, C. Facilitated Hexose Transporters: New Perspectives on Form and Function. *Physiology* **2007**, *22*, 234–240.

10. McQuade, D. T., Plutschack, M. B. & Seeberger, P. H. Passive Fructose Transporters in Disease: A Molecular Overview of Their Structural Specificity. *Org. Biomol. Chem.* **2013**, *11*, 4909–4920.

11. Mueckler, M.; Thorens, B. The SLC2 (GLUT) Family of Membrane Transporters. *Mol. Asp. Med.* **2013**, *34*.

12. Long, W.; Cheeseman, C. I. Structure and Functional Insights into GLUT Family of Membrane Transporters. *Cell Health Cytoskelet.* **2015**, *7*, 167–183.

13. Deng, D.; Yan, N. GLUT, SGLT, and SWEET: Structural and Mechanistic Investigation of the Glucose Transporters. *Protein Sci.* **2016**, *25*, 546–558.

14. Mueckler, M.; Caruso, C.; Baldwin, S. A.; Panico, M.; Blench, I.; Morris, H. R.; Allard, W. J.; Lienhard, G. E.; Lodish, H. F. Sequence and Structure of a Human Glucose Transporter. *Science* **1985**, *229*, 941–945.

15. Deng, D.; Xu, C.; Sun, P.; Wu, J.; Yan, C.; Hu, M.; Yan, N. Crystal Structure of the Human Glucose Transporter GLUT1. *Nature* **2014**, *510*, 121–125.

16. Joost, H.-G.; Thorens, B. The Extended GLUT-Family of Sugar/Polyol Transport Facilitators: Nomenclature, Sequence Characteristics, and Potential Function of Its Novel Members. *Mol. Membr. Biol*. **2001**, *18*, 247–256.

17. Joost, H.-G.; Bell, G. I.; Best, J. D.; Birnbaum, M. J.; Charron, M. J.; Chen, Y. T.; Doege, H.; James, D. E.; Lodish, H. F.; Moley, K. H.; Moley, J. F.; Mueckler, M.; Rogers, S.; Schurmann, A.; Seino, S.; Thorens, B. Nomenclature of the 53 GLUT/SLC2A Family of Sugar/Poloyl Transport Facilitators. *Am. J. Physiol. Endocrinol. Metab.* **2002**, *282*, E974–E976.

18.Wood, S.; Trayhurn, P. Glucose Transporters (GLUT and SGLT): Expanded Families of Sugar Transport Proteins. *Br. J. Nutr.* **2003**, *89*, 3–9.

19. Simpson, I. A.; Cushman, S. W. Hormonal Regulation of Mammalian Glucose Transport. *Annu. Rev. Biochem.* **1986**, *55*, 1059–1089.

20. Bryant, N. J.; Govers, R.; James, D. E. Regulated Transport of the Glucose Transporter GLUT4. *Nat. Rev. Mol. Cell Biol.* **2002**, *2*, 267–277.

21. Rumsey, S. C.; Darnwala, R.; Al-Hasani, H.; Zarnowski, M. J.; Simpson, I. A.; Levine, M. Dehydroascorbic Acid Transport by GLUT4 in Xenopus Oocytes and Isolated Rat Adipocytes. *J. Biol. Chem.* **2000**, *275*, 28246–28253.

22. Uldry, M.; Ibberson, M.; Horisberger, J.-D.; Chatton, J.-Y.; Riederer, B. M.; Thorens, B. Identification of a Mammalian H_-Myo-Inositol Symporter Expressed Predominantly in the Brain. *EMBO J.* **2001**, 4467–4477.

23. Kasahara, M.; Hinkle, P. C. Recognition and Purification of D-Glucose Transporter from Human Erythrocytes. *J. Biol. Chem.* **1977**, *252*, 7380–7390.

24. Morgello, S.; Uson, R. R.; Schwartz, E. J.; Haber, R. The Human Blood-Brain Barrier Glucose Transporter (GLUT1) Is a Glucose Transporter of Gray Matter Astrocytes. *Glia.* **1995**, *14*, 43–54.

25. Kumagai, K. A. Glucose Transport in Brain and Retina: Implications in the Management and Complications of Diabetes. *Diabetes Metab Res Rev* **1999**, *15*, 261–273.

26. Postic, C.; Burcelin, R.; Rencurel, F.; Pegorier, J.-P.; Loizeau, M.; Girard, J.; Leturque, A. Evidence for a Transient Inhibitory Effect of Insulin on GLUT2 Expression in the Liver: Studies in Vivo and in Vitro. *Biochem. J.* **1993**, *293*, 119–124.
27. Pang, K.; Mukonoweshuro, C.; Wong, G. G. Beta Cells Arise from Glucose Transporter 2 (GLUT2)-Expressing Epithelial Cells of the Developing Rat Pancreas. *Proc. Natl. Acad. Sci. USA* **1994**, *91*, 9559–9563.
28. Maher, F.; Davies-Hill, T. M.; Lysko, P. G.; Henneberry, R. C.; Simpson, I. A. Expression of Two Glucose Transporters, GLUT1 and GLUT3, in Cultured Cerebellar Neurons: Evidence for Neuron-Specific Expression of GLUT3. *Mol. Cell Neurosci.* **1991**, *2*, 351–360.
29. Haung, S.; Czech, P. The GLUT4 Glucose Transporter. *Cell. Metab.* **2007**, *5*, 237–252.
30. Band, E. B.; Depaoli, A. M.; Davidson, N. O.; Bell, C. I.; Burant, C. F. Sequence, Tissue Distribution, and Functional Characterization of the Rat Fructose Transporter GLUT5. *Am. J. Physiol. Gastrointest. Liver Physiol.* **1993**, *264*, G1169-1176.
31. Zhao, F.-Q.; Keating, A. F. Functional Properties and Genomics of Glucose Transporters. *Curr. Genomics* **2007**, *8*, 113–129.
32. Cheeseman, C. GLUT7: A New Intestinal Facilitated Hexose Transport. *Am J. Physiol. Endocrinol. Metab.* **2008**, *295*, E238 E241.
33. Preitner, F.; Bonny, O.; Laverriere, A.; Rotman, S.; Firsov, D.; Costa, A. D.; Metref, S.; Thorens, B. GLUT9 Is a Major Regulator of Urate Homostasis and Its Genetic Inactivation Induces Hyperuricosuria and Urate Nephropathy. *Proc. Natl.Acad. Sci. USA* **2009**, *106*, 15501–15506.
34. Deng, D.; Xu, C.; Sun, P.; Yan, C.; Ke, M.; Jiang, X.; Xiong, L.; Ren, W.; Hirata, K.; Yamamoto, M.; Fan, S.; Yan, N. Molecular Basis of Ligand Recognition and Transport by Glucose Transporters. *Nature* **2015**, *526*, 391–396.
35. Seatter, M. J.; De La Rue, S. A.; Porter, L. M.; Gould, G. W. QLS Motif in Transmembrane Helix VII of the Glucose Transporter Family Interacts with the C-1 Position of D-Glucose and Is Involved in Substrate Selection at the Exofacial Binding Site. *Biochemistry* **1998**, *37*, 1322–1326.

36. Olson, A. L.; Pessin, J. E. Structure, Function, and Regulation of the Mammalian Facilitative Glucose Transporter Gene Family. *Annu. Rev. Nutr.* **1996**, *16*, 235–256.

37. Mueckler, M.; Weng, W.; Kruse, M. Glutamine 161 of GLUT1 Glucose Transporter Is Critical for Transport Activity and Exofacial Ligand Binding. *J. Biol. Chem.* **1994**, *269*, 20533–20538.

38. Long, W.; Panwar, P.; Witkowska, K.; Wong, K.; O'Neill, D.; Chen, X.-Z.; Lemieux, M. J.; Cheeseman‡, C. I. Critical Roles of Two Hydrophobic Residues within Human Glucose Transporter 9 (HSLC2A9) in Substrate Selectivity and Urate Transport. *J. Biol. Chem.* **2015**, *290*, 15292–15303.

39. Neame, K. D.; Richards, T. G. *Elementary Kinetics of Membrane Carrier Transport.*, Ist.; London, UK: *Blackwell Scientific Publications*;, 1972.

40. Fisher, R. B.; Parsons, D. S. Glucose Movements across the Wall of the Rat Small Intestine. *J. Physiol.* **1953**, *119*, 210–223.

41. Widdas, W. Inability of Diffusion to Account for Placental Glucose Transfer in the Sheep and Consideration of the Kinetics of a Possible Carrier Transfer. *J. Physiol.* **1952**, *118*, 23–39; Augustin, R; Mayoux, E. Mammalian sugar transporters. In *Glucose homeostasis*. IntechOpen, **2014.**

42. Naftalin, R. J. Alternating Carrier Models of Asymmetric Glucose Transport Violate the Energy Conservation Laws. *Biophys. J.* **2008**, *95*, 4300=4314.

43. Vollers, S. S.; Carruthers, A. Sequence Determinants of GLUT1-Mediated Accelerated-Exchange Transport: Analysis by Homology-Scanning Mutagenesis. *J. Biol. Chem.* **2012**, *287*, 42533–42544.

44. Anthony Carruthers. Will the Original Glucose Transporter Isoform Please Stand Up! *Am. J. Physiol. Endocrinol. Metab.* **2009**, *297*, E836–E848.

45. Nomura, N.; Verdon, G.; Kang, H. J.; Shimamura, T.; Nomura, Y.; Sonoda, Y.; Hussien, S. A.; Qureshi, A. A.; Coincon, M.; Sato, Y.; Abe, H.; Nakada-Nakura, Y.; Hino, T.; Arakawa, T.; Kusano-Arai, O.; Iwanari, H.; Murata, T.; Kobayashi, T.; Hamakubo, T.; Kasahara, M.; Iwata, S.; Drew, D. Structure and Mechanism of Mammalian Fructose Transporter GLUT5. *Nature.* **2015**, *526*, 397–401.

46. Gallagher, B. M.; Fowler, J. S.; Gutterson, N. I.; MacGregor, R. R.; Wan, C.-N.; Wolf, A. P. Metabolic Trapping as a Principle of Radiopharmaceutical Design: Some Factors Responsible for the Biodistribution of [18F]-2-Deoxy-2-Fluoro-D-Glucose. *J. Nucl. Med.* **1978**, *19*, 1154–1161.

47. Angyal, S. J. The Composition and Conformation of Sugars in Solution. *Angew. Chem. Int. Ed. Engl.* **1969**, *8*, 157–166.

48. Tajmir-Riahi, H. A. Carbohydrate Complexes with Alkaline Earth Metal Ions. Interactions of D-Glucono-1,5-Lacton with the Mg (II), Ca (II), Sr (II) and Ba (II)Cations in the Crystalline Solid and Aqueous Solution. *J. Inorg. Chem.* **1990**, *39*,33–37.

49. Kahlenberg, A.; Urman, B.; Dolansky, D. Preferential Uptake of D-Glucose by Isolated Human Erythrocyte Membranes. *Biochemistry* **1971**, *10*, 3154–3162.

50. Barnett, J. E.; Holman, G. D.; Munday, K. A. Structural Requirements for Binding to the Sugar-Transport System of the Human Erythrocyte. *Biochem. J.* **1973**, *131*, 211–221.

51. Kahlenberg, A.; Dolansky, D. Structural Requirements of D-Glucose for Its Binding to Isolated Human Erythrocyte Membranes. *Can. J. Biochem.* **1972**, *50*, 638–643.

52. Rees, W. D.; Holman, G. D. Hydrogen Bonding Requirements for the Insulin-Sensitive Sugar Transport System of Rat Adipocytes. *Biochim. Biophys. Acta Biomembr.* **1981**, *646*, 251–260.

53. Gatley, S. J. Labeled Glucose Analogs in the Genomic Era. *J. Nucl. Med.* **2003**, *44*, 1082–1086.

54. Tatibouët, A.; Yang, J.; Morin, C.; Holman, G. D. Synthesis and Evaluation of Fructose Analogues as Inhibitors of the D-Fructose Transporter GLUT5. *Bioorg. Med. Chem.* **2000**, *8*, 1825–1833.

55. Trayner, B. J.; Grant, T. N.; West, F. G.; Cheeseman, C. I. Synthesis and Characterization of 6-Deoxy-6-Fluoro-D-Fructose as a Potential Compound for Imaging Breast Cancer with PET. *Bioorg. Med. Chem.* **2009**, *17*, 5488–5495.; Girniene, J.; Tatibouët, A.; Sackus, A.; Yang, J.; Holman, G. D.; Rollin, P. Inhibition

of the D-Fructose Transporter Protein GLUT5 by Fused-Ring Glycol-1,3-Oxazolidin-2-Thiones and Oxazolidin-2-Ones. *Carbohydr. Res.* **2003**, *338*, 711–719.

56. Yang, J.; Dowden, J.; Tatibouët, A.; Hatanaka, Y.; Holman, G. D. Development of High Affinity Ligands and Photoaffinity Labels for the D Fructose Transporter GLUT5. *Biochem. J.* **2002**, *367*, 533–539.

57. Yang, J.; Tatibouët, A.; Hatanaka, Y.; Holman, G. D. Fructose Analogues with Enhanced Affinity for GLUT5. *Diabetes* **2001**, *50*, A277–A277.

58. Kondapi, V. P. K. .; Soueidan, O.-M.; Cheeseman, C. I.; West, F. G. Tunable GLUT–Hexose Binding and Transport via Modulation of Hexose C-3 Hydrogen-Bonding Capabilities. *Chem. Eur. J.* **2017**, *23*, 8073–8081.

59. Xu, X. D.; Shao, S. X.; Jiang, H. P.; Cao, Y. W.; Wang, Y. H.; Yang, X. C.; Wang, Y. L.; Wang, X. S.; Niu, H. T. Warburg Effect or Reverse Warburg Effect? A Review of Cancer Metabolism. Oncology Research and Treatment. *Oncol. Res. Treat.* **38**, 117–122.

60. Nakagawa, T.; Lanaspa, M. A.; Millan, I. S.; Fini, M.; Rivard, C. J.; Sanchez-Lozada, L. G.; Andres-Hernando, A.; Tolan, D. R.; Johnson, R. J. Fructose Contributes to the Warburg Effect for Cancer Growth. *Cancer Metab.* **2020**, *8*, 1–12.

61. Lassen, U.; Daugaard, G.; Eigtved, A.; Damgaard, K.; Friberg, L. 18F-FDG Whole Body Positron Emission Tomography (PET) in Patients with Unknown Primary Tumours (UPT). *Eur. J. Cancer* **1993**, 1076–1082.

62. Nakagawa, T.; Johnson, R. J.; Andres-Hernando, A.; Roncal-Jimenez, C.; Sanchez-Lozada, L. G.; Tolan, D. R.; Lanaspa, M. A. Fructose Production and Metabolism in the Kidney. *J. Am. Soc. Nephrol.* **2020**, *31*, 898–906.

63. Aparicio, L. M.; Villaamil, V. M.; Calvo, M. B.; Rubira, L. V.; Rois, J. M.; Valladares-Ayerbes, M.; Campelo, R. G.; Bolós, M. V.; Pulido, E. G. Glucose Transporter Expression and the Potential Role of Fructose in Renal Cell Carcinoma: A Correlation with Pathological Parameters. *Mol. Med. Rep.* **2010**, *3*, 575–580.

64. Zamora-León, S. P.; Golde, D. W.; Concha, I. I.; Rivas, C. I.; Delgado-López, F.; Baselga, J.; Nualart, F.; Vera, J. C. Expression of the Fructose Transporter GLUT5 in Human Breast Cancer. *Proc. Natl. Acad. Sci. USA* **1996**, *93*, 1847–1842.

65. Godoy, A.; Ulloa, V.; Rodríguez, F.; Reinicke, K.; Yañez, A. J.; García, M. D. L. A.; Medina, R. A.; Carrasco, M.; Barberis, S.; Castro, T.; Martínez, F.; Koch, X.; Vera, J. C.; Poblete, M. T.; Figueroa, C. D.; Peruzzo, B.; Nualart, F. Differential Subcellular Distribution of Glucose Transporters GLUT1-6 and GLUT9 in Human Cancer: Ultrastructural Localization of GLUT1 and GLUT5 in Breast Tumor Tissues. *J. Cell Physiol.* **2005**, *207*, 614–627.

66. Jegatheesan, P.; Bandt, J. P. D. Fructose and NAFLD: The Multifaceted Aspects of Fructose Metabolism. *Nutrients* **2017**, *9*, 1–13.

67. DiNicolantonio, J.; Subramonian, A. M.; O'Keefe, J. H. Added Fructose as a Principal Driver of Non-Alcoholic Fatty Liver Disease: A Public Health Crisis. *Open Heart* **2017**, *4*, 1–6.

68. Villaamil, V. M.; Gallego, G. A.; Rubira, L. V.; Campelo, R. G.; Valladares-Ayerbes, M.; Pulido, E. G.; Bolós, M. V.; Caínzos, I. S.; Villaamil, V. M. Fructose Transporter GLUT5 Expression in Clear Renal Cell Carcinoma. *Oncol. Rep.* **2011**, *25*, 315–323.

69. Weng, Y.; Zhu, J.; Chen, Z.; Fu, J.; Zhang, F. Fructose Fuels Lung Adenocarcinoma through GLUT5. *Cell Death Dis.* **2018**, *9*, 1–4.

70. Fan, X.; Liu, H.; Liu, M.; Wang, Y.; Qiu, L.; Cui, Y. Increased Utilization of Fructose Has a Positive Effect on the Development of Breast Cancer. *Peer J.* **2017**, *5*, 1–15.

71. Hamann, I.; Krys, D.; Glubrecht, D.; Bouvet, V.; Marshall, A.; Vos, L.; Mackey, J. R.; Wuest, M.; Wuest, F. Expression and Function of Hexose Transporters GLUT1, GLUT2, and GLUT5 in Breast Cancer-Effects of Hypoxia. *FASEB J.* **2018**, *32*, 5104–5118.

72. James, M. L.; Gambhir, S. S. A Molecular Imaging Primer: Modalities, Imaging Agents, and Applications. *Physiol. Rev.* **2012**, *92*, 897–965.

73. Wang, D. S.; Dake, M. D.; Park, J. M.; Kuo, M. D. Molecular Imaging: A Primer for Interventionalists and Images. *J. Vasc. Interv. Radiol.* **2006**, *17*, 1405–1423.

74. Pysz, M. A.; Gambhir, S. S.; Willmann, M. D. Molecular Imaging: Current Status and Emerging Strategies. *Clin. Radiol.* **2010**, *65*, 500–516.

75. Gambhir, S. S. Molecular Imaging of Cancer with Positron Emission Tomography. *Nat. Rev. Cancer* **2002**, *2*, 683–693.

76. Imam, S. K. Review of Positron Emission Tomography Tracers for Imaging of Tumor Hypoxia. *Cancer Biother. Radiopharm.* **2010**, *25*, 365–374.

77. Muehllehner, G.; Karp, J. S. Positron Emission Tomography. *Phys. Med. Biol.* **2006**, *51*, R117–R137.

78. Couturier, O.; Luxen, A.; Chatal, J. F.; Vuillez, J. P.; Rigo, P.; Hustinx, R. Fluorinated Tracers for Imaging Cancer with Positron Emission Tomography. *Eur J. Nucl. Med. Mol. Imaging* **2004**, *31*, 1182–1206.

79. Zanzonico, P. Positron Emission Tomography: A Review of Basic Principles, Scanner Design and Performance, and Current Systems. *Semin. Nucl. Med*. **2004**, *34*, 87–111.

80. Wood, K. A.; Hoskin, P. J.; Saunders, M. I. Positron Emission Tomography in Oncology: A Review. *Clin. Oncol. R. Coll. Radiol.* **2007**, *19*, 237–255.

81. Pagani, M.; Stone-Elander, S.; Larsson, S. A. Alternative Positron Emission Tomography with Non-Conventional Positron Emitters: Effects of Their Physical Properties on Image Quality and Potential Clinical Applications. *Eur. J. Nucl. Med.* **1997**, *24*, 1304–1327.

82. Maschauer, S.; Prante, O. Sweetening Pharmaceutical Radiochemistry by 18F Fluoroglycosylation: A Short Review. *Bio. Med. Res. Int.* **2014**, *Article ID 214748*.

83. Wester, H. J. *Pharmaceutical Radiochemistry (I)*; Munich Molecular Imaging Handbook Series; *Scintomics,* 1, 2010.

84. Kilbourn, M. R.; Huizenga, J. R. Fluorine-18 Labeling of Radiopharmaceuticals. *Natl. Acad.* **1994**, *3203*.

85. Rozen, S. Elemental Fluorine as a Legitimate Reagent for Selective Fluorination of Organic Compounds. *Acc. Chem. Res.* **1988**, *21*, 307–312.

86. Ramsden, C. A. *Xenon Difluoride in the Organic Laboratory: A Tale of Substrates, Solvents and Vessels.*; *Arkivoc*, 2013; Vol. 109.

87. Furuya, T.; Kamlet, A. S.; Ritter, T. Catalysis for Fluorination and Trifluoromethylation. *Nature* **2011**, *473*, 470–477.

88. Lal, G. S.; Pez, G. P.; Syvret, R. G. Electrophilic NF Fluorinating Agents. *Chem. Rev*. **1996**, *96*, 1737–1756.

89. Singh, R. P.; Shreeve, J. M. Recent Highlights in Electrophilic Fluorination with 1-Chloromethyl-4-Fluoro-1,4-Diazoniabicyclo[2.2.2]Octane Bis(Tetrafluoroborate). *Acc. Chem. Res.* **2004**, *37*, 31–44.

90. Nyffeler, P. T.; Durón, S. G.; Burkart, M. D.; Vincent, S. P.; Wong, C.-H. Selectfluor: Mechanistic Insight and Applications. *Angew. Chem. Int. Ed.* **2004**, *44*, 192–212.

91. Umemoto, T.; Harasawa, K.; Tomizawa, G.; Kawada, K.; Tomita, K. N-F 19-Fluorine Nuclear Magnetic Resonance of N-Fluoropyridinium Salts. *J. Fluor. Chem.* **1991**, *53*, 369–377.

92. Kiselyov, A. S. Chemistry of N-Fluoropyridinium Salts. *Chem. Soc. Rev.* **2005**, *34*, 1031–1037.

93. Champagne, P. A.; Desroches, J.; Hamel, J. D.; Vandamme, M.; Paquin, J.-F. Monofluorination of Organic Compounds: 10 Years of Innovation. *Chem. Rev.* **2015**, *115*, 9073–9174.

94. Nguyen, T.-H.; Abarbri, M.; Guilloteau, D.; Mavel, S.; Emond, P. Nucleophilic Fluorination of Alkynyliodonium Salts by Alkali Metal Fluorides: Access to Fluorovinylic Compounds. *Tetrahedron* **2011**, *67*, 3434–3439.

95. Kim, D. W.; Jeong, H. J.; Lim, S. T.; Sohn, M. H.; Katzenellenbogen, J. A.; Chi, D. Y. Facile Nucleophilic Fluorination Reactions Using Tert-Alcohols as a Reaction Medium: Significantly Enhanced Reactivity of Alkali Metal Fluorides and Improved Selectivity. *J. Org. Chem.* **2008**, *73*, 957–962.

96. Bouvet, V.; Jans, H. S.; Wuest, M.; Soueidan, O.-M.; Mercer, J.; McEwan, A. J. B.; West, F. G.; Cheeseman, C. I.; Wuest, F. Automated Synthesis and Dosimetry of 6-Deoxy-6-[(18)F]Fluoro-D-Fructose (6-[(18)F]FDF): A Radiotracer for Imaging of GLUT5 in Breast Cancer. *Am. J. Nucl. Med. Mol. Imaging* **2014**, *4*, 248–259.

97. Akiyama, Y.; Hiramatsu, C.; Fukuhara, T.; Hara, S. Selective Introduction of a Fluorine Atom into Carbohydrates and a Nucleoside by Ring-Opening Fluorination Reaction of Epoxides. *J. Fluor. Chem.* **2006**, *127*, 920–923.

98. Soueidan, O.-M.; Trayner, B. J.; Grant, T. N.; Henderson, J. R.; Wuest, F.; West, F. G.; Cheeseman, C. I. New Fluorinated Fructose Analogs as Selective Probes of the Hexose Transporter Protein GLUT5. *Org. Biomol. Chem.* **2015**, *13*, 6511–6521.

99. L'Heureux, A.; Beaulieu, F.; Bennettl, C.; Bill, D. R.; Clayton, S.; LaFlamme, M. M.; Tadayon, S.; Tovell, D.; Couturier, M. Aminodifluorosulfinium Salts: Selective Fluorination Reagents with Enhanced Thermal Stability and Ease of Handling. *J. Org. Chem.* **2010**, *75*, 3401–3411.

100. Ni, C.; Hu, M.; Hu, J. Good Partnership between Sulfur and Fluorine: Sulfur-Based Fluorination and Fluoroalkylation Reagents for Organic Synthesis. *Chem. Rev.* **2015**, *115*, 765–825.

101. Clark, A. E.; Holman, G. D. Exofacial Photolabelling of the Human Erythrocyte Glucose Transporter with an Azitrifluoroethylbenzoyl-Substituted Bismannose. *Biochem. J.* **1990**, *269*, 615–622.

102. Koumanov, F.; YANG, J.; JONES, E. A.; Hatanaka, Y.; Holman, G. D. Cell-Surface Biotinylation of GLUT4 Using Bis-Mannose Photolabels. *Biochem. J.* **1998**, *330*, 1209–1215.

103. Hashimoto, M.; Hatanaka, Y.; Yang, J.; Dhesi, J.; Holman, G. D. Synthesis of Biotinylated Bis(D-Glucose) Derivatives for Glucose Transporter Photoaffinity Labelling. *Carbohydr. Res* **2001**, *331*, 119–127.

104. Zou, C.; Wang, Y.; Shen., Z. 2-NBDG as a Fluorescent Indicator for Direct Glucose Uptake Measurement. *ChemBioChem,* **2005**, *64*, 207–215.

105. Levi, J.; Cheng, Z.; Gheysens, O.; Patel, M.; Chan, C. T.; Wang, Y. B.; Namavari, M.; Gambhir, S. S. Fluorescent Fructose Derivatives for Imaging Breast Cancer Cells. *Bioconj. Chem.* **2007**, *18*, 628–634.

106. Tanasova, M.; Plutschack, M.; Muroski, M. E.; Sturla, S. J.; Strouse, G. F.; McQuade, D. T. Fluorescent THF-based Fructose Analogue Exhibits Fructose-dependent Uptake. *ChemBioChem* **2013**, *14*, 1263–1270.

107. Soueidan, O.-M.; Scully, T. W.; Kaur, J.; Panigrahi, R.; Belovodskiy, A.; Do, V.; Matier, C. D.; Lemieux, M. J.; Wuest, F.; Cheeseman, C.; West, F. G. Fluorescent Hexose Conjugates Establish Stringent Stereochemical Requirement by Glut5 for

Recognition and Transport of Monosaccharides. *ACS Chem. Biol.* **2017**, *12*, 1087–1094.

108. Begoyan, V. V.; Weseliński, Ł. J.; Xia, S.; Fedie, J.; Kannan, S.; Ferrier, A.; Rao, S.; Tanasova, M. Multicolor GLUT5-Permeable Fluorescent Probes for Fructose Transport Analysis. *Chem. Comm.* **2018**, *54*, 3855–3858.

109. Ido, T.; Wan, C. N.; Casella, V.; Fowler, J. S.; Wolf, A. P.; Reivich, M.; Kuhl, D. E. Labeled 2-deoxy-D-glucose Analogs. 18F-labeled 2-deoxy-2-fluoro-D-glucose, 2-deoxy-2-fluoro-D-mannose and 14C-2-deoxy-2-fluoro-D-glucose. *J. Label. Compd. Radiopharm.* **1978**, *14*, 175–183.

110. Tanasova, M.; Fedie, J. R. Molecular Tools for Facilitative Carbohydrate Transporters (Gluts). *ChemBioChem* **2017**, *18*, 1774–1788.

111. Kim, J.; Lee, J.; Chang, E.; Kim, S.; Suh, K.; Sul, J.; Song, I.; Kim, Y.; Lee, C. Selective Sentinel Node plus Additional Non-Sentinel Node Biopsy Based on an FDG-PET/CT Scan in Early Breast Cancer Patients: Single Institutional Experience. *World J. Surg.* **2009**, *33*, 943–949.

112. Haradahira, T.; Tanaka, A.; Maeda, M.; Kanazawa, Y.; Ichiya, Y. I.; Masuda, K. Radiosynthesis, Rodent Biodistribution, and Metabolism of 1-Deoxy-1-[18F] Fluoro-D-Fructose. *Nucl. Med. Biol.* **1995**, *22*, 719–725.

113. Wuest, M.; Trayner, B. J.; Grant, T. N.; Jans, H. S.; Mercer, J. R.; Murray, D.; West, F. G.; McEwan, A. J.; Wuest, F.; Cheeseman, C. I. Radiopharmacological Evaluation of 6-Deoxy-6-[18F] Fluoro-D-Fructose as a Radiotracer for PET Imaging of GLUT5 in Breast Cancer. *Nucl. Med. Biol.* **2011**, *38*, 461–475.

114. Niu, B.; Wen, X.; Jia, Z.; Wu, X.; Guo, W.; Sun, H. Synthesis and Preliminary Evaluation of 1-[18F] Fluoro-1-deoxy-2, 5-anhydro-D-mannitol as a PET Radiotracer for Breast Cancer Imaging. *Chin. J. Chem.* **2013**, *3*, 1159–1163.

115. Calvaresi, E. C.; Hergenrother, P. J. Glucose Conjugation for the Specific Targeting and Treatment of Cancer. *Chem. Sci.* **2013**, *4*, 2319–2333.

116. Tanaka, M.; Kataoka, H.; Yano, S.; Ohi, H.; Kawamoto, K.; Shibahara, T.; Mizoshita, T.; Mori, Y.; Tanida, S.; Kamiya, T.; Joh, T. Anti-Cancer Effects of Newly

Developed Chemotherapeutic Agent, Glycoconjugated Palladium (II) Complex, against Cisplatin-Resistant Gastric Cancer Cells. *BMC Cancer* **2013**, *13*, 1–9.

117. Patra, M.; Awuah, S. G.; Lippard, S. J. Chemical Approach to Positional Isomers of Glucose–Platinum Conjugates Reveals Specific Cancer Targeting through Glucose-Transporter-Mediated Uptake in Vitro and in Vivo. *J. Am. Chem. Soc.* **2016**, *138*, 12541–12551.

118. Yang, K.; Gao, T.; Bao, Z.; Su, J.; Chen, X. Preparation and Characterization of a Novel Thermosensitive Nanoparticle for Drug Delivery in Combined Hyperthermia and Chemotherapy. *J. Mater. Chem. B* **2013**, *1*, 6442–6448.

119. Li, J.; Ma, F. K.; Dang, Q. F.; Liang, X. G.; Chen, X. G. Glucose-Conjugated Chitosan Nanoparticles for Targeted Drug Delivery and Their Specific Interaction with Tumor Cells. *Front. Mater. Sci.* **2014**, *8*, 363–372.

120. Raffaghello, L.; Lee, C.; Safdie, F. M.; Wei, M.; Madia, F.; Bianchi, G.; Longo, V. D. From the Cover: Reactive Oxygen Species Special Feature: Starvation-Dependent Differential Stress Resistance Protects Normal but Not Cancer Cells against High-Dose Chemotherapy. *Proc. Natl. Acad. Sci. U. S. A.* **2008**, *105*, 8215.

121. Barnett, J. E.; Holman, G. D.; Chalkley, R. A.; Munday, K. A. Evidence for Two Asymmetric Conformational States in the Human Erythrocyte Sugar-Transport System. *Biochem. J.* **1975**, *145*, 417–429.

122. Pinkofsky, H. B.; Rampal, A. L.; Cowden, M. A.; Jung, C. Y. Cytochalasin B Binding Proteins in Human Erythrocyte Membranes. Modulation of Glucose Sensitivity by Site Interaction and Partial Solubilization of Binding Activities. *J. Biol. Chem.* **1978**, *253*, 4930–4937.

123. Kapoor, K.; Finer-Moore, J. S.; Pedersen, B. P.; Caboni, L.; Waight, A.; Hillig, R. C.; Bringmann, P.; Heisler, I.; Müller, T.; Siebeneicher, H.; Stroud, R. M. Mechanism of Inhibition of Human Glucose Transporter GLUT1 Is Conserved between Cytochalasin B and Phenylalanine Amides. *Proc. Natl. Acad. Sci.* **2016**, *113*, 4711–4716.

124. Strobel, P.; Allard, C.; Perez-Acle, T.; Calderon, R.; Aldunate, R.; Leighton, F. Myricetin, Quercetin and Catechin-Gallate Inhibit Glucose Uptake in Isolated Rat Adipocytes. *Biochem. J.* **2005**, *386*, 471–478.

125. Nomura, M.; Takahashi, T.; Nagata, N.; Tsutsumi, K.; Kobayashi, S.; Akiba, T.; Yokogawa, K.; Moritani, S.; Miyamoto, K. I. Inhibitory Mechanisms of Flavonoids on Insulin-Stimulated Glucose Uptake in MC3T3-G2/PA6 Adipose Cells. *Biol. Pharm. Bull.* **2008**, *31*, 1403–1409.

126. Pérez, A.; Ojeda, P.; Ojeda, L.; Salas, M.; Rivas, C. I.; Vera, J. C.; Reyes, A. M. Hexose Transporter GLUT1 Harbors Several Distinct Regulatory Binding Sites for Flavones and Tyrphostins. *Biochemistry* **2011**, *50*, 8834–8845.

127. Siebeneicher, H.; Cleve, A.; Rehwinkel, H.; Neuhaus, R.; Heisler, I.; Müller, T.; Bauser, M.; Buchmann, B. Identification and Optimization of the First Highly Selective GLUT1 Inhibitor BAY-876. *ChemMedChem* **2016**, *11*, 2261–2271.

128. Ung, P. M. U.; Song, W.; Cheng, L.; Zhao, X.; Hu, H.; Chen, L.; Schlessinger. Inhibitor Discovery for the Human GLUT1 from Homology Modeling and Virtual Screening. *ACS Chem. Biol.* **2016**, *11*, 1908–1916.

129. George Thompson, A. M.; Ursu, O.; Babkin, P.; Iancu, C. V.; Whang, A.; Oprea, T. I.; Choe, J. Y. Discovery of a Specific Inhibitor of Human GLUT5 by Virtual Screening and in Vitro Transport Evaluation. *Sci. Rep.* **2016**, *6*, 1–9.

CHAPTER 2

Towards selective binding to GLUT5 transporter-synthesis, molecular dynamics and in vitro evaluation of novel C-3 modified 2,5-Anhydro-D-mannitol Analogs[a]

2.1. Introduction

Nutrient uptake across the cell membrane, facilitated through the SLC (solute carrier) family of transmembrane proteins, plays an essential role in the internalization of compounds such as monosaccharides, amino acids, vitamins, hormones, neurotransmitters, etc.[1–3] Facilitative hexose transporters (GLUTs), from the same gene family (SLC2), perform the process of influx and efflux of monosaccharides in a gradient-dependent manner, furnishing fuels for cellular metabolic processes.[4–6] So far, 14 subtypes of GLUTs (GLUT1-14) have been identified and classified based on sequence homology, tissue-specific expression, substrate affinities, and transport kinetic properties.[7,8] In recent years, deregulation in GLUTs' expression has gained wide attention, as this phenomenon is reported to be linked to various conditions, such as cancer, obesity, metabolic disorders, and diabetes.[9–13] Specific tissue dependent activity and overexpression of GLUTs make them interesting diagnostic and therapeutic targets for biomarker imaging as well as for selective delivery of drugs.[1–3]

Among these hexose transporters, GLUT1, a ubiquitous glucose transporter, represents the most common target for biomarker imaging application, especially when utilizing the ^{18}F-labeled fructose derivative 2-deoxy-2-fluoro-D-glucose ([^{18}F]FDG) for positron emission tomography (PET), based on the well-known increased glucose requirement of cancer cells as compared to normal cells, a phenomenon known as the Warburg effect.[14] However, D-glucose is known to be a substrate for multiple GLUT transporters, including GLUT1, 2, 3, and 4, posing a challenge for the selective

[a]The contents of this chapter have been copied and/or adapted from the following publication: Towards selective binding to GLUT5 transporter-synthesis, molecular dynamics, and in vitro evaluation of novel C-3 modified 2,5-anhydro-d-mannitol analogs: Natasha Rana, Marwa A. Aziz, Ahmed K. Oraby Melinda Wuest, Jennifer Dufour, Khaled A. M. Abouzid, Frank Wuest, and F. W. West. *Pharmaceutics,* **2022***, 14,* 828

development of ligands targeting individual GLUTs.[1–5,15]

In specific cases, cancer cells may switch their metabolic demand and increase their utilization of another common hexose sugar, fructose, when they have access to this alternative energy source.[16] Fructose is transported almost selectively through facilitative hexose transporter GLUT5 in millimolar (mM) concentration ranges. Affinities of 11–15 mM have been determined using D-[^{14}C]fructose in GLUT5 (human isoform) expressing oocytes or in brush border membrane vesicles from rat and human intestine, the organ with the highest GLUT5 protein expression in the human organism.[17] Fructose transport through GLUT5 occurs at one order of magnitude lower affinities (1-2 mM) compared to the glucose transport through its major transporter GLUT1, albeit still in the millimolar concentration range.[17]

GLUT5 was found to be overexpressed in different types of cancers, including lung cancer, renal cell carcinoma, pancreatic cancer, and acute myeloid leukemia, among others.[18-20] The protein expression profile of GLUT5 was found to be increased in breast cancer, depending on the type of breast cancer.[21] Compared to estrogen receptor positive breast cancer, triple-negative breast cancer cells, and tissues express significantly higher protein levels of GLUT5, which also was detected for mRNA levels, as analyzed from breast cancer patient samples, making it an intriguing target for diagnosis and therapeutic applications.[22] The mechanism of fructose transport by GLUT5 is proposed to occur in a “gated pore” fashion, involving a conformational change between outward-open and inward-open conformations through an occluded state.[23] Inhibition constants (K_i) of bicyclic furanose analogs for GLUT5 transport were reported in the 9–32 mM concentration range, as measured against [^{14}C]D-fructose uptake by GLUT5 expressed in CHO cells.[24] Early studies by Holman and co-workers demonstrated that the presence of hydroxyl groups and their stereochemical configuration on D-fructose derivatives strongly influenced the GLUT5-mediated binding and transport.[25-30] These structure-activity relationship studies also revealed that hydroxyl groups in positions C-2 and C-6 only play a minor role in binding to GLUT5, rendering these carbons attractive sites for structural modifications in the design of fructose analogs.[25-30] As a result, the development of C-6 modified

fluorescent and radiolabeled probes of fructose has been evaluated to study their transport and uptake profiles through GLUT5 expressing breast cancer cells.[31-33] However, these probes, which lack a C-6 hydroxyl group, also underwent efflux. This was attributed to their structural unsuitability to undergo metabolic trapping inside the cells through phosphorylation by hexokinase. When exploring modifications at C-3 and C-4 positions of the fructose molecule, decreased potencies were observed, likely due to interference with critical hydrogen bonding interactions in the GLUT5 binding pocket.[34] Removal of the C-2 hemiacetal hydroxyl group in the furanose form of fructose affords the known carbohydrate derivative 2,5-anhydromannitol (2,5-AM), whose affinity for GLUT5 was found to be similar to that of fructose.[25-30,33,35-36] Conjugates of 2,5-anhydro-mannitol also inhibit fructose uptake through GLUT5. Recently we had estimated an IC_{50} value against the uptake of the probe 6-[^{18}F]FDF of ~20 mM for 1-deoxy-1-fluoro-2,5-anhydro-mannitol (1-FDAM), substantially better than D-fructose itself (~300 mM).[33] Fluorescent derivative 1-amino-2,5-anhydro-D-mannitol (NBDM) is transported twice as efficiently than D-fructose through GLUT5 transporters, as measured in human MCF7 breast cancer cells with a K_i range of 2.3–2.7 mM.[37] The lack of a hemiacetal at C-2 leaves 2,5-AM permanently locked in a furanose form, with a C_2 symmetry that renders the C-1 and C-6 hydroxyl groups equivalent and potentially subjectable to phosphorylation at either site by hexokinase or ketohexokinase (fructokinase). If a reporter group could be attached via C-3 or C-4, the efflux issues noted with fructose derivatives modified at C-6 might be overcame.

We have previously examined a series of C-3 modified derivatives of 2,5-AM for their ability to inhibit the uptake of radiolabeled fructose in murine EMT6 mammary carcinoma cell lines. This study highlighted the importance of strong hydrogen bond donor properties by the C-3 substituent; in particular, two electron-deficient anilines and two amides displayed IC_{50} values comparable to or lower than that of the natural substrate, fructose.[38,39] With the goal of optimizing the binding, transport, and metabolic trapping of 2,5-AM derivatives, we describe efforts to prepare a series of derivatives that retain hydrogen bond donor capability at C-3 with a variety of functionalities and encompassing a range of steric demands. These compounds were

screened for their inhibition of the uptake of the potent and well-studied radiolabeled GLUT5 substrate, [^{18}F]-6-deoxy-6-fluoro-D-fructose (6-[^{18}F]FDF), in EMT6 cells. In addition, docking and molecular dynamics (MD) simulations were carried out to further evaluate the interactions between these novel compounds and GLUT5 protein at a molecular level. These studies were pursued to identify key interactions with the binding pocket that could be harnessed in the future refinement of probe structure to optimize affinity, with an eventual goal of developing the next generation molecular imaging probes targeting GLUT5 through the incorporation of the appropriate reporter groups at C-3 of the 2,5-AM scaffold.

2.2. Results and Discussion

2.2.1. Synthesis of C-3 modified 2,5-AM compounds

Previously, it was observed that GLUT5 tolerates substitution of OH at C-3 of the 2,5-AM scaffold with NHR, so long as its capacity for effective hydrogen bond donation is retained.[38] With an eventual goal of developing non-invasive imaging probes, we specifically targeted a new set of compounds containing carbon-fluorine bond (with the potential for eventual radiofluorination) or fluorophores (with the potential for optical detection), linked to the C-3 nitrogen atom with a wider range of functionalities, such as ureas, thioureas, and sulfonamides (Figure 2.1). We also selected groups ranging from simple fluorinated phenyl to larger polycyclic moieties to permit refinement of our understanding of the size limits for the molecular payloads that can be transported by the GLUT5 machinery.

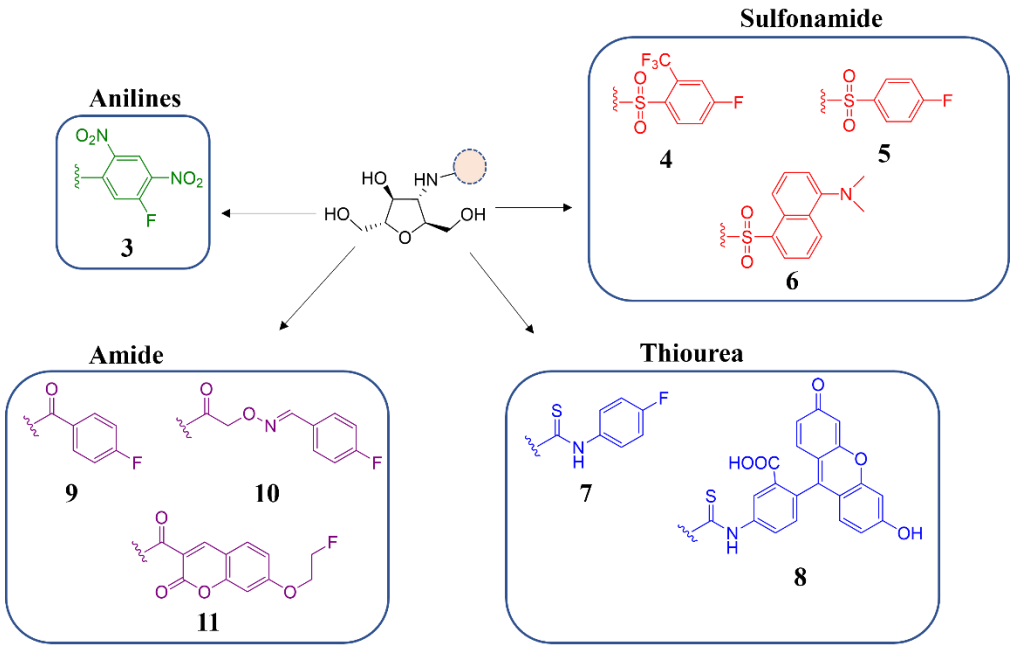

Figure 2.1. A selection of C-3 modified 2,5-AM compounds

The synthetic route to the desired compounds began from 3-azido-3-deoxy-2,5-dianhydro-D-mannitol (**1**), synthesized according to the reported procedure.[40] Afterwards, it was reduced through Pd/C-catalyzed hydrogenation to give 3-amino-3-deoxy-2,5-anhydro-D-mannitol (**2**), which served as the key intermediate to be functionalized to several C-3 modified 2,5-AM derivatives. (Scheme 2.1).

Fluorinated aniline derivative **3** was prepared directly through ipso substitution reaction between the amine **2** and 1,5-difluoro-2,4-dinitrobenzene. Sulfonamide derivatives **4**, **5**, and **6** were synthesized by following the same reaction condition involving the treatment of amine **2** with different sulfonyl chloride reagents in the presence of sodium bicarbonate. Similarly, for thiourea derivatives **7** and **8**, amine **2** was treated with 4-fluorophenyl isothiocyanate or fluorescein isothiocyanate, giving the desired products in good yields. To afford the amide derivatives, different routes were employed for each target. To obtain **9**, amine **2** was benzoylated directly with NHS ester of 4-fluorobenzoic acid, giving 3-fluorobenzamido-3-deoxy-2,5-anhydro-D-mannitol (**9**) in moderate yield **(Scheme 1)**.

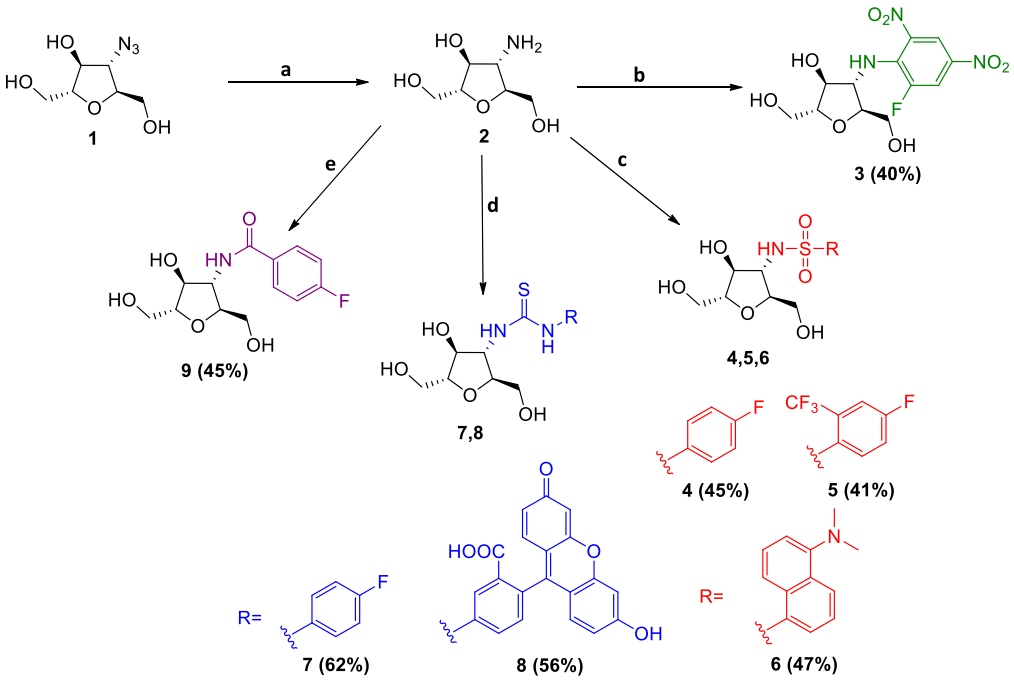

Scheme 2.1. Synthesis of C-3 modified 2,5-AM compounds **3**–**9**. Reagents and conditions. a) Pd/C, MeOH, H_2 (1 atm), RT, 3 h, quant. b) 1,5-difluoro-2,4-dinitrobenzene, $NaHCO_3$, DMF, RT, 4 h, 40%; c) Sulfonyl chloride derivatives (4-fluorobenzene sulfonyl chloride, 4-fluoro-2-(trifluoromethyl) benzenesulfonyl chloride, dansyl chloride), MeCN, Na_2CO_3, RT, 16 h; d) Isothiocyanate reagents (4-fluorophenyl isothiocyanate, fluorescein isothiocyanate isomer I), MeOH, RT, 15 h; e) NHS ester of 4-fluorobenzoic acid, MeOH, RT, 15h, 45%

On the other hand, the synthesis of **10** and **11** was accomplished by employing a multistep sequence, according to the routes depicted in Schemes 2.2 and 2.3. Synthesis of compound **10** was initiated via coupling of amine **2** with *N*-(Boc-aminooxy)acetic acid, followed by deprotection of the Boc protecting group in an acidic medium, affording **II**.[41] The resulting primary amine was coupled further with 4-fluorobenzaldehyde to form oxime ether **10**. We also synthesized a fluorescent amide derivative **11** containing a coumarin moiety. The synthesis began from 2,4-dihydroxybenzaldehyde, which upon heating at reflux with Meldrum's acid in the water, provided 7-hydroxy-coumarin-3-carboxylic acid (**III**). This was followed by conversion of **III** to its activated NHS ester **(V)**. Next, the corresponding ester obtained was treated with amino-2,5-AM **2**, giving the coumarin analog of 2,5-AM (**V**). The phenolic hydroxyl group of compound **V** was alkylated selectively with 2-fluoroethyl *p*-toluenesulfonate by taking advantage of its greater acidity relative to the alcohol

moieties in the 2,5-AM scaffold, affording 3-(7-fluoroethoxy coumarin-3-formamide)-2,5-anhydro-D-mannitol **(11)** in moderate yield.

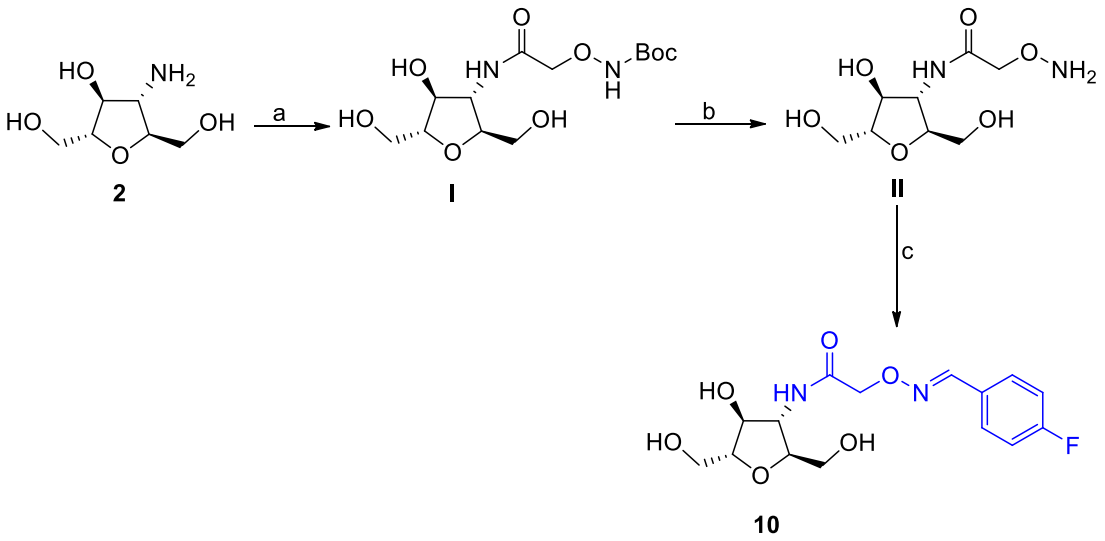

Scheme 2.2. Synthetic route for compound **10.** Reagents and conditions. a) (*N*-Boc aminooxy) acetic acid, *N-hydroxysuccinimide* (*NHS*), MeOH, RT, 12 h, 55%; b) DCM/TFA (1:1), DMF, RT, 8 h, quant. c) 4-F-C_6H_4CHO, NEt_3, MeOH, RT, 4 h, 70%

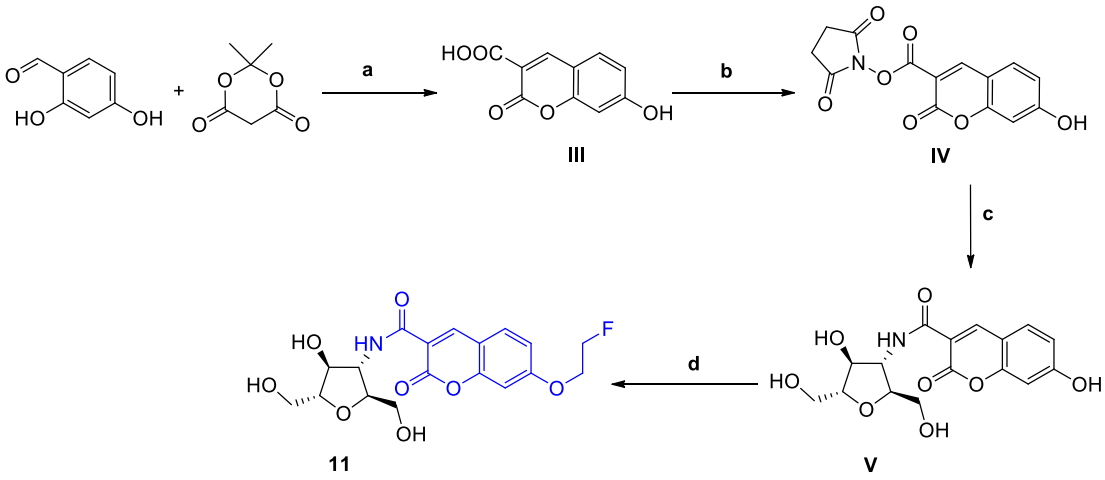

Scheme 2.3. Synthetic route for compound **11**. Reagents and conditions. a) H_2O, 120°C, 12 h, 90% b) NHS, EDCI, DMF, RT, 3 h, 75% c) Compound **2**, MeOH, RT, 15 h, 85% d) 2-fluoroethyl p toluenesulfonate, K_2CO_3, DMF, 110°C, 1 h, 50%

2.2.2. In vitro cell experiments

To analyze the interaction of these novel C-3 modified 2,5-anhydro-D-mannitol analogs with GLUT5, in vitro experiments were carried out in GLUT5-expressing

murine mammary carcinoma cancer cells (EMT6) to determine how the varied substitution patterns would impact GLUT5 binding. Furthermore, fructose derivative 6-FDF was used as the reference compound, as it has been analyzed for its uptake profile through GLUT5 in the past.[42-43,33] Inhibition experiments revealed that for D-fructose, a half-maximum inhibition concentration (IC_{50}) of 322 mM was determined, while 6-FDF resulted in an IC_{50} value of 19 mM.[43] First, these data confirmed the millimolar concentration range for fructose transport in the utilized murine EMT6 breast cancer cells, and second that 6-FDF was more than an order of magnitude potent than D-fructose itself. In addition, D-fructose also inhibits the uptake of radiolabeled D-glucose derivative 2-deoxy-2-[^{18}F]fluoro-D-glucose ([^{18}F]FDG) with an IC_{50} of 80 mM in murine EMT6 cells and 220 mM in human MDA-MB231 cells, confirming the presence and function of facilitative hexose transporter GLUT2 in breast cancer cells.[33] The latter data confirmed that both D-fructose and 6-FDF are being transported through both GLUT2 and GLUT5 in breast cancer cells in a millimolar concentration range. Therefore, when designing novel specific inhibitors for the GLUT5 transporter, it would be reasonable to expect their GLUT5 transport also in a millimolar concentration range, especially when using a radiometric assay established with radiolabeled fructose derivative 6-[^{18}F]FDF in murine EMT6 breast cancer cells and inhibition using D-fructose and reference compound 6-FDF as internal controls.[33,43]

Competition binding experiments against the uptake of radiolabeled 6-[^{18}F]FDF in the presence of the C-3 modified derivatives were performed in a dose-dependent manner, followed by determining their half-maximum inhibition concentration (IC_{50}) values (Figure 2.2 and Table 2.1). Our analysis began with the evaluation of the aniline-derivative 3, which is the fluorinated analog of the previously reported GLUT5 substrate, 3-(*N*-2,4-dinitrophenyl)amino-2,5-anhydro-D-mannitol[38] (Table 2.1). In comparison to reference 6-FDF, compound **3** displayed a 10–12-fold better inhibition of 6-[^{18}F]FDF uptake into EMT6 cells. This may be attributed to the electron withdrawing effect exerted by the ortho and para nitro groups on the aniline, which is expected to reduce the electron density at the amine nitrogen. This would be expected

to enhance its ability to donate a hydrogen bond to complementary acceptor moieties in the binding pocket. The aromatic nitro and fluorophenyl groups may contribute further favorable interactions, as was suggested in docking studies.

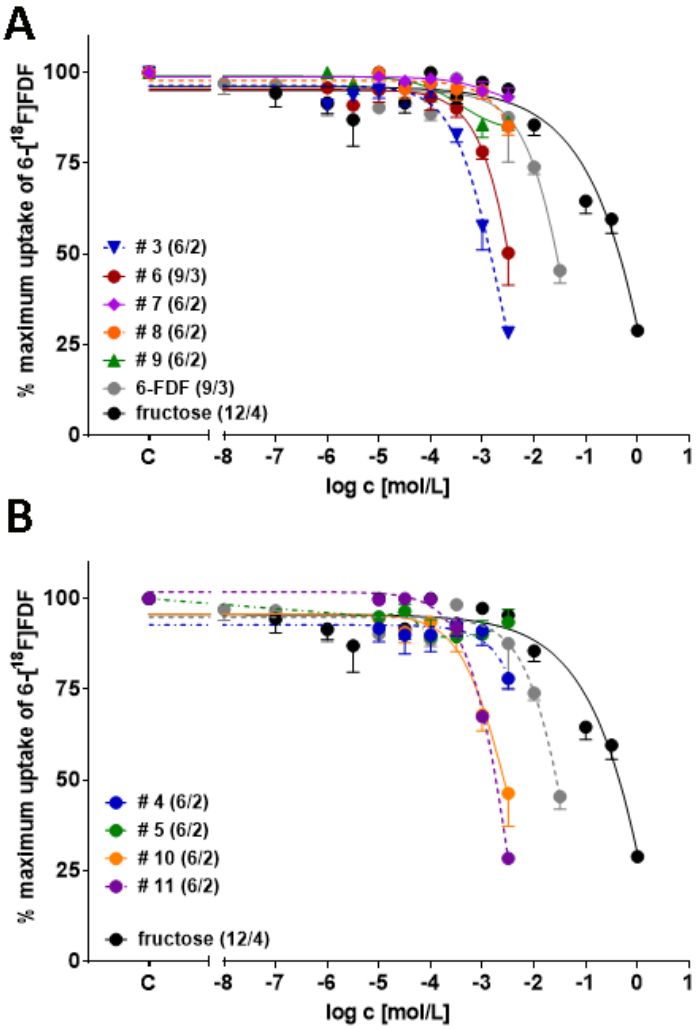

Figure 2.2. Concentration-dependent inhibition of 6[^{18}F]FDF uptake into EMT6 cells of C-3 modified 2,5-AM compounds (**3**-**11**), 6-FDF, and **fructose**). Data are shown as mean ± SEM of n data points from 2–4 experiments

Regarding the sulfonamide derivatives, compound **4** did not show a better IC_{50} value than 6-FDF, while **5** failed to inhibit 6-[^{18}F]FDF uptake transport at all. On the contrary, compound **6**, connected to the bulky fluorescent dansyl group, displayed a 5-fold stronger inhibitory effect on 6-[^{18}F]FDF uptake compared to 6-FDF, indicating the tolerance and affinity of the GLUT5 binding pocket for greater steric bulk at C-3. On

the other hand, functionalization with a thiourea handle (compound **7**) resulted in no effect on 6-[^{18}F]FDF uptake into EMT6 cancer cells, while compound **8**, bearing the bulky fluorescent fluorescein group, showed a similar inhibition as 6-FDF itself.

Table 2.1. Half-maximum Inhibition Concentrations (IC_{50}) for C-3 Modified 2,5-AM Compounds against 6-[^{18}F]FDF Uptake into EMT6 Cells

Compound	n/x	IC_{50} (mM)[a]
3	**6/2**	**1.10 ± 0.17**
4	**6/2**	**~ 6** *(estimated)*
5	**6/2**	**n.d.[b]**
6	**9/3**	**2.29 ± 0.18**
7	**6/2**	**n.d.**
8	**6/2**	**~ 20** *(estimated)*
9	**6/2**	**n.d.**
10	**6/2**	**2.31 ± 0.35**
11	**6/2**	**1.71 ± 0.08**
6-FDF	**9/3**	**17.02 ± 0.75**
fructose	**12/4**	**342 ± 74**

[a]Data shown as mean ± SEM from *n* data points out of 2-4 experiments; n.d.[b] – not determined.

Amide derivative **9** displayed no inhibitory activity in the selected concentration range, aligning with the results obtained for the sulfonamide and thiourea derivatives (**4**, **5**, and **7)** having a small spacer between the anhydromannitol NH and aryl group. Finally, both compound **11**, with a bicyclic coumarin, and compound **10**, with a longer linker, resulted in a significant increase in the potency to inhibit 6-[^{18}F]FDF uptake by ~10-fold relative to 6-FDF. Taken together, the improved inhibitory potency, as determined for compounds **10** and **11**, suggested that an aromatic group attached with a tether and localized aromatic rings at position C-3 could be well tolerated by the GLUT5 binding pocket. Out of the novel library of 2,5-anhydro-mannitol derivatives, four compounds were found to possess IC_{50} values of 1.1 to 2.3 mM, which would be one order of magnitude more potent than 1-FDAM or 6-FDF and about two orders of magnitude more potent than D-fructose itself.[33,43] This is in line

with the findings of Tanasova et al.[37] that derivatives of 2,5-anhydro-D-mannitol can be transported with about one order of magnitude higher affinity through GLUT5 versus natural substrate D-fructose. However, the expression of the low-affinity fructose transporter protein GLUT2 by EMT6 cells also represents a potential complicating factor. As previously mentioned, 6-[^{18}F]FDF is transported by both GLUT5 and GLUT2, though with a higher affinity via the GLUT5 pathway, although experiments with the 2,5-AM derivative 1-FDAM suggest that it may not show a similar uptake profile, indicating that it may be more specific towards GLUT5 transport only.[21,31,34] A complete assessment of the extent of inhibition of 6-[^{18}F]FDF uptake in EMT6 cells by the 2,5-AM analogs discussed here will require further evaluation of their specific interactions with GLUT2, which is beyond the scope of the present study.

The results described above compare well with previous efforts to identify GLUT5 inhibitors. Plant natural products, such as astragalin-6-glucoside and rubusoside, have been shown to possess IC_{50} values of 1.8 mM and 10.3 mM, as measured against D-[^{14}C]fructose.[44] Also, MSNBA (N-(4-methanesulfonyl-2-nitrophenyl)-2H-1,3-benzodioxol-5-amine), generated as a specific GLUT5 inhibitor from a virtual screening library, exhibits an IC_{50} value against D-[^{14}C]fructose of 5.8 mM in MCF7 human breast cancer cells and 0.10 mM in a proteoliposome GLUT5 expression system.[45]

2.2.3. In silico studies

We sought to examine the origins of the substantially different 6-[^{18}F]FDF inhibitory properties detected for the structurally related 2,5-AM derivatives **3–11**. We started by docking each of the compounds, as well as fructose, into the central cavity at the transmembrane domain (TMD) of the open-inward facing conformation of GLUT5 (PDB accession: 4YB9).[23] Docking of fructose showed hydrogen bonding interactions with the C-domain residues of helix 7, namely Q167, Y32, S392 and N294, in agreement with poses and interactions previously reported by Nomura and others, as essential residues for fructose binding and uptake (Figure 2.3).[23,46]

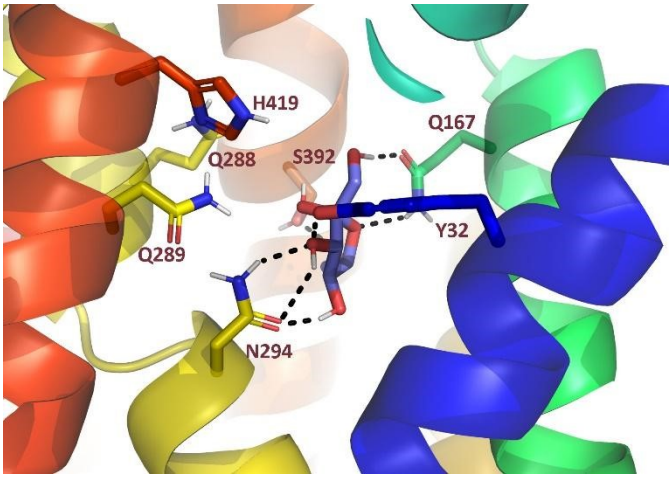

Figure 2.3. Docking pose and putative interactions of fructose with GLUT5. (Hydrogen bonds are shown as black dotted lines)

To get a more accurate representation and validation of the binding poses suggested by molecular docking, we then chose three compounds, **3**, **10**, and **11** for further computational studies by molecular dynamics (MD) to explore whether the compounds will remain in the proposed binding pocket. We expected these molecular dynamics simulations to provide insights into the impact of structural changes at the C-3 position on the ability of these molecules to occupy the GLUT5 fructose binding pocket. The selected compounds were submitted for a 50 ns long MD simulation to simulate atomic motions and to validate the stability and the poses of docked ligands. The MD simulations were carried out in a membrane environment of POPC lipids to mimic the environment of the protein (Figure 2.4) using AMBER18 and the ff14SB forcefield combined with the GAFF force field.[47,48] Analysis of the MD trajectories revealed that all complexes equilibrated at around 30 ns with average RMSD values of 2.7 Å, 2.1 Å, 2.7 Å, and 2.3 Å for fructose, compounds **3**, **10**, and **11**, respectively (Figure 2.5). However, some fluctuations in the RMSD of fructose were observed around 45 ns of the simulation; these could be the result of a low hydrogen bond occupancy with binding residues at this time of the simulation and the probability that the compound is moving down the cavity for uptake, as can be seen during the process of the simulation trajectory using VMD software.

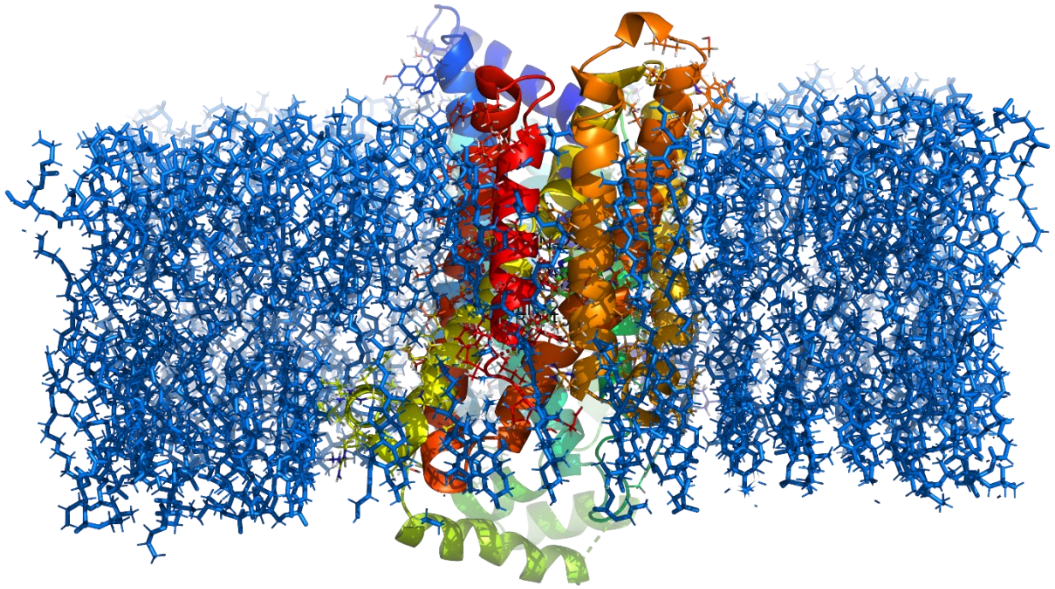

Figure 2.4. Embedded GLUT5 complex (colored ribbons) in a lipid membrane (blue sticks) used for molecular dynamics simulations. (Figure generated in Pymol)

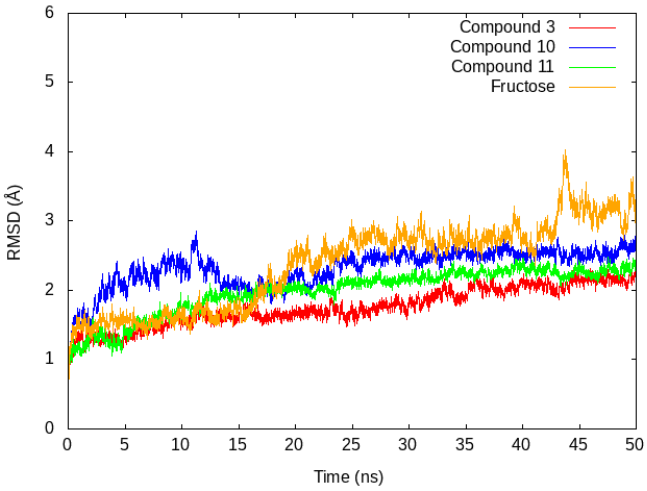

Figure 2.5. Root mean square deviations (RMSD) of ligands-GLUT5 complex systems as a function of simulation time

Hydrogen bond occupancies are used to study the interaction between the ligands and target proteins.[49] Residue Q167 has been suggested previously to be very crucial for the recognition, interaction, and specificity of fructose to the GLUT5 protein compared to other GLUTs.[23] Analysis of the hydrogen bond occupancies of the complexes through the MD trajectories revealed that fructose formed hydrogen bonds

to residues Q167, N325, Q289, and S392, in agreement with previous reports (Figure 2.6).[23,45] Similarly, compounds **3**, **10**, and **11** formed hydrogen bonds to Q167, Q289, and Q288 (Figure 2.7).

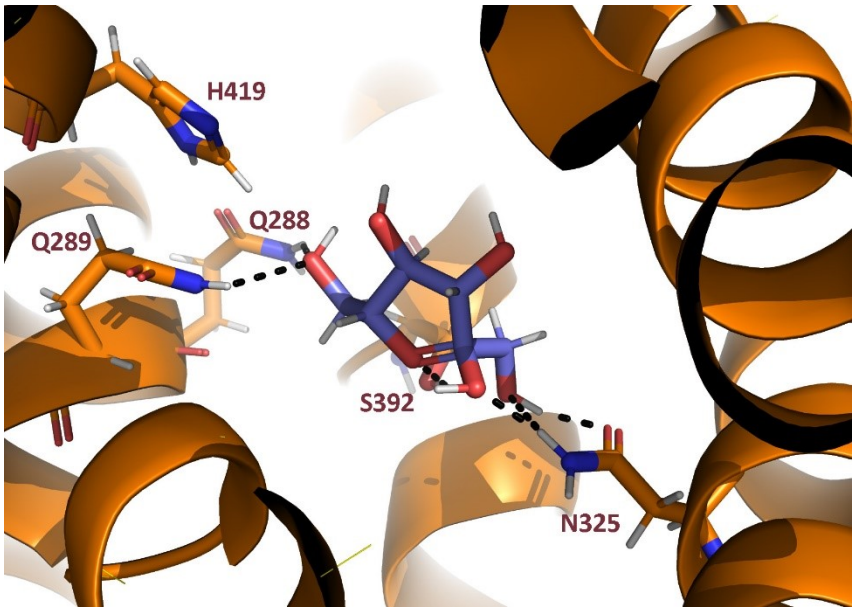

Figure 2.6. 3D snapshot of fructose during MD simulation. Hydrogen bonds are shown as black dashed lines

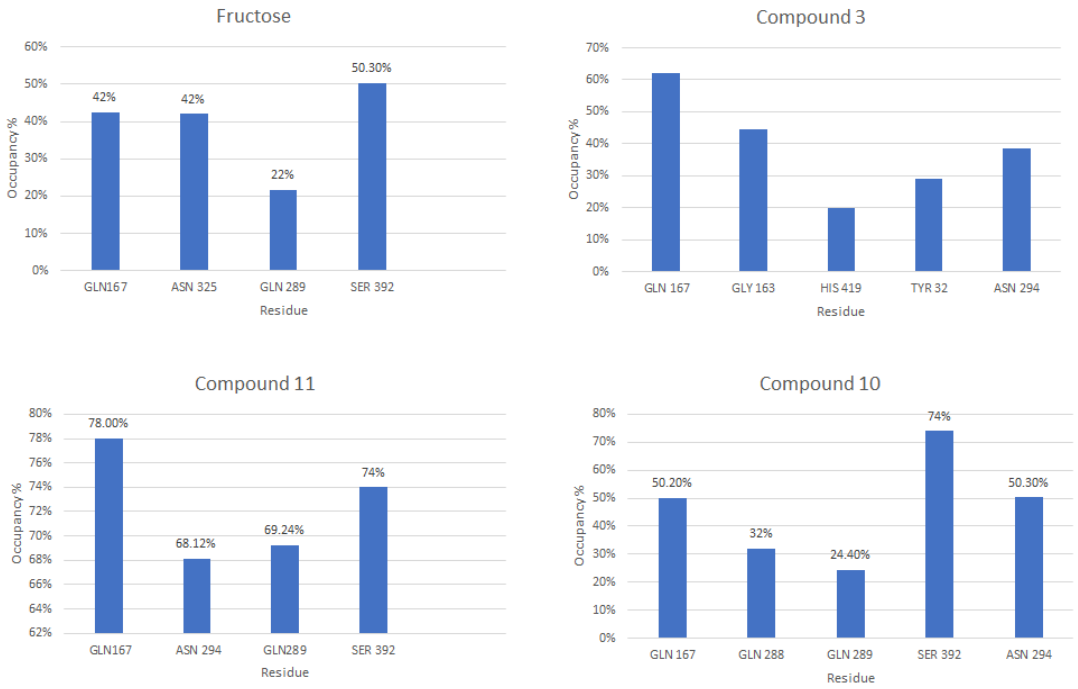

Figure 2.7. Hydrogen bond occupancies of compounds used in MD simulations

Further investigation of hydrogen bonds formed throughout the simulation trajectories showed that compound **3**, which exhibited the most potent IC_{50} value and strongest interactions with GLUT5, formed extra hydrogen bonds between the oxygen of the nitro group and the backbone NH of G163, in addition to hydrogen bonds between H419, Y32 and N294 side chains and the sugar part of the molecule (Figure 2.8). We used clustering in AMBER tools via the average-linkage algorithm to obtain a representative structure of the last 20 ns of simulation for all ligands. Examination of this representative structure for compound **3** revealed a pi-cation interaction, frequently observed between the positively charged nitro group nitrogen atom and the His imidazole sidechain, which might contribute to the stability of the complex and the greater inhibition of uptake of this compound. Similarly, hydrogen bonds occurred between the amide oxygen and C4 hydroxyl of compound **10** to N294, which also might contribute to the better inhibitory activity of this class of C-3 substituted 2,5-AM derivatives (Figure 2.9). Three more hydrogen bonds were observed between the amide NH at C-3, oxygen of the (-O-N=CH-) and C-6 hydroxyl of compound **10** to Q167. Similarly, the amide NH at C-3 of compound **11** formed the essential hydrogen bond contact with Q167 (Figure 2.10).

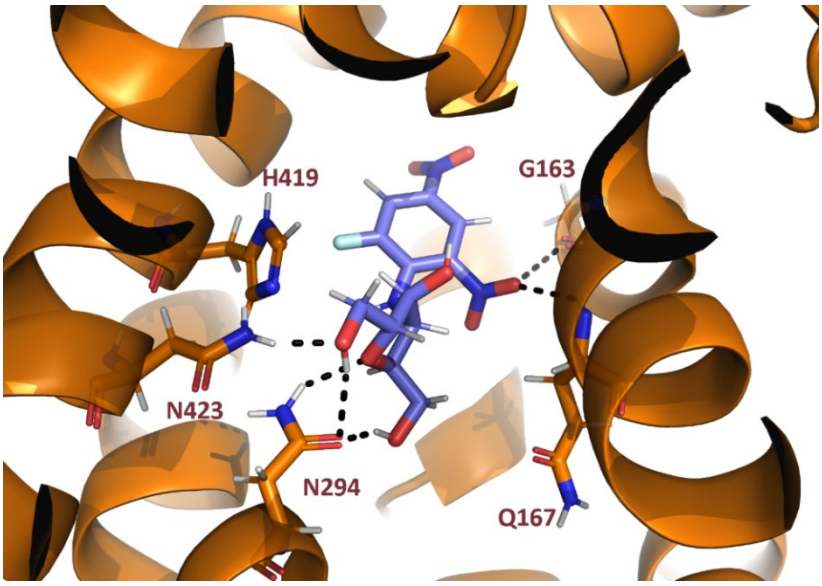

Figure 2.8. Snapshot of compound **3** during MD simulation. Hydrogen bonds are shown as black-dashed lines

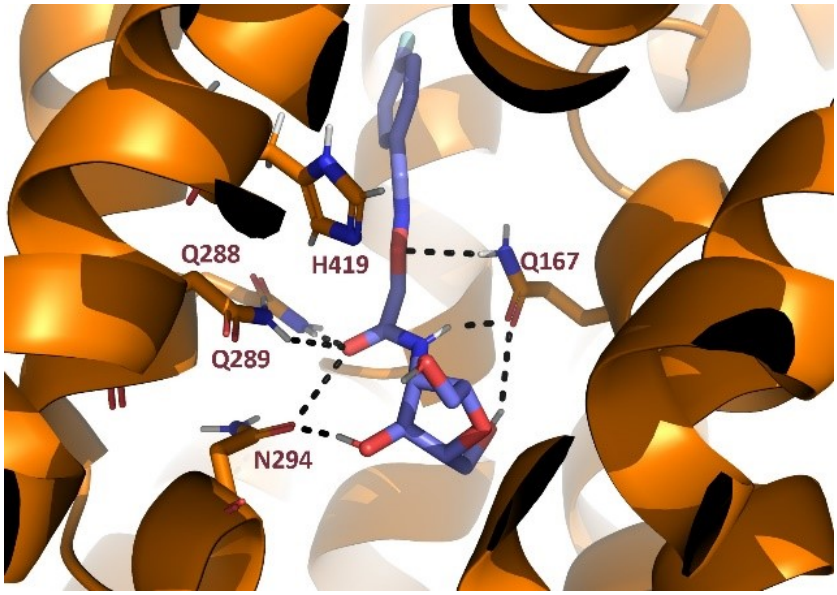

Figure 2.9. 3D snapshot of compound **10** during MD simulation. Hydrogen bonds are shown as black dashed lines

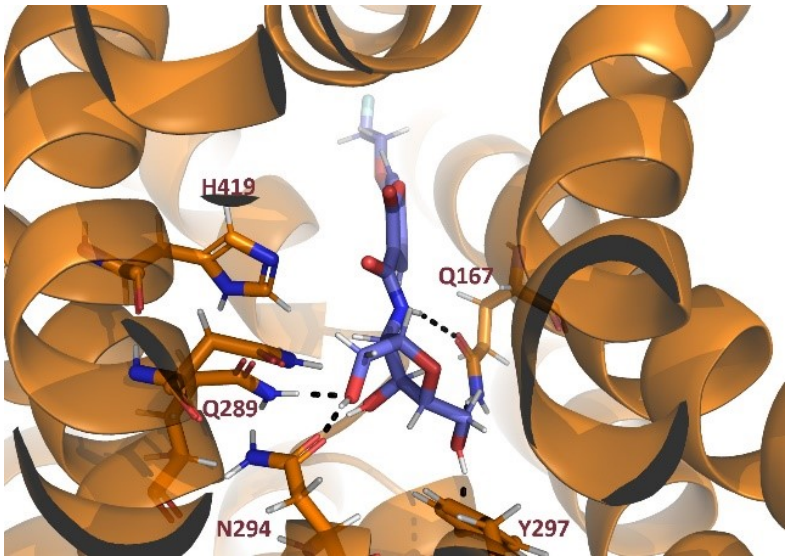

Figure 2.10. 3D snapshot of compound **11** during MD simulation. Hydrogen bonds are shown as black dashed lines

It is worth noting that hydrogen bonding interactions between fructose hydroxyl groups to N294 have been reported previously to be essential to the interaction with the GLUT5 protein structure.[50] These observations might contribute to the ability of the C-3 modified 2,5-AM derivatives to be involved in hydrogen bond contacts with important GLUT5 binding residues and the tolerability of the binding pocket to

accommodate a variety of sterically demanding groups (e.g., coumarins, nitrophenyl, Figure 2.11). The stability of the simulations was confirmed by the radius of gyration for all the simulated complexes (Figure 2.12). Root mean square fluctuations (RMSF) showed similar fluctuation patterns of the protein backbone of GLUT5 in complexes with all compounds analyzed (Figure 2.13).

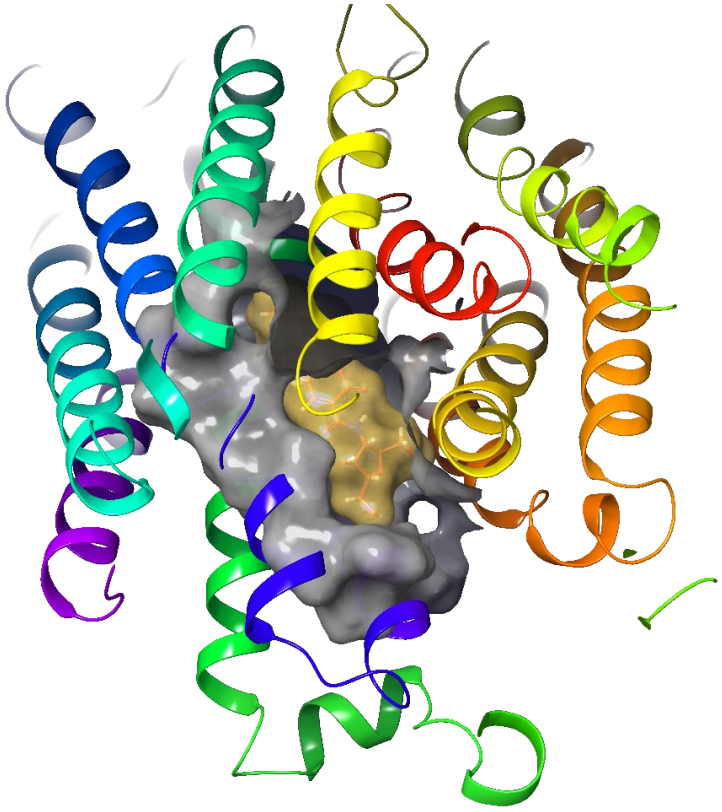

Figure 2.11. Compound 11 (orange surface) is accommodated in the GLUT5 binding pocket (gray surface)

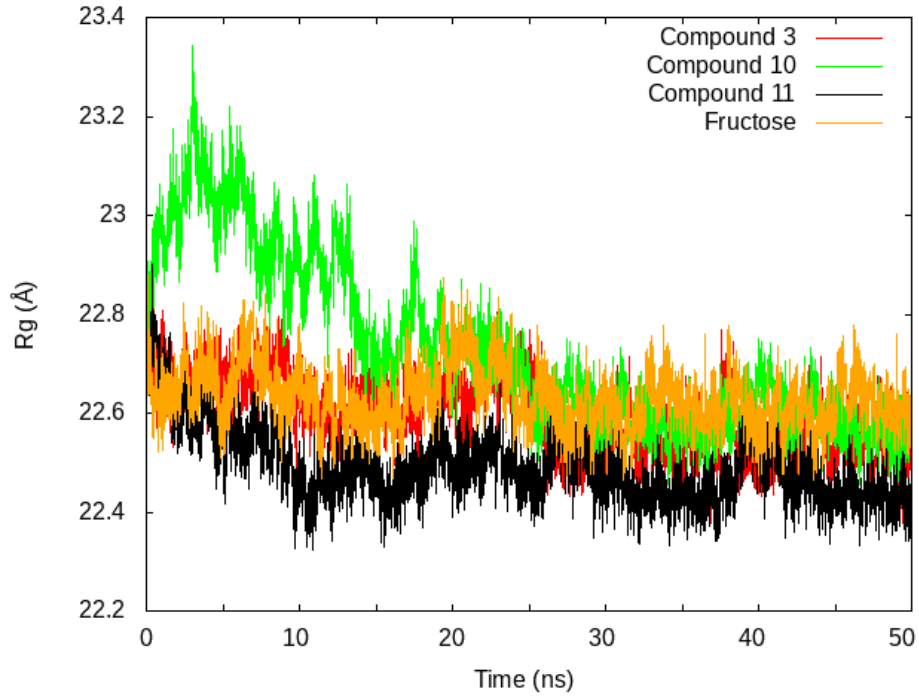

Figure 2.12. Radius of gyration (*R*g) fluctuation versus time of GLUT5 complexed with compounds 3,10, 11, and fructose

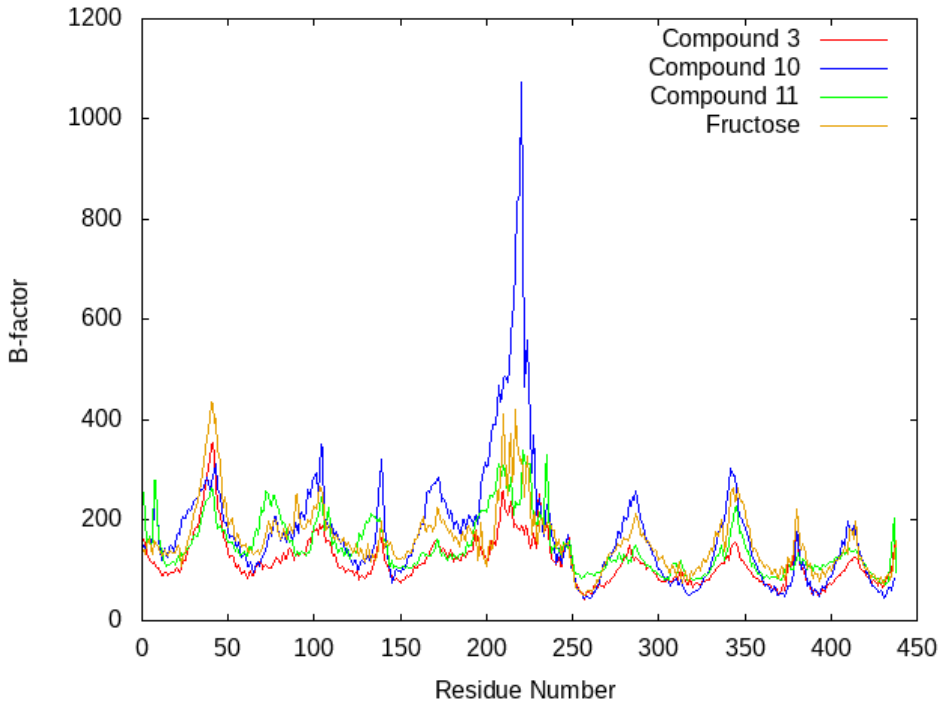

Figure 2.13. RMSF as a function of B-factor and residues of GLUT5 in complex with compounds 3,10,11, and fructose

In order to get a better insight into the contribution of the selected ligands to the stability of their complexes with GLUT5, we have employed the MMGBSA method to measure the free binding energy of the complexes.[51,52] The calculated binding energies were similar for the GLUT5 complexes with compounds **3**, **10**, and **11** with –48.64 ± 2.3 kcal mol^{-1}, –43.30 ± 3.2 kcal mol^{-1}, 45.26 ± 2.9 kcal mol^{-1}, respectively, and significantly lower than the one calculated for fructose (–16.95 ± 2.3 kcal mol^{-1}). It is worth mentioning that the binding free energy calculated for fructose is similar to that obtained by Ainsley et al.[46] These findings could be correlated to the observed activity of each ligand in stabilizing the GLUT5 complexes with good insight into the possible future modification of the 2,5 AM to design more potent inhibitors. Overall, the computational results are in agreement with the observed inhibitory activities of these novel probe molecules. Moreover, the MD studies support previous reports of the essential residues involved in the binding of fructose and its analogs to GLUT5.[46]

2.3. Conclusion

In summary, different derivatives of 2,5-AM were synthesized and evaluated in vitro against radiolabeled fructose derivative 6-[^{18}F]FDF. Several compounds displayed concentration-dependent inhibitory effects on cellular uptake of 6[^{18}F]FDF at levels 100-fold or better than the natural GLUT5 substrate, fructose. These results will help to refine the understanding of the structural requirements of the GLUT5 transport machinery with respect to the molecular cargoes attached to fructose mimics that are tolerated by the protein. Since elevated GLUT5 expression and abnormal fructose metabolism are associated with several cancers and other diseases, this work will contribute to the development of novel PET, fluorescent, and dual imaging probes targeting the GLUT5 transporter. The development of molecular probes that are mimicking the fructose uptake and metabolism has a high potential for detection of elevated GLUT5 expressing metabolic disorders. As a result, the present findings can lead to improved designs of fructose-based inhibitors and potential selective GLUT5 targeting pharmaceutical and radiopharmaceutical agents.

2.4. Experimental section

Materials and methods

Reactions were carried out in oven-dried glassware under a positive argon or nitrogen atmosphere unless otherwise stated. Transfer of anhydrous solvents and reagents was accomplished with oven-dried syringes or cannula. Solvents were distilled before use, and dimethylformamide (DMF) and acetonitrile (MeCN) were distilled from calcium hydride. Chemicals were purchased from Sigma-Aldrich Inc. and were used without further purification. Thin layer chromatography was performed on glass plates preloaded with 0.25 mm silica gel matrix. Flash chromatography columns were packed with 230–400 mesh silica gel. Optical rotations were measured with Perkin Elmer 241 polarimeter, at 22 ± 2 °C. Proton nuclear magnetic resonance spectra (^{1}H NMR) were recorded at 500 MHz or 700 MHz and coupling constants (*J*) are reported in Hertz (Hz). Standard notation was used to describe the multiplicity of signals observed in ^{1}H NMR spectra: broad (br), multiplet (m), singlet (s), doublet (d), triplet (t), etc. Carbon nuclear magnetic resonance spectra (^{13}C NMR) were recorded at 100 MHz or 125 MHz and are reported δ (ppm) relative to the center line of the septet from methanol-d_4 (49.3 ppm), triplet of chloroform-d (77.2 ppm), or septet of DMSO-d_6 (39.5 ppm). Infrared (IR) spectra were measured with a FT-IR 3000 spectrophotometer. Mass spectra were determined on a high-resolution electrospray positive ion mode spectrometer.

2.4.1. Synthesis

3-Azido-3-deoxy-2,5-dianhydro-D-mannitol **(1)** was prepared via diastereoselective ring-opening of 2,5:3,4-dianhydro-D-allitol according to the reported procedure. [40,52]

3-deoxy-3-amino-2,5-anhydro-D-mannitol (2)

Azide **1** (0.25 g, 1.3 mmol) was dissolved in MeOH in (25 mL), and 10% Pd/C (0.05 g, 20 % by weight) was added, followed by stirring the resulting heterogeneous mixture at room temperature under H_2 atmosphere (1 atm) attained via a balloon. After stirring for 3 h, solids were removed by filtration over a celite pad and washed with DCM and MeOH (20 mL). The filtrate was evaporated completely under reduced pressure to yield the amine **2** as pale-yellow thick syrup. The amine obtained (quant.) was used for the next step without further purification.[40]

3-deoxy-3-[N-(5-fluoro-2,4-dinitro-phenyl)amino]-2,5-anhydro-D-mannitol (3)

To a stirred solution of amine **2** (0.12 g, 0.76 mmol) in dry DMF (10 mL) in an oven-dried flask maintained under N_2 atmosphere, excess $NaHCO_3$ was added. After stirring for 30 min, 1,5-difluoro-2,4-dinitrobenzene (0.19 g, 0.91 mmol) was added slowly, and the resultant heterogeneous mixture was allowed to stir at room temperature for 4 h. Upon completion of the reaction (monitored by TLC with 10% MeOH/ DCM eluent system), excess $NaHCO_3$ was filtered off. Then, the solvent was concentrated under reduced pressure, yielding a brown viscous syrup, which was purified through silica gel column chromatography, using a DCM/MeOH solvent mixture (gradient from 100:0 to 95:5). Fractions containing the desired product were combined and concentrated under vacuum to yield pure compound **3** as a yellow solid (0.085 g, 40%). R_f 0.34 (DCM/MeOH, 90:10) $[\alpha]_D^{20}$ +29.82 (*c* 0.23, MeOH); IR (cast film) 3359, 3097, 2932, 2879, 1626, 1581, 1508, 1448, 1401, 1259, 1052 cm^{-1}; ^1H NMR (700 MHz, CD_3OD): δ 9.05 (d, *J* = 8.0 Hz, 1H), 7.27 (d, *J* = 14.3 Hz, 1H), 4.30 (t, *J* = 5.2 Hz, 1H), 4.26 (t, *J* = 5.2 Hz, 1H), 4.08 (dt, *J* = 5.6, 4.7 Hz, 1H), 4.00 (ddd, *J* = 5.2, 3.9, 2.7 Hz, 1H), 3.81 (dd, *J* = 11.9, 4.9 Hz, 1H), 3.77 (dd, *J* = 11.9, 2.7 Hz, 1H), 3.69–3.67 (m, 1H), 3.6 –3.64 (m, 1H); ^{13}C NMR (176 MHz, CD_3OD): δ 159.5 (d, J_{C-F} = 267.8 Hz), 149.0 (d, *J* = 13.9 Hz), 127.7, 126.9, 125.6, 102.2 (d, *J* = 28.1 Hz), 85.4, 83.2, 77.2, 62.0, 61.6, 61.2; HRMS (ESI) calcd for $C_{12}H_{15}FN_3O_8$ $[M+H]^+$ 348.0765; found 348.0764.

General Procedure to Synthesize 4, 5 and 6:

A 50 mL round bottom flask, maintained under N_2 atmosphere, was charged with amine **2** (0.15 g, 0.95 mmol) and acetonitrile (15 mL). After the amine was dissolved completely, the sulfonyl chloride derivative (0.14 g, 0.74 mmol of 4-fluorobenzenesulfonyl chloride for **4**, 0.14 g, 0.74 mmol of 4-fluoro-2-(trifluoromethyl) benzenesulfonyl chloride for **5**, and 0.30 g, 1.1 mmol of dansyl chloride for **6**) was added to the flask, followed by addition of excess Na_2CO_3 (0.51 g, 4.7 mol). This heterogeneous mixture was allowed to stir at room temperature for 16 h. Solids were filtered off and washed with an excess of MeCN. The filtrate was

evaporated under vacuum to yield a crude product, which was subjected to silica gel column chromatography eluted with a DCM/MeOH solvent mixture (100:0 to 92:8 for **4**, 100:0 to 95:5 for **5**, and 100:0 to 92:8 for **6**). Fractions containing compounds were combined and concentrated under a vacuum to yield a pure product.

3-deoxy-3-[N-(4-fluorobenzenesulfonamide)amino]-2,5-anhydro-D-mannitol (4)

Colorless oil (0.09 g, 45%). R_f 0.24 (DCM/MeOH, 90:10); $[\alpha]_D^{20}$ +14.80 (*c* 0.20, MeOH); IR (cast film) 3349, 2924, 2881, 1709, 1684, 1592, 1495, 1329, 1293, 1237, 1155 cm^{-1}; ^1H NMR (500 MHz, D_2O): δ 8.04 (dd, *J* = 8.8, 5.0 Hz, 2H), 7.42 (app t), 4.05 (t, *J* = 7.6 Hz, 1H), 3.91–3.87 (m, 1H), 3.87–3.84 (m, 1H), 3.80 (dd, *J* = 12.5, 2.8 Hz, 1H), 3.75 (t, *J* = 7.6 Hz, 1H), 3.68 (dd, *J* = 12.5, 4.9 Hz, 1H), 3.63 (dd, *J* = 12.5, 2.8 Hz, 1H), 3.46 (dd, *J* = 12.5, 4.9 Hz, 1H); ^{13}C NMR (126 MHz, D_2O): δ 166.3 (d, *J* = 253.0 Hz), 136.6, 130.7 (d, *J* = 9.8 Hz), 117.5 (d, *J* = 23.0 Hz), 83.1, 81.5, 75.7, 61.6, 61.4, 60.3; HRMS (ESI) calcd for $C_{12}H_{16}FNO_6SNa$ $[M+Na]^+$ 344.0682; found 344.0683.

3-deoxy-3-[N-(4-fluoro-2-(trifluoromethyl)benzenesulfonamide)amino]-2,5-anhydro-D-mannitol (5)

Colorless oil (0.08 g, 41%). R_f 0.28 (DCM/MeOH, 90:10); $[\alpha]_D^{20}$ +14.00 (*c* 0.10, MeOH); IR (cast film) = 3341, 2929, 2885, 1593, 1482, 1416, 1311, 1264, 1166, 1096 cm^{-1}; ^1H NMR (700 MHz, D_2O): δ 8.33 (dd, *J* = 9.2, 5.1 Hz, 1H), 7.81 (dd, *J* = 9.2, 2.6 Hz, 1H), 7.58 (ddd, *J* = 9.2, 7.6, 2.6 Hz, 1H), 4.02 (t, *J* = 8.3 Hz, 1H), 3.87 (ddd, *J* = 8.3, 4.6, 2.6 Hz, 1H), 3.78 (d, *J* = 4.1 Hz, 1H), 3.76 (d, *J* = 8.3 Hz, 1H), 3.73 (dd, *J* = 12.5, 2.8 Hz, 1H), 3.65 (dd, *J* = 12.5, 2.8 Hz, 1H), 3.61 (dd, *J* = 12.5, 5.0 Hz, 1H), 3.47 (dd, *J* = 12.5, 5.0 Hz, 1H); ^{13}C NMR (176 MHz, D_2O) δ 164.5 (d, *J* = 255.5 Hz), 135.5 (d, *J* = 9.5 Hz), 135.1, 130.2, 122.9 (d, *J* = 273.4 Hz), 120.2 (d, *J* = 21.4 Hz), 117.9 (d, *J* = 23.1 Hz), 82.8, 80.9, 75.1, 61.5, 61.2, 60.1. HRMS (ESI) calcd for $C_{13}H_{14}F_4NO_6S$ $[M-H]^-$ 388.0559; found 388.0559.

3-deoxy-3-[N-(5-(dimethylamino)naphthalene-1-sulfonamide)amino]-2,5-anhydro-D-mannitol (6)

Yellow sticky solid (0.11 g, 47%). R_f 0.48 (DCM/MeOH, 90:10); $[\alpha]_D^{20}$ +20.90 (*c* 1.30, MeOH); IR (cast film) 3349, 2924, 2854, 1678, 1457, 1204, 1141, 1060, 790 cm^{-1}; ^1H

NMR (700 MHz, CD_3OD) δ 8.54 (dt, *J* = 8.5, 1.1 Hz, 1H), 8.34 (dt, *J* = 8.7, 0.9 Hz, 1H), 8.27 (dd, *J* = 7.3, 1.3 Hz, 1H), 7.56 (ddd, *J* = 9.8, 8.6, 7.4 Hz, 2H), 7.25 (dd, *J* = 7.6, 0.9 Hz, 1H), 3.88 (t, *J* = 6.6 Hz, 1H), 3.69 – 3.65 (m, 1H), 3.65–3.62 (m, 1H), 3.61 (d, *J* = 3.0 Hz, 1H), 3.54 (dd, *J* = 7.1, 6.4 Hz, 1H), 3.50 (dd, *J* = 11.9, 4.9 Hz, 1H), 3.25 (dd, *J* = 11.8, 2.8 Hz, 1H), 3.10 (dd, *J* = 11.8, 5.5 Hz, 1H), 2.87 (s, 6H); ^{13}C NMR (176 MHz, CD_3OD) δ 153.2, 137.8, 131.2, 131.1, 130.9, 130.3, 129.0, 124.3, 120.7, 116.3, 84.9, 83.7, 77.5, 63.0, 62.9, 62.3, 45.8.; HRMS (ESI) calcd. for $C_{18}H_{24}N_2O_6SNa$ $[M+Na]^+$ 419.1247; found 419.1242.

General Procedure to Synthesize 7 and **8:**

Amine **2** (0.13 g, 0.79 mmol) was dissolved in MeOH (15 mL) in a 50 mL round bottom flask, maintained under N_2 atmosphere. To this clear solution, the isothiocyanate derivative (0.14 g, 0.95 mmol of 4-fluorophenyl isothiocyanate for **7** and 0.34 g, 0.87 mmol of fluorescein isothiocyanate isomer I (Sigma) for **8**) was added slowly and the reaction mixture was stirred for 15 h at ambient temperature. MeOH was then removed under vacuum, and the crude compound was subjected to silica gel column chromatography using a DCM/MeOH solvent mixture (gradient from 100:0 to 94:6 for **7** and 100:0 to 90:10 for **8**). Fractions containing the desired product were combined and concentrated under a vacuum to yield the pure compound.

3-deoxy-3-[N-(1-(4-fluorophenyl)thiourea)amino]-2,5-anhydro-D-mannitol (7)

Brown oil (0.12 g, 62%). R_f 0.25 (DCM/MeOH, 90:10); $[\alpha]_D^{20}$ –5.33 (*c* 0.30, MeOH); IR (cast film) 3297, 3070, 2939, 1611, 1544, 1509, 1460, 1415, 1339, 1219, 1046 cm^{-1}; ^1H NMR (700 MHz, D_2O): δ 7.24 (dd, *J* = 8.8, 5.0 Hz, 2H), 7.14 (app t), 4.12 (t, *J* = 6.9 Hz, 1H),), 3.9–3.92 (m, 1H), 3.9–3.88 (m, 1H), 3.76 (dd, *J* = 12.5, 3.1 Hz, 1H), 3.7–3.70 (m, 1H) , 3.70–3.66(m, 1H), 3.69–3.65 (m, 1H), 3.59 (dd, *J* = 12.5, 4.4 Hz, 1H); ^{13}C NMR (176 MHz, D_2O): δ 181.5, 162.2 (d, *J* = 244.8 Hz), 129.46, 129.41, 117.2 (d, *J* = 22.1 Hz), 84.0, 82.7, 76.1, 63.0, 62.1, 61.8. ; HRMS (ESI) calcd for $C_{13}H_{17}FN_2O_5Na$ $[M+Na]^+$ 323.0893; found 323.0892.

3-deoxy-3-[N-(3-(fluorescein)-5-yl)thiourea)amino]-2,5-anhydro-D-mannitol (8)

Orange sticky solid (0.19 g, 56%). R_f 0.44 (DCM/MeOH, 90:10); $[\alpha]_D^{20}$ –10.64 (*c* 0.25, MeOH); IR (cast film) 3261, 2935, 2853, 1748, 1597, 1462, 1370, 1232, 1190, 1067 cm^{-1}; ^1H NMR (500 MHz, CD_3OD) δ 8.16–8.03 (m, 1H), 7.78–7.65 (m, 1H), 7.16 (d, *J* = 8.2 Hz, 1H), 6.82 (d, *J* = 8.8 Hz, 2H), 6.66 (d, *J* = 2.4 Hz, 2H), 6.57 (dd, *J* = 8.8, 2.4 Hz, 2H), 4.21 (t, *J* = 5.7 Hz, 1H), 3.98 (td, *J* = 5.8, 3.5 Hz, 1H), 3.94 (q, *J* = 3.5 Hz, 1H), 3.81 (d, *J* = 3.5 Hz, 1H), 3.78 (d, *J* = 5.6 Hz, 1H), 3.77–3.75 (m, 1H), 3.74 (d, *J* = 2.8 Hz, 1H), 3.64 (dd, *J* = 12.0, 4.2 Hz, 1H).; ^{13}C NMR (126 MHz, CD_3OD) δ 181.6, 170.2, 164.0, 154.0, 140.4, 129.6, 129.3, 129.1, 125.9, 120.2, 114.4, 111.3, 102.2, 102.0, 84.7, 83.8, 76.2, 71.7, 63.1, 62.4, 61.7; HRMS (ESI) calcd. for $C_{27}H_{23}N_2O_9S$ $[M-H]^-$ 551.1133; found 551.1133.

3-deoxy-3-[N-(4-fluorobenzamide)amino]-2,5-anhydro-D-mannitol (9)

To a homogenous solution of amine **2** (0.15 g, 0.92 mmol) in MeOH (10 mL), NHS ester of 4-fluoro benzoyl chloride (prepared using the reported procedure,[53] 0.17g, 1.1 mmol) was added. The clear solution was stirred for 15 h at room temperature. Evaporation of MeOH under reduced pressure afforded the crude compound, which was purified using silica gel column chromatography eluted with a DCM/MeOH solvent mixture (gradient from 100:0 to 93:3). Fractions containing the desired product were combined and concentrated under vacuum to yield clear oil **9** (0.09 g, 45%). R_f 0.46 (DCM/MeOH, 90:10); $[\alpha]_D^{20}$ +4.28 (*c* 0.70, MeOH); IR (cast film) 3381, 2925, 2485, 1635, 1605, 1446, 1235, 1053, 852cm^{-1}; ^1H NMR (700 MHz, D_2O): δ 7.83 (dd, *J* = 8.7, 5.4 Hz, 2H), 7.26 (app t), 4.51 (t, *J* = 8.0 Hz, 1H), 4.30 (t, *J* = 7.9 Hz, 1H), 4.05 (ddd, *J* = 8.3, 5.4, 2.9 Hz, 1H), 4.02 (ddd, *J* = 8.0, 5.2, 2.9 Hz, 1H), 3.85 (dd, *J* = 12.5, 2.9 Hz, 1H), 3.81 (dd, *J* = 12.5, 3.0 Hz, 1H), 3.77–3.74 (m, 1H), 3.74–3.71 (m, 1H). ^{13}C NMR (176 MHz, D_2O): δ 171.2, 165.7 (d, *J* = 249.7 Hz), 130.5 (d, *J* = 9.3 Hz), 130.5, 116.5 (d, *J* = 22.2 Hz), 83.4, 81.6, 75.4, 62.3, 61.7, 58.0; HRMS (ESI) calcd. for $C_{13}H_{16}FNO_5Na$ $[M+Na]^+$ 308.0905; found 308.0905.

3-deoxy-3-[N-(tert-butyl-2-amino-2-oxoethoxycarbamate)]-2,5-anhydro-D-mannitol (I)

In a 50 mL round bottom flask, maintained under N_2 atmosphere, amine **2** (0.22 g, 1.3 mmol) was dissolved in MeOH (20 mL). NHS ester of aminoxy acetic acid

(prepared using reported procedure,[54] 0.75 g, 2.5 mmol) was added in the flask and vigorous stirring was continued for 12 h at room temperature. The solvent was removed under vacuum, providing the crude compound, which was subjected to silica gel column chromatography using a DCM/MeOH solvent mixture (gradient from 100:0 to 95:5). Fractions containing the desired product were combined and concentrated under vacuum to yield clear oil **10a** (0.22 g, 55%). R_f 0.61 (DCM/MeOH, 80:20); $[\alpha]_D^{20}$ +22.76 (*c* 1.0, MeOH); IR (cast film) 3274, 2979, 2934, 1715, 1659, 1459, 1370, 1286, 1164, 1116, 1047, 849 cm^{-1}; ^1H NMR (700 MHz, CD_3OD): δ 4.32 (d, *J* = 15.9 Hz, 1H), 4.27 (q, *J* = 8.3, 7.8 Hz, 1H), 4.14 (t, *J* = 7.0 Hz, 1H), 3.88 (dd, *J* = 5.2, 2.6 Hz, 1H), 3.87–3.85 (m, 1H), 3.75 (dd, *J* = 12.0, 3.0 Hz, 1H), 3.70 (dd, *J* = 12.0, 3.1 Hz, 1H), 3.63(m, 1H), 3.67–3.59 (m, 1H), 3.31 (m, 1H), 1.48 (s, 9H); ^{13}C NMR (176 MHz, CD_3OD): δ 172.0, 159.9, 85.1, 83.3, 83.2, 76.8, 76.4, 63.5, 62.9, 58.8, 28.5.; HRMS (ESI) calcd. for $C_{13}H_{24}N_2O_8Na$ $[M+Na]^+$ 359.1425; found 359.1423.

3-deoxy-3-[N-(2-(((4-fluorobenzylidene)amino)oxy)acetamide)amino]-2,5-anhydro-D-mannitol (10)

The tert-butyl carbamate intermediate obtained from the previous step **10a**, dissolved in DMF (10 mL) was treated with 5 mL of DCM/TFA (1/1 v/v) under N_2 atmosphere. After 8 h of stirring at room temperature, the solvent was removed under vacuum, yielding the corresponding amine **10b**, which was used for the next step without purification.

2-Fluorobenzaldehyde (102 µL, 0.95 mmol) and Et_3N (159 µL, 1.1 mmol) were added to a solution of amine **10b** (0.15 g, 0.60 mmol) in MeOH (5 mL). The reaction was allowed to stir at room temperature for 4 h under N_2 atmosphere. Then, the reaction mixture was concentrated under reduced pressure, providing a crude residue, which was purified through silica gel column chromatography using a DCM/MeOH solvent mixture (gradient from 100:0 to 93:7). Fractions containing the desired product were combined and concentrated under vacuum to yield compound **10** as a white solid (0.15 g, 70 %). R_f 0.45 (DCM/MeOH, 90:10); $[\alpha]_D^{20}$ +11.76 (*c* 0.50, MeOH); IR (cast film) 3326, 3108, 2925, 2873, 2486, 1653, 1511, 1467, 1230, 1157, 1078, 1018 cm^{-1}; ^1H NMR (700 MHz, CD_3OD): δ 8.26 (s, 1H), 7.67–7.64 (m, 2H), 7.16–7.12 (m,

2H), δ 4.62 (d, *J* = 4.5 Hz, 2H), 4.30 (t, *J* = 6.5 Hz, 1H), 4.12 (t, *J* = 6.2 Hz, 1H), 3.88–3.87 (m, 1H), 3.87–3.85 (m, 1H), 3.73 (dd, *J* = 12.0, 2.8 Hz, 1H), 3.67 (dd, *J* = 11.9, 3.4 Hz, 1H), 3.64–3.61 (m, 1H), 3.61–3.59 (m, 1H); ^{13}C NMR (176 MHz, CD_3OD): δ 172.5,165.3 (d, *J* = 249.3 Hz), 151.1,130.4 (d, *J* = 8.6 Hz), 129.5 (d, *J* = 3.2 Hz), 116.8 (d, *J* = 22.3 Hz), 85.7, 84.2, 77.0, 73.8, 63.7, 63.0, 58.9; HRMS (ESI) calcd. for $C_{15}H_{19}FN_2O_6Na$ $[M+Na]^+$ 365.1119; found 365.1118.

3-deoxy-3-[N-(7-hydroxy-2-oxo-2H-chromene-3-carboxamide)amino]-2,5-anhydro-D-mannitol (V)

Amine **2** (0.15 g, 0.92 mmol) was dissolved in MeOH (5 mL) under N_2 atmosphere. NHS ester of 7-hydroxy coumarin-3-carboxylic acid (prepared using reported procedure,[55,56] 0.33 g, 1.1 mmol) was added to this homogenous solution, and vigorous stirring of the mixture was continued at room temperature for 15 h. MeOH was removed under reduced pressure, and the crude compound was purified via silica gel column chromatography using a DCM/MeOH solvent mixture (gradient from 100:0 to 93:7). Fractions containing the desired product were combined and concentrated under vacuum to yield yellow oil **11c** (0.29 g, 85%). R_f 0.55 (DCM/MeOH, 90:10); $[\alpha]_D^{20}$ – 2.96 (*c* 0.25, MeOH); IR (cast film) 3470, 2989, 2945, 2523, 1705, 1653, 1410, 1231, 1081, 998, 816 cm^{-1}; ^{1}H NMR (700 MHz, CD_3OD): δ 8.78 (s, 1H), 7.67 (d, *J* = 8.6 Hz, 1H), 6.89 (dd, *J* = 8.6, 2.3 Hz, 1H), 6.77 (d, *J* = 2.2 Hz, 1H), 4.40 (t, *J* = 6.7 Hz, 1H), 4.22 (t, *J* = 6.4 Hz, 1H), 3.98–3.94 (m, 1H), 3.94–3.90 (m, 1H), 3.79–3.76 (m, 1H), 3.76–3.73 (m, 1H), 3.70 (m, 1H), 3.67 (m, 1H)); ^{13}C NMR (176 MHz, CD_3OD): δ 165.9, 164.9, 163.1, 158.3, 149.9, 133.0, 115.7, 114.1, 112.7, 103.1, 85.6, 84.4, 77.4, 63.8, 63.0, 60.0; HRMS (ESI) calcd. for $C_{16}H_{16}NO_8$ $[M-H]^-$ 350.0881; found 350.0881.

3-deoxy-3-[N-(7-(2-fluoroethoxy)-2-oxo-2H-chromene-3-carboxamide)amino]-2,5-anhydro-D-mannitol (11)

Compound **11c** (0.19 g, 0.57 mmol) and DMF (15 mL) were stirred in a 50 mL round bottom flask, maintained under N_2 atmosphere, until it was completely dissolved. K_2CO_3 (0.12 g, 0.85 mmol) was the added in the flask, followed by the addition of 2-fluoro ethyl tosylate (prepared using the reported procedure,[57] 0.375 g, 1.7 mmol), and the resulting mixture was heated at 110 °C for 1 h. After this time, the solids were

filtered off, and the filtrate was then concentrated under reduced pressure. The resultant crude compound was subjected to silica gel column chromatography eluted with a DCM/MeOH solvent mixture (gradient from 100:0 to 95:5). Fractions containing the desired product were combined and concentrated under vacuum to yield yellow oil **11** (0.11 g, 50%). R_f 0.65 (DCM/MeOH, 90:10); $[\alpha]_D^{20}$ +10.20 (*c* 0.05, MeOH); IR (cast film) ύ = 3332, 2919, 1710, 1616, 1601, 1561, 1454, 1370, 1226, 1149, 1062, 912 cm^{-1}; ^1H NMR (700 MHz, D_2O): δ 8.72 (s, 1H), 7.75 (d, *J* = 8.7 Hz, 1H), 7.08 (dd, *J* = 8.8, 2.3 Hz, 1H), 7.03 (s, 1H), 4.89 (dt, *J* = 47.5, 3.7 Hz, 2H), 4.52 (t, *J* = 7.2 Hz, 1H), 4.49–4.40 (m, 2H), 4.36 (t, *J* = 7.0 Hz, 1H), 4.13 (ddd, *J* = 8.2, 5.4, 3.0 Hz, 1H), 4.05 (ddd, *J* = 7.9, 5.4, 2.6 Hz, 1H), 3.86 (dd, *J* = 12.3, 2.8 Hz, 1H), 3.83 (dd, *J* = 12.4, 3.1 Hz, 1H), 3.77 (t, *J* = 5.0 Hz, 1H), 3.75 (d, *J* = 4.4 Hz, 1H); ^{13}C NMR (176 MHz, D_2O): δ 165.7, 164.1, 162.8, 158.1, 149.6, 132.7, 115.6, 115.3, 113.9, 102.0, 85.6, 84.4, 82.7 (d, *J* = 169.7 Hz), 77.4, 69.5 (d, *J* = 19.8 Hz), 63.8, 63.0, 60.1; HRMS (ESI) calcd. for $C_{18}H_{20}FNO_8Na$ $[M+Na]^+$ 420.1065; found 420.1069.

2.4.2. In vitro cell experiments

Instruments

WIZARD2 automatic *γ*-counter (Perkin Elmer, Waltham, MA, USA).

Buffer solutions

Glucose-free Krebs–Ringer buffer solution (120 mM NaCl, 25 mM $NaHCO_3$, 4 mM KCl, 1.2 mM KH_2PO_4, 2.5 mM $MgSO_4$, 70 μM $CaCl_2$, pH 7.4) was used for the studies with EMT6 cells. Cold phosphate-buffered saline (PBS) was used to wash the extracellular probes (137 mM NaCl, 2.7 mM KCl, 10 mM Na_2HPO_4, 2 mM KH_2PO_4). RIPA buffer (Sigma-Aldrich, St. Louis, MO, U.S.A.) was used for cell lysis.

Radiotracer synthesis

Radiotracer 6-[^{18}F] FDF was synthesized at the Division of Oncologic Imaging at the Department of Oncology using a GE TracerLab MX automated synthesis unit (GE Healthcare Canada Inc., Mississauga, Ontario, Canada). The synthesis was accomplished according to the well-established reported radiosynthesis procedure.[31,43]

Cell culture

Murine EMT6 mammary gland tumor cells were grown in a humidified 5% CO_2 incubator at 37 °C, in Gibco DMEM/F-12 media supplemented with 15 mM HEPES, l-glutamine, 10% fetal bovine serum (GIBCO 12483; Gibco, Gaithersburg, MD) and 1% penicillin/streptomycin with media renewal every 2 to 3 d.

General procedure for in vitro inhibition of 6-[^{18}F]FDF Cell Uptake

Competition binding experiments of 2,5-anhydro-D-mannitol derivatives and D-fructose were carried out in a dose-dependent manner to determine half-maximum inhibition concentrations (IC_{50}).

EMT6 cells were grown to confluence in 12-well cell culture plates, with media renewal every 2 d. One hour prior to the experiment, cell culture media were removed, and the plates were washed twice with glucose–free Krebs–Ringer buffer solution. To each well, 1 mL of glucose-free Krebs–Ringer buffer solution was added, and incubation at 37 °C was continued for 1 h under the glucose-free condition. After 1 h, the Krebs–Ringer buffer was removed. To each well, 400 µL of glucose-free Krebs–Ringer buffer was added containing 0.1–0.5 MBq of 6-[^{18}F]FDF and different concentrations of the 2,5-AM derivatives **3-11** (10^{-8}–10^{-3} –3 × 10^{-2} M) or fructose (10^{-5}–1 M) and no compound at all for comparison (= 100% uptake).

After 60 min incubation time, radiotracer uptake was stopped with 1 mL of ice-cold PBS, and the cells were washed twice with PBS and lysed in 0.4 mL radioimmunoprecipitation assay buffer (RIPA buffer). Then, the radioactivity in the cell lysates was determined as counts per minute (CPM) using a WIZARD2 automatic γ-counter (Perkin Elmer, Waltham, MA, U.S.A.) and converted to the radioactivity dose SI unit Becquerel (Bq). Data were analyzed as a percent of maximum uptake of 6-[^{18}F]FDF. Graphs were constructed using GraphPad Prism 5.0 (GraphPad Software, San Diego, CA, U.S.A.), and half-maximum inhibition concentrations (IC_{50}) were determined from the concentration-inhibition curves by graphical analysis.

2.4.3. Molecular docking

The molecular structures of the ligands were built using ChemBioDraw Ultra version 14.0, and their energy was minimized using the MMFF94x force field with ChemBio3D Ultra to produce the lowest energy conformer, followed by another

preparation using the LigPrep module using the Schrödinger Small Molecule Discovery Suite. The crystal structure of the GLUT5 receptor in the inward-open conformation (PDB ID: 4YB9) was used for our computational studies. The Protein Preparation Wizard module was used to add hydrogen atoms, minimize energy, and create appropriate protonation states of amino acid side chains. The Sitemap module in the Schrödinger suite was used to aid the prediction of the possible binding sites. Parameters were set to produce five sites, which were compared carefully to the reported binding site of GLUT5. A receptor grid file was generated, based on the prepared protein active site accounting for the most probable binding pocket. The docking algorithm Glide in extra precision (XP) was used to perform all molecular docking studies.[58] The docking generated 10 poses for each complex in which the top scoring poses were selected for further evaluation by MD simulations.

Molecular dynamics simulations

All systems were embedded in a lipid membrane of POPC lipids using the CHARMM-GUI server.[59] The systems were solvated with TIP3P water molecules, and Na^+ and Cl^- ions were added to create a neutral system with an ion concentration of 0.15 M and box dimensions of 100 Å × 100 Å × 110 Å. Then, the systems for MD were setup using leap for Amber18 with the AmberFF14SB forcefield with the additional lipid14 forcefield for the POPC membrane.

The ligands were parametrized using the Antechamber package in AMBER18 using the AM1-BCC charge model with the GAFF forcefield. The solvated systems were subject to 5000 steps of steepest descent minimization, followed by 5000 steps of conjugate gradient minimization using pmemd. Initially, the systems were heated as an NVT ensemble to 100 K using a Langevin thermostat for 2500 steps, while the membrane was restrained with a force constant of 10 kcal/mol. The system's pressure was equilibrated with as an NPT ensemble to 1 atm with gradual heating to 300 K, which was performed for 50000 steps, while restraining the lipid membrane. This was followed by a short MD run of 5 ns, without lipid restraints as an NVT ensemble. The simulations were continued for 50 ns. During the MD simulations, the equations of motion were integrated using a 2 fs time step, and the atomic coordinates were saved

to the trajectory, producing 5000 frames. The analysis of the resultant trajectories was performed using CPPTRAJ and VMD. [60,61] Figures were rendered from snapshots using Pymol. For MD snapshots extracted from the production simulations, we calculated the enthalpic portion of the binding energy using the Molecular Mechanics/Generalized Born Surface Area (MM/GBSA) method implemented in the MMPBSA.py script.[51] In MM/GBSA, the free energy change due to ligand binding is calculated as:

$$\Delta G_{\text{bind,solv}} = \Delta G_{\text{MM,vac}} + \Delta G_{\text{solv,complex}} - (\Delta G_{\text{solv,ligand}} + \Delta G_{\text{solv,protein}})\, T\Delta S \quad (1)$$

where $\Delta G_{\text{MM,vac}}$ includes averaged non-bonded molecular mechanics terms (electrostatic and van der Waals) occurring between protein and ligand. Solvation terms are modeled as:

$$\Delta G_{\text{solv}} = \Delta G_{\text{solv,polar}} + \Delta G_{\text{solv,non-polar}} \quad (2)$$

2.5. References

1. Lin, L.; Yee, S. W.; Kim, R. B.; Giacomini, K. M. SLC transporters as therapeutic targets: emerging opportunities. *Nat. Rev. Drug Discov.* **2015***, 14*, 543–560.

2. Colas, C.; Ung P. M.; Schlessinger, A. SLC transporters: structure, function, and drug discovery. *Med. Chem. Comm.* **2016**, *7*, 1069–1081.

3. Kotsampasakou, E.; Ecker, G. F.; Sitte, H. H.; Mannhold, R.; Buschmann, H.; Clausen, R. P.; Transporters as Drug Targets. Eds **2017**, 271-324.

4. Marger, M. D.; Saier Jr, M. H. A major superfamily of transmembrane facilitators that catalyse uniport, symport and antiport. *Trends Biochem. Sci.* **1993**, *18*, 13–20.

5. Manolescu, A. R.; Witkowska, K.; Kinnaird, A.; Cessford, T.; Cheeseman, C. Facilitated hexose transporters: new perspectives on form and function. *Physiology* **2007**, *22*, 234–240.

6. García-Álvarez, I.; Garrido, L.; Fernández-Mayoralas, A. Studies on the uptake of glucose derivatives by red blood cells. *ChemMedChem* **2007**, *2*, 496–504.

7. McQuade, D. T.; Plutschack, M. B.; Seeberger, P. H. Passive fructose transporters in disease: a molecular overview of their structural specificity. *Org. Biomol. Chem.* **2013**, *11*, 4909–4920.

8. Mueckler, M.; Thorens, B. The SLC2 (GLUT) family of membrane transporters. *Mol. Aspects Med.* **2013***, 34,* 121–138.

9. Tappy, L.; Lê, K. A. Metabolic effects of fructose and the worldwide increase in obesity. *Physiol. Rev.* **2010***, 90,* 23–46.

10. Gaby, A. R. Adverse effects of dietary fructose. *Altern. Med. Rev.* **2005**, *10*, 294-306.

11. Camps, M.; Castelló, A.; Muñoz, P.; Monfar, M.; Testar, X.; Palacín, M.; Zorzano, A. Effect of diabetes and fasting on GLUT-4 (muscle/fat) glucose-transporter expression in insulin-sensitive tissues. Heterogeneous response in heart, red and white muscle. *Biochem. J.* **1992***, 282*, 765–772.

12. Medina, R. A.; Owen, G. I. Glucose transporters: expression, regulation, and cancer. *Biol. Res.* **2002***, 35*, 9–26.

13. Adekola, K.; Rosen, S. T.; Shanmugam, M. Glucose transporters in cancer metabolism. *Curr. Opin. Oncol.* **2012**, *24*, 650–654.

14. Kostakoglu, L.; Agress Jr. H.; Goldsmith, S. J. Clinical role of FDG PET in evaluation of cancer patients. *RadioGraphics* **2003,** *23*, 315–340.

15. Joost, H. G.; Bell, G. I.; Best, J. D.; Birnbaum, M. J.; Charron, M. J.; Chen, Y. T.; Doege, H.; James, D. E.; Lodish, H. F.; Moley, K. H.; Moley, J. F.; Mueckler, M.; Rogers, S.; Schürmann, A.; Seino, S.; Thorens, B. Nomenclature of the GLUT/SLC2A family of sugar/polyol transport facilitators. *Am. J. Physiol. Metab.* **2002**, *282*, E974–E976.

16. Fan, X.; Liu, H.; Liu, M.; Wang, Y.; Qiu, L.; Cui, Y. Increased utilization of fructose has a positive effect on the development of breast cancer. *PeerJ.* **2007**, *5*, e3804.

17. Douard, V.; Ferraris RP. Regulation of the fructose transporter GLUT5 in health and disease. *Am. J. Physiol. Endocrinol. Metab.* **2008**, *238*, E227-E237; original literature: Kane, S.; Seatter, M. J.; Gould, G. W. Functional studies of human GLUT5:effect of pH on substrate selection and an analysis of substrate interactions. *Biochem. Biophys. Res. Commun.* **1997***, 238*, 503-505; Mate, A.; Barfull, A.; Hermosa, A. M.; Planas, J. M.; Vazquez, C. M. Regulation of D-fructose transporter GLUT5 in the ileum of spontaneously hypertensive rats. *J. Membr. Biol.* 199 (2004), 173-179; Gorovits, N.; Charron, M. J; What we know about facilitative glucose transporters:

lessons from cultured cells, animal models, and human studies. *Biochem. Mol. Biol. Educ.* **2008**, *31*, 163-172.

18. Chen, W. L.; Wang, Y. Y.; Zhao, A.; Xia, L.; Xie, G.; Su, M.; Zhao, L.; Liu, J.; Qu, C.; Wei, R.; Rajani, C.; Ni, Y.; Cheng, Z.; Chen, Z.; Chen, S.; Jia, W. Enhanced fructose utilization mediated by SLC2A5 is a unique metabolic feature of acute myeloid leukemia with therapeutic potential. *Cancer Cell* **2016***, 30*, 779–791.

19. Weng, Y.; Zhu, J.; Chen, Z.; Fu, J.; Zhang, F. Fructose fuels lung adenocarcinoma through GLUT5. *Cell Death Dis.* **2018***, 9*, 1-4.

20. Villaamil, V. M.; Gallego, G. A.; Rubira, L. V.; Campelo, R. G.; Valladares-Ayersbes, M.; Pulido, E. G.; Bolós, M. V.; Caínzos, I. S.; Aparicio, L. M. A. Fructose transporter GLUT5 expression in clear renal cell carcinoma. *Oncol. Rep.* **2011**, *25*, 315–323.

21. Zamora-León, S. P.; Golde, D. W.; Concha, I. I.; Rivas, C. I.; Delgado-López, F.; Baselga, J.; Nualart, F.; Vera, J. C. Expression of the fructose transporter GLUT5 in human breast cancer. *Proc. Natl. Acad. Sci.* **1996**, *93*, 1847–1852.

22. Hamann, I.; Krys, D.; Glubrecht, D.; Bouvet, V.; Marshall, A.; Vos, L.; Mackey, J. R.; Wuest, M.; Wuest, F.; Expression and function of hexose transporters GLUT1, GLUT2, and GLUT5 in breast cancer—effects of hypoxia. *FASEB J.* **2018**, *32*, 5104-5118.

23. Nomura, N.; Verdon, G.; Kang, H. J.; Shimamura, T.; Nomura, Y.; Sonoda, Y.; Hussien, S. A.; Qureshi, A. A.; Coincon, M.; Sato, Y.; Abe, H.; Nakada-Nakura, Y.; Hino, T.; Arakawa, T.; Kusano-Arai, O.; Iwanari, H.; Murata, T.; Kobayashi, T.; Hamakubo, T.; Kasahara, M.; Iwata, S.; Drew, D. Structure and mechanism of the mammalian fructose transporter GLUT5. *Nature* **2015***, 526,* 397–401.

24. Review literature: Tanasova, M.; Fedie, JR. Molecular tools for facilitative carbohydrate transporters (Gluts). *Chembiochem* **2017**, *18*, 1774-1788; original literature: Girniene, J.; Tatibouët, A.; Sackus, A.; Yang, J.; Holman, G. D.; Rollin, P. Inhibition of the D-fructose transporter protein GLUT5 by fused-ring glyco-1, 3-oxazolidin-2-thiones and-oxazolidin-2-ones. *Carbohydr. Res.* **2003**, *338*, 711-719.

25. Barnett, J. E. G.; Holman, G. D.; Munday, K. A. Structural requirements for binding

to the sugar-transport system of the human erythrocyte. *Biochem. J.* **1973***, 131*, 211–221.

26. Barnett, J. E.; Holman, G. D.; Chalkley, R. A.; Munday, K. A. Evidence for two asymmetric conformational states in the human erythrocyte sugar-transport system. *Biochem. J.* **1975***, 145*, 417–429.

27. Rees, W. D.; Holman, G. D. Hydrogen bonding requirements for the insulin-sensitive sugar transport system of rat adipocytes. *Biochim. Biophys. Acta- Biomembr.* **1981***, 646*, 251–260.

28. Holman, G. D.; Rees, W. D. Side-specific analogues for the rat adipocyte sugar transport system. *Biochim. Biophys. Acta - Biomembr.* **1982,** *685*, 78–86.

29. Holman, G. D.; Midgley, P. J. W. Synthesis of novel bis (d-mannose) compounds. *Carbohydr. Res.* **1985**, *135*, 337–341.

30. Abbadi, M.; Holman, G. D.; Morin, C.; Rees, W. D.; Yang, J. Synthesis of symmetrical 4, 4′-and 6, 6′-bis (d-glucose)-based probes as tools for the study of d-glucose transport proteins. *Tetrahedron Lett.* **1999,** *40*, 5861–5864.

31. Bouvet, V.; Jans, H. S.; Wuest, M.; Soueidan, O. M.; Mercer, J.; McEwan, A. J. B.; West, F. G.; Cheeseman, C. I.; Wuest, F. Automated synthesis and dosimetry of 6-deoxy-6-[18F] fluoro-D-fructose (6-[18F] FDF): a radiotracer for imaging of GLUT5 in breast cancer. *Am. J. Nucl. Med. Mol. Imaging* **2014***, 4,* 248–259.

32. Soueidan, O. M.; Scully, T. W.; Kaur, J.; Panigrahi, R.; Belovodskiy, A.; Do, V.; Matier, C. D.; Lemieux, M. J.; Wuest, F.; Cheeseman, C. I.; West, F. G. Fluorescent hexose conjugates establish stringent stereochemical requirement by glut5 for recognition and transport of monosaccharides. *ACS Chem. Biol.* **2017***, 12*, **1**087–1094.

33. Wuest, M.; Hamann, I.; Bouvet, V.; Glubrecht, D.; Marshall, A.; Trayner, B.; Soueidan, O. M.; Krys, D.; Wagner, M.; Cheeseman, C.; West, F.; Wuest, F. Molecular imaging of GLUT1 and GLUT5 in breast cancer: a multitracer positron emission tomography imaging study in mice. *Mol. Pharmacol.* **2018**, *93*, 79-89.

34. Tatibouët, A.; Yang, J.; Morin, C.; Holman, G. D. Synthesis, and evaluation of fructose analogues as inhibitors of the D-fructose transporter GLUT5. *Bioorg. Med. Chem.* **2000**, *8*, 1825-1833.

35. Inukai, K.; Katagiri, H.; Takata, K.; Asano, T.; Anai, M.; Ishihara, H.; Nakazaki, M.; Kikuchi, M.; Yazaki, Y.; Oka, Y. Characterization of rat GLUT5 and functional analysis of chimeric proteins of GLUT1 glucose transporter and GLUT5 fructose transporter. *Endocrinology* **1995**, *136*, 4850-4857.

36. Soueidan, O. M.; Trayner, B. J.; Grant, T. N.; Henderson, J. R.; Wuest, F.; West, F. G.; Cheeseman, C. I. New fluorinated fructose analogs as selective probes of the hexose transporter protein GLUT5. *Org. Biomol. Chem.* **2015***, 13*, 6511-6521.

37. Tanasova, M.; Plutschack, M.; Muroski, M. E.; Sturla, S. J.; Strouse, G. F.; McQuade, D. T. Fluorescent THF-based fructose analogue exhibits fructose-dependent uptake. *ChemBioChem.* **2013***, 14,* 1263–1270.

38. Kumar Kondapi, V. P.; Soueidan, O. M.; Cheeseman, C. I.; West, F. G. Tunable GLUT–Hexose Binding and Transport via Modulation of Hexose C-3 Hydrogen-Bonding Capabilities. *Chem. Eur. J.* **2017***, 23,* 8073–8081.

39. For an alternative strategy relying on C-1 modification of 2,5-AM with fluorophores, see: Begoyan, V. V.; Weseliński, Ł. J.; Xia, S.; Fedie, J.; Kannan, S.; Ferrier, A.; Rao, S.; Tanasova, M. Multicolor GLUT5-permeable fluorescent probes for fructose transport analysis. *Chem Commun* **2018**, *54*, 3855-3858.

40. Kumar Kondapi, V. P.; Soueidan, O. M.; Hosseini, S. N.; Jabari, N.; West, F. G. Efficient and Easy Access to Optically Pure Tetrasubstituted Tetrahydrofurans via Stereoselective Opening of C2-Symmetric Epoxide and Aziridine Rings. *Eur. J. Org. Chem.* **2016**, *7*, 1367–1379.

41. Tang, F.; Yang, Y.; Tang, Y.; Tang, S.; Yang, L.; Sun, B.; Jiang, B.; Dong, J.; Liu, H.; Huang, M.; Geng, M.Y.; Huang, W. One-pot N-glycosylation remodeling of IgG with non-natural sialylglycopeptides enables glycosite-specific and dual-payload antibody–drug conjugates. *Org. Biomol. Chem.* **2016***, 14*, 9501–9518.

42. Trayner, B. J.; Grant, T. N.; West, F. G.; Cheeseman, C. I. Synthesis and characterization of 6-deoxy-6-fluoro-D-fructose as a potential compound for imaging breast cancer with PET. *Bioorg. Med. Chem.* **2009**, *17*, 5488-5495.

43. Wuest, M.; Trayner, B. J.; Grant, T. N.; Jans, H. S.; Mercer, J. R.; Murray, D.; West, F. G.; McEwan, A. J. B.; Wuest, F.; Cheeseman, C. I. Radiopharmacological

evaluation of 6-deoxy-6-[18F] fluoro-D-fructose as a radiotracer for PET imaging of GLUT5 in breast cancer. *Nucl. Med. Biol.* **2011**, *38*, 461-475.

44. Thompson, A. M. G.; Iancu, C. V.; Nguyen, T. T. H.; Kim, D.; Choe, J. Y. Inhibition of human GLUT1 and GLUT5 by plant carbohydrate products; insights into transport specificity. *Sci Rep.* **2015**, *5*, 1-10.

45. George Thompson, A. M.; Ursu, O.; Babkin, P.; Iancu, C. V.; Whang, A.; Oprea, T. I.; Choe, J. Y. Discovery of a specific inhibitor of human GLUT5 by virtual screening and in vitro transport evaluation. *Sci. Rep.* **2016**, *6*, 24240.

46. a) Ainsley, J.; Chaturvedi, S. S.; Karabencheva-Christova, T. G.; Tanasova, M.; Christov,C. Z. Integrating molecular probes and molecular dynamics to reveal binding modes of GLUT5 activatory and inhibitory ligands. *Chem Commun* 54 (2018), 9917-9920. b) Ferreira, R. S.; Pons, J.-L.; Labesse, G. Insights into Substrate and Inhibitor Selectivity among Human GLUT Transporters through Comparative Modeling and Molecular Docking, *ACS Omega*, **2019**, *4*, 4748-4760.

47. Tian, C.; Kasavajhala, K.; Belfon, K. A. A.; Raguette, L.; Huang, H.; Migues, A. N.; Bickel, J.; Wang, Y.; Pincay, J.; Wu, Q.; Simmerling, C. ff19SB: Amino-acid-specific protein backbone parameters trained against quantum mechanics energy surfaces in solution. *J. Chem. Theory Comput.* **2019,** *16*, 528-552.

48. Wang, J.; Wang, W.; Kollman, P. A.; Case, D. A. Automatic atom type and bond type perception in molecular mechanical calculations.*J. Mol. Graph. Model.* **2006***,* 25, 247-260.

49. Bai, Q.; Zhang, Y.; Li, X.; Chen, W.; Liu, H.; Yao, X. Computational study on the interaction between CCR5 and HIV-1 entry inhibitor maraviroc: insight from accelerated molecular dynamics simulation and free energy calculation. *Phys. Chem. Chem. Phys.* 16 (2014), 24332-24338.

50. Genheden, S.; Ryde, U. The MM/PBSA and MM/GBSA methods to estimate ligand-binding affinities. *Expert Opin. Drug. Discov.* **2015,** *10*, 449-461.

51. Miller, B. R.; McGee, T. D.; Swails, J. M.; Homeyer, N.; Gohlke, H.; Roitberg, A.E. MMPBSA. py: an efficient program for end-state free energy calculations. *J. Chem. Theory Comput.* **2012**, *8*, 3314-3321.

52. Horton, D.; Philips, K. D. The nitrous acid deamination of glycosides and acetates of 2-amino-2-deoxy-D-glucose. *Carbohydr. Res.* **1973**, *30*, 367–374.

53. Brennauer, A. Acylguanidines as bioisosteric groups in argininamide-type neuropeptide Y Y1 and Y2 receptor antagonists: synthesis, stability and pharmacological activity (Doctoral dissertation) **2006**.

54. Tang, F.; Yang, Y.; Tang, Y.; Tang, S.; Yang, L.; Sun, B.; Jiang, B.; Dong, J.; Liu, H.; Huang, M.; Geng, M. Y.; Huang, W. One-pot N-glycosylation remodeling of IgG with non-natural sialylglycopeptides enables glycosite-specific and dual-payload antibody–drug conjugates. *Org. Biomol. Chem.* **2016**, *14*, 9501–9518.

55. Gnaccarini, C.; Ben-Tahar, W.; Mulani, A.; Roy, I.; Lubell, W. D.; Pelletier, J. N.; Keillor, J. W. Site-specific protein propargylation using tissue transglutaminase. *Org. Biomol. Chem.* **2012**, *10*, 5258–5265.

56. Shiota, S.; Yamamoto, S.; Shimomura, A.; Ojida, A.; Nishino, T.; Maruyama, T. Quantification of amino groups on solid surfaces using cleavable fluorescent compounds. *Langmuir* **2015**, *31*, 8824–8829.

57. Neumann, K. T.; Lindhardt, A. T.; Bang-Andersen, B.; Skrydstrup, T. *J. Label. Compd.* Synthesis and selective 2H-, 13C-, and 15N-labeling of the Tau protein binder THK-523. *Radiopharm.* **2017**, *60*, 30–35.

58. Halgren, T. A.; Murphy, R. B.; Friesner, R. A.; Beard, H. S.; Frye, L. L.; Pollard, W. T.; Banks, J. L. Glide: a new approach for rapid, accurate docking and scoring. 2.Enrichment factors in database screening. *J. Med. Chem.* 2004, 47, 1750-1759.

59. Jo, S.; Kim, T.; Iyer, V. G.; Im, W. CHARMM-GUI: a web-based graphical user interface for CHARMM. *J. Comput. Chem.* **2008**, *29*, 1859-1865.

60. Roe, D. R.; Cheatham III, T. E. PTRAJ and CPPTRAJ: software for processing and analysis of molecular dynamics trajectory data. *J. Chem. Theory Comput*. **2013**, *9*, 3084-3095.

61. Humphrey, W.; Dalke, A.; Schulten, K. VMD: visual molecular dynamics. *J. Mol. Graph.* **1996**, *14*, 27-38.

Chapter 3

Development and analysis of 2,5-anhydro-D-mannitol derivatives as radiotracer and fluorescent probes for imaging breast cancer cells

3.1. Introduction

Breast cancer constitutes to be second leading cause of cancer deaths and most common diagnosed malignancies in women worldwide.[1] With an early detection and better treatment, the survival rate of breast cancer patients has increased to 78-90% in the last three decades.[2] Specific biomarker detection and precision medicine concept involving diagnostic test of patient followed by selecting optimal and appropriate therapies is one of the optimal targeted therapies for monitoring a disease at the molecular level.[3] To date, physical examination or mammography is the most widely used method for the detection of primary breast cancer.[4,5] However, mammography offers some limitation in sensitivity and specificity as this method only relies on anatomical differences between normal and metabolically compromised cells with no specific information about molecular changes and processes at a cellular level.[4,5] As a result, other imaging methodologies offering functional imaging such as positron emission tomography (PET), single photon emission computed tomography (SPECT), magnetic resonance imaging (MRI) or higher resolution ultrasound are investigated and increasingly gaining importance to complement and increase the diagnostic accuracy in detection of breast cancer specifically metastatic disease.[6,7,8] In the clinics, the most common and widely used PET imaging agent, the glucose derivative 2-deoxy-2-[^{18}F]-fluoro-D-glucose (2-[^{18}F]FDG or [^{18}F]FDG), is utilized to detect increased glucose uptake and metabolism in variety of different cancers.[9,10] It is also used in assessing changes in tumor metabolism in response to therapy.[11] This radiolabeled hexose takes advantage of the characteristic overexpression of several members of the facilitative hexose transporter (GLUT) family.[12] GLUT1, GLUT3, GLUT4 and GLUT12 have been reported to be responsible for increased uptake of glucose and [^{18}F]FDG in malignant tissue.[13-15] Like glucose itself, [^{18}F]FDG upon entering the cells undergoes a first step

of metabolism, phosphorylation by kinase enzyme (hexokinase II).[16,17] However, [^{18}F]FDG-phosphate cannot be further metabolized, in contrast to glucose-6-phosphate, as it, as it is not a substrate for aldolase, the enzyme involved in second phosphorylation step. Thus, the increased glucose transport and metabolism within tumor cells results in an increasing accumulation of [^{18}F]FDG, allowing their detection via PET.[18,19]

However, several limitations of [^{18}F]FDG in specific tumor cell detection have spurred the development of alternative PET radiotracers.[20,21] Due to high glucose uptake/transport by macrophages and other immune cells involved in inflammation processes, increased uptake in areas of inflammation can create confusion between normal and tumor tissues, leading to the possibility of a false positive diagnosis.[22-24] In addition, it also has been reported that [^{18}F]FDG-PET demonstrates variable sensitivity and specificity specifically in breast cancer detection.[25] Several clinical studies analyzing the GLUT1 protein expression in breast cancer patients revealed that 28-47% of the patient samples were GLUT1 negative.[26] These findings may help explain the lower sensitivity of [^{18}F]FDG-PET in different types of breast cancer.[27] As a result, health regulatory bodies advise not to use [^{18}F]FDG-PET as a stand-alone methodology for diagnosis and treatment of both primary and metastatic breast cancer.[28] Therefore, there is a need for alternative biomarkers for abnormal cellular metabolism in breast tumors.

In addition to [^{18}F]FDG, alternative PET radiotracers targeting different receptors, transporters, enzymes over-expressed in breast cancer cells or changes in tumor microenvironment have been developed and tested for breast cancer imaging.[28] Among those were [^{18}F]16α-fluorestradiol ([^{18}F]FES) targeting estrogen receptors, ^{64}Cu- and ^{89}Zr-labeled monoclonal antibodies such as trastuzumab or pertuzumab targeting HER2 positive breast cancers, ^{18}F-fluorothymidine ([^{18}F]FLT) targeting tumor cell proliferation, ^{11}C-methionine or other radiolabeled amino acids such as ^{18}F-fluciclovine targeting amino acid transport and metabolism as well as ^{18}F-fluomisonidazole ([^{18}F]FMISO) targeting tumor hypoxia.[29] In 1996, Zamora-Leon et al. reported the elevated protein expression of the high affinity fructose transporter GLUT5 in human breast cells, proposing it as an alternative biomarker for diagnosis

and treatment of breast cancer.[30] Along with GLUT5, class I glucose/fructose transporting isoform GLUT2 is also involved in fructose transport across the cell membrane, although, there is a significant difference between their affinity for fructose (GLUT2 (76 mmol/L) < GLUT5 (6 mmol/L).[31] Both GLUT2 and GLUT5 were found to be overexpressed in breast cancer as wells as other cancers: close to 37% of breast tumor samples expressed GLUT5 and 31% expressed GLUT2.[32,33] This increased expression of fructose transporter proteins indicates that fructose uptake could contribute as an alternative energy fuel also leading to cancer progression. Besides increased glucose metabolism tumor cells could broaden/switch their nutrient pool in order to compensate for their increased demand of energy metabolism.[34] Due to the lower affinity and lack of selectivity (transporting both glucose and fructose displayed by GLUT2), GLUT5 has gained more attention due to its specific substrate preference for fructose only.[35] This has led to the development of development of D-fructose or 2,5-anhydro-D-mannitol (2,5-AM) derivatives labeled with radionuclide or fluorescent reporter groups that target GLUT5 (see Chapter 1).[29]

This direction may open new avenues for an alternative and improved diagnosis of breast cancer as well as other types of cancer which also exhibit similar GLUT protein expression profiles. While designing an ^{18}F-labeled fructose for PET imaging and fluorescently labeled fructose derivatives for optical imaging purposes, it is very important to decide on which position the fluorine atom should sit on fructose molecule as it may have major implications towards its proper binding with the transporter protein and subsequent intracellular metabolism through its specific enzyme reaction (kinases).[29] One of the important factors that should be considered is to ensure that the tracer is retained within the cancer cell once transported inside, as in the case of [^{18}F]FDG getting internalized and phosphorylated leading to its intracellular accumulation to facilitate prolonged imaging with PET.[34] Intracellular phosphorylation (first step of glycolysis) occurs via two distinct enzymes: ketohexokinase (fructokinase) at C-1 position and hexokinase at C-6 position.[36,37,38] Depending on the expression profile of the kinase enzymes in the tumor cells, the optimal labeling position of the fructose molecule should be selected. In mammalian cells, there are four

hexokinase isoforms expressed and out of those, the hexokinase I and II proteins are found to be overexpressed in many tumor cells with hexokinase II being the main isoform linked with high glycolytic rates.[39] Cell lines such as human MCF7 breast cancer show high levels of hexokinase I and II protein while other cell lines such as human MDA-MB-435 and MDA-MB-231 breast cancer display considerably lower protein expression levels of both hexokinases.[11]

However, the first fructose-derived PET tracer developed, 1-deoxy-1-[^{18}F]fluoro-D-fructose (Figure 3.1), studied by Haradahira et al., was evaluated in in a fibrosarcoma tumor bearing mouse model, but no GLUT5 levels were evaluated and also no trapping of 1-[^{18}F]FDF was observed.[40] Experiments in EMT6 tumor bearing mice confirmed that 1-[^{18}F]FDF was not trapped in these murine breast tumor cells,[28] indicating that this radiotracer was not strongly recognized by any kinases present in the cells, although, it should have been by hexokinase II as predicted by Haradahira et al. As derivatization at position C-1 of the fructose molecule prevents recognition by ketohexokinase, the next idea was to generate a fructose derivative substituted at position C-6.[41] In one approach, the Cheeseman, West, and Wuest groups carried out extensive studies on the fructose derivative 6-deoxy-6-[^{18}F]fluoro-D-fructose (6-[^{18}F]FDF), which was observed to be accumulated in GLUT5 expressing cell lines (Figure 3.1).[34,41] In addition, its non-radiolabeled version 6-FDF was observed to be more potent (IC_{50} = 19 mM) than natural substrate of GLUT5, fructose with an IC_{50} of 322 mM, indicating higher affinity of GLUT5 for 6-FDF than for its natural substrate.[34] However, in vitro radiotracer efflux experiments, substantial efflux was also detected by 6-[^{18}F]FDF in both EMT6 and MCF7 cell lines indicating no metabolic trapping via ketohexokinase-mediated phosphorylation. In vitro phosphorylation experiments with both hexokinase II and ketohexokinase enzymes showed that 6-[^{18}F]FDF was not phosphorylated by hexokinase II but it was indeed phosphorylated by ketohexokinase over 60 min incubation time.[34]

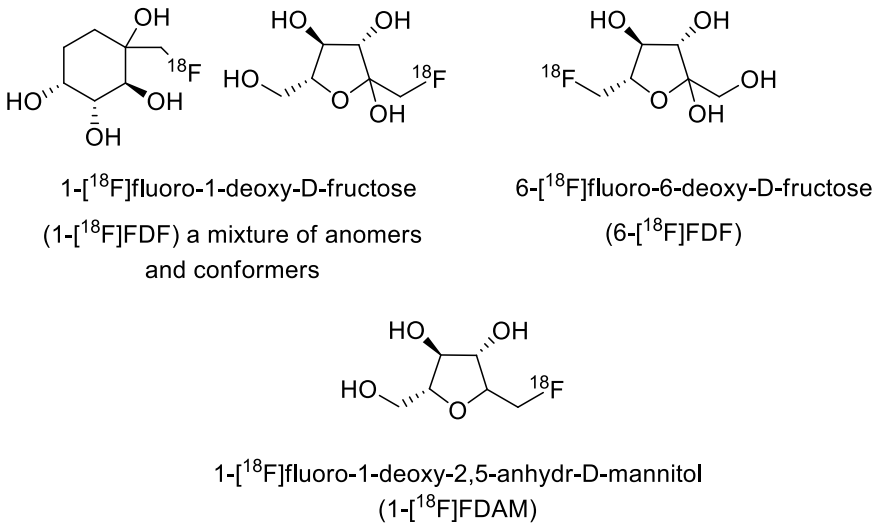

Figure 3.1. Radiolabeled fructose and 2,5-AM derivatives used for targeting GLUT5

However, 6-[^{18}F]FDF was also found to interact with and be transported by GLUT2.[29] Therefore, there was still the need to generate a radiolabeled molecule specifically targeting the GLUT5 transporter. Prior work suggested a focus on derivatives of 2,5-anhydro-D-mannitol (2,5-AM), which had demonstrated good specificity towards GLUT5 (see Chapter 1 and 2).

Initial generation of 1-deoxy-1-[^{18}F]fluoro-2,5-anhydro-mannitol (1-[^{18}F]FDAM) and it's in vitro and in vivo analysis in the murine mammary EMT6 model resulted in low cell and tumor tissue uptake with subsequent washout again (Figure 3.1), however its initial tumor uptake was somewhat higher than for 1-[^{18}F]FDF.[28] Based on those observations, further structural modification of the 2,5-AM scaffold seemed to be warranted.

We have previously examined a series of C-3 modified derivatives of 2,5-AM for their ability to inhibit the uptake of radiolabeled fructose in murine EMT6 mammary carcinoma cell lines. This study highlighted the importance of a strong hydrogen bond donor attached at C-3. With the goal of optimizing binding, transport and metabolic trapping of 2,5-AM derivatives, the next efforts were focused on a preparation of a series of derivatives that retain hydrogen bond donor capability at C-3 with a variety of functionalities and encompassing a range of steric demand.

Regarding the development of fluorescent derivatives, small compounds/molecules labeled with fluorescent tags exhibits a broader application in imaging as a safer, economical and an effective method to obtain higher and spatial resolution images. Several fructose based fluorescent probes have been developed and studied ranging from blue to red emission region (see Chapter 1).

Here I will discuss the development of various 2,5-AM derivatives as potential novel PET tracer and fluorescent probes. The goal of this study is to (A) evaluate and study the most potent compounds that were screened and identified in the previous chapter and based on that, to design and develop a novel PET radiotracer out of the library of C-3 modified 2,5-AM derivatives; and (B) label C-3 position of 2,5-AM with different fluorophores and perform confocal microscopy experiments to study the uptake of these probes into breast cancer cells in presence of both glucose and fructose.

3.2. Development of PET tracer

3.2.1. Radiotracer synthesis

In order to estimate the affinity of non-radiolabeled 2,5-AM derivatives for fructose mediated transport into breast cancer cells, half maximum inhibitory concentrations (IC_{50}) of all the compounds were determined in a cell-based competition assay. This assay involved measurement of cellular uptake (EMT6) of 6-[^{18}F]FDF in the absence and presence of increasing concentrations of various C-3 modified 2,5-AM derivatives, as well as D-fructose and cold 6-FDF as positive controls (Figure 3.2). Figure 3.3 depicts the calculated concentration response curves for the analyzed 2,5-AM derivatives inhibiting 6-[^{18}F]FDF uptake in comparison to control compounds 6-FDF and D-fructose.

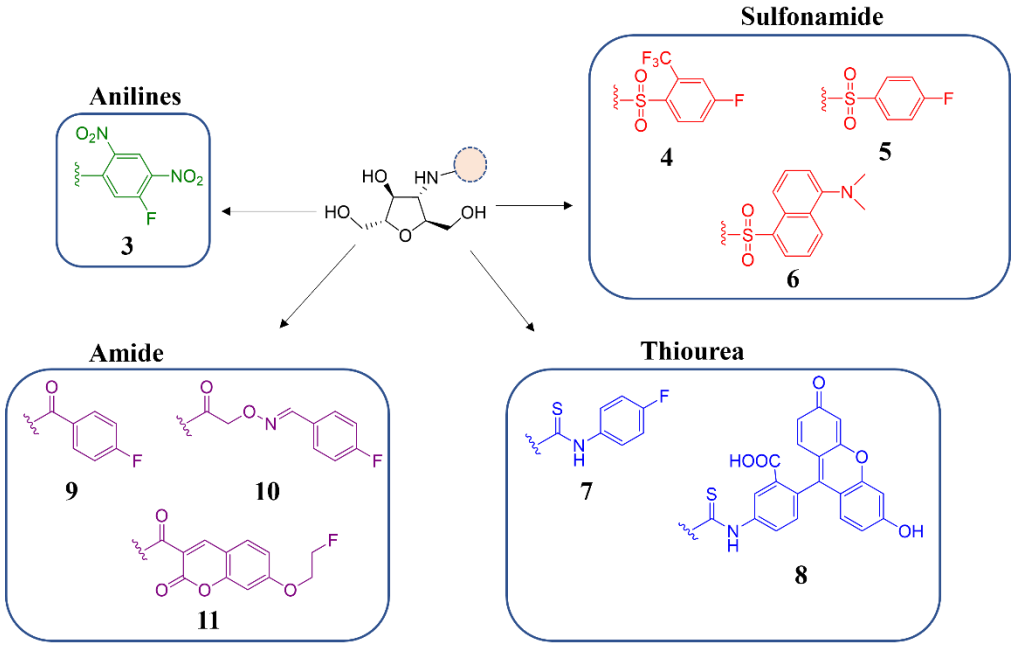

Figure 3.2. A selection of C-3 modified 2,5-AM compounds

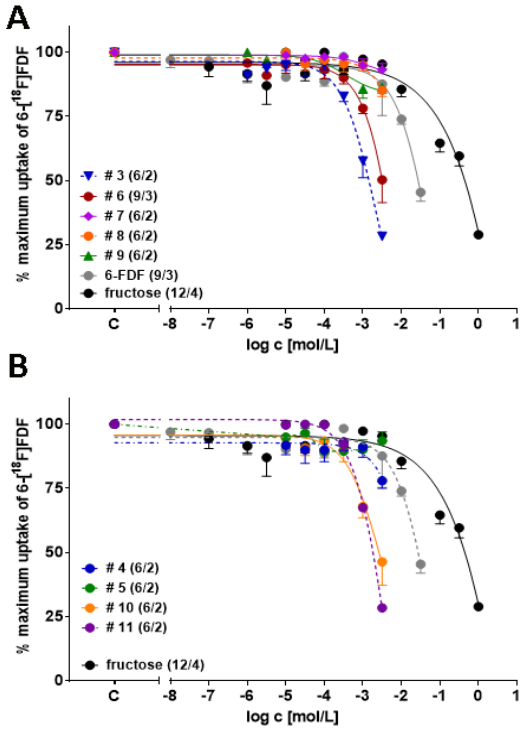

Figure 3.3. Concentration-dependent inhibition of 6[^{18}F]FDF uptake into EMT6 cells of C-3 modified 2,5-AM compounds (**4,5,10,11**), 6-FDF and, **fructose**). Data are shown as mean ± SEM of n data points from 2–4 experiments.

Out of this library of compounds, three 2,5-AM compounds displayed greater potency than 6-FDF and D-fructose (Figure 3.4). Nonlinear regression analysis furnished IC_{50} values of 1.10±0.17 mM **(3)**, 2.31±0.35 mM **(10)**, 1.71±0.08 mM **(11)** and 342±74 mM for fructose, suggesting that the potency of all those three compounds and their affinity for GLUT5 was approximately 10-fold higher than 6-FDF and 100-fold higher than fructose. Fructose possesses a low affinity for GLUT2 (K_m ~76 mM) versus GLUT5 (K_m ~15 mM), whereas glucose possesses a high affinity for both GLUT2 (K_m ~1 mM) and GLUT1 (K_m ~5 mM). This indicates that in the presence of high extracellular glucose/fructose concentrations, transport of a radiolabeled derivative of **3**, **10,** and **11** should occur almost exclusively via the GLUT5 machinery, since extracellular glucose should saturate GLUT2. Therefore, these three 2,5-AM derivatives were further selected to be developed as ^{18}F-radiolabeled compounds.

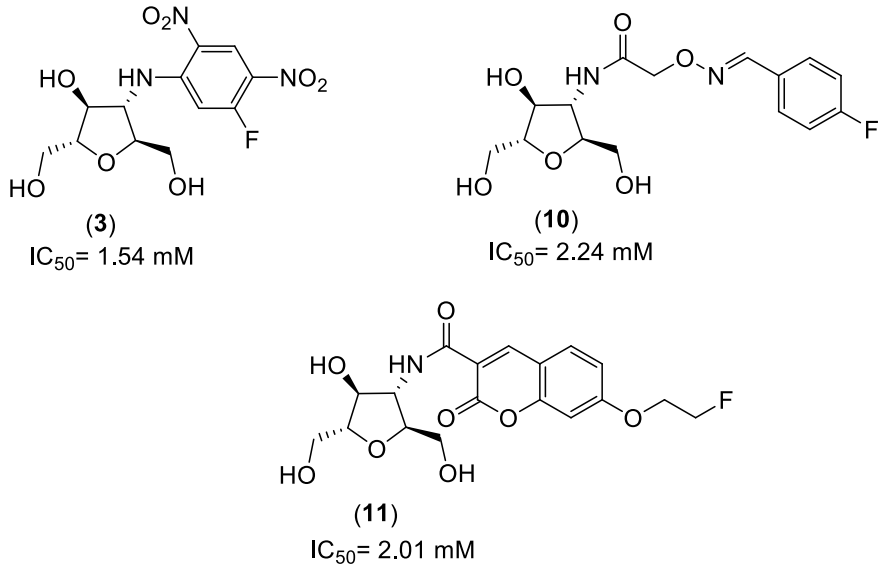

Figure 3.4. List of the three most potent C-3 modified 2,5-AM derivatives

Different strategies were proposed to incorporate ^{18}F into the compounds of interest. As depicted in Scheme 3.1, for the development of a cold reference compound **3,** it was hypothesized that radiofluorination could be achieved from nucleophilic

aromatic substitution (S_NAr) on the chloro dinitrophenyl substituent of precursor **12** with the fluoride. Unfortunately, no clean formation of the desired product was obtained (as confirmed through aromatic protons of the reaction mixture, in which no evidence of new $^{1}H–^{19}F$ couplings was observed).

Unfortunately, NMR analysis indicated the presence of only starting material. In the presence of cesium fluoride and crown ether (18-Crown-6, Table 3.1, entry 4), a mixture of starting material and product was obtained. However, due to almost nearly identical R_f values on TLC, their separation was a challenge.

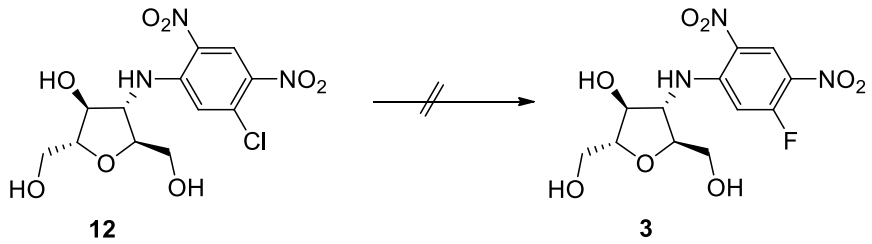

Scheme 3.1. Proposed synthesis of reference compound **3**

Table 3.1. Optimisation studies for synthesis of **3**

S. No.	Reagents	Solvent	Temp.	Observations
1.	KF (5equiv.) nBu_4NCl (5 eqiv.)	DMF	140˚C	Messy NMR
2.	CsF (5equiv.) nBu_4NCl (5 eqiv.)	DMF	140˚C	Messy NMR
3.	CsF (5eqiv.) 18-Crown-6	DMF	140˚C	Mixture of SM and product
4.	CsF (5equiv.) 18-Crown-6	Acetonitrile	140˚C	S.M. recovered
5.	CsF (5equiv.) t-BuOH	DMF	140˚C	Messy NMR

In a control experiment using 1,3-dichloro-4,6-dinitrobenzene as a model system (Scheme 3.2), a mixture of the mono- and di-fluorinated products **13** and **14** was obtained, as determined by ^{19}F NMR analysis.

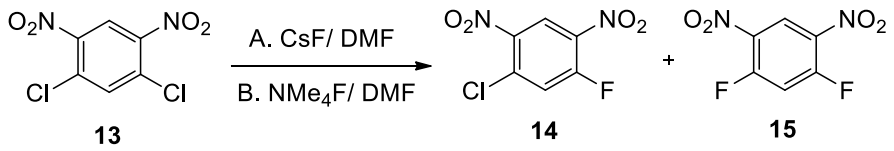

Scheme 3.2. Control (test) reaction

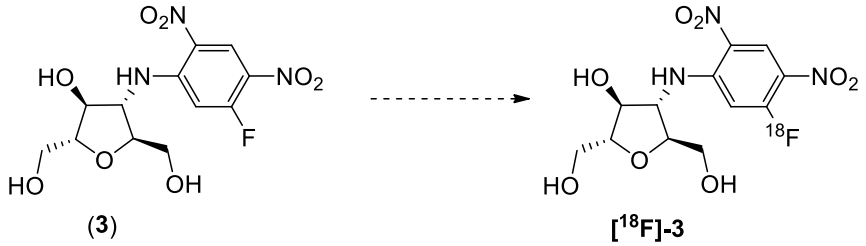

Scheme 3.3. Proposed scheme for synthesis of radiolabeled **[^{18}F]-3**

In radiochemical reactions, there are reports for substituting ^{19}F with ^{18}F, under specific reaction conditions in which a large concentration of ^{18}F is treated with starting material and radiochemical yield of the labeled product can be confirmed with HPLC analysis.[42] However, such reactions exhibit limitations with purity and final separation of the product. Due to contamination of ^{18}F labeled compound with non-radiolabeled starting material and traces of unreacted ^{18}F, low decay corrected yield makes it a challenge to develop a more efficient and atom economical reaction. Therefore, we focused on developing alternative compound **10** as an ^{18}F-labeled radiotracer.

Due to the well-established process for the synthesis of compound **10,** the non-radioactive reference compound was obtained by following the same steps starting with the readily available, glucosamine hydrogen chloride furnishing the final product with an overall 26% yield (Scheme 3.4) (see Chapter 2).

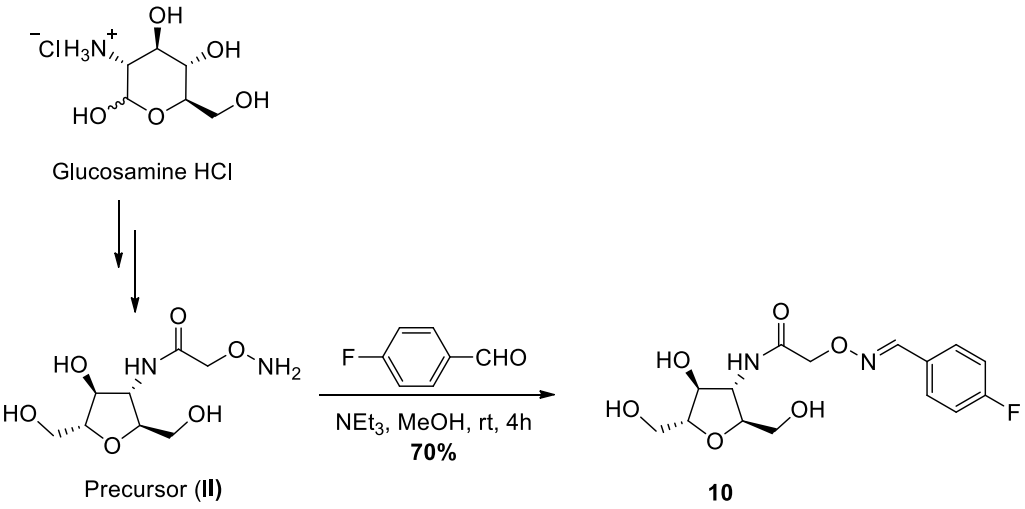

Scheme 3.4. Synthesis of reference compound **10**

The radiosynthesis of compound **10** was performed in a remotely controlled synthesis via two step procedure starting from deprotection of the boc protected precursor **I** followed by reaction of free amine **(II)** with radiolabeled building block, 4-[^{18}F]-fluorobenzaldehyde **([^{18}F]FBA**) in acetonitrile at 50 ℃ (Scheme 3.5). For optimization of the radiotracer synthesis different test reactions (Table 3.3) were performed by varying amount of precursor and time to optimize the best yielding

reaction conditions. All the test reactions resulted in the formation of the desired radiotracer product indicating the robustness of these conditions. The best reaction condition (Table 3.2, entry 1) was obtained in the presence of trifluoroacetic acid with 1 mg of precursor. Incorporation of ^{18}F by condensation reaction formed an oxime ether linkage giving [^{18}F]-**10** in a range of 23-61% radiochemical yield (non-decay corrected) within 60 min including HPLC purification. Therefore, [^{18}F]-**10** was then further used for in vitro and in vivo analysis and its properties were compared to 6-[^{18}F]-FDF to determine its in vitro and in vivo profile.

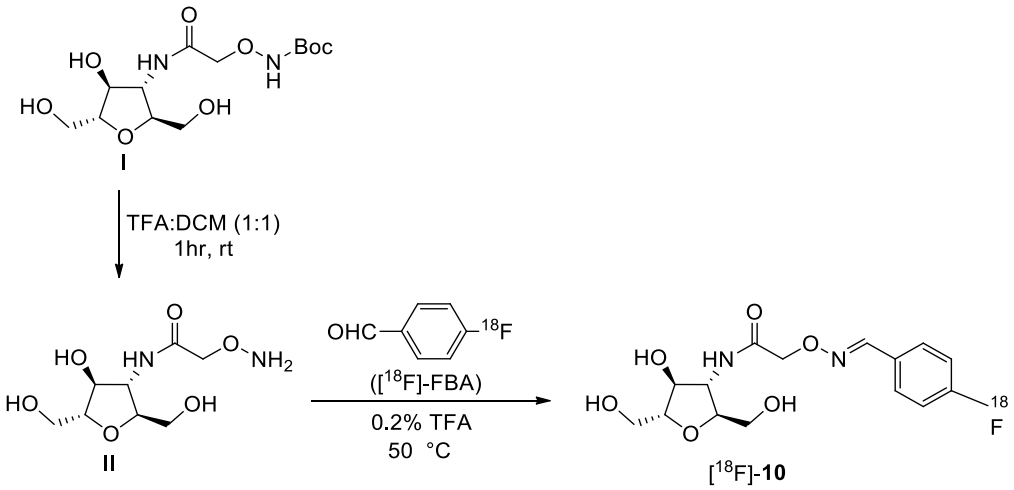

Scheme 3.5. Synthesis of radiolabeled [^{18}F]-**10**

Table 3.2. Optimization reaction conditions for [^{18}F]-**10**

No. of test reaction	Amount of precursor (mg)	Time(min)	% Yield (Radio-TLC)
1	1	30	**61**
2	1	30	56
3	1	20	41
4	1	5	48
5	0.5	5	48
6	0.25	5	23
7	1	10	57
8	0.5	10	58
9	0.25	1	28
10	1	15	59
11	0.5	15	50
12	0.25	15	31

3.2.2. Cell uptake studies

Radiotracer uptake (Figure 3.5) of [^{18}F]-**10** in murine breast cancer cell line EMT6 and in human triple negative breast cancer cell line MDA-MB-231 were compared to the uptake of 6-[^{18}F]FDF. In EMT6 cells, cellular uptake of 6-[^{18}F]FDF reached 26.3 ± 2.6 % radioactivity / mg protein (n=9/3) after 60 min incubation time, whereas uptake of [^{18}F]-**10** was determined at 2.2 ± 0.3 % radioactivity / mg protein (n=9/3) after 60 min. In MDA-MB-231 cells, a similar trend was observed for both radiotracers, with higher uptake again for 6-[^{18}F]FDF (3.2 ± 0.3 % radioactivity / mg protein , n=9/3) in comparison to [^{18}F]-**10** (1.8 ± 0.2 % radioactivity / mg protein , n=9/3).

Cellular uptake of 6-[^{18}F]FDF was observed to be around 9-fold higher in murine EMT6 cells versus MDA-MB-231 cells. However, in both the cell lines uptake of radiotracer [^{18}F]-**10** was determined to be lower than 6-[^{18}F]FDF. Older data concerning 1-[^{18}F]FDAM had shown a similar uptake range of ~2 % radioactivity / mg protein in EMT6 cells as measured for [^{18}F]-**10.**[28] As cited before, higher uptake of 6-[^{18}F]FDF could be based on its uptake through both, GLUT2 and GLUT5, which are found in both cell lines EMT6 and MDA-MB231.[35] The observed differences in cellular uptake levels can be based on a variety of reasons: (a) difference in expression profile of proteins of interest (GLUTs) in both cell lines; (b) size/bulk of substitution required for recognition and transport of the radiotracer; (c) presence of specific kinase

enzymes to phosphorylate the radiotracer and therefore retain it inside the cell. Next analysis steps would involve in vitro blocking studies in the MDA-MB-232 cell line using both glucose and fructose to confirm the involvement of GLUT5 and potentially exclude involvement of GLUT2 for the uptake of [^{18}F]-**10**.

In addition, it has been observed that TNBC cell lines such as MDA-MB-231 show higher protein expression of hexokinase II than MCF-10A and MCF7 cell lines.[43] Also, expression of ketohexokinase (fructokinase) may be of importance in different breast cancer as it drives development of metastasis.[44]

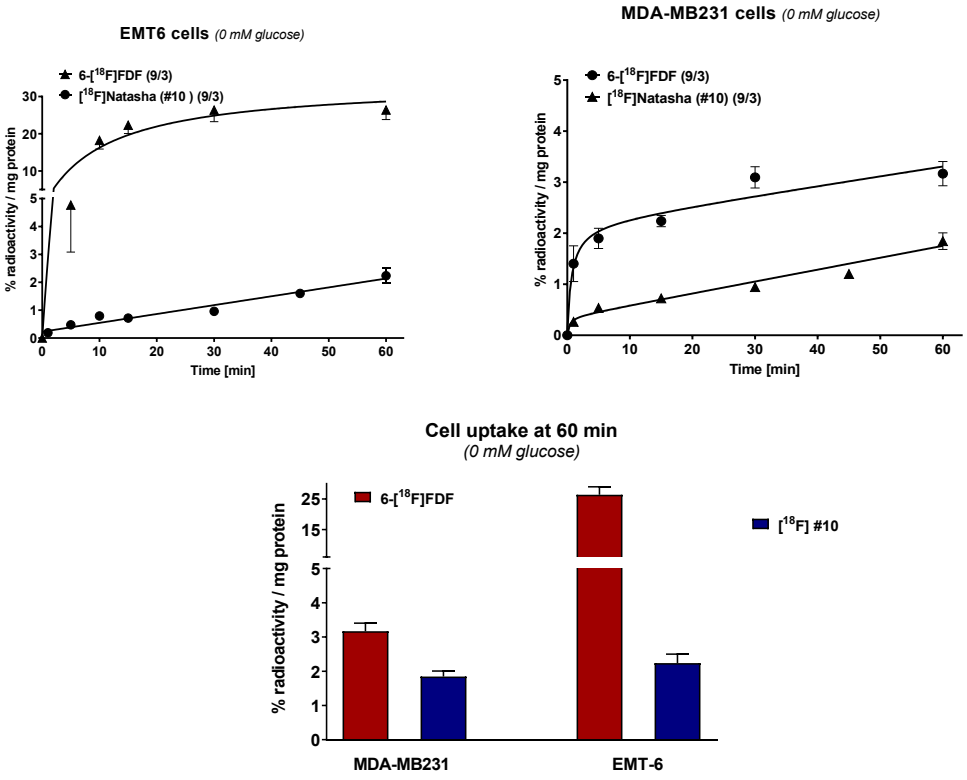

Figure 3.5. Cellular uptake experiments of 6-[^{18}F]FDF and [^{18}F]-10 into murine EMT6 mammary cancer cells and human MDA-MB-231 breast cancer cells. Data are shown as % radioactivity/mg protein over 60 min. Data are shown as mean ± SEM of 9 data points from 3 different experiments.

3.2.3. In vivo studies of tumor bearing mice

In this study, PET experiments were performed using human MDA-MB-231 tumor-bearing NIH-III xenograft mice and imaging experiments were done with both, 6-[^{18}F]FDF and [^{18}F]-**10**. Results revealed significant differences in muscle and tumor

uptake as well as in clearance parameters through heart (blood pool), liver and kidneys as well as differences in bone and brain uptake.

Figure 3.6 depicts selected PET images presented as maximum intensity projections for 6-[^{18}F]FDF and [^{18}F]-**10** at 5-, 20-, 60- and 120 min post injection (p.i.) as collected over 2 h dynamic PET scans. After 5-20 min, tumor uptake was clearly visible after injection of fructose derivative 6-[^{18}F]FDF, whereas after injection of 2,5-AM derivative [^{18}F]-**10,** a much lower overall tumor uptake was observed. After injection of 6-[^{18}F]FDF a high initial tumor uptake was detected at 20 min p.i.. After 120 min p.i., sufficient washout of radioactivity from non-targeting muscle tissue and background resulted in a good tumor-to-background ratio to visualize the tumor. In addition, bone uptake was also detected, which was indicative of an in vivo defluorination of 6-[^{18}F]FDF over time. In contrast, injection of [^{18}F]-**10** did not reach such a dominant tumor uptake, but also muscle tissue and therefore background levels remained low. There was also no visible bone structure and therefore no in vivo defluorination observed. At 120 min p.i. tumor uptake of [^{18}F]-**10** reached a sufficient contrast to be visualized in the maximum intensity projection image at a higher image resolution (see Figure 3.6 lower right image).

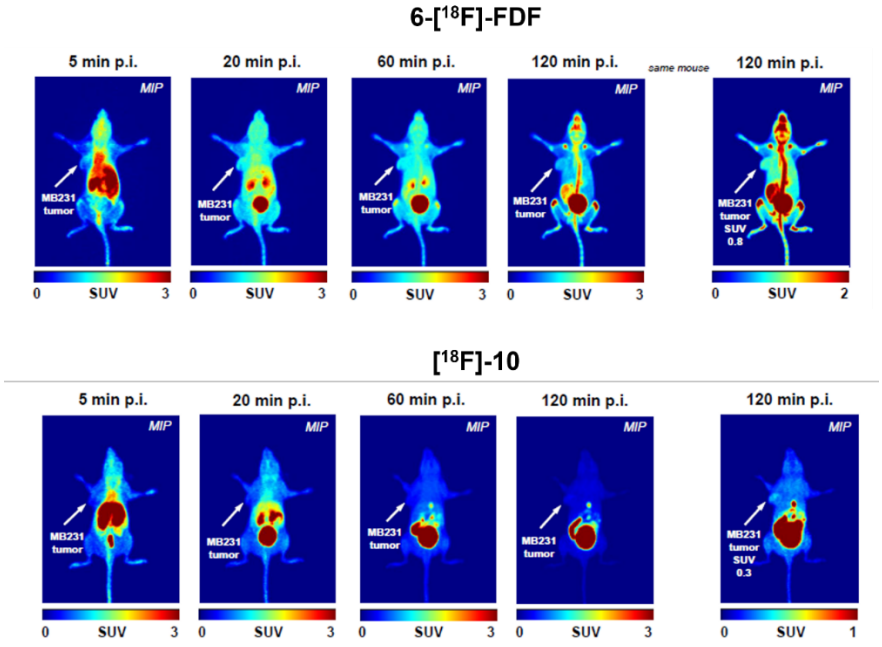

Figure 3.6. Representative PET after injection of 6-[^{18}F]FDF and [^{18}F]-**10** into the same MDA-MB-231 tumor-bearing NIH-III nu/nu mouse after 5-, 20-, 60- and 120-min post injection. Images at far right are shown as maximum intensity projections (MIP).

Figure 3.7 summarises time-activity curves (TACs) generated for the uptake profile of both radiotracers into tumor and muscle tissue. In the case of 6-[^{18}F]FDF, rapid uptake of the radioactivity was observed into MDA-MB-231 tumors reaching a maximum level of SUV 0.84 ± 0.05 (n=3) after 20 min. At later time points, tumor uptake of 6-[^{18}F]FDF started to slightly decrease reaching a SUV of 0.74±0.05 (n=4) after 120 min p.i.. In contrast to fructose derivative 6-[^{18}F]FDF, the 2,5-AM analog, [^{18}F]-**10** showed moderate tumor uptake peaking at 20 min p.i. (0.45±0.02, n=4) and decreased over time reaching SUV of 0.23±0.02 (n=3) after 120 min p.i.. Surprisingly, [^{18}F]-**10** displayed somewhat greater muscle uptake at 20 min p.i. (SUV 0.54±0.08, n=4) in comparison to the tumor tissue which eventually started to decrease rapidly reaching similar uptake levels at 120 min p.i. (SUV 0.17±0.02 (n=3) indicating radioactivity washout from both muscle and tumor tissue over time. In summary, [^{18}F]-**10** displayed much lower uptake levels in comparison to 6-[^{18}F]FDF with significant differences between specific (tumor) and nonspecific (muscle) uptake. However,

skeletal muscle cells also express different GLUTs including GLUT5 which could contribute to the higher uptake levels of 6-[^{18}F]FDF.

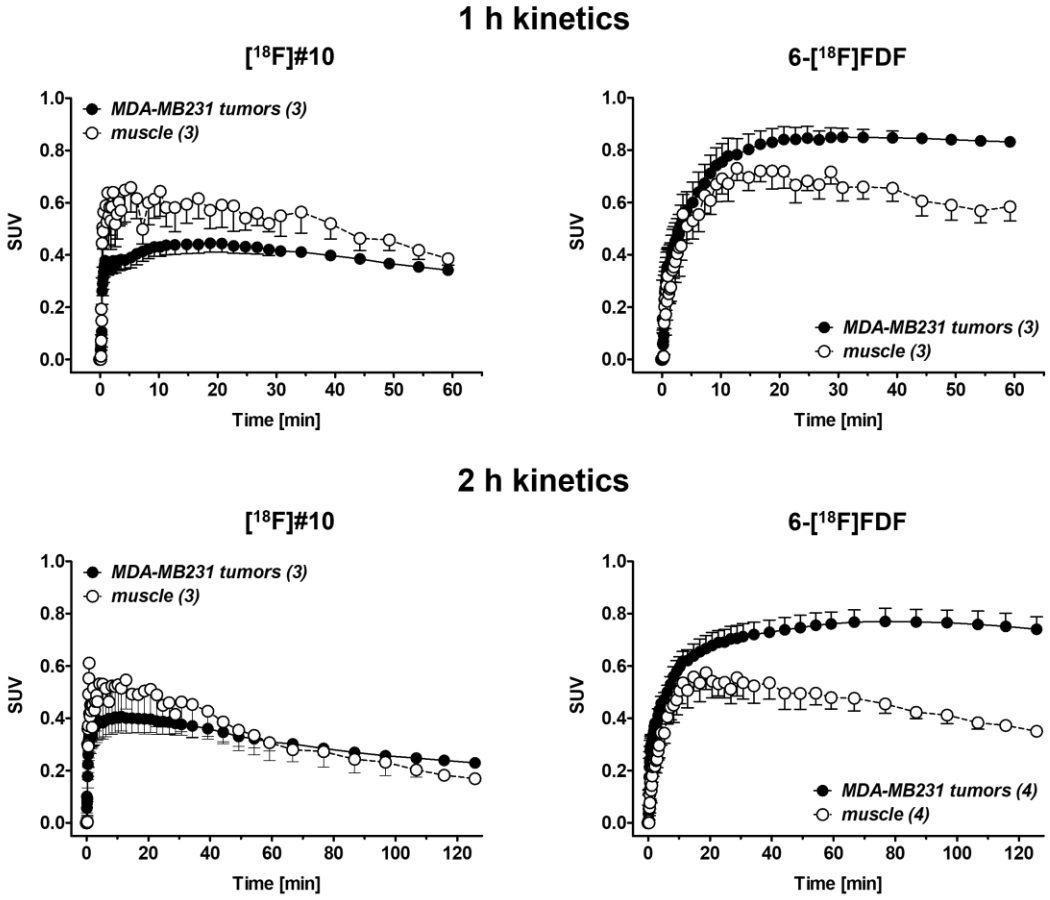

Figure 3.7. TACs for MDA-MB-231 tumor and muscle tissue uptake for 6-[^{18}F]FDF and [^{18}F]-**10** over 1 h and 2 h p.i. TACs are presented as semiquantitative SUV and mean ± S.E.M. from n experiments.

Figure 3.8 depicts the TACs for the clearance profile of both radiotracers over 60 min from MDA-MB231 tumor bearing mice. By analysing the region of the heart as indication for the blood pool, rapid clearance was observed over the time course of 60 min with some difference between 6-[^{18}F]FDF and [^{18}F]-**10**: after 60 min, 2-times more blood radioactivity was detected after injection of 6-[^{18}F]FDF (SUV 0.92±0.05; n=3) versus [^{18}F]-**10** (SUV 0.44±0.04; n=3). [^{18}F]-**10** cleared more through the renal system and the kidneys than 6-[^{18}F]FDF, reaching a maximum SUV of 9.54±1.23 (n=6/3) after 6 min.

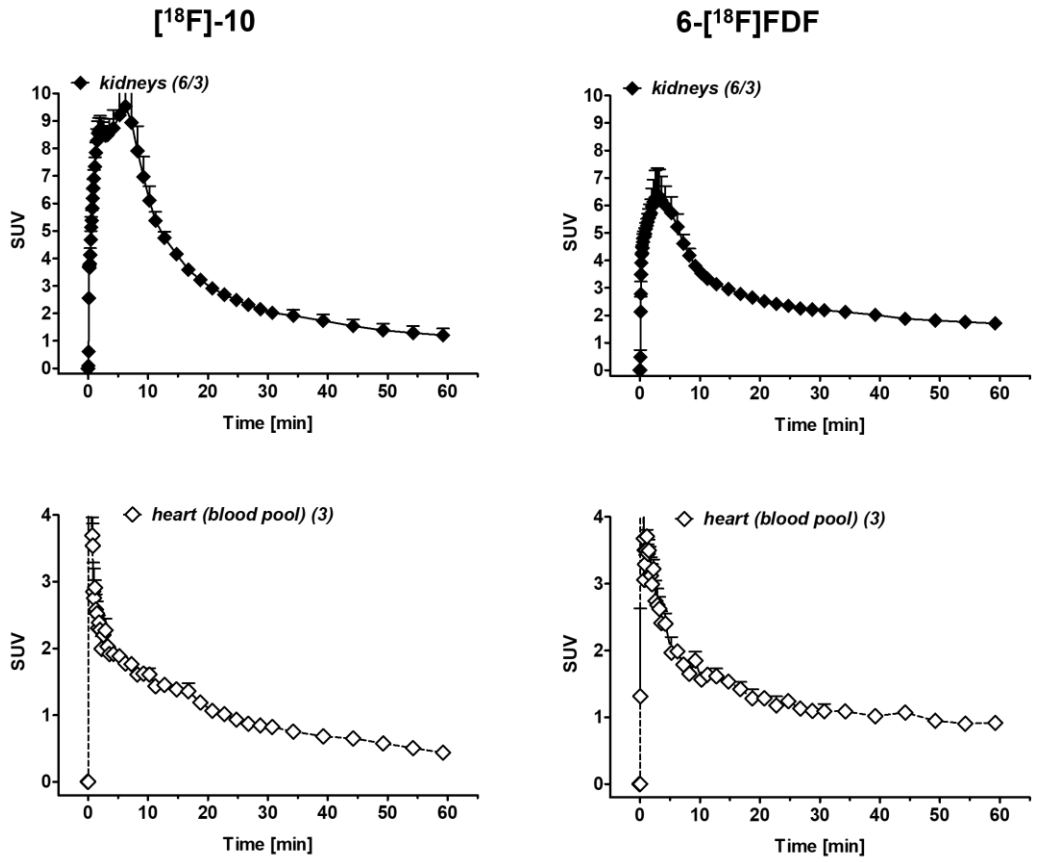

Figure 3.8. TACs of the radioactivity profile in kidney and heart (blood pool) after single intravenous injection of 6-[^{18}F]FDF and [^{18}F]-**10.** Data are shown as SUV and means ± S.E.M. from n MDA-MB-231 tumor bearing NIH-III nu/nu mice.

Besides renal clearance both radiotracers also got cleared through the hepatobiliary system. As shown in Figure 3.9, clearance of 6-[^{18}F]FDF through liver occured faster than [^{18}F]-**10,** but remained at higher levels after 60 min: SUV 0.95±0.04 (n=3) versus 0.55±0.04 (n=3), respectively. This was similar to the blood clearance levels.

As reported before, the TAC of 6-[^{18}F]FDF in bone showed uptake based on a metabolic process in vivo. While initial uptake was observed after ~10 min (SUV 0.92±0.05, levels increased to SUV 1.48±0.15 (n=3) after 60 min p.i.. This observation was an indication of defluorination of 6-[^{18}F]FDF followed by subsequent bone uptake of fluoride. After injection of [^{18}F]-**10,** no bone uptake was detected indicating that this radiotracer was not defluorinated in vivo.

Another big difference between 6-[^{18}F]FDF and [^{18}F]-**10** is related to brain uptake. After injection of 6-[^{18}F]FDF, brain uptake clearly increased over time reaching a constant steady state level after 60 min p.i. (SUV 0.96±0.06; n=3) and [^{18}F]-**10** was just observed to be washed through the brain in the initial blood flow during the distribution phase but did not reach any sufficient uptake levels (SUV 0.09±0.01; n=3 after 60 min p.i..

About 3 decades ago, in 1990, a study was unable to detect GLUT5 in several types of cancer,[13,45] then in 1996 studies performed by Zamora-Leon *et al.* reported elevated protein expression levels of GLUT5 in two breast cancer cell lines.[29] As a result, 6-[^{18}F]FDF and [^{18}F]-**10** were studied simultaneously in the present breast cancer models, the murine EMT6 and the human MDA-MB-231 cell lines. However, their uptake, accumulation and retention profiles were significantly different in both the cell lines (in vitro) and in the MDA-MB231 tumor model (in vivo). Both the cell lines (EMT6 and MDA-MB-231) are reported to express GLUT2, GLUT5, hexokinase II and ketohexokinase (fructokinase).[46] Differences between the two investigated radiotracers can be reasoned due to involvement of both, GLUT2 and GLUT5 in the uptake of 6-[^{18}F]FDF as well as fructokinase into the trapping mechanism. On the other hand, [^{18}F]-**10** might have got transported through GLUT5 with no interaction with either hexokinase II or ketohexokinase resulting in washout from the tumor tissue. As a result, it appears that developing a radiotracer that facilitates uptake via GLUT5 and undergoes phosphorylation through HK/KHK could be a key determinant of specific detection of GLUT5 in breast cancer as well as other types of cancer expressing GLUT5.

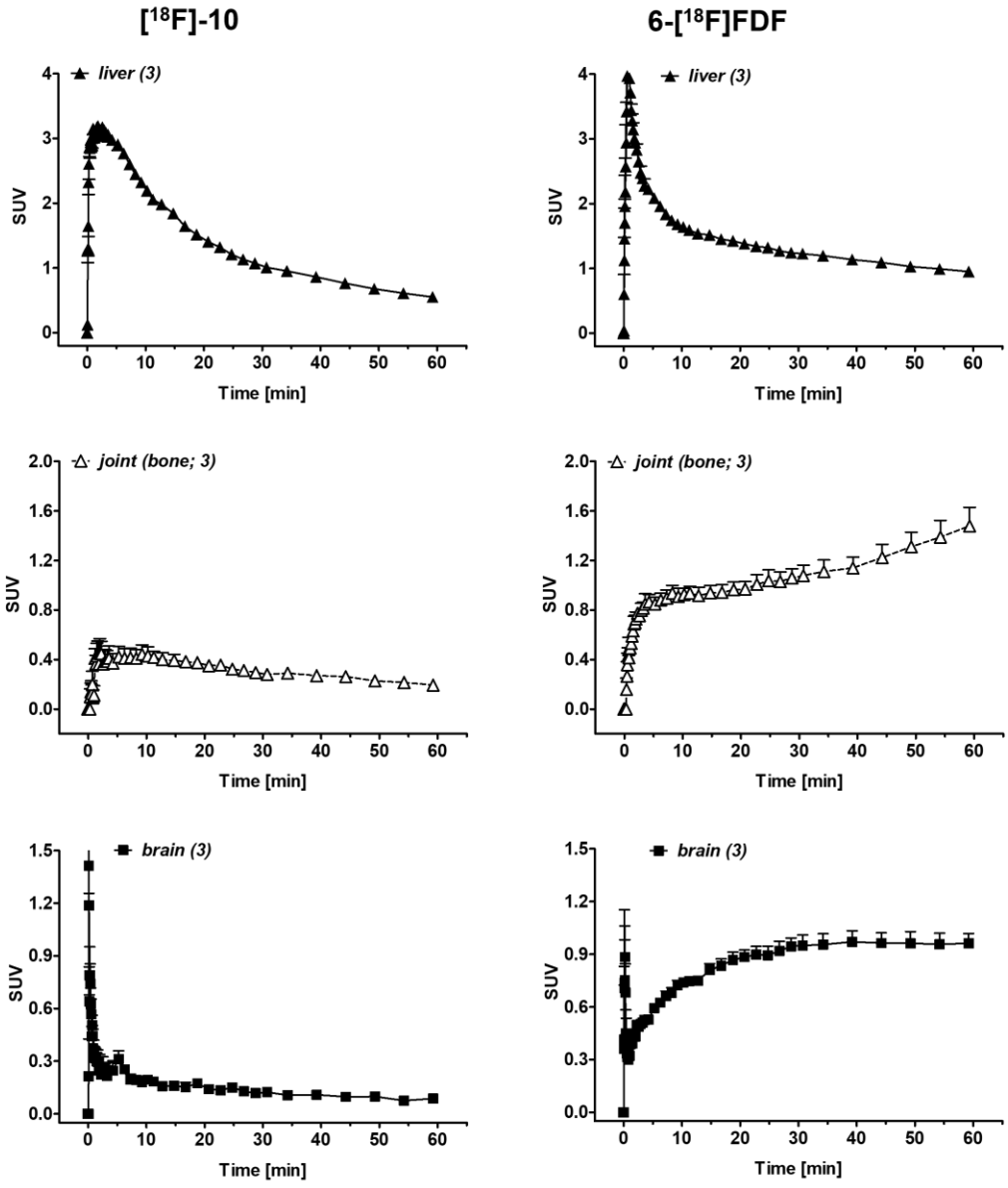

Figure 3.9. TACs of the radioactivity profile in liver, joint and brain after single intravenous injection of 6-[^{18}F]FDF and [^{18}F]-**10.** Data are shown as SUV and means ± S.E.M. from n MDA-MB-231 tumor bearing NIH-III nu/nu mice.

3.3. Development of fluorescent 2,5-AM derived tracer

3.3.1. Introduction to fluorescent hexose probe

In order to access the metabolic state of the cell, analysis of GLUT expression is studied through the development and investigation of GLUT targeting affinity labeled and modified sugar analogs. As mentioned in Chapter 1, fluorescent sugar derivatives are

evaluated to review their transport efficiency (how large fluorophore can be accommodated by the central pore of GLUTs) along with their phosphorylation kinetics. In addition, to alleviate the limitations associated with radiolabeling (time constraint due to half-life, handling of radioactive materials, set up, and waste management), there is a need to develop high affinity fluorescently labeled hexose derivatives. For localization of fluorescent probes in tumor cell over normal cells, a high quality diagnostic image of the tumor needs to be obtained.

Since GLUT1 is often observed to be over expressed in many tumor cells, several probes have been developed which could successfully achieve localization and accumulation at the site of tumor.[32] Fig. 3.10 represents some probes that have been utilized to target GLUT1. 2-[N-(7-Nitrobenz-2-oxa-1,3-diazol-4-yl)amino]-2-deoxy-D-glucose (**2-NBDG**) is reported to be delivered in various tumor cells through GLUT1.[47,48,49] Cy5.5-2DG (**17**)[49] and Pyro-2DG[50] (**18**) represent the near infrared fluorescent deoxy analog that was developed to target GLUT1 machinery. In the case of Pyro-2DG (**18**), preliminary confocal studies displayed that uptake of this probe can be inhibited in presence of D-glucose suggesting Pyro-2DG as a substate of GLUT1. Confocal studies of Cy5.5-DG demonstrated the tumor cell uptake by several tumor cell lines; however, its uptake was not observed to be blocked by D-glucose. Interestingly, Glc-SiR-COOH (**19,** net charge = 0), showed GLUT mediated cellular uptake whereas its methyl analog Glc-SiR-Me (net charge = -1) failed to show any uptake, indicating the significance of net charge of the glyconjugate for efficient cellular uptake.[51] A recent study has developed dual probe (**2-FBDG**) having an [^{18}F] radiolabel and a fluorophore and was observed it to be selectively taken up through GLUT1.[52]

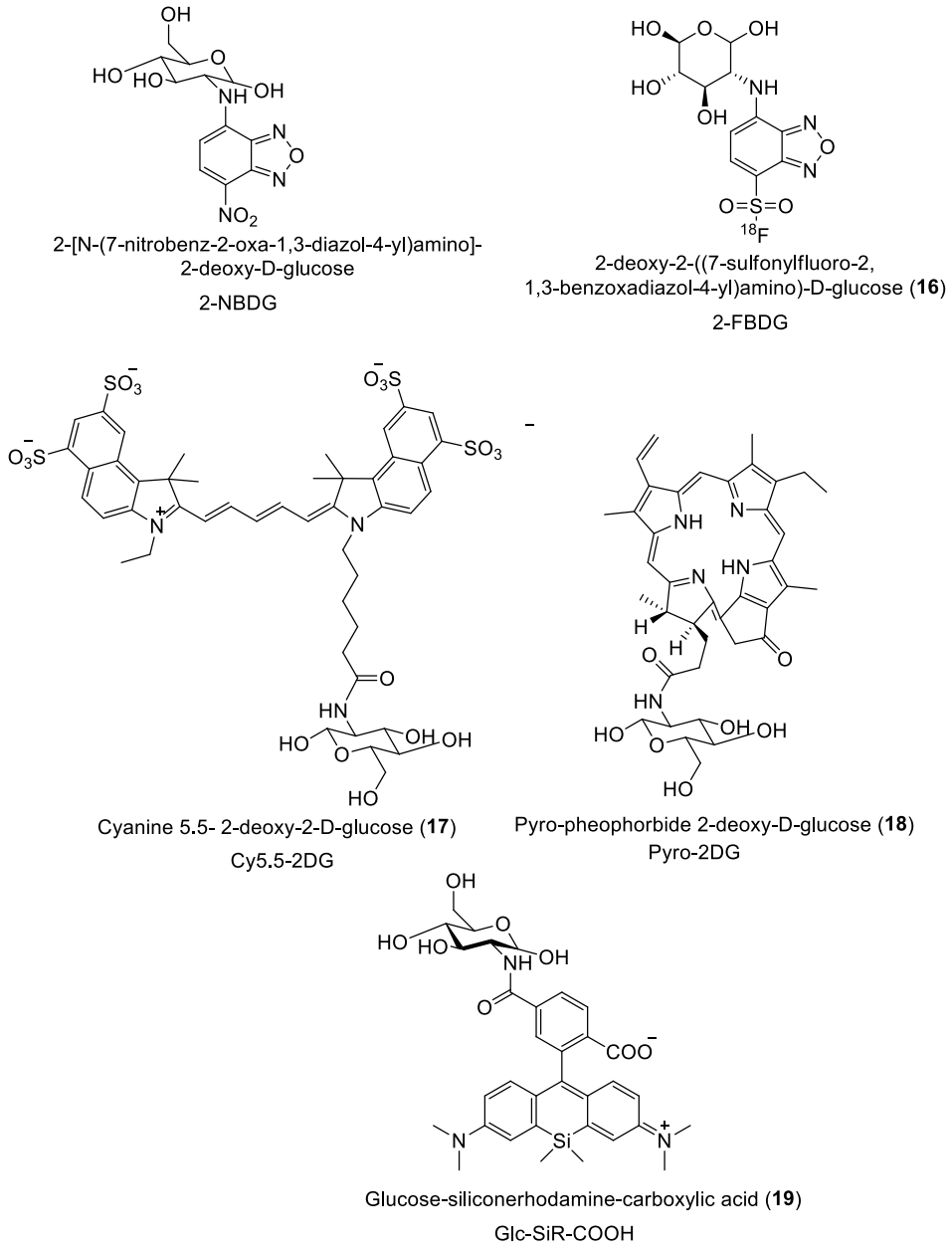

Figure 3.10. Fluorescent probes utilized to target GLUT1.

However, due to inconsistent expression levels of GLUT1 in early-stage breast cancer cells, there is a need to develop probes targeting other transporters, such as the fructose transporters GLUT2 and GLUT5. Due to the unique substrate preference of GLUT5 for fructose, development of probes for this biomarker has gained more attention in the past decade. Development of such probes which could undergo enzymatic phosphorylation would help in improving the quality of diagnostic image by

preventing the efflux of the probes. Reduced efflux of a probe would permit greater accumulation in the target cells, resulting in a higher signal to noise ratio. Moreover, the absence of radioactive decay in the case of fluorescence detection would also help preserve a strong cellular signal. Along with localization of tumor, such probes can also aid in understanding the mechanism of transport of D-fructose in healthy and tumor cells. As a result, in this section, we will be discussing the synthesis and evaluation of list of fluorescent probes with potential to display high affinity for GLUT5.

3.3.2. Previous studies

This section contains the development of D-fructose and 2,5-AM based probes to target GLUT5 (Figure 3.11.). Probes such as **1-NBDF**[11], **1-NBDAM**[53], **6-NBDF**[54] and **3-NBDAM**[55] were observed to be selectively transported through GLUT5 and it was observed that transport of some probes into cells was independent of extracellular D-glucose but dependent on D-fructose. This specific targeting of GLUTs could render a differentiation in imaging between GLUT5 expressing vs GLUT5 deficient cells. The authors designed **1-NBDF**, substituting C-1 position of D-fructose as position C-6 would be available for phosphorylation with hexokinase. However, in competitive studies (with D-glucose and D-fructose) uptake of **1-NBDF** seemed to be diminished suggesting the involvement of GLUT2 transporter. The same groups of authors also reported the fructose-cyanine conjugate (1-Cy5.5-F, **20**)[11] in order to study the tolerance of fructose transporter for a bulky fluorophore as selected red dye probe could provide real time, low background, reduced scattering, enhanced tissue penetration, and in depth imaging along with various applications such as NIR light therapy. Unfortunately, uptake of 1-Cy5.5-F was observed to be hexose independent as unconjugated cyanine dye also displayed similar uptake indicating uptake of probe due to endocytosis. **6-NBDF** displayed selective uptake through GLUT5 but was observed to undergo rapid efflux due to absence of C6-OH for hexokinase in order to get trapped inside the cells. With **1-NBDAM**, longer retention was expected due to presence of C6-OH. However, efflux of the majority of the internalized probe was observed after multiple washes of the cells. This could indicate either slow phosphorylation or its complete absence. The C-3 modified 2,5-AM probe, **3-NBDAM** exhibited GLUT5

dependent transport into breast cancer cells. In addition, **3-NBDAM** was observed to be accumulated inside the cells with slower efflux as compared to **1-NBDAM**. Based on these observations, it can be noted that NBD being a smaller fluorophore does not increase the bulk of overall hexose-conjugate enabling smooth passage through GLUTs. However, there are no such reports of study of bulky fluorophores at C-3 position of 2,5-AM. Recently, coumarin conjugates of 2,5-AM (**MannCou)** have been evaluated as probes for GLUT5.[56] Inspired from such results, we have generated a list of fluorescent probes bearing different fluorophores varying in size and optical properties to study their applicability to the GLUT5 transport mechanism.

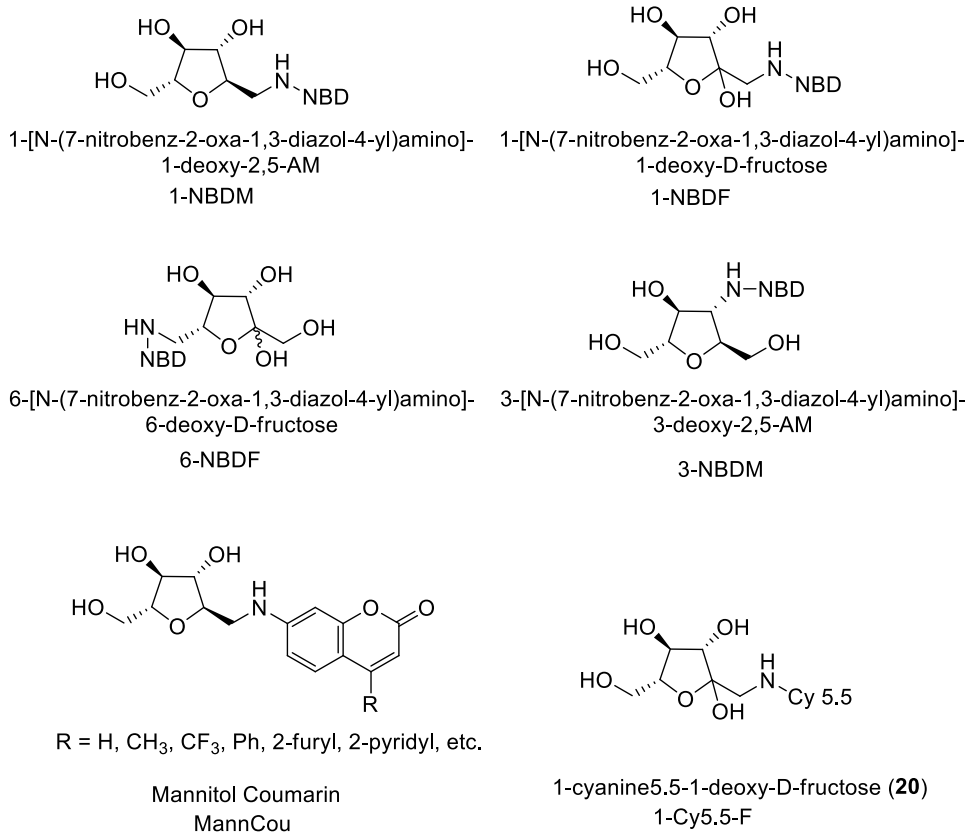

Figure 3.11. D-fructose and 2,5-AM based probes to target GLUT5

3.3.3. Design and synthesis of C-3 modified 2,5-AM fluorescent probes

Chapter 2 summarized the GLUT5 recognition for 2,5-AM derivatives and it was described that presence of a hydrogen bond donor at the C-3 position of 2,5-AM is crucial for protein ligand interactions and provides high affinity GLUT5 ligands. In

addition, it was also reported that presence of hydrogen bond acceptor at same C-3 position can also generate derivatives exhibiting moderate GLUT1 affinity.[55] However, strong binding (as demonstrated through inhibition of cellular uptake of a known GLUT ligand) does not necessarily indicate transport of the inhibitor. Therefore, to evaluate the ability of GLUT5 to transport the 2,5-AM, we designed multicolor fluorescent probes to understand the uptake of these probes via GLUT5 in tumor cells. The range of these fluorophores would allow greater understanding of the structural limits for transport, as determined by varying steric demand and polar features found on the various fluorophores while holding the 2,5-AM scaffold constant. It would also encourage in understanding the GLUT5 uptake efficiency in presence of D-glucose and D-fructose. The compounds shown in the Figure 3.12 were designed to retain the critical hydrogen bond donor moiety at C-3 that appears to be necessary for recognition by GLUT5, while varying the size and optical properties of the fluorescent label.

These studies would measure the relative fluorescence of probes inside the tumor cells which would also give an insight on the amount of the probe taken up by the tumor cells. The availability of free primary alcohols at C-1 and C-6 of the 2,5-AM scaffold (mimicking the D-fructofuranose) should allow enzymatic phosphorylation of the probe in presence of intracellular kinases. As a result, these probes were expected to exhibit a GLUT5 dependent uptake with low efflux.

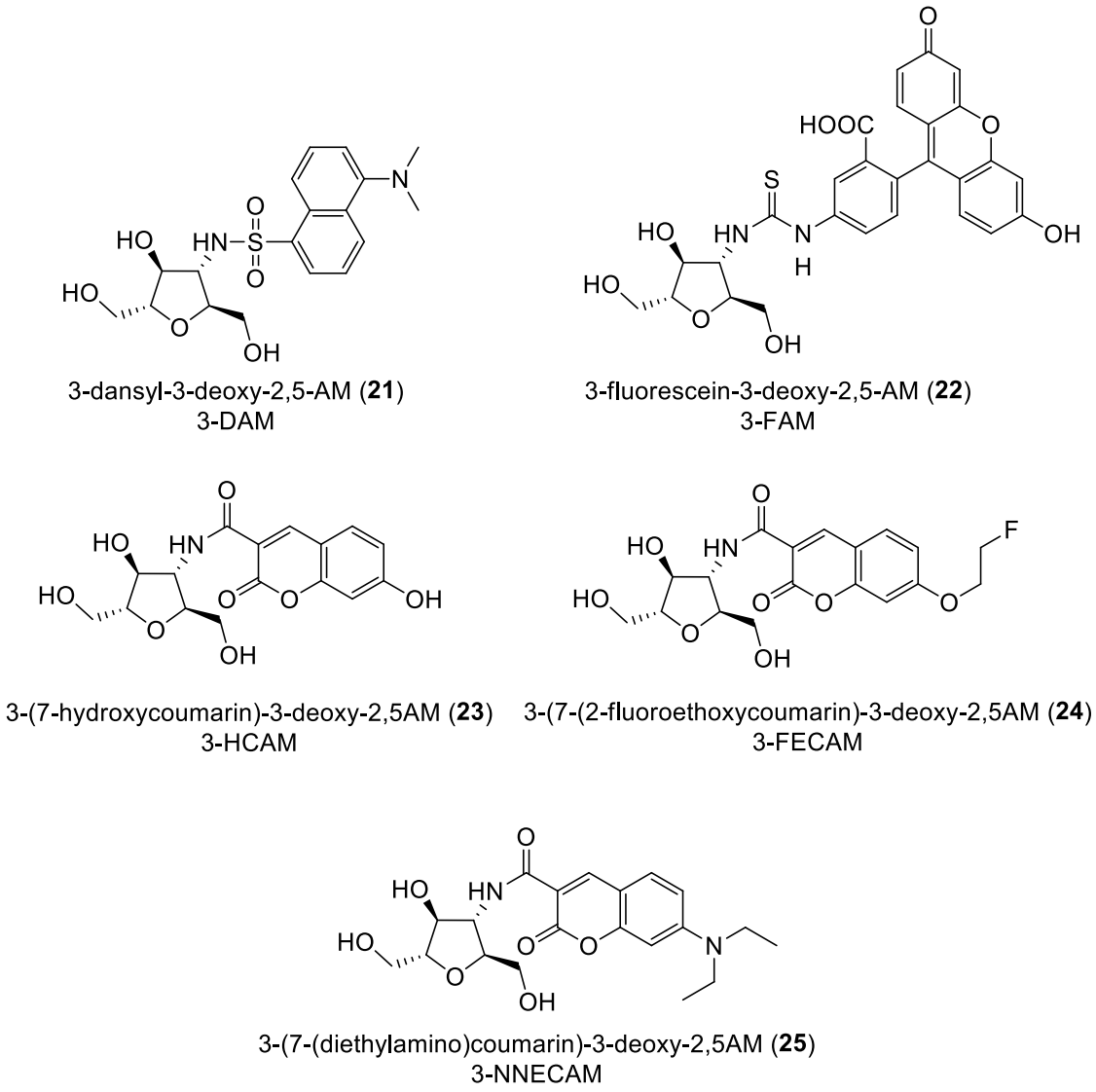

Figure 3.12. List of synthesized 2,5-AM derived fluorescent probes

The synthesis of fluorescent derivatives is shown in Scheme 3.6. Labeling of C-3 amino group of 2,5-AM with fluorophore was performed by treating primary amine functionality of unprotected 2,5-AM with the corresponding fluorophore containing reagents. For synthesis of **21** and **22**, the C-3 amino group of 2,5-AM was conjugated with dansyl chloride or fluorescein isothiocyanate isomer I respectively in presence of methanol at room temperature without addition of strong base. In the case of **21**, reaction proceeded through simple displacement of chloride with amine forming HCl as the by product. Compound **22** was synthesized by adding FITC isomer I to form

corresponding thiourea linkage. The synthesis of **23** and **24** is already mentioned in Chapter 2 in which synthesis of NHS ester of the coumarin fluorophore was carried out separately[57,58] and then it was conjugated to corresponding amino moiety of 2,5-AM. Compound **24** was synthesized from **23** via one additional step involving alkylation of corresponding **23** with 2-fluoroethyl tosylate in DMF at 140℃. Several attempts were made to form the amide bond between the carboxylic acid of the coumarin reagent and amino group of 2,5-AM in presence of various coupling conditions. However due to the high polarity of the starting materials and reagents used, separation of product from polar impurities (side products, starting materials etc.) posed a challenge in obtaining acceptable yields with higher product purity. Therefore, treating amino group of 2,5-AM with the NHS ester of the coumarin carboxylate was examined[57,58], and resulted in a higher yielding reaction with easier separation. For the same reasons, probe **25** was generated by reacting NHS ester of commercially available 7-(diethylamino)coumarin-3-carboxylic acid with corresponding amine.[57]

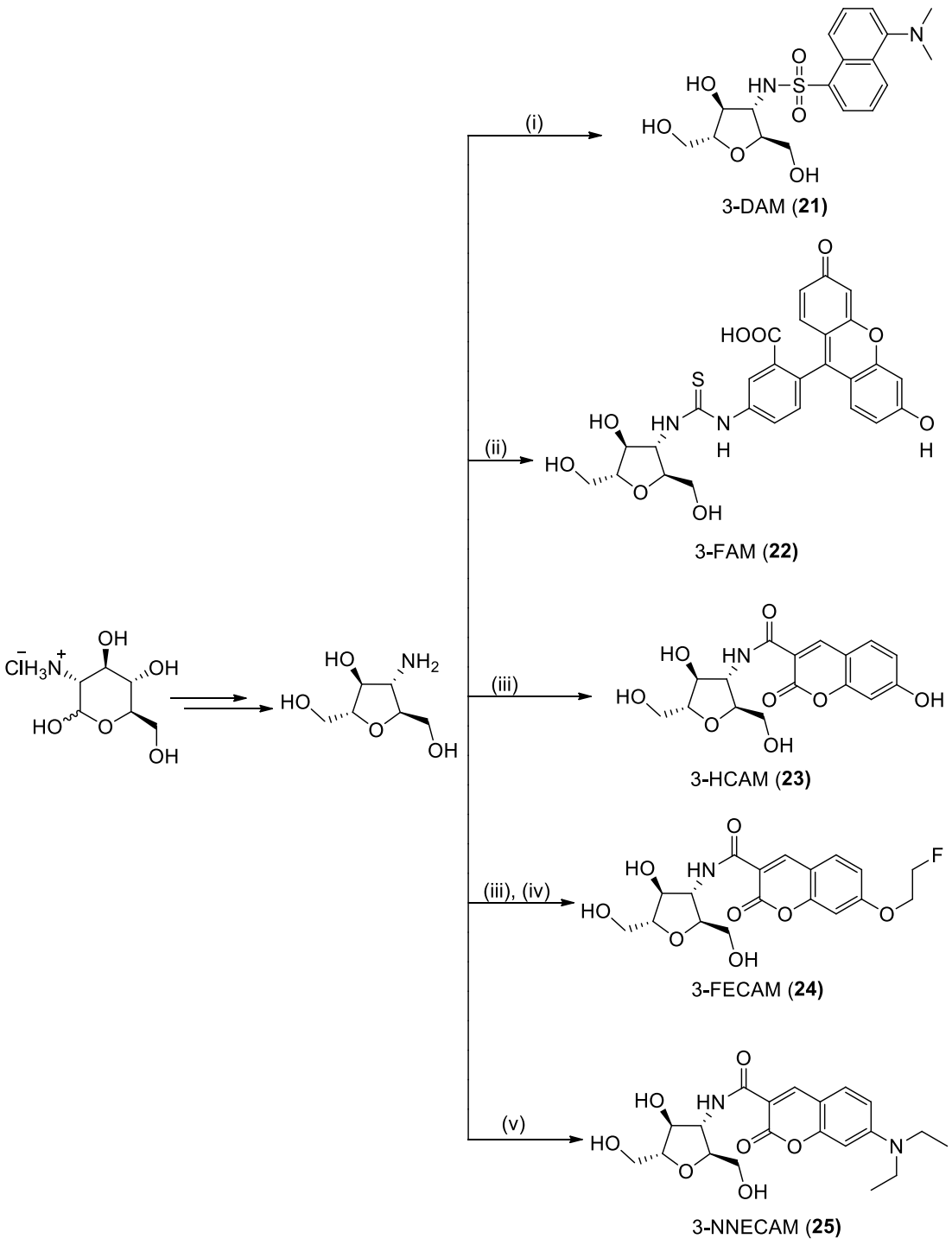

Scheme 3.6. Synthesis of fluorescent probes (i) dansyl chlorie, CH_3CN, Na_2CO_3, rt, 16h, 35% (ii) fluorescein isothiocyanate isomer I, MeOH, rt, 15h, 55% (iii) NHS ester of 7-hydroxycoumarin-3-carboxylic acid, MeOH, RT, 15 h, 85% (iv) 2-fluoroethyl p toluenesulfonate, K_2CO_3, DMF, 110°C, 1 h, 50% (v) NHS ester of 7-(diethylamino) coumarin-3-carboxylic acid, MeOH, rt, 1h, 78%.

For the synthesis of the rhodamine conjugated derivative **28,** Schemes 3.7, 3.8 and Table 3.3 describe the optimization methods that were explored to generate the red fluorescent probe. As shown in Scheme 3.7, synthesis was started from activating the carboxylic acid of rhodamine B (**26**) as its NHS ester. After obtaining the N-hydroxy succinimide analog (**27**), coupling of **27** with the amino group of 2,5-AM resulted in only small traces of desired product **28**, along with mostly recovered starting material. Table 3.4 describes the optimization conditions used to directly couple rhodamine B with the amino group of 2,5-AM in the presence of various coupling agents. Unfortunately, all the conditions gave only trace amounts of product (as detected via LC-MS) which could not be isolated after chromatographic purification, along with mostly recovered starting materials. Given the difficulties observed with conjugation via amide linkage, we then turned our attention to rhodamine isothiocyanate **29** as the derivatizing reagent. However, after carrying out this reaction, a complex mixture was obtained, and its separation into homogeneous products proved to be challenging. In light of the number of other diverse fluorescent probes in hand (Table 3.4), we elected to proceed to confocal microscopy studies without the desired rhodamine conjugate.

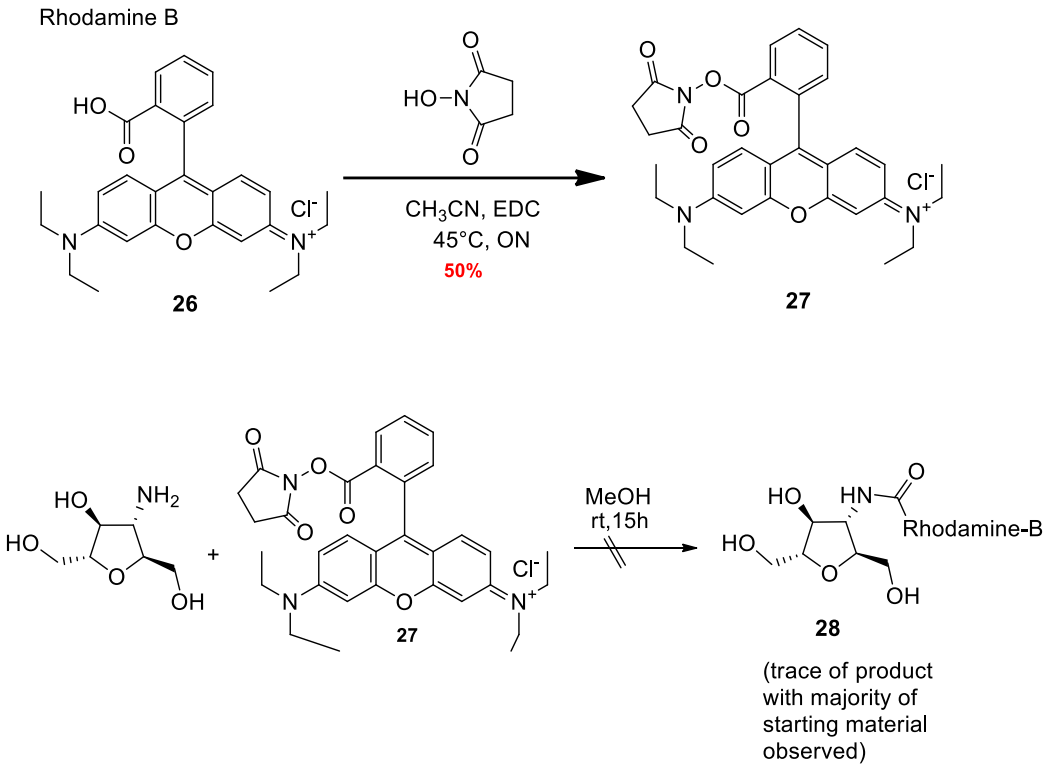

Scheme 3.7. Attempted synthesis of rhodamine B conjugate mannitol derivative

Table 3.3. Optimisation studies for coupling of rhodamine B with C-3 amino 2,5-AM

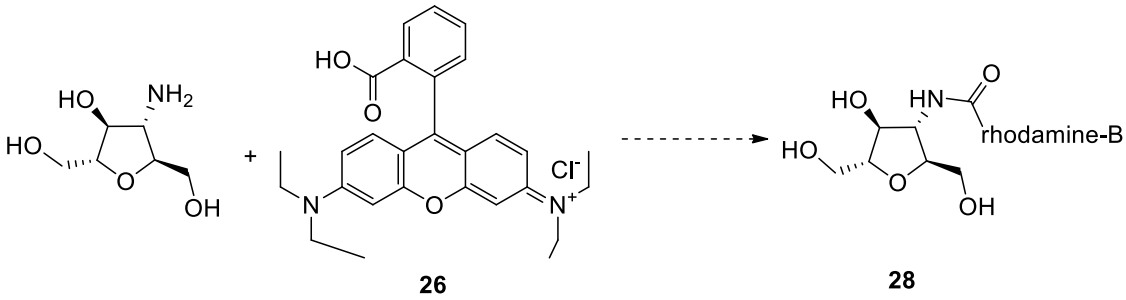

No. of conditions	Coupling agents	Solvent	Temperature	Observations
1	EDC	DMF	rt	SM recovered
2	EDC	DMF	100 ℃	Messy NMR
3	HBTU, TEA	DMF	rt	Messy NMR

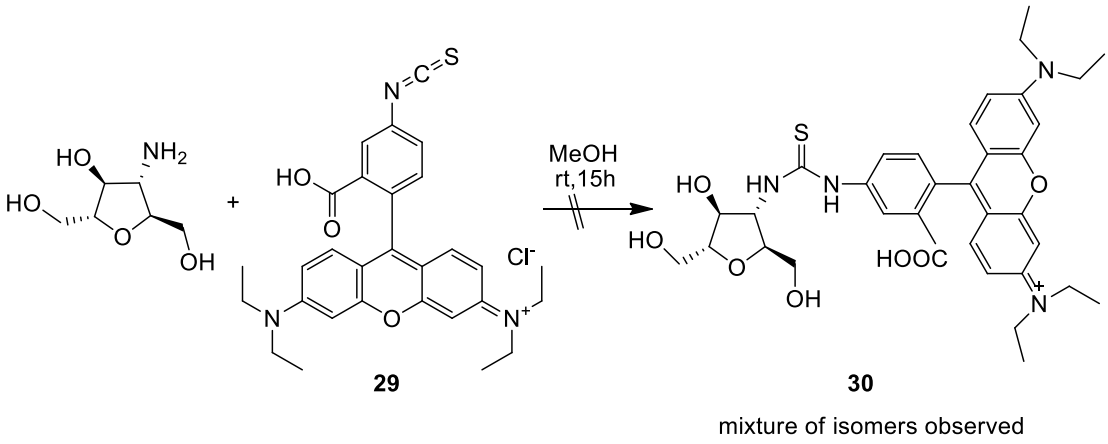

Scheme 3.8. Attempted synthesis of rhodamine isothiocyanate conjugate 2,5-AM derivative

Table 3.4. Observed optical properties of fluorescent probes

Compound	λ (excitation, nm)	λ (emission, nm)
3-DAM	334	519
3-FAM	492	519
3-HCAM	342	447
3-FECAM	347	402
3-NMCAM	406	473

3.3.4. Confocal Microscopy

To further analyze and confirm that the synthesized fluorescent probes were taken up via GLUT5 (as opposed to other GLUTs or passive diffusion across the cell membrane), qualitative confocal microcopy experiments were performed using the murine breast cancer cell line EMT6. As observed from the optical properties of the probes (Table 3.4), all of the compounds emited light in the blue to green spectral region, in which interference from endogenous fluorophores could confound the microscopy studies.

Therefore, it was important to determine the intrinsic fluorescence of the cells. Before each probe was evaluated, cells were subjected to a blank sample containing 0.1% DMSO to measure for autofluorescence using a fluorescence microscope with different filter sets. All the samples having blank displayed autofluorescence of low intensity suggesting small interference in studying the uptake of probes. All these experiments were performed by incubating a fixed concentration of the probe (e.g.,100 μM) for 1 hour at 37℃. In case of probes 3-DAM (**21**) and 3-FAM (**22**), DAPI was

used for labeling of nucleus to study distribution and accumulation of probes. In this section, we will be discussing the images obtained for each fluorescent probe in uptake and competition experiments.

(A) **3-DAM (21)**

As shown in Figure 3.13, there is evident cytosolic uptake of the dansyl probe, 3-DAM. In addition to greater fluorescence intensity in comparison to DMSO, incubation of this probe resulted in a significant cell fluorescence indicating involvement of hexose transporters in mechanism of uptake. To further confirm the role of GLUT5 in this uptake, coincubation studies were performed in presence of large concentration of extracellular D-glucose and D-fructose. In presence of D-glucose, intracellular uptake of 3-DAM wasn't significantly affected as no inhibition in fluorescence was observed. Interestingly, with an addition of D-fructose, dramatic reduction in the fluorescent signal confirmed the significant role of fructose transporter GLUT5 as the principal transporter of probe. It is difficult to state the role of GLUT2 in the uptake as this transporter mediates passage of both D-glucose (high affinity) and D-fructose, and so one would expect minimal inhibition in fluorescence of probe in the presence of the preferred GLUT2 substrate (D-glucose).

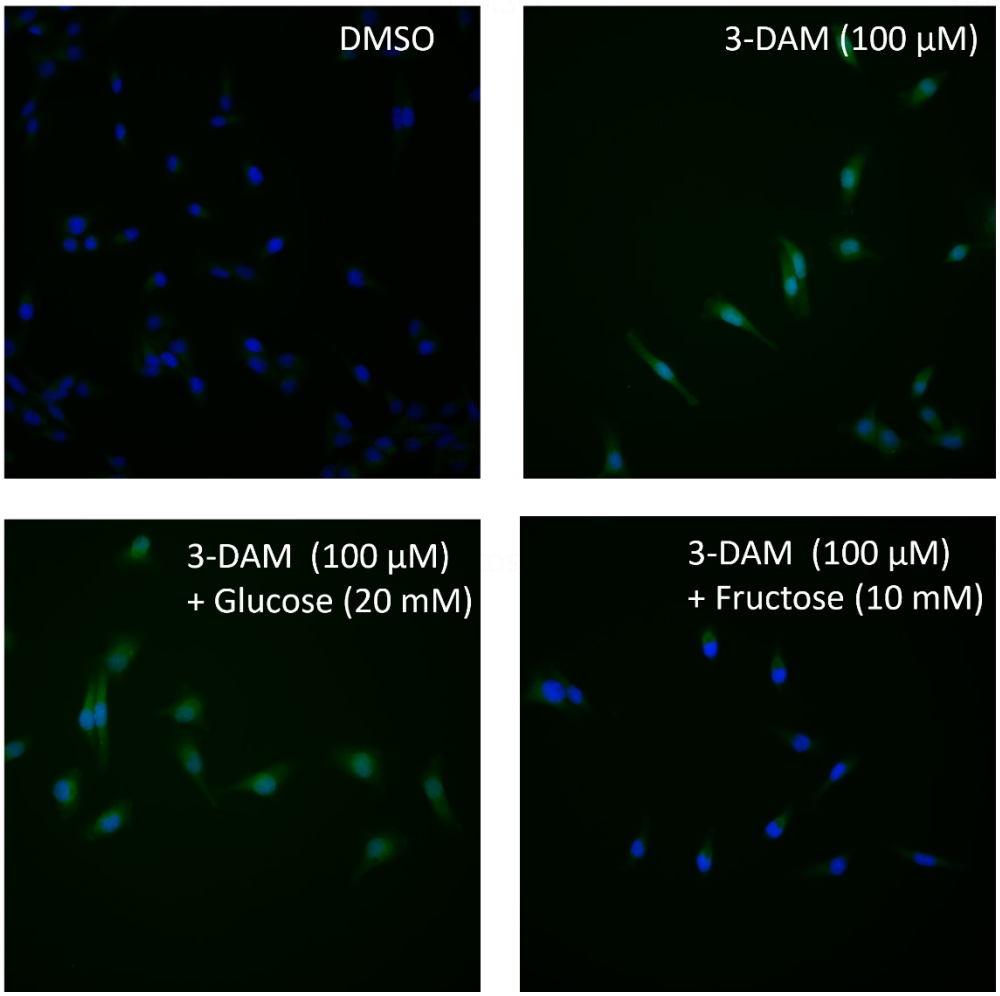

Figure 3.13. Confocal images obtained after incubation of EMT6 cells with **3-DAM** and the response to the presence of extracellular D-glucose (20mM) or D-fructose (10 mM). Green fluorescence = 3-DAM(334/519 nm), Blue fluorescence =DAPI to visualize the nuclei.

(B) **3-FAM (22)**

Microscopy experiments using fluorescein conjugate 3-FAM were the first to employ a probe bearing a much bulkier fluorophore at C-3 position of 2,5-AM (Figure 3.14). As judged by the low fluorescence intensity in the case of DMSO blank, no significant autofluorescence was observed in this filter set (FITC). Incubation of EMT6 cells with 100 µM of probe (3-FAM, **22**) resulted in an increased intracellular fluorescence signal suggesting that 3-FAM was also taken up into these cells. To investigate the internalization of 3-FAM, competitive studies with D-glucose and D-fructose were performed. No diminution of fluorescence intensity was observed on coincubation with

D-glucose. In the presence of D-fructose, we observed a complete reduction of the overall fluorescence signal including the background. In that case, the present results may suggest that 3-FAM is also transported through GLUT5 indicating that these transporters possess the tolerance to transport the fluorescein moiety as a cargo attached to 2,5-AM.

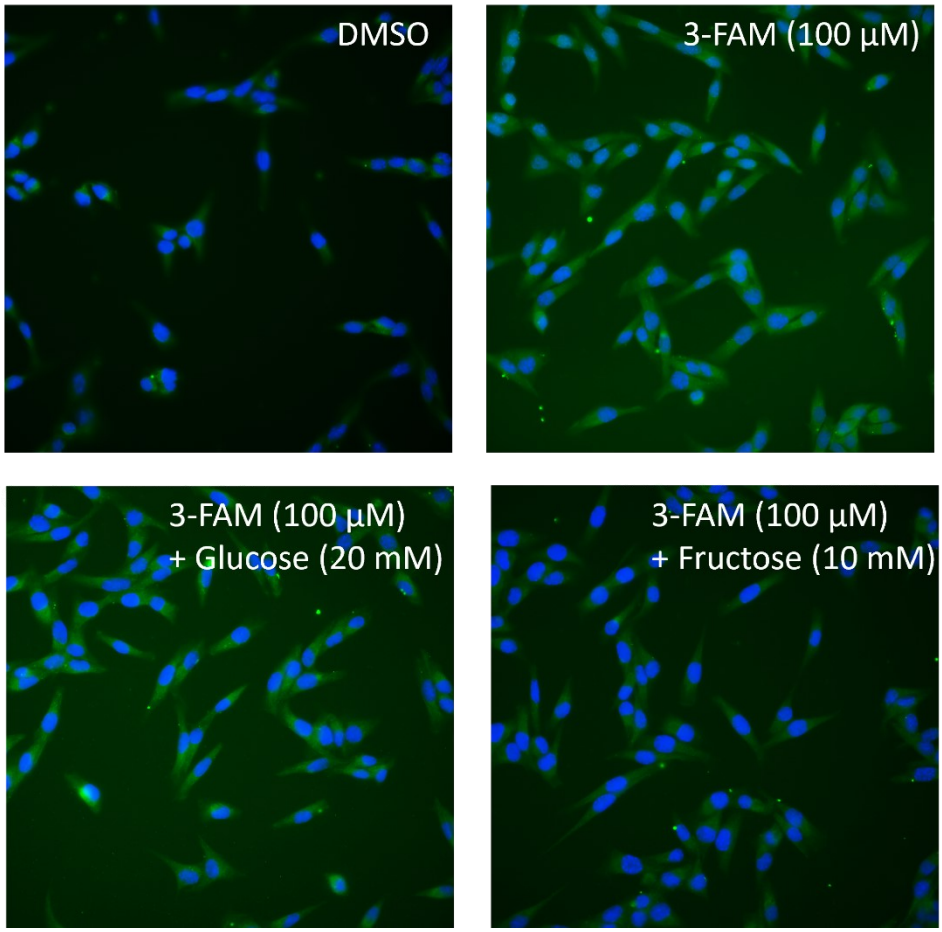

Figure 3.14. Confocal images obtained after incubation of EMT6 cells with **3-FAM** and the response to the presence of extracellular D-glucose (20mM) or D-fructose (10 mM). Green fluorescence = 3-FAM(492/519 nm), Blue fluorescence =DAPI to visualize the nuclei.

(C) **3-HCAM (23)**

Incubation of EMT6 cells with the hydroxy coumarin conjugate **23** produced a bright blue fluorescence signal indicating internalization by the cells (Figure 3.15). Addition of a large excess of extracellular D-glucose had a minor effect on the fluorescence signal. In presence of large amount of D-fructose, significant inhibition in intensity of

signal was observed with nucleus voids more clearly visible. As with the earlier examples, these results provide positive evidence for the principal involvement of GLUT5 in the uptake of this probe molecule.

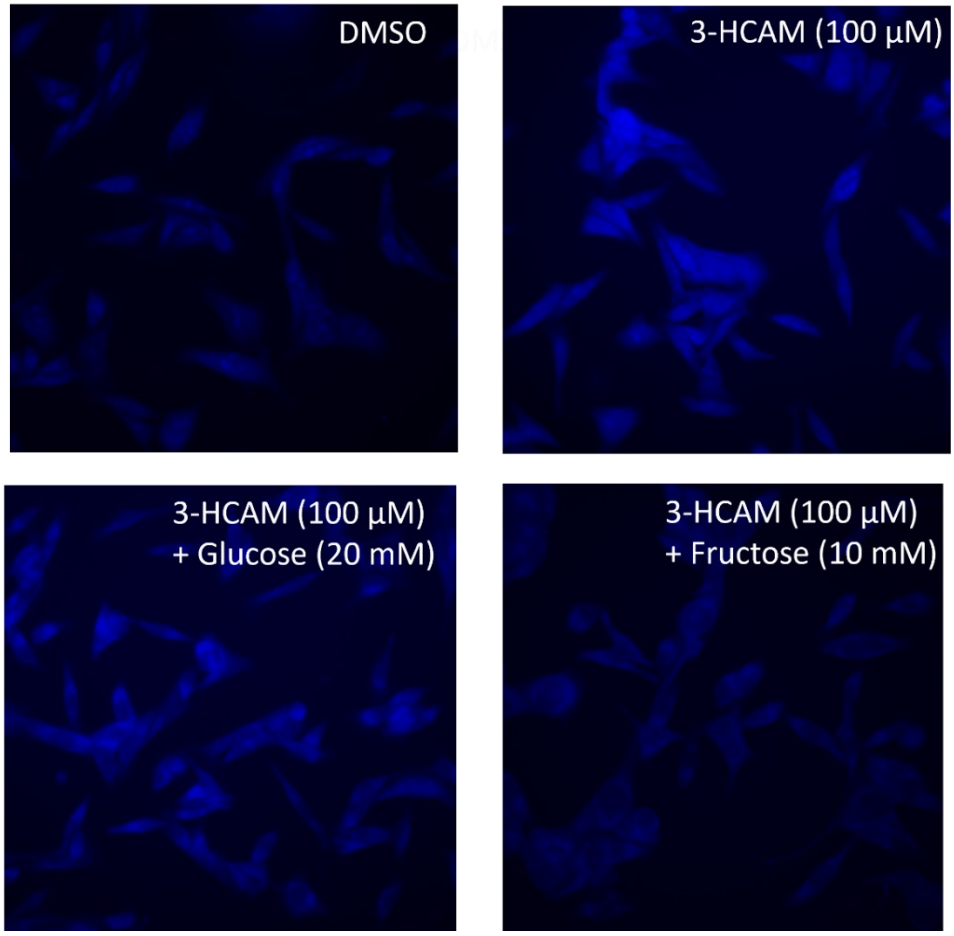

Figure 3.15. Confocal images obtained after incubation of EMT6 cells with **3-HCAM** and the respnse to the presence of extracellular D-glucose (20mM) or D-fructose (10 mM). Blue fluorescence = 3-HCAM(342/447 nm).

(D) **3-FECAM (24)**

Probe molecule **24** (3-FECAM) is the alkylated version of the coumarin conjugate **23** (Figure 3.16.). As evident from optical properties, this alkylation resulted in subsequent quenching of emission wavelength. This reduction in excitation/emission wavelength posed a challenge in finding optimal filter set for imaging. Cells incubated with this probe were imaged under the same filter set as DAPI. As observed from the images, uptake of 3-FECAM was clearly visualized due to increase in the fluorescence signal.

However, the coincubation experiments indicated no evidence for significant inhibition of fluorescence in the presence of either D-glucose or D-fructose.

This suggests that this probe doesn't selectively use the GLUT5 transporter to enter the cell. Even though this probe displayed some potency to inhibit 6-[^{18}F]-FDF uptake (IC_{50}=2.01 mM) which would be indicative of an interaction with the GLUT transporters, the confocal imaging experiments exclude an active cell uptake. On the contrary, we did observe some localized accumulation of the probe inside the cell indicating of a potential passive uptake of 3-FECAM. Further studies are needed to understand its molecular uptake mechanism.

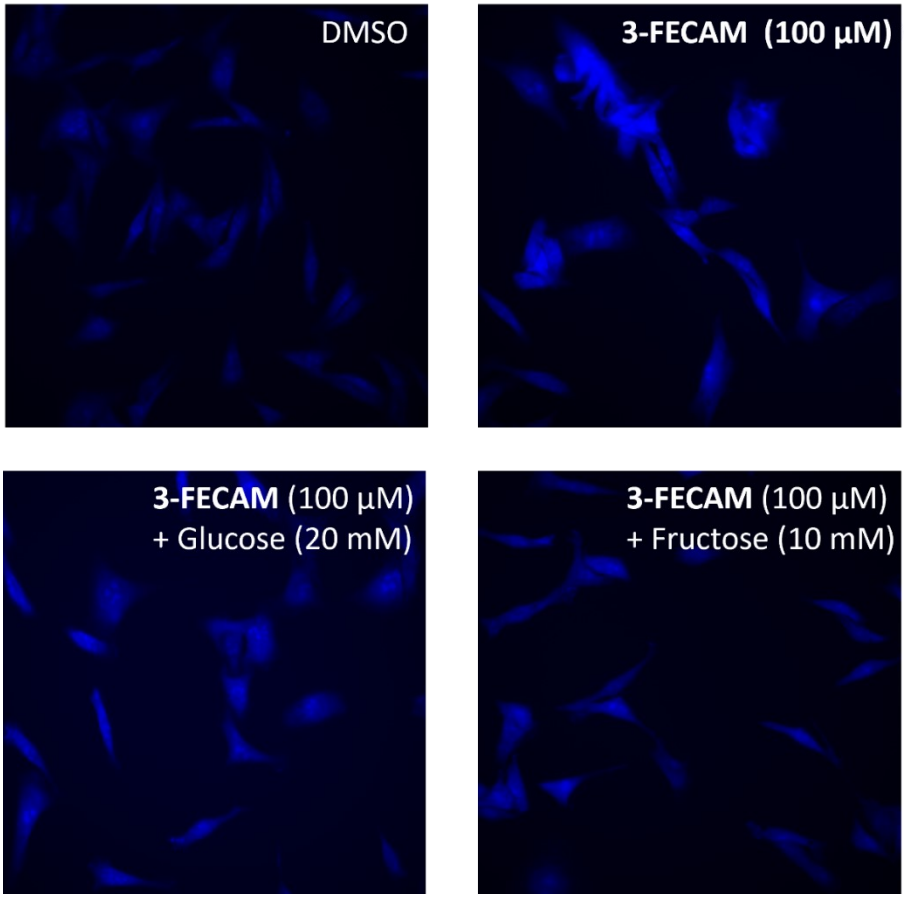

Figure 3.16. Confocal images obtained after incubation of EMT6 cells with **3-FECAM** and the response to the presence of extracellular D-glucose (20mM) or D-fructose (10 mM). Blue fluorescence = 3-FECAM(347/402 nm).

(F) **3-NNECAM (25)**

Confocal microscopy experiments with aminocoumarin conjugate **25** produced similar uptake behaviour to what was seen with the previous probes (Figure 3.17). Significantly greater fluorescence intensity was observed relative to the DMSO blank, but the effect of extracellular D-glucose or D-fructose resulted in the overall reduction of the signal. Coincubation with D-fructose produced a less bright signal as compared to D-glucose. This might suggest the transport of this probe through both GLUT2 and GLUT5.

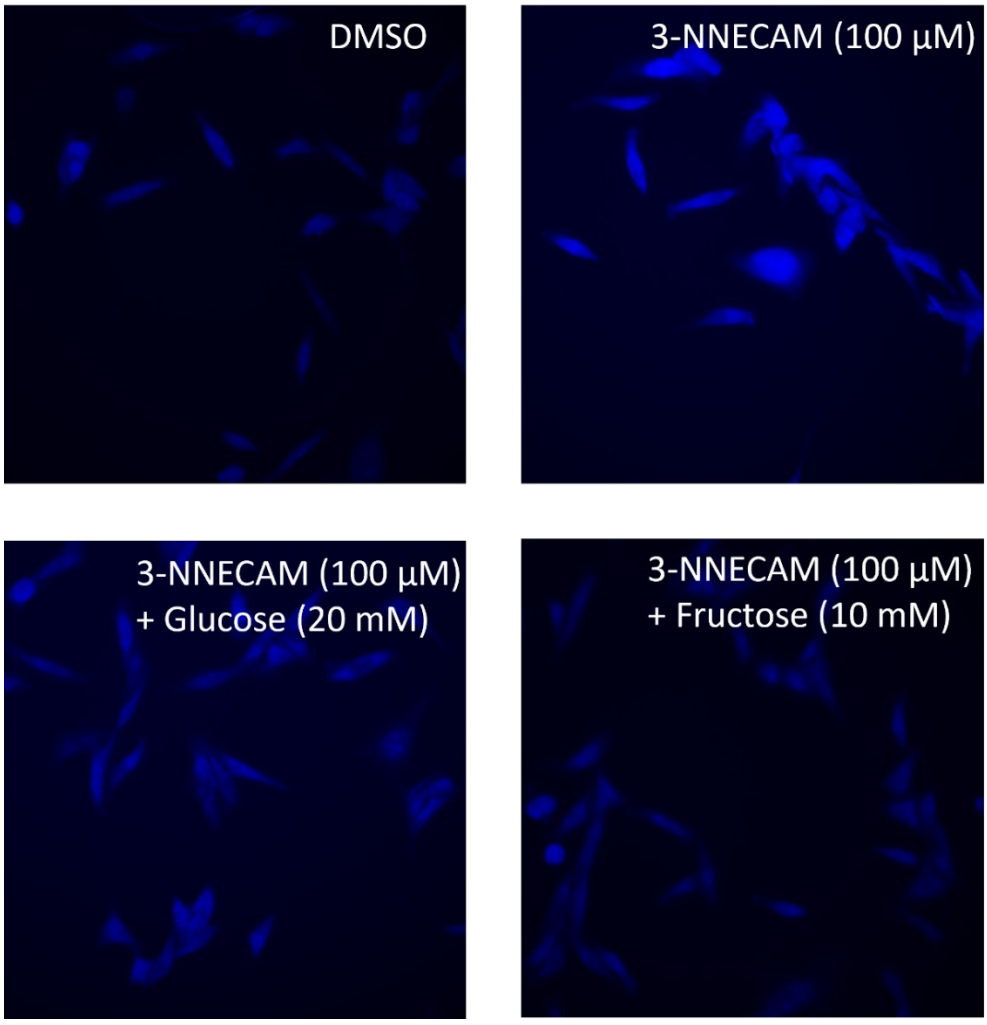

Figure 3.17. Confocal images obtained after incubation of EMT6 cells with **3-NNECAM** and the response to the presence of extracellular D-glucose (20mM) or D-fructose (10 mM). Blue fluorescence = 3-HCAM(406/473 nm).

3.4. Conclusion

In summary, presented experimental results demonstrates the importance of developed molecular probes to image selective uptake through GLUT5 in breast cancer cells and tumors. [^{18}F]-**10** was envisioned as a novel PET radiotracer for imaging of GLUT5 expression in vitro and in vivo. The goal of the present study was to investigate the radiopharmacological profile of [^{18}F]-**10** in comparison to 6-[^{18}F]FDF in murine EMT6 and human MDA-MB-231 tumor cells. It was found that 6-[^{18}F]-FDF exhibits an overall higher cell uptake than [^{18}F]-**10** in both cell lines. However, while, 6-[^{18}F]-FDF resulted in a higher overall MDA-MB231 tumor uptake after 2 h post injection, it also possesses a significant muscle tissue uptake, and it is not selective as it is transported by both GLUT2 and GLUT5. It also shows some metabolic instability as it was observed to be defluorinated over time in vivo. Compound [^{18}F]-**10** on the other hand, maybe more specific for GLUT5, results in a lower tumor and muscle uptake with no increasing tumor-to-muscle ratio in vivo. [^{18}F]-**10** also displayed a slower metabolism in vivo and therefore better stability in comparison to 6-[^{18}F]-FDF as it was evident from radioactivity levels analyzed in the bone. Further studies are needed to confirm the selective uptake of [^{18}F]-**10** via GLUT5 and its potential phosphorylation pattern via fructokinase, although its MDA-MB231 tumor tissue washout pattern over time may be indicative of no phosphorylation.

In addition to the radiotracer [^{18}F]-**10**, five fluorescent 2,5-AM derivatives were synthesised and evaluated in cell culture for their ability in detecting GLUT5 in breast cancer. All the five derivatives displayed good uptake (cytosolic accumulation) in cancer cells. Importantly, it was found out that three out five derivatives displayed uptake behaviour suggestive of its utilization of the D-fructose uptake machinery (especially GLUT5). The size of the fluorophore did not seem to affect the transport of the probe molecules via GLUT5. This indicates the potential of labeling 2,5-AM with fluorophores in the NIR region useful for in vitro and in vivo. In contrast, the remainder two fluorescent probes displayed only nonspecific uptake into EMT6 breast cancer cells and are therefore not useful for specific targeting of GLUT5. Overall, the work here provides support for the objective of developing radiolabeled and fluorescent

probe molecules targeting the GLUT5 biomarker as an approach for imaging breast cancer in vitro and in vivo.

Future studies will include further study of [18F]-**10**, including effect of extracellular D-fructose and D-glucose, as well as careful analysis of its phosphorylation kinetics in the presence of KHK or hexokinase II.

3.5. Experimental section

3.5.1. Chemical synthesis

Materials and methods

Reactions were carried out in oven-dried glassware under a positive argon or nitrogen atmosphere unless otherwise stated. Transfer of anhydrous solvents and reagents was accomplished with oven-dried syringes or cannula. Solvents were distilled before use, and dimethylformamide (DMF) and acetonitrile (MeCN) were distilled from calcium hydride. Chemicals were purchased from Sigma-Aldrich Inc. and were used without further purification. Thin layer chromatography was performed on glass plates preloaded with 0.25 mm silica gel matrix. Flash chromatography columns were packed with 230–400 mesh silica gel. Optical rotations were measured with Perkin Elmer 241 polarimeter, at 22 ± 2 °C. Proton nuclear magnetic resonance spectra (^{1}H NMR) were recorded at 500 MHz or 700 MHz and coupling constants (*J*) are reported in Hertz (Hz). Standard notation was used to describe the multiplicity of signals observed in ^{1}H NMR spectra: broad (br), multiplet (m), singlet (s), doublet (d), triplet (t), etc. Carbon nuclear magnetic resonance spectra (^{13}C NMR) were recorded at 100 MHz or 125 MHz and are reported δ (ppm) relative to the center line of the septet from methanol-d_4 (49.3 ppm), triplet of chloroform-d (77.2 ppm), or septet of DMSO-d_6 (39.5 ppm). Infrared (IR) spectra were measured with a FT-IR 3000 spectrophotometer. Mass spectra were determined on a high-resolution electrospray positive ion mode spectrometer.

Synthesis of the probes (**3, 10, 11, and 21-24** employed the procedures described in Chapter 2).

3-deoxy-3-[N-(7-(diethylamino) coumarin-3-carboxamide)amino]-2,5-anhydro-D-mannitol, NNECAM (25)

In a one-neck 50 mL round bottom flask, maintained under N_2 atmosphere, C-3 amine 2,5-AM (0.13 g, 0.61 mmol) was dissolved in MeOH (10 mL). NHS ester of 7-diethylamino coumarin-3-carboxylic acid[57,58] (0.33 g, 0.91 mmol) was added to the flask and vigorous stirring of the homogenous mixture was continued at room temperature for 15 h. MeOH was removed under reduced pressure and the crude compound was purified via silica gel column chromatography using a DCM/MeOH solvent mixture (gradient from 100:0 to 94:6). Fractions containing the desired product were combined and concentrated under vacuum to provide **NNECAM (25)** (0.16 g, 64%) as a bright yellow sticky solid. R_f 0.45 (DCM/MeOH, 90:10); $[\alpha]_D^{20}$ = -8.84 (*c* 0.26, MeOH); FT-IR (cast film) 3308, 2966, 2931, 2878, 1698, 1617, 1581, 1536, 1513, 1454, 1420, 1379, 1353 cm^{-1}; ^1H NMR (700 MHz, CD_3OD): δ= 8.64 (d, *J* = 0.7 Hz, 1H), 7.56 (d, *J* = 9.0 Hz, 1H), 6.83 (dd, *J* = 9.0, 2.5 Hz, 1H), 6.59 (d, *J* = 2.3 Hz, 1H), 4.38 (t, *J* = 6.8 Hz, 1H), 4.20 (t, *J* = 6.5 Hz, 1H), 3.95 (ddd, *J* = 7.1, 5.5, 3.6 Hz, 1H), 3.91 (ddd, *J* = 6.5, 4.7, 3.0 Hz, 1H), 3.77 (dd, *J* = 11.9, 2.9 Hz, 1H), 3.75 – 3.73 (m, 1H), 3.69 (dd, *J* = 12.0, 5.5 Hz, 1H), 3.66 (dd, *J* = 11.9, 4.6 Hz, 1H), 3.54 (q, *J* = 7.1 Hz, 4H), 1.24 (t, *J* = 7.1 Hz, 6H); ^{13}C NMR (176 MHz, CD_3OD): δ= 164.4, 162.6, 157.8, 153.3, 148.9, 131.3, 110.3, 108.3, 108.0, 95.8, 84.10, 83.0, 76.0, 62.4, 61.6, 58.5, 44.5, 11.2; HRMS (ESI) calcd for $C_{20}H_{26}NaN_2O_7$ $[M+Na^+]$ 429.163; found 429.1632.

Radiotracer Synthesis

[^{18}F]-**10**

^{18}[F]-FBA (4-[^{18}F]-fluorobenzaldehyde) can be made either on the automated synthesis unit (ASU) or manually. The preference is to do this on the ASU as it allows for much higher amounts of ^{18}F to be used (up to 20 GBq rather than 1 GBq doing it manually) which allows for a much higher concentration of [^{18}F]-4-fluorobenzaldehyde. 5-10 mg of the trimethylammonium-benzaldehyde precursor is dissolved in a minimal amount of the extra-dry acetonitrile (usually 300 uL, or 1 mL on the ASU). Corresponding solution is added to the ^{18}F and reacted for 15 minutes at 85 ◦C. Purification is done using a C-18 Strata cartridge (primed with ACN and water) and eluted in acetonitrile (typically in 1.5 mL when done manually, or 3 mL on the ASU). This is then analyzed by TLC using 30% ethyl acetate in hexane (Rf = 0.8) or HPLC. While synthesis of

^{18}[F]-FBA is going on, synthesis of [^{18}F]-**10** is carried out in a separate chamber. 1 mg of the precursor **I** is treated with 50/50 solution (20 total µL) of TFA and DCM to remove boc for 1 hour. Once deprotected, 400 µL of H_2O and 400 µL of the **^{18}[F]-FBA** (350 MBq of [^{18}F]-**FBA** with purity >90%) containing acetonitrile is added (total 800 µL) to deprotected precursor **II** and reacted at 50 °C for 30 minutes. It has been shown the reaction goes well in slightly acidic conditions (0.2% TFA in water mixed with acetonitrile), allowing the aldehyde to react to form oxime. The compound is then purified via HPLC (3 ml/min, 20% ACN in 0.2% TFA water for 5 minutes, increasing to 30% over 5 more minutes, then up to 90% over an additional 10 minute, holding at 90% acetonitrile for 10 minutes). Retention time was observed at 16.7 minutes (16.6 on UV detector, 16.8 on radio detector). TFA and organic solvent were evaporated, and the product was diluted in appropriate buffer for cell studies.

3.5.2. Biological experiments

Buffer solutions

Glucose-free Krebs–Ringer buffer solution (120 mM NaCl, 25 mM $NaHCO_3$, 4 mM KCl, 1.2 mM KH_2PO_4, 2.5 mM $MgSO_4$, 70 µM $CaCl_2$, pH 7.4) was used for the studies with EMT6 cells. Cold phosphate-buffered saline (PBS) was used to wash the extracellular probes (137 mM NaCl, 2.7 mM KCl, 10 mM Na_2HPO_4, 2 mM KH_2PO_4). RIPA buffer (Sigma-Aldrich, St. Louis, MO, U.S.A.) was used for cell lysis.

Cell culture

Murine mammary gland tumor cells EMT6 (ATTC CRL-2755TM) and human BC cells MDA-MB231 (ATCC® HTB-26™) were grown in a CO_2 incubator at 37°C, in Gibco® DMEM/F-12 supplemented with 10% fetal bovine serum (GIBCO, 12483) and 1% penicillin/streptomycin and split every 2-3 days.

In vitro cell uptake of ^{18}F-labeled radiotracers

For radiotracer uptake studies, cells were grown to confluence in 12-well plates using in Gibco® DMEM/F-12 medium (containing 10% fetal bovine serum (GIBCO, 12483) and 1% penicillin/streptomycin). One hour prior to the experiment, the media was removed, and the cells were washed two times with phosphate-buffered saline solution

(PBS). Next, glucose-free Krebs-Ringer solution (120 mM NaCl, 4 mM KCl, 1.2 mM KH_2PO4, 2.5 mM $MgSO_4$, 25 mM $NaHCO_3$, 70 µM $CaCl_2$, pH 7.4) was added to the cells. 500 µl Krebs-Ringer (with or without 5 mM glucose or 30 mM fructose) solution with 0.1-0.5 MBq ^{18}F-labeled radiotracer was added to each well and the plates were incubated at 37℃ for specific periods of time (5, 10, 15, 30, 45 and 60 min). Radiotracer uptake was stopped with 1mL ice-cold PBS, the cells were washed twice with PBS and lysed in 0.4mL radioimmunoprecipitation assay buffer (RIPA buffer). Radioactivity in the cell lysates was determined as counts per minute [CPM] using a WIZARD2 Automatic gamma counter (Perkin Elmer; Waltham, MA, USA) and converted to the radioactivity dose SI unit Bequerel [Bq]. Total protein concentration in the samples was determined by the bicinchoninic acid method (BCA; Pierce, Thermo Scientific 23227) using bovine serum albumin as protein standard. Data were calculated as percent of measured radioactivity per mg protein (% radioactivity / mg protein). Cell uptake of 6-[^{18}F]FDF and [^{18}F]-**10** over a 60 min incubation time was compared in murine EMT6 versus human MDA-MB231 BC cells. Graphs were constructed using GraphPad Prism 5.0 (GraphPad Software).

In Vitro inhibition of 6-[^{18}F]FDF cell uptake

Competition binding experiments of 2,5-anhydro-D-mannitol derivatives and D-fructose were carried out in a dose-dependent manner to determine half-maximum inhibition concentrations (IC_{50}). Solubility: A) Fructose - freely soluble in Krebs–Ringer buffer; B) 2,5-AM derivatives - all the samples were first dissolved in ≤0.1% DMSO and were further diluted using Krebs–Ringer buffer according to the desired concentration maintaining ≤0.1% DMSO; C) Blank - 0.1% DMSO. EMT6 cells were grown to confluence in 12-well cell culture plates with media renewal every 2 days. One hour prior to the experiment, cell culture media was removed, and the plates were washed twice with glucose-free Krebs–Ringer buffer solution. To each well, 1 mL of glucose-free Krebs–Ringer buffer solution was added and incubation at 37°C was continued for 1 h under the glucose-free condition. After one hour, Krebs–Ringer buffer was removed. To each well 400 µL of glucose-free Krebs–Ringer buffer was added containing 0.1–0.5 MBq of 6-[^{18}F]FDF and different concentrations of the 2,5-

AM derivatives (solution prepared in Krebs–Ringer buffer of desired concentration) 3–11 (10^{-8}–10^{-3} and $3x10^{-2}$ M) or fructose (10^{-5} – 1 M) and no compound at all for comparison (=100% uptake). After 60 min incubation time, radiotracer uptake was stopped with 1 mL of ice cold PBS, and the cells were washed twice with PBS and lysed in 0.4 mL radioimmunoprecipitation assay buffer (RIPA buffer). Radioactivity in the cell lysates was then determined as counts per minute (CPM) using a WIZARD2 automatic g-counter (Perkin Elmer, Waltham, MA, USA) and converted to the radioactivity dose SI unit Becquerel (Bq). Data was analyzed as percentage of maximum uptake of 6-[18F]FDF. Graphs were constructed using GraphPad Prism 5.0 (GraphPad Software, San Diego, CA, USA) and half-maximum inhibition concentrations (IC_{50}) were determined by graphical analysis of the concentration-inhibition curves.

Animal model

All animal experiments were carried out in accordance with guidelines of the Canadian Council on Animal Care (CCAC) and were approved by the local animal care committee of the Cross Cancer Institute. Human MDA-MB-231 cells, which form xenografts in female mice, were injected subcutaneously ($2\text{-}5\times10^6$ cells in 100 µL PBS) into 8-10 weeks old female NIH-III nu/nu mice (Charles River, Wilmington, MA, USA). Tumors were imaged after 3-4 weeks when reaching sizes ranging from 300–500 mm^3.

In vivo PET experiments

MDA-MB-231 tumor bearing NIH-III nu/nu mice were anesthetized with isoflurane in 40% oxygen / 60% nitrogen (gas flow, 1 L/min) and body temperature was kept constant at 37°C for the entire experiment. Mice were positioned and immobilized in the prone position into the centre of the field of view of an INVEON® PET scanner (Siemens Preclinical Solutions, Knoxville, TN, U.S.A.). A transmission scan for attenuation correction was not acquired. The amount of radioactivity [Bq] present in the injection solution in a 0.5 mL syringe was determined with a dose calibrator (AtomlabTM 300, Biodex Medical Systems, New York, U.S.A.). After the emission scan was started, radioactivity was injected with a delay of approximately 15 s. Data

acquisition continued for up to 120 min in 3D list mode. 4-8 MBq of ^{18}F-labeled radiotracer in 100 -150 µL saline was injected through a tail vein catheter. The list mode data were sorted into sinograms with 59 time frames (10 x 2 s, 8 x 5 s, 6 x 10 s, 6 x 20 s, 8 x 60 s, 10 x 120 s, 10 x 300 s). The frames were reconstructed using maximum a posteriori (MAP) reconstruction mode. No correction for partial volume effects was performed. The image files were further processed using the ROVER v2.0.51 software (ABX GmbH, Radeberg, Germany).

Masks defining 3D regions of interest (ROI) were set and the ROIs were defined by thresholding. ROIs covered all visible tumor mass of the subcutaneous tumors, and the thresholds were defined by 50% of the maximum radioactivity uptake level for each EMT6 tumor in each animal. Mean standardized uptake values [SUVmean = (activity [Bq]/mL tissue)/(injected activity [Bq]/body weight), mL/kg] were calculated for each ROI. Time-activity curves (TAC) were generated from the dynamic scans. All semi-quantified PET data are presented as means ± SEM. Time-activity curves were constructed using GraphPad Prism 5.0 (GraphPad Software).

Confocal microscopy experiments

For probes: **3-DAM (21)**, **3-FAM (22)**

The procedure was adapted from Kondapi *et al.*[55] EMT6 cells were grown on coverslips to ~90% confluency. 1 h before the assay, the cell media was removed, and the cells were rinsed with pH 7.4 PBS twice. The cells were then incubated at 37 °C with 1 mL of Krebs buffer. The buffer was aspirated, and the cells were treated with 1 mL of either 100 µM **Probe** or 100 µM **Probe** + 20 mM D-glucose or 100 µM **Probe** + 10 mM D-fructose (in pH 7.4 Krebs buffer) for 1 h at 37 °C. The treatment was aspirated, then the cells were washed with ice-cold PBS twice. The cells were then incubated for 7 min at rt with 1 mL of 3.5% PFA in PBS. After PFA removal, the cells were permeabilized using 1 mL of 0.02% Triton X-100 in PBS for 5 min. The permeabilizing solution was removed and the cells were washed with PBS. Then the cells were treated with 1 mL of 0.3 µmol mL^{-1} DAPI in PBS for 15 min. The DAPI solution was removed and the cells were rinsed with PBS. The coverslips were then

mounted onto microscopy slides using 15 μL of Mowiol. The slides were then imaged using the same settings on the Leica SP8 Falcon STED.

For probes: **3-HCAM (23)**, **3-FECAM(24),** and **3-NNECAM (24)**.

The procedure was adapted from Kondapi *et al.*[55] EMT6 cells were grown on coverslips to ~90% confluency. 1 h before the assay, the cell media was removed, and the cells were rinsed with pH 7.4 PBS twice. The cells were then incubated at 37 °C with 1 mL of Krebs buffer. The buffer was aspirated, and the cells were treated with 1 mL of either 100 μM **Probe** or 100 μM **Probe** + 20 mM D-glucose or 100 μM **Probe** + 10 mM D-fructose (in pH 7.4 Krebs buffer) for 1 h at 37 °C. The treatment was aspirated, then the cells were washed with ice-cold PBS twice. The cells were then incubated for 7 min at rt with 1 mL of 3.5% PFA in PBS. After PFA removal, cells were rinsed with PBS. The coverslips were then mounted onto microscopy slides using 15 μL of Mowiol. The slides were then imaged using the same settings on the Leica SP8 Falcon STED.

3.6. References

1. Siegel, R. L.; Miller, K. D.; Jemal, A. Cancer Statistics 2017. *CA Cancer J. Clin.* **2017**, *67*, 7–30.

2. DeSantis, C.; Siegel, R.; Bandi, P.; Jemal, A. Breast Cancer Statistics, 2011. *CA Cancer J. Clin.* **2011**, *61*, 409–418.

3. Jameson, J. L.; Longo, D. L. Precision Medicine--Personalized, Problematic, and Promising. *N. Engl. J. Med.* **2015**, *372*, 2229–2234.

4. Buist, D. S.; Porter, P. L.; Lehman, C.; Taplin, S. H.; White, E. Factors Contributing to Mammography Failure in Women Aged 40-49 Years. *J. Natl. Cancer Inst.* **2004**, *96*, 1432–1440.

5. Berlin, L. The Missed Breast Cancer Redux: Time for Educating the Public about the Limitations of Mammography? *AJR Am. J. Roentgenol.* **2001**, *176*, 1131–1134.

6. Koomen, M.; Pissano, E. D.; Kuzmiak, C.; Pavic, D.; McLelland, R. Future Directions in Breast Imaging. *J. Clin. Oncol.* **2005**, *23*, 1674–1677.

7. Lehman, C. D.; Schnall, M. D. Imaging in Breast Cancer: Magnetic Resonance Imaging. *Breast Cancer Res.* **2005**, *7*, 215–219.

8. Benard, F.; Turcotte, E. Imaging in Breast Cancer: Single-Photon Emission Computed Tomography and Positron Emission Tomography. *Breast Cancer Res.* **2005**, *7*, 153–162.

9. Jadvar, H.; Alavi, A.; Gambhir, S. S. 18F-FDG Uptake in Lung, Breast, and Colon Cancers: Molecular Biology Correlates and Disease Characterization. *J. Nucl. Med.* **2009**, *50*, 182–1827.

10. Buerkle, A.; Weber, W. A. Imaging of Tumor Glucose Utilization with Positron Emission Tomography. *Cancer Metastasis Rev.* **2008**, *27*, 545–554.

11. Levi, J.; Cheng, Z.; Gheysens, O.; Patel, M.; Chan, C. T.; Wang, Y. B.; Namavari, M.; Gambhir, S. S. Fluorescent Fructose Derivatives for Imaging Breast Cancer Cells. *Bioconj. Chem.* **2007**, *18*, 628–634.

12. Flier, J. S.; Mueckler, M. M.; Usher, P.; Lodish, H. F. Elevated Levels of Glucose Transport and Transporter Messenger RNA Are Induced by Ras or Src Oncogenes. *Science* **1985**, *235*, 1492–1495.

13.Yamamoto, T.; Seino, Y.; Fukumoto, H.; Koh, G.; Yano, H.; Inagaki, N.; Yamada, Y.; Inoue, K.; Manabe, T.; Imura, H. Over-Expression of Facilitative Glucose Transporter Genes in Human Cancer. *Biophys. Res. Commun.* **1990**, *170*, 223–230. Barbosa, A,M.; Martel, F. Targeting Glucose Transporters for Breast Cancer Therapy: The Effect of Natural and Synthetic Compounds. *Cancers (Basel)* **2020**, *12*, 154

14. Younes, M.; Lechago, L. V. .; Somoano, J. R.; Mosharaf, M.; Lechago, J. Wide Expression of the Human Erythrocyte Glucose Transporter Glut1 in Human Cancers. *Cancer Res. 56* (1996), 1164–1167.

15. Medina, R. A.; Owen, G. I. Glucose Transporters: Expression, Regulation and Cancer. *Biol. Res.* **2002**, *35*, 9–26.

16. Ak, I.; Stokkel, M. P.; Pauwels, E. K. Positron Emission Tomography with 2-[18F]Fluoro-2-Deoxy-D-Glucose in Oncology. Part II. The Clinical Value in Detecting and Staging Primary Tumours. *J. Cancer Res. Clin. Oncol.* **2000**, *126*, 560–574.

17. Weir, L.; Worsley, D.; Bernstein, V. The Value of FDG Positron Emission Tomography in the Management of Patients with Breast Cancer. *Breast J.* **2005**, *11*, 204–209.

18. Santiago, J. F.; Gonen, M.; Yeung, H.; Macapinlac, H.; Larson, S. A. A Retrospective Analysis of the Impact of 18F-FDG PET Scans on Clinical Management of 133 Breast Cancer Patients. *Q J. Nucl. Med. Mol. Imaging* **2006**, *50*, 61–67.

19. Mavi, A.; Urhan, M.; Jian, Q. Y.; Zhuang, H.; Houseni, M.; Cermik, T. F.; Thiruvenkatasamy, D.; Czerniecki, B.; Schnall, M.; Alavi, A. Dual Time Point 18F-FDG PET Imaging Detects Breast Cancer with High Sensitivity and Correlates Well with Histologic Subtypes. *J. Nucl. Med.* **2006**, *47*, 1440–1446.

20. Sundararajan, L.; Linden, H. M.; Link, J. M.; Krohn, K. A.; Mankoff, D. A. 18F-Fluoroestradiol. *Semin. Nucl. Med.* **2007**, *37*, 470–476.

21. Buck, A. K.; Schirrmeister, H.; Mattfeldt, T.; Reske, S. N. Biological Characterisation of Breast Cancer by Means of PET. *Eur J. Nucl. Med. Mol. Imaging* **2004**, *31(Suppl 1)*, S80–S87.

22. Alavi, A.; Zhuang, H. Finding Infection-Help from PET. *Lancet* **2001**, *358*, 1386.

23. Schirmer, M.; Calamia, K. T.; Wenger, M.; Klauser, A.; Salvarani, C.; Moncayo, R. 18F-Fluorodeoxyglucose-Positron Emission Tomography: A New Explorative Perspective. *Exp. Gerontol.* **2003**, *38*, 463–470.

24. Kubota, R.; Kubota, K.; Yamada, S.; Tada, M.; Ido, T.; Tamahashi, N. Microautoradiographic Study for the Differentiation of Intratumoral Macrophages, Granulation Tissues and Cancer Cells by the Dynamics of Fluorine-18-Fluorodeoxyglucose Uptake. *J. Nucl. Med.* **1994**, *35*, 102–112.

25. Younes, M.; Brown, R. W.; Mody, D. R.; Fernandez, L.; Laucirica, R. GLUT1 Expression in Human Breast Carcinoma: Correlation with Known Prognostic Markers. *Anticancer. Res.* **1995**, *15*, 2895–2898.

26. Ravazoula, P.; Batistatou, A.; Aletra, C.; Ladopoulos, J.; Kourounis, G.; Tzigounis B. Immunohistochemical Expression of Glucose Transporter Glut1 and Cyclin D1 in Breast Carcinomas with Negative Lymph Nodes. *Eur. J. Gynaecol. Oncol.* **2003**, *24*, 544–546.

27. Kuo, S. J.; Wu, Y. C.; Chen, C. P.; Tseng, H. S.; Chen, D. R. Expression of Glucose Transporter-1 in Taiwanese Patients with Breast Carcinoma — a Preliminary Report. *Kaohsiung J. Med. Sci.* **2006**, *22*, 339–345.

28. Wuest, M.; Hamann, I.; Bouvet, V.; Glubrecht, D.; Marshall, A.; Trayner, B. J.; Soueidan, O.-M.; Krys, D.; Wagner, M.; Cheeseman, C. I.; West, F. G.; Wuest, F. Molecular Imaging of GLUT1 and GLUT5 in Breast Cancer: A Multitracer PET Imaging Study in Mice. *Mol. Pharmacol.* **2018**, *93*, 79–89. Mankoff D.A.; Eubank W.B. Current and future use of positron emission tomography (PET) in breast cancer. J. Mammary Gland. Biol. Neoplasia. 2006, *11*, 125-36.

29. Henry, K.E.; Ulaner, G.A.; Lewis, J.S. Clinical Potential of Human Epidermal Growth Factor Receptor 2 and Human Epidermal Growth Factor Receptor 3 Imaging in Breast Cancer. *PET Clin.* **2018**, *13*, 423-435; Ulaner, G.A.; Schuster, D.M. Amino Acid Metabolism as a Target for Breast Cancer Imaging. *PET Clin.* **2018**, *13*, 437-444; Fleming, I. N.; Gilbert, F.J.; Miles, K. A.; Cameron, D. Opportunities for PET to deliver clinical benefit in cancer: breast cancer as a paradigm. *Cancer Imag.* 2010, *10,* 144-52; Wibmer, A. G.; Hricak, H.; Ulaner, G. A.; Weber, W. Trends in oncologic hybrid imaging.Eur. J. Hybrid Imaging. **2018**, *2*, 1.

30. Zamora-León, S. P.; Golde, D. W.; Concha, I. I.; Rivas, C. I.; Delgado-López,F.; Baselga, J.; Nualart, F.; Vera, J. C. Expression of the Fructose Transporter GLUT5 in Human Breast Cancer. *Proc. Natl. Acad. Sci. U.S.A.* **1996**, *93*, 1847–1842.

31. Barron, C. C.; Bilan, P. J.; Tsakiridis, T.; Tsiani, E. Facilitative Glucose Transporters: Implications for Cancer Detection, Prognosis and Treatment. *Metabolism* **2016**, *65*, 124–139. Macheda, M. L.; Rogers, S.; Best, J. D. Molecular and Cellular Regulation of Glucose Transporter (GLUT) Proteins in Cancer. *J. Cell Physiol.* **2005**, *202*, 654–662.

32. Godoy, A.; Ulloa, V.; Rodríguez, F.; Reinicke, K.; Yañez, A. J.; García, M. D. L. A.; Medina, R. A.; Carrasco, M.; Barberis, S.; Castro, T.; Martínez, F.; Koch, X.; Vera, J. C.; Poblete, M. T.; Figueroa, C. D.; Peruzzo, B.; Nualart, F. Differential Subcellular Distribution of Glucose Transporters GLUT1-6 and GLUT9 in Human Cancer:

Ultrastructural Localization of GLUT1 and GLUT5 in Breast Tumor Tissues. *J. Cell Physiol.* **2005**, *207*, 614–627.

33. Chan, K. K.; Chan, J. Y.; Chung, K. K.; Fung, K. P. Inhibition of Cell Proliferation in Human Breast Tumor Cells by Antisense Oligonucleotides against Facilitative Glucose Transporter. *J. Cell Biochem.* **2004**, *93*, 1134–1142.

34. Wuest, M.; Trayner, B. J.; Grant, T. N.; Jans, H. S.; Mercer, J. R.; Murray, D.; West, F. G.; McEwan, A. J.; Wuest, F.; Cheeseman, C. I. Radiopharmacological Evaluation of 6-Deoxy-6-[18F] Fluoro-D-Fructose as a Radiotracer for PET Imaging of GLUT5 in Breast Cancer. *Nucl. Med. Biol.* **2011**, *38*, 461–475.

35. Manolescu, A. R.; Witkowska, K.; Kinnaird, A.; Cessford, T.; Cheeseman, C. Facilitated Hexose Transporters: New Perspectives on Form and Function. *Physiology* **2007**, *22*, 234–240.

36. Raushel, F. M.; Cleland, W. W. The Substrate and Anomeric Specificity of Fructokinase. *J. Biol. Chem.* **1973**, *248*, 8174.

37. Raushel, F. M.; Cleland, W. W. Bovine Liver Fructokinase: Purification and Kinetic Properties. *Biochemistry* **1977**, *16*, 2169–2175.

38. Chenault, H. K.; Mandes, R. F.; Hornberger, K. R. Synthetic Utility of Yeast Hexokinase. Substrate Specificity, Cofactor Regeneration, and Product Isolation. *J. Org. Chem.* **1977**, *62*, 331–336.

39. Aloj, L.; Caraco, C.; Jagoda, E.; Eckelman, W. C.; Neumann, R. D. Glut-1 and Hexokinase Expression: Relationship with 2-Fluoro-2-Deoxy-D-Glucose Uptake in A431 and T47D Cells in Culture. *Cancer Res.* **1999**, *59*, 4709–4714.

40. Haradahira, T.; Tanaka, A.; Maeda, M.; Kanazawa, Y.; Ichiya, Y. I.; Masuda, K. Radiosynthesis, Rodent Biodistribution, and Metabolism of 1-Deoxy-1-[18F] Fluoro-D-Fructose. *Nucl. Med. Biol.* **1995**, *22*, 719–725.

41. Trayner, B. J.; Grant, T. N.; West, F. G.; Cheeseman, C. I. Synthesis and Characterization of 6-Deoxy-6-Fluoro-D-Fructose as a Potential Compound for Imaging Breast Cancer with PET. *Bioorg. Med. Chem.* **2009**, *17*, 5488–5495.

42. Wester, H. J. *Pharmaceutical Radiochemistry (I)*; Munich Molecular Imaging Handbook Series; *Scintomics*, 1, 2010.

43. Zancan, P.; Sola-Penna, M.; Furtado, C. M.; Da Silva, D. Differential Expression of Phosphofructokinase-1 Isoforms Correlates with the Glycolytic Efficiency of Breast Cancer Cells. *Mol. Genet. Metab.* **2010**, *100*, 372–378.

44. Kim, J.; Kang, J.; Kang, Y. L.; Woo, J.; Kim, Y.; Huh, J.; Park, J. W. Ketohexokinase-A Acts as a Nuclear Protein Kinase That Mediates Fructose-Induced Metastasis in Breast Cancer. *Nat. Comm.* **2020**, *11*, 1–20.

45. Gowrishankar, G.; Zitzmann-Kolbe, S.; Junutula, A.; Reeves, R.; Levi, J.; Srinivasan, A.; Bruus-Jensen, K.; Cyr, J.; Dinkelborg, L.; Gambhir, S. S. GLUT 5 Is Not Over-Expressed in Breast Cancer Cells and Patient Breast Cancer Tissues. *PLoS One* **2011**, *6*, e26902.

46. Kang, H.; Kim, H.; Lee, S.; Youn, H.; Youn, B. Role of Metabolic Reprogramming in Epithelial–Mesenchymal Transition (EMT). *Int. J. Mol. Sci.* **2019**, *20*, 2042.

47. Yoshioka, K.; Takahashi, H.; Homma, T.; Saito, M.; Oh, K. B.; Nemoto, Y.; Matsuoka, H. A Novel Fluorescent Derivative of Glucose Applicable to the Assessment of Glucose Uptake Activity of Escherichia Coli. *Biochim. Biophys. Acta Biomembr.* **1996**, *1289*, 5–9.

48. Yoshioka, K.; Saito, M.; Oh, K. B.; Nemoto, Y.; Matsuoka, H.; Natsume, M.; Abe, H. Intracellular Fate of 2-NBDG, a Fluorescent Probe for Glucose Uptake Activity, in Escherichia Coli Cells. *Biosci. Biotechnol. Biochem.* **1996**, *60*, 1899–1901.

49. Cheng, Z.; Levi, J.; Xiong, Z.; Gheysens, O.; Keren, S.; Chen, X.; Gambhir, S. S. Near-Infrared Fluorescent Deoxyglucose Analogue for Tumor Optical Imaging in Cell Culture and Living Mice. *Bioconj. Chem.* **2006**, *17*, 662–669.

50. Zhang, M.; Zhang, Z.; Blessington, D.; Li, H.; Busch, T. M.; Madrak, V.; Miles, J.; Chance, B.; Glickson, J. D.; Zheng, G. Pyropheophorbide 2-Deoxyglucosamide: A New Photosensitizer Targeting Glucose Transporters. *Bioconj. Chem.* **2003**, *14*, 709–714.

51. Jo, A.; Sung, J.; Lee, S.; Nam, H.; Lee, H. W.; Park, J.; Kim, H. M.; Kim, E.; Park, S. B. Near-IR Fluorescent Tracer for Glucose-Uptake Monitoring in Live Cells. *Bioconj. Chem.* **2018**, *29*, 3394–3401.

52. Yuen, R.; Wagner, M.; Richter, S.; Dufour, J.; Wuest, M.; West, F. G.; Wuest, F. Design, Synthesis, and Evaluation of Positron Emission Tomography/Fluorescence Dual Imaging Probes for Targeting Facilitated Glucose Transporter 1 (GLUT1). *Org. Biomol. Chem.* **2021**, *19*, 3241–3254.

53. Tanasova, M.; Plutschack, M.; Muroski, M. E.; Sturla, S. J.; Strouse, G. F.; McQuade, D. T. Fluorescent THF-based Fructose Analogue Exhibits Fructose-dependent Uptake. *ChemBioChem* **2013**, *14*, 1263–1270.

54. Soueidan, O.-M.; Scully, T. W.; Kaur, J.; Panigrahi, R.; Belovodskiy, A.; Do, V.; Matier, C. D.; Lemieux, M. J.; Wuest, F.; Cheeseman, C.; West, F. G. Fluorescent Hexose Conjugates Establish Stringent Stereochemical Requirement by Glut5 for Recognition and Transport of Monosaccharides. *ACS Chem. Biol.* **2017**, *12*, 1087–1094.

55. Kondapi, V. P. K. .; Soueidan, O.-M.; Cheeseman, C. I.; West, F. G. Tunable GLUT–Hexose Binding and Transport via Modulation of Hexose C-3 Hydrogen-Bonding Capabilities. *Chem. Eur. J.* **2017**, *23*, 8073–8081.

56. Begoyan, V.V.; Weseliński, Ł.J.; Xia, S.; Fedie, J.; Kannan, S.; Ferrier, A.; Rao, S.; Tanasova, M. 2018. Multicolor GLUT5-permeable fluorescent probes for fructose transport analysis. *Chem. Comm.*, **2018,** *54*, 3855-3858.

57. Gnaccarini, C.; Ben-Tahar, W.; Mulani, A.; Roy, I.; Lubell, W. D.; Pelletier, J. N.; Keillor, J. W. Site-specific protein propargylation using tissue transglutaminase. *Org. Biomol. Chem.* **2012**, *10*, 5258–5265.

58. Shiota, S.; Yamamoto, S.; Shimomura, A.; Ojida, A.; Nishino, T.; Maruyama, T. Quantification of amino groups on solid surfaces using cleavable fluorescent compounds. *Langmuir* **2015**, *31*, 8824–8829.

Chapter 4

A novel fluorescence-based assay for the identification of GLUT5 inhibitors through systematic screening of 2,5-anhydro-D-mannitol derivatives[a]

4.1. Introduction

Hexoses are an explicit energy source and the most essential fuel for cellular metabolism.[1] Bearing polyhydroxy substitutions, hexoses are very hydrophilic moieties that are not able to traverse the lipid cell membrane via simple diffusion. Instead, mammalian facilitative hexose transporters (GLUTs) mediate hexose trafficking from extracellular space to intracellular space and vice versa.[2,3] Two main distinct types of hexose transporters have been identified; sodium-glucose co-transporters (SGLTs) and glucose transporters (GLUTs). In SGLTs, energy for active hexose transport is fueled by the sodium ion gradient across the cell membrane, whereas the GLUTs allow the passage of hexoses across the plasma membrane employing a facilitated diffusion mechanism, using existing chemical or electrochemical gradients.[2,4–6]

These GLUT proteins, encoded by the solute carrier (SLC2) genes, have been further divided into fourteen known isoforms, all of which have well established roles and a distinct pattern of tissue distribution, acting as transporters in different tissues and cell types.[7] For instance, GLUT1 is mostly localized in erythrocytes as well as the blood-brain barrier and responsible for the vital transport of glucose into the brain,[8,9] while GLUT4 is the major insulin-responsive glucose transporter that is distributed in the skeletal muscles, adipocytes, and cardiomyocytes.[10] GLUT5 is predominantly expressed in the small intestine and one of its primary functions is mediating dietary

---

[a]The contents of this chapter have been copied and/or adapted from the following manuscript in preparation: Rana, N.; Aziz, M.A.; Serya, R.A.T.; Lasheen, D. S.; Samir, N; Abouzid, K.A.M.; West, F.G. A novel fluorescence-based assay for the identification of GLUT5 inhibitors through systematic screening of 2,5-anhydro D-mannitol derivatives.

fructose uptake across the apical membrane of the small intestine.[11] Based on amino acid sequence, substrate preferences, tissue specificity, and structural similarity, GLUTs have been classified into three major groups. Class I comprises GLUTs 1-4 and 14 and primarily facilitates D-glucose transport. Class-II is composed of GLUTs 5, 7, 9, and 11, showing relatively high specificity towards D-fructose. However, the Class III family (GLUTs 6, 8, 10, 12, and 13) is structurally atypical and its functional activity is still poorly understood.[4,7,12–15]

Plenty of disease states such as obesity, insulin resistance diabetes, gout, and non-alcoholic fatty liver diseaseare characterized by alteration in the expression patterns of hexose transporters (GLUTs).[16–20] Consequently, interest in these GLUT transporters have grown recently as they were found to be overexpressed in tumor cells owing to faster cell division and altered metabolic profiles, demanding a continuous supply of hexose fuel.[20–22] Of the 14 GLUT family members, GLUT5 shows a unique substrate preference towards D-fructose, the second most abundant energy substrate in tumor cells.[11]Intrestingly, this high affinity fructose transporter exhibits overexpression in breast carcinoma cell lines,[23,24] along with other numerous cancers,[25,26] while tightly regulated in normal healthy tissues.[11,23] Such dependence of the metabolically compromised cancer cells on high nutrient uptake provides avenues to exploit GLUT5 as a valuable target in anticancer imaging and therapeutic approaches.

GLUT5, together with other GLUT transporter proteins, belongs to the larger major facilitator superfamily (MFS), having a barrel structure in which two clusters of six transmembrane helices surround the central aqueous pore containing the substrate binding site.[27–29] Recent X-ray crystal structure analyses suggest that hexose transport is achieved through a conformational shift of the protein folding between outward-open, occluded, and inward-open conformational states.[27–30] The existence of certain critical hydroxyl substituents as well as their stereochemistry on the D-fructose molecule tends to play a fundamental role in the D-fructose–GLUT5 binding process. The carbon skeleton of D-fructose, in addition, is believed to be responsible for the nonpolar interactions between D-fructose and hydrophobic amino acid residues of the GLUT5 protein.[3,16,28,31]

Previously performed structure activity relationship studies on GLUT5 substrates demonstrated the ability of its binding pocket to accept D-fructose in its furanose and pyranose ring forms.[32] Moreover, the C-1, C-3 and C-4 hydroxyl groups of the D-fructose molecule appear to form essential hydrogen bonding interactions with specific amino acid residues within the binding pocket for efficient uptake.[16,32,33] In contrast, the role of the hydroxyl groups at C-2 and C-6 was found to play a insignificant role in substrate recognition, rendering several C-6 labeled D-fructose analogs readily handled by GLUT5.[16,32–35] Nevertheless, after GLUT5 mediated transport into intracellular space, accumulation of these probes inside the cells is hampered and substantial efflux occurs due to masking of C-6 hydroxyl group as a potential site for phosphorylation by hexokinase enzymes, resulting in loss of metabolic trapping.[36,37] Elimination of the C-2 hemiacetal hydroxyl group of D-fructose attained a fructose analog with C_2-symmetry, 2,5-anhydro-D-mannitol (2,5-AM), which closely resembles the methyl-β-D-fructofuranoside structure and exhibit slightly higher affinity to GLUT5 than D-fructose.[32] To resolve the high efflux property observed with C-6 modified D-fructose analogs, the two primary hydroxyl groups at C-1/C-6 of 2,5-AM should be left untouched, while modifications at C-3 or C-4 positions could be evaluated for their tolerability by GLUT5.

In an early thorough study conducted by our group, a detailed structure activity relationship analysis was carried out through a series of C-3 modified 2,5-AM-based derivatives, exhibiting different hydrogen bond donor/acceptor properties. It was emphasized that retention of hydrogen bond donor ability at the C-3 position is key for GLUT5 mediated uptake with very high affinity.[38] In a further complementary study, aiming to provide more broad insight into GLUT5 structural demands and binding pocket requirements, we have synthesized a selection of C-3 derived 2,5-AM probes, installed with different hydrogen bond donor moieties.[39] The transport properties of these probes were investigated in the GLUT5-expressing murine breast cancer cell line EMT6 against the radiolabeled GLUT5 substrate, 6-[^{18}F]-deoxy-6-fluoro-D-fructose (6-[^{18}F] FDF), using the non-radiolabeled fructose derivative and 6-FDF **(I)** as the reference compound (Figure 4.1).[35,37] Relative to 6-FDF, several compounds displayed

strong inhibitory activity on 6-[^{18}F]FDF uptake into EMT6 cells (refer to Chapter 2). Figure 4.1 presents reported analogs and inhibitors that acts through different GLUT pathways.[35,38,40-42]

In this current study, a novel fluorescence-based assay has been developed with the ultimate purpose of evaluating the affinity of various C-3 modified 2,5-AM compounds to GLUT5, using our own synthesized reference compound, 6-NBDF **(II)** (Figure 4.1). This fluorescently labeled fructose analog is exploited as an alternative reference compound to 6-[^{18}F]FDF, eliminating the need to synthesize any radiolabeled moiety. Accordingly, an extended series of our previously synthesized C-3 derived 2,5-AM compounds, bearing hydrogen bond donor functionalities (namely anilines, amides, sulfonamides, ureas, and thioureas) were evaluated in murine EMT6 mammary cells utilizing this new fluorescent-based assay (Figure 4.2). In addition, we also performed this assay with compounds depicted in Figure 4.1 by treating them as reference compounds.

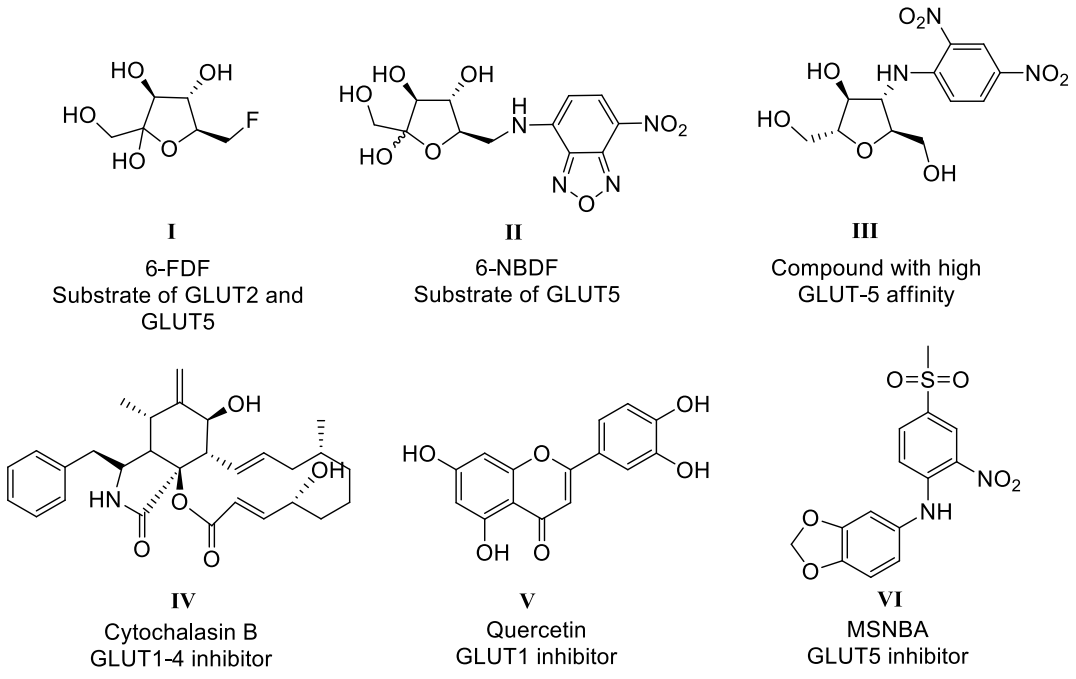

Figure 4.1. Compounds acting on different GLUT pathway

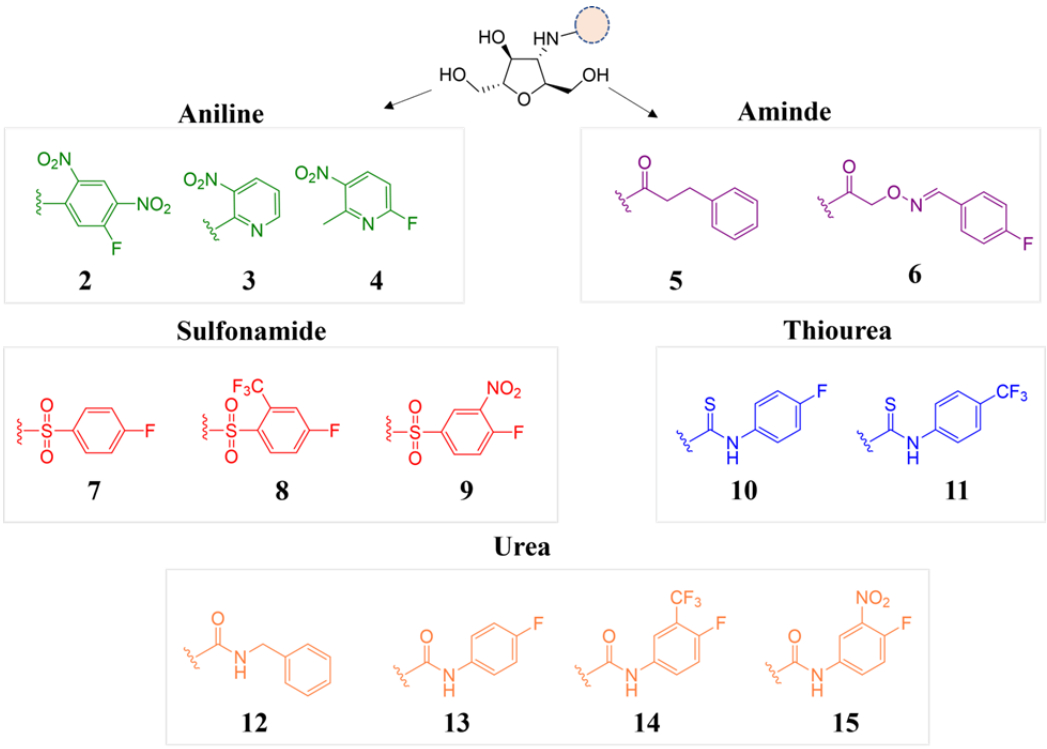

Figure 4.2. A series of C-3 derived 2,5-AM compounds

4.2. Results and Discussion

4.2.1. Synthesis of C-3 modified 2,5-AM derivatives

Various C-3 derived 2,5-AM compounds **(2-15)** were synthesized according to the synthetic route depicted in Scheme 4.1. The key intermediate 3-amino-3-deoxy-2,5-anhydro-D-mannitol **(1)** was prepared according to the procedure reported in our previous study,[39,] and was then functionalized to different C-3 modified 2,5-AM derivatives. (Scheme 4.1) Compounds **2**, **6**, **7**, **8**, and **10** were synthesized according to the reported procedure.[39] Herein, the pyrido aniline derivatives (**3** and **4**) were obtained through reacting amine (**1**) with 2-chloro-3-nitropyridine and 2,6-difluoro-3-nitropyridine, respectively in DMF, while the synthesis of the amide derivative **(5)** was accomplished by treating the amine (**1**) with *N*-succinimidyl 3-phenylpropanoate in methanol. Formation of compounds **3** and **4** occurred via ipso substitution. In case of **4,** regioselectivity was observed as amino group of 2,5-AM displaced fluoro group at C-2 position of pyridine reagent. Formation of compound **5** proceeed through the

reaction of NHS ester with amino group of 2,5-AM forming an amide bond and N-hydroxy succinimide as the by product. Regarding sulfonamide derivative (**9)**, its preparation involved condensation reaction between amine (**1)** and 4-fluoro-3-nitrobenzenesulfonyl chloride in presence of sodium carbonate and acetonitrile at ambient temperature. To afford thiourea compound (**11)**, amine (**1)** was reacted in with 4-fluorophenyl-2-(trifluoromethyl) phenyl isothiocyanate in methanaol for 15 hours. Finally, amine (**1)** was treated with different isocyanate derivatives in DMF at room temperature affording the urea derivatives (**12-15**) in good to moderate yields. (Scheme 4.1)

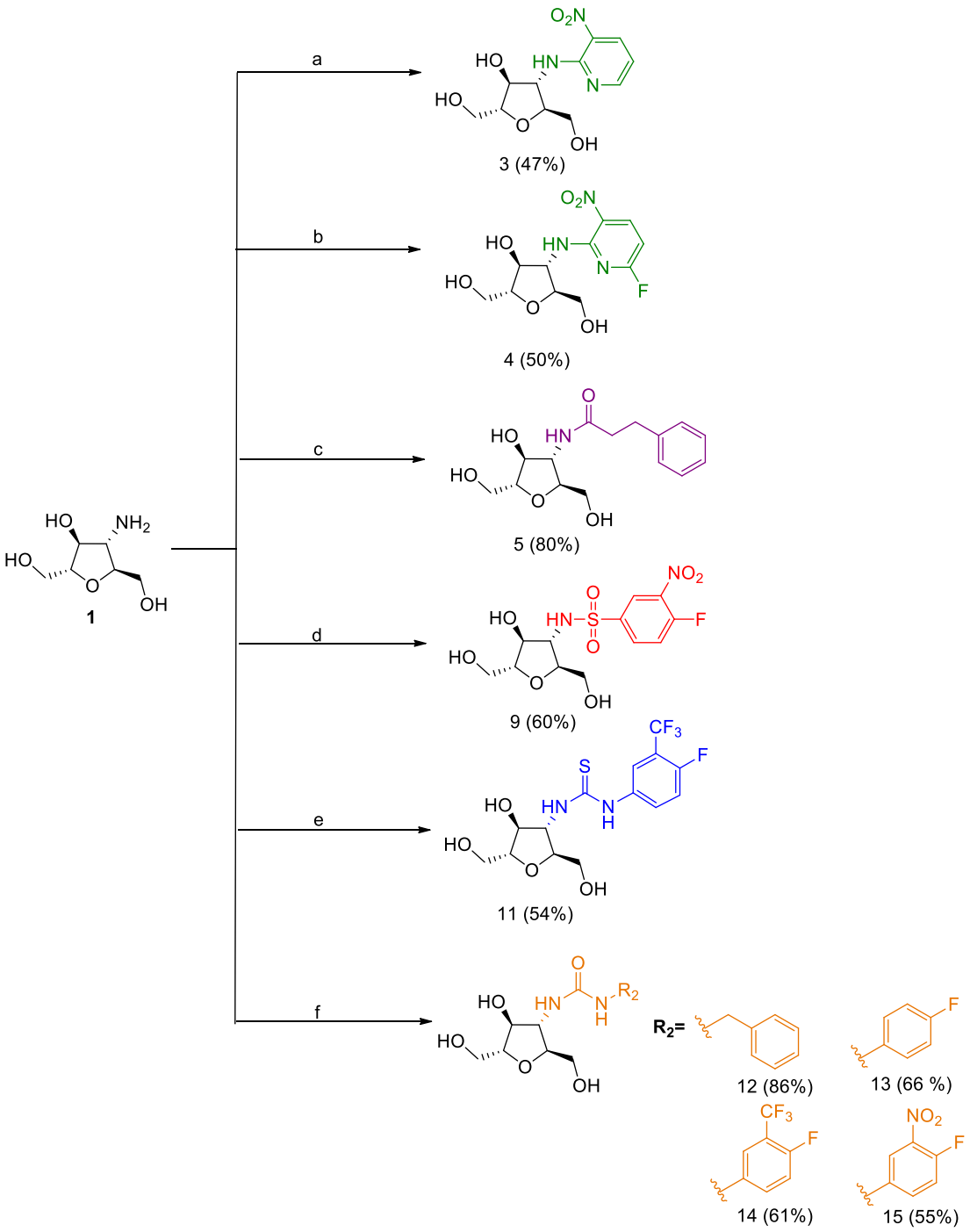

Scheme 4.1. Synthesis of C-3 derived 2,5-AM compounds. Reagents and conditions: a) 2-chloro-3-nitropyridine, $NaHCO_3$, DMF, RT, 12 h then 80 °C, 15 h, 47%; b) 2,6-difluoro-3-nitropyridine, $NaHCO_3$, DMF, RT, 2 h, 50%; c) *N*-succinimidyl 3-phenylpropanoate, MeOH, RT, 2 h, 80%; d) 4-fluoro-3-nitrobenzenesulfonyl chloride, Na_2CO_3, MeCN, RT, 16 h, 60%; e) 4-fluorophenyl-2-(trifluoromethyl)phenyl isothiocyanate, MeOH, RT, 15 h, 54%; f) Isocyanate derivatives: Benzyl isocyanate, 4-fluorophenyl isocyanate, 4-fluoro-3-(trifluoromethyl)phenyl isocyanate, 4-fluoro-3-nitrophenyl isocyanate, DMF, RT, 15 h

4.2.2. Biological Evaluation

4.2.2.1. Validation of 6-NBDF as a reference compound

6-NBDF probe **II**, the reference compound used in the assay under development here has been previously reported to be transported via GLUT5 pathway and could have the potential to serve as a laboratory tool for assessing the trafficking of D-fructose mimics inside GLUT5-expressing breast cancer cells.[38] It was observed that 6-NBDF was taken up rapidly into the mammalian EMT6 cell line via GLUT5 machinery and competitively inhibited the uptake of [^{14}C]-D-fructose, the natural substrate of GLUT5, with an IC_{50} = 2.9 ± 1.14 mM.[31] In addition, complementary qualitative confocal microscopy experiments were conducted, offering solid evidence for 6-NBDF cell internalization. Furthermore, uptake was inhibited in the presence of D-fructose but was unaffected by D-glucose, indicating primary uptake via GLUT5 rather than GLUT2.[38] These studies provided key support for the hypothesis that 6-NBDF **II** could serve as a reference compound in our proposed fluorescence-based GLUT5 assay.

To evaluate the suitability of the fluorescent probe molecule **II** as a reference compound in this assay, several preliminary experiments were conducted. First, the concentration-dependent uptake of **II** by EMT6 cell lines was examined. It was observed that a linear relationship of fluorescence intensity occurred with the incubation of EMT6 cells with increasing concentrations of probe **II**. (Figure 4.3 Panel A). Secondly, 350 μM (0.35 mM) of **II** was incubated in EMT6 cells at different intervals for 2 h to determine the time-dependent uptake of the probe compound. As anticipated, the fluorescence signal was detected to be continuously increasing with time (Figure 4.3 Panel B). An increase in fluorescence intensity in both concentration and time-based manner would set the basis for optimization of an inhibition assay to determine the optimal time and concentration of 6-NBDF to be used for further steps.

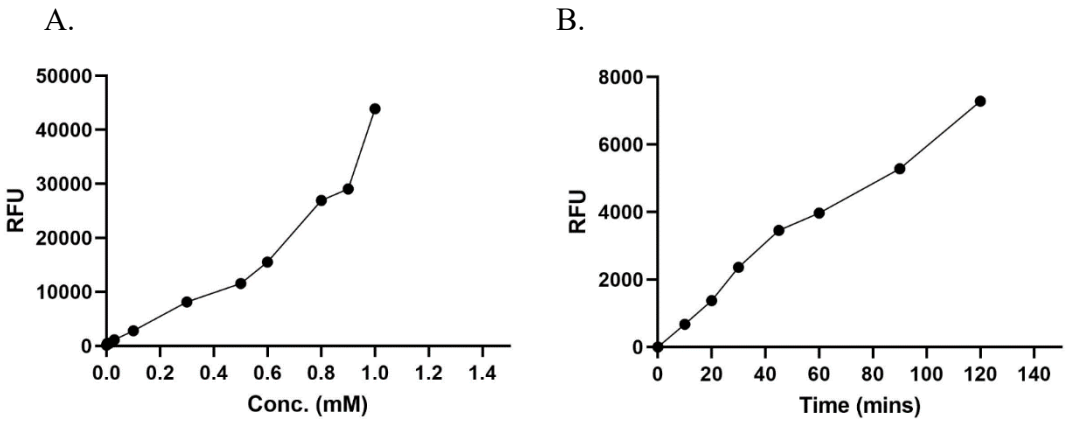

Figure 4.3. A) Concentration-dependent uptake of 6-NBDF into EMT6 cells with different concentrations ranging from 10^{-4}-10^{-1}-9×10^{-1}-1 M); **B)** Time-dependent uptake of 6-NBDF into EMT6 cells measured at different time intervals up to 2h

4.2.2.2. In vitro 6-NBDF uptake inhibition assay by C-3 modified 2,5-AM compounds

The effect of structural variation among the novel C-3 modified 2,5-AM derivatives described above was investigated to gain a better understanding of the interactions required for GLUT5 recognition. The murine mammary carcinoma cell line EMT6, previously shown to express the GLUT5 transporter, was used in these experiments to measure the concentration-dependent inhibition of their uptake of **II** by derivatives **2-15**. Table 4.1 and Figures 4.4-4.9 depict the concentration dependent inhibition of 6-NBDF uptake into EMT6 cells in presence of different compounds (**2-15**) and their IC_{50} values.

Table 4.1. Half-maximum inhibition concentrations (IC_{50}) for C-3 derived 2,5-AM compounds **(2-15)**, D-fructose, GLUT5 substrate **(III)**, cytochalasin B **(IV)**, quercetin **(V),** and MSNBA **(VI)** against the uptake of 6-NBDF and 6-[^{18}F]FDF[39] into EMT6 cells. Data shown as mean ± SEM from n data points out of x experiments; n.d. = not determined,– not performed, [b]50% inhibition was observed.[43]

Compound	n/x	IC_{50} (mM) against 6-NBDF	IC_{50} (mM) against 6-[^{18}F]FDF(refer to chapter 2)[39]
2	**9/3**	1.05	1.10 ± 0.17
3	**9/3**	2.24	-
4	**9/3**	0.99	-
5	**9/3**	n.d.	-
6	**9/3**	1.48	2.31 ± 0.35
7	**9/3**	n.d.	~6 (estimated)
8	**9/3**	4.63	n.d.
9	**9/3**	1.61	-
10	**9/3**	n.d.	-
11	**9/3**	6.84	-
12	**9/3**	2.16	-
13	**9/3**	n.d.	-
14	**9/3**	2.88	-
15	**9/3**	5.04	-
Cytochalasin B	**9/3**	n.d.	b
Quercetin	**9/3**	n.d.	-
MSNBA	**9/3**	n.d.	n.d.
III	**9/3**	2.92	-
D-Fructose	**9/3**	1710	342 ± 74

We initiated our study by investigating the effect of D-fructose as a reference to study its inhibitory effect on 6-NBDF uptake. An IC_{50} of 1.7 M was observed which is quite high even though D-fructose is the natural substrate of GLUT5.

Aniline derivatives **2, 3,** and **4** were found to be potent inhibitors of 6-NBDF uptake into the EMT6 cells, compared to D-fructose, with IC_{50} values of 1.05, 2.24, and 0.99 mM respectively (Table 4.1 and Figure 4.4). These findings are consistent with our previously reported result of compound **3** (refer to Chapter 2)[39], which was found to be a potent inhibitor of 6-[^{18}F]FDF uptake by EMT6 cells. Such potent activity exerted by these probes may be due to the collective electron withdrawing influence of the benzene ring substituents. These substituents are expected to remove electron density from the aniline nitrogen, rendering it a better hydrogen bond donor.

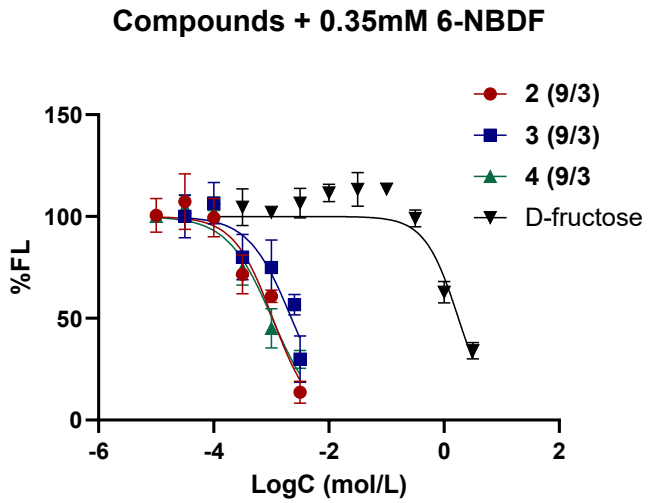

Figure 4.4. Concentration-dependent inhibition of 6-NBDF uptake into EMT6 cells of C-3 derived 2,5-AM compounds **2**, **3, 4,** and **D-fructose.** Data are shown as mean ± SEM of n data points from 2-4 experiments

Moving to the amide-bearing derivatives (Figure 4.5, Table 4.1), compound **5** exhibited no effect on 6-NBDF uptake into EMT6 cells. However, compound **6,** with an aryl ring incorporated by a slightly long tether compared to **5**, displayed a significant inhibitory activity with an IC_{50} of 1.48 mM, demonstrating the affinity and tolerability of GLUT5 binding pocket to an oxime ether linkage in the tether. Again, some

consistency was noticed with our previous 6-[^{18}F]FDF uptake result, where **6** showed potency in inhibiting the uptake of 6-[^{18}F]FDF with an IC_{50} of 2.31 ± 0.35 mM. (refer to Chapter 2)

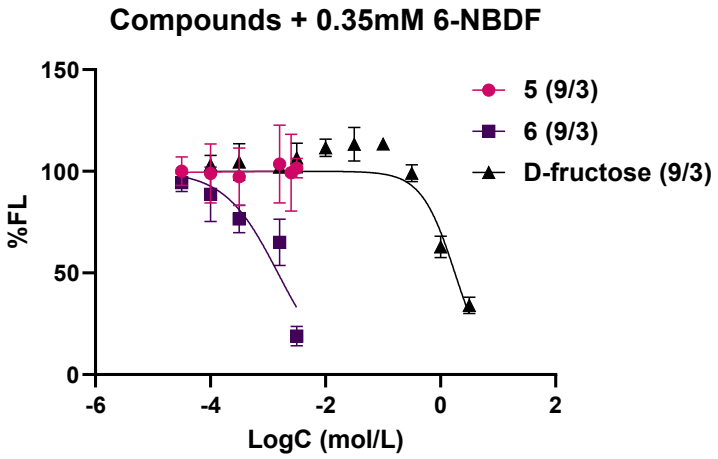

Figure 4.5. Concentration-dependent inhibition of 6-NBDF uptake into EMT6 cells of C-3 derived 2,5-AM compounds **5, 6,** and **D-fructose.** Data are shown as mean ± SEM of n data points from 2-4 experiments

Sulfonamide **7** displayed no inhibition of uptake of **II** by EMT6 cells. Interestingly, sulfonamides **8** and **9** showed strong inhibitions with IC_{50} values of 4.63 mM and 1.61 mM respectively (Figure 4.6 and Table 4.1). On the contrary, sulfonamide **7** did moderately inhibit the uptake of 6-[^{18}F]FDF with an approximate IC_{50} of 6 mM. For compounds **8** and **9,** the mentioned observations could be delineated due to the presence of electron withdrawing groups (-CF_3 and -NO_2) leading to diminishing of electron density on the amine linker with nitro group being a strong electron withdrawing than the trifluoromethyl group.

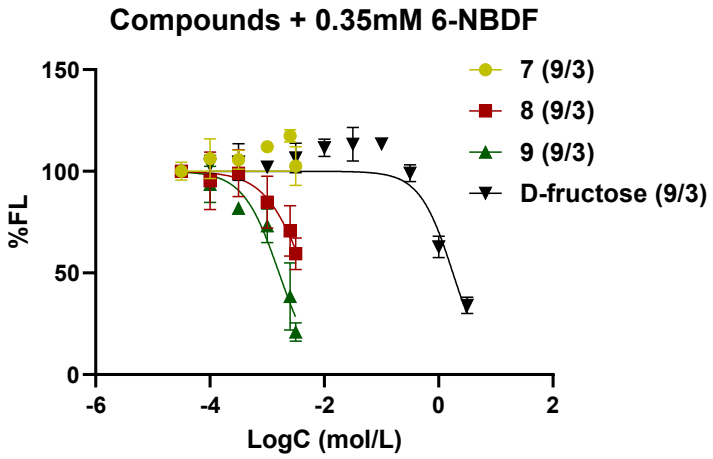

Figure 4.6. Concentration-dependent inhibition of 6-NBDF uptake into EMT6 cells of C-3 derived 2,5-AM compounds **7, 8, 9,** and **D-fructose.** Data are shown as mean ± SEM of n data points from 2-4 experiments

Compound **10** containing a thiourea moiety, exerted no inhibitory effect aligning with the results obtained in case of 6-[^{18}F]FDF transport. However, compound **11** displayed relatively weak inhibitory effect with an IC_{50} of 6.84 mM (Figure 4.7 and Table 4.1).

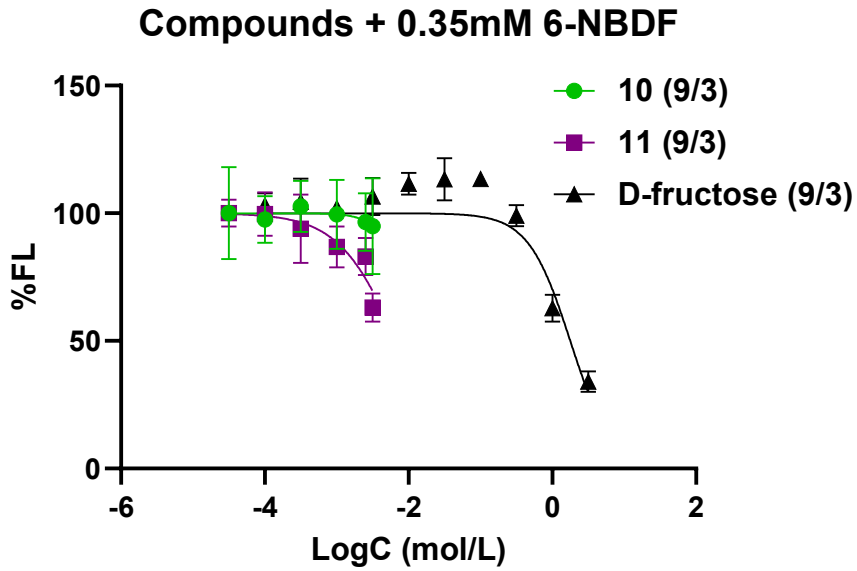

Figure 4.7. Concentration-dependent inhibition of 6-NBDF uptake into EMT6 cells of C-3 derived 2,5-AM compounds **10,11,** and **D-fructose.** Data are shown as mean ± SEM of n data points from 2-4 experiments. Further measurements of **11** and **12** were limited due to their poor solubility in buffer

Finally, upon evaluating novel urea-linked 2,5-AM derivatives **12-15** (Figure 4.8 and Table 4.1), we observed that urea functionalization at C-3 in compounds **12, 14,** and **15** is generally tolerated and resulted in a significant increase in the inhibition efficacy, in comparison to D-fructose, with IC_{50} values of 2.16, 2.35 and 5.04 mM respectively. In the case of urea and thiourea containing derivatives, substituents on the benzyl ring are not involved in conjugation with NH at C-3, and the presence of these substituents on the remote aryl ring would not participate in influencing the hydrogen bonding capacity of NH at C-3. Compound **13** having the same para fluorine atom substituent similar to that of thiourea derivative **10,** exhibited no inhibitory effect suggesting similar type of binding interactions of these two compounds with GLUT5. In the case of **14** and **11,** also bearing the same substituents, a slight difference in IC_{50} values (6.84 vs 2.88 mM) was noted. Lastly, compound **15,** demonstrated a moderate inhibitory activity with an IC_{50} of 5.04 mM. These findings suggests that there must be other interactions are involved with the amino acid residues in the GLUT5 binding pocket, causing the observed difference in potencies.

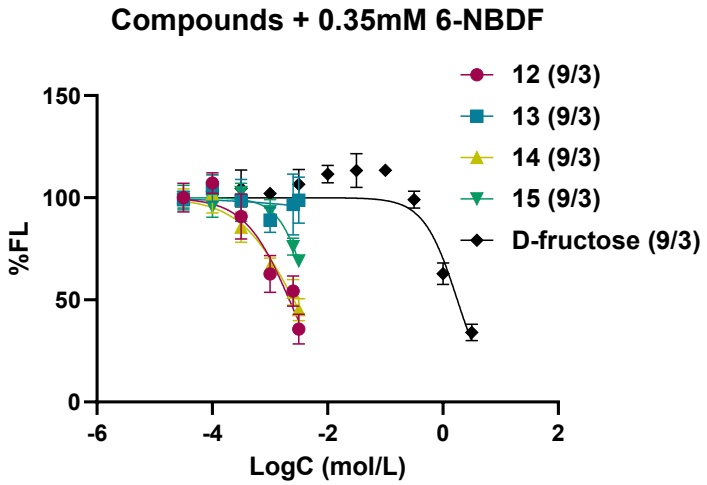

Figure 4.8. Concentration-dependent inhibition of 6-NBDF uptake into EMT6 cells of C-3 derived 2,5-AM compounds **12, 13, 14, 15, and D-fructose** Data are shown as mean ± SEM of n data points from 2-4 experiments. Further measurements of **15** were limited due to its poor solubility in buffer

Furthermore, we examined the 6-NBDF uptake profile in the presence of different GLUT inhibitors (Figure 4.9 and Table 4.1). Cytochalasin B **IV**, an

established inhibitor of GLUT1-4 facilitated transport,[41] as well as quercetin **V**, which competitively inhibits glucose entry via GLUT2,[42] afforded no decrease in the uptake of 6-NBDF by EMT6 cells. The absence of any apparent effects by known Class I GLUT inhibitors provides good evidence that uptake of 6-NBDF **II** occurs via the principal fructose transporter, GLUT5. In addition, the effect of MSNBA **VI**, the first reported selective inhibitor of GLUT5, displayed an IC_{50} of 5.8±0.5 µM to test the inhibition of yeast expressed GLUT5,[44] was also studied against 6-NBDF entry into the EMT6 cancer cell line. Surprisingly, no drop in 6-NBDF uptake was observed till 0.1 mM concentration of MSNBA **VI**, after which further measurements were limited by the poor solubility of **VI** (Table 4.1 and Figure 4.9). Compound **III**, which was previously shown to be a potent inhibitor of [^{14}C]-D-fructose uptake, was also investigated against the uptake of 6-NBDF **II**. Predictably, it was found to strongly inhibit 6-NBDF uptake with an IC_{50} of 2.92 mM. These preliminary studies can indicate that any novel compound from subsequent screens employing **II** as a reference probe can be viewed as a potential GLUT5 inhibitor.

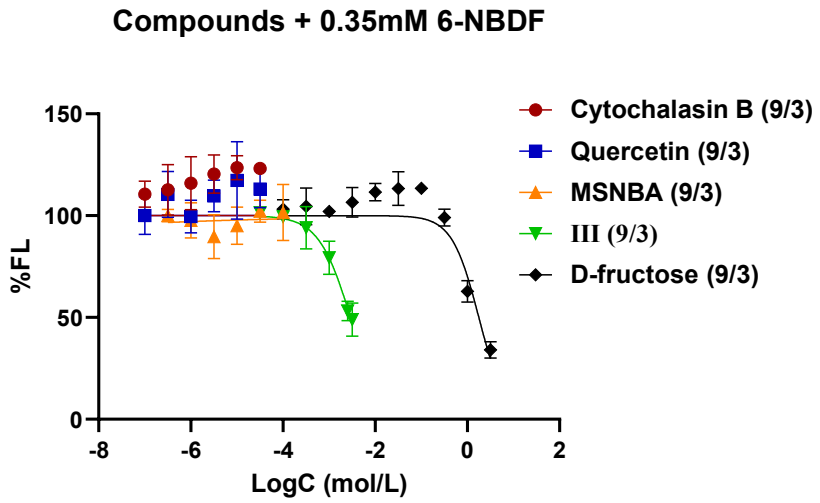

Figure 4.9. Concentration-dependent inhibition of 6-NBDF uptake into EMT6 cells of C-3 derived 2,5-AM compounds **Cytochalasin B, Quercetin, MSNBA,** GLUT5 substrate **III,** and **D-fructose.** Data are shown as mean ± SEM of n data points from 2-4 experiments

As a result, out of different functional group linkers tested, compounds having electron deficient aniline displayed maximum potency followed by compounds having

sulfonamide linkers. In addition, some compounds gave contradictory results in two assays reported: (1) measurement of inhibition of uptake of 6-NBDF and (2) measurement of inhibition of uptake of 6-[^{18}F]FDF. Since the inhibition is measured against the uptake of two different reference compounds, these conflicting results might be due to different types of interactions of both reference compounds with GLUT5 and the involvement of more than one transporter in their transport as 6-[^{18}F]FDF is reported to be transported through both GLUT2 and GLUT5. Compound **8** displayed inhibition of 6-NBDF uptake whereas no inhibition was observed in 6-[^{18}F]FDF uptake. This might suggest that maybe a higher concentration of this compound is needed to cause inhibition of 6-[^{18}F]FDF uptake and it is more selective to GLUT5 causing strong inhibition in fluorescence of 6-NBDF. On the contrary, in case of compound **7,** inhibition in uptake of 6-[^{18}F]FDF was observed with no inhibition observed in uptake of 6-NBDF. This might suggest that **7** is getting transported through the same route as 6-[^{18}F]FDF, selectively through GLUT2 to cause inhibition in its uptake Further cytotoxicity studies and inhibition studies of 6-NBDF using 6-FDF are needed to understand these contradictory results and to study selectivity of fructose transporters. Regarding different inhibitors of GLUTs tested, none of the inhibitors caused any measurable inhibition of uptake of 6-NBDF. Surprisingly, the previously reported GLUT5 inhibitor, MSNBA did not show even slight inhibition at the concentration reported at which it exerts 50% inhibition in D-[^{14}C]-fructose uptake. This work helps to understand the structure activity relationship between 2,5-AM analogs and GLUT5 concerning the importance of hydrogen bonding requirements and recognition of different linkers with different affinity.

4.3. Conclusions

In summary, we have shown that 6-NBDF can be used as a reference standard to study the inhibition of small molecules to determine GLUT5 affinity for such molecules. We also observed that inhibition values were in the same range for the same compounds that were tested in the 6-[^{18}F]FDF inhibition assay, except D-fructose. Similar performance by 6-NBDF **II** relative to the earlier radiolabeled probe 6-[^{18}F]FDF raises the possibility of easy generalization and automation of the assay, potentially allowing

for a high-throughput screen for GLUT5 inhibitors. However, one important limitation of any fluorescence-based assay is the potential for confounding results due to the intrinsic fluorescence of some compounds in the screening library. Along with this newly developed fluorescent assay, **11-14** novel and previously reported C-3 modified 2,5-AM derivatives were characterized for their ability to be recognized and transported by the facilitated hexose transporter GLUT5. Out of the library, **4-5** compounds displayed much greater potency than the reference D-fructose itself. In addition, it was observed that D-fructose displayed an IC_{50} of 1.7M, which is 5-fold higher than the IC_{50} value observed (322 mM) in the 6-[^{18}F]FDF inhibition assay. This observation suggests that GLUT5 has a greater affinity for **II** than it does for 6-[^{18}F]FDF requiring a greater concentration of D-fructose to exert an inhibitory effect on uptake of 6-NBDF. Future studies are needed to understand the binding kinetics of this inhibition to provide better understanding on behavior of GLUT5 binding. The assay reported here shows another method for monitoring the inhibition effect and transport of different derivatives. In addition, it would help to study transporter kinetics to analyze the type of inhibition (competitive, allosteric, noncompetitive) exhibited by these compounds. Further studies are underway to determine the role and fate of these compounds in hopes that these studies will help to identify and design another generation of selective GLUT5 substrates.

4.4. Experimental Section

.4.4.1. Synthesis

Materials and Methods

Reactions were carried out in oven-dried glassware under a positive argon or nitrogen atmosphere unless otherwise stated. Transfer of anhydrous solvents and reagents was accomplished with oven-dried syringes or cannula. Solvents were distilled before use, and dimethylformamide (DMF) and acetonitrile (MeCN) were distilled from calcium hydride. Chemicals were purchased from Sigma-Aldrich Inc. and were used without further purification. Thin layer chromatography was performed on glass plates preloaded with 0.25 mm silica gel matrix. Flash chromatography columns were packed

with 230–400 mesh silica gel. Optical rotations were measured with Perkin Elmer 241 polarimeter, at 22 ± 2 °C. Proton nuclear magnetic resonance spectra (^{1}H NMR) were recorded at 500 MHz or 700 MHz and coupling constants (*J*) are reported in Hertz (Hz). Standard notation was used to describe the multiplicity of signals observed in ^{1}H NMR spectra: broad (br), multiplet (m), singlet (s), doublet (d), triplet (t), etc. Carbon nuclear magnetic resonance spectra (^{13}CNMR) were recorded at 100 MHz or 125 MHz and are reported δ (ppm) relative to the center line of the septet from methanol-d_4 (49.3 ppm), triplet of chloroform-d (77.2 ppm), or septet of DMSO-d_6 (39.5 ppm). Infrared (IR) spectra were measured with a FT-IR 3000 spectrophotometer. Mass spectra were determined on a high-resolution electrospray positive ion mode spectrometer

GLUT inhibitors, cytochalasin B **IV** and quercetin **V** were purchased from Sigma–Aldrich Inc. in solid state. GLUT5 inhibitor, MSNBA **VI**, was synthesized based on the reported procedures.[44] Key amine compound, 3-Amino-3-deoxy-2,5-anhydro-D-mannitol **(1),** was prepared from 3-Azido-3-deoxy-2,5-anhydro-D-mannitol according to the reported procedure.[39]

3-deoxy-3-[N-(3-nitropyridyl)amino]-2,5-anhydro-D-mannitol (3)

Amine **1** (0.12 g, 0.73 mmol) and dry DMF (12 mL) were stirred in a one-neck 50 mL round bottom flask, maintained under N_2 atmosphere, until it is completely dissolved. Excess amount of $NaHCO_3$ (0.42 g, 5.1 mol) was added to the flask, followed by the addition of 2-chloro-3-nitropyridine (0.24 g, 1.4 mmol). The resulting mixture was left to stir at room temperature for 12 h before it was heated at 80 °C for 15 h. After overnight stirring, the solution was allowed to cool to room temperature, solids were filtered off and the filtrate was then concentrated under reduced pressure. The obtained crude compound was subjected to silica gel column chromatography eluted with a DCM/MeOH solvent mixture (gradient from 100:0 to 95:5). Fractions containing the desired product were combined and concentrated under vacuum providing yellow sticky solid **(3)** (0.095 g, 47%). R_f 0.40 (DCM/MeOH, 90:10); $[\alpha]_D^{20}$ = -2.94 (*c* 0.17, MeOH); IR (cast film) 3341, 2956, 2920, 2851, 2102, 1733, 1609, 1508, 1444, 1411, 1377, 1358, 1314 cm^{-1}; ^{1}H NMR (700 MHz, CD_3OD): δ 8.49 (dd, *J* = 8.3, 1.8 Hz, 1H), 8.44 (dd, *J* = 4.5, 1.8 Hz, 1H), 6.79 (dd, *J* = 8.3, 4.5 Hz, 1H), 4.76 (t, *J* = 6.0 Hz, 1H),

4.26 (t, J = 5.8 Hz, 1H), 4.04 (ddd, J = 6.4, 5.5, 3.6 Hz, 1H), 3.98 (ddd, J = 5.9, 4.4, 2.8 Hz, 1H), 3.79 (dd, J = 5.5, 3.3 Hz, 1H), 3.78 (dd, J = 5.6, 3.2 Hz, 1H), 3.74 (dd, J = 12.0, 5.5 Hz, 1H), 3.69 (dd, J = 11.9, 4.4 Hz, 1H); ^{13}C NMR (176 MHz, CD_3OD): δ 156.3, 153.6, 136.5, 130.0, 113.5, 86.1, 85.2, 78.2, 63.8, 63.2, 61.3; HRMS (ESI) calcd for $C_{11}H_{14}N_3O_6$ $[M-H]^-$ 284.0888; found 284.0895.

3-deoxy-3-[N-(5-fluoro-2-nitropyridyl)amino]-2,5-anhydro-D-mannitol (4)

Amine **1** (0.14 g, 0.86 mmol) was dissolved in freshly distilled DMF (20 mL) under N_2 atmosphere. Excess amount of $NaHCO_3$ (0.53 g, 6.3 mol) and 2,6-difluoro-3-nitropyridine[45,46] (0.14 g, 0.86 mmol) was subsequently added, and vigorous stirring was continued at room temperature for 2 h. Solids were removed by filtration before the resultant filtrate was concentrated under reduced pressure. The obtained crude compound was purified via silica gel column chromatography using a DCM/MeOH solvent mixture (gradient from 100:0 to 95:5). Fractions containing the desired product were combined and concentrated under vacuum to yield yellow solid **(4)** (0.13 g, 50%). R_f 0.3 (DCM/MeOH, 90:10); $[\alpha]_D^{20}$ = -1.06 (*c* 0.17, MeOH); FT-IR (cast film) 3327, 2951, 2919, 2851, 1624, 1582, 1544, 1458, 1432, 1362, 1331, 1259 cm^{-1}; ^{1}H NMR (400 MHz, CD_3OD): δ 8.62 (dd, J = 8.9, 7.0 Hz, 1H), 6.36 (dd, J = 8.9, 3.2 Hz, 1H), 4.69 (t, J = 5.4 Hz, 1H), 4.27 (t, J = 5.3 Hz, 1H), 4.04 (td, J = 5.6, 3.8 Hz, 1H), 3.98 (ddd, J = 5.5, 4.0, 2.7 Hz, 1H), 3.80 – 3.75 (m, 2H), 3.68 (dd, J = 11.9, 4.0 Hz, 1H), 3.62 (dd, J = 7.9, 5.5 Hz, 1H); ^{13}C NMR (176 MHz, D_2O): δ 164.1 (d, J = 375.1 Hz), 153.4, 143.1 (d, J = 12.6 Hz), 126.9, 99.3 (d, J = 40.3 Hz), 84.2, 82.9, 76.5, 62.2, 62.1, 59.2; HRMS (ESI) calcd for $C_{11}H_{13}FN_3O_6$ $[M-H]^-$ 302.0794; found 302.0787.

3-deoxy-3-[N-(dihydrocinnamide)amino]-2,5-anhydro-D-mannitol (5)

Amine **1** (0.25 g, 1.5 mmol) was dissolved in MeOH (5 mL) under N_2 atmosphere. To the homogeneous mixture, NHS ester of dihydro-cinnamoyl chloride (0.38 g, 1.5 mmol) was added and stirred for 24 h at room temperature. The reaction mixture was concentrated under reduced pressure. The obtained crude compound was purified via silica gel column chromatography using a DCM/MeOH solvent mixture (gradient from 100:0 to 95:5). Fractions containing the desired product were combined and concentrated under vacuum to obtain yellow solid (0.37 g, 80%). R_f 0.5 (DCM/MeOH,

90:10); $[\alpha]_D^{20}$ = 5.00 (*c* 0.10, MeOH); IR (cast film) 3278, 3064, 2920, 2852, 2919, 1649, 1557, 1453, 1378, 1323, 1050, 718 cm^{-1}; ^1H NMR (400 MHz, CD_3OD): δ 7.26 (t, *J* = 7.6 Hz, 2H), 7.22 – 7.19 (m, 2H), 7.18 – 7.15 (m, 1H), 4.14 (t, *J* = 7.4 Hz, 1H), 3.99 (t, *J* = 7.0 Hz, 1H), 3.81 (ddd, *J* = 7.3, 5.0, 3.0 Hz, 1H), 3.70 (dd, *J* = 12.0, 3.0 Hz, 1H), 3.66 (ddd, *J* = 7.6, 5.6, 3.1 Hz, 1H), 3.62 – 3.58 (m, 1H), 3.58 – 3.55 (m, 1H), 3.51 (dd, *J* = 12.0, 5.6 Hz, 1H), 2.91 (dd, *J* = 15.7, 8.0 Hz, 2H), 2.51 (td, *J* = 7.5, 4.3 Hz, 2H); ^{13}C NMR (176 MHz, CD_3OD): δ 174.3, 140.6, 128.05, 128.01, 125.8, 83.6, 82.0, 75.2, 62.2, 61.4, 57.7, 37.4, 31.4; HRMS (ESI) calcd for $C_{15}H_{21}NNaO_5$ $[M+Na]^+$ 318.1308; found 318.1312.

3-deoxy-3-[N-(4-Fluoro-3-nitrobenzenesulfonamide)amino]-2,5-anhydro-D-mannitol (9)

A 50 mL round bottomed flask, maintained under N_2 atmosphere, was charged with amine **1** (0.22 g, 1.3 mmol) which was dissolved in freshly distilled MeCN (15 mL). 4-Fluoro-3-nitrobenzenesulfonyl chloride[48] (0.39 g, 1.6 mmol) was then added to the flask, followed by addition of excess Na_2CO_3 (0.55 g, 5.2 mol). This heterogeneous mixture was allowed to stir at room temperature. After 16 h, solids were filtered off and washed with excess of MeCN. The filtrate was then evaporated under vacuum to yield a crude product, which was subjected to silica gel column chromatography eluting with a DCM/MeOH solvent mixture (gradient from 100:0 to 92:8). Fractions containing compounds were combined and concentrated under vacuum to yield a pure product of **9** as yellow sticky solid (0.37 g, 60%). R_f 0.4 (DCM/MeOH, 90:10); $[\alpha]_D^{20}$ = +4.53 (*c* 0.19, MeOH); IR (cast film) 3328, 3113, 2929, 1664, 1609, 1530, 1486, 1459, 1350, 1269, 1241 cm^{-1}; ^1H NMR (700 MHz, D_2O): δ 8.71 (dd, *J* = 6.8, 2.4 Hz, 1H), 8.30 (dq, *J* = 8.9, 2.7 Hz, 1H), 7.71 – 7.64 (m, 1H), 4.00 (t, *J* = 7.8 Hz, 1H), 3.86 (dddd, *J* = 8.2, 4.5, 2.6, 1.0 Hz, 1H), 3.82 – 3.78 (m, 1H), 3.78 – 3.76 (m, 1H), 3.75 – 3.72 (m, 1H), 3.70 (dd, *J* = 12.5, 2.7 Hz, 1H), 3.61 (dd, *J* = 12.6, 5.0 Hz, 1H), 3.52 (dd, *J* = 12.5, 4.5 Hz, 1H); ^{13}C NMR (176 MHz, CD_3OD): δ 158.5 (d, *J* = 268.7 Hz), 140.5, 135.5, 135.4, 126.7, 120.5 (d, *J* = 22.2 Hz), 84.6, 83.0, 76.7, 62.6, 62.4, 61.7; HRMS (ESI) calcd for $C_{12}H_{14}FN_2O_8S$ $[M-H]^-$ 365.0460; found 365.0459.

3-deoxy-3-[N-(1-(4-fluorophenyl-3-(trifluoromethyl)phenyl)thiourea]-2,5-anhydro-D-mannitol (11)

In a one-neck 50 mL round bottom flask, maintained under N_2 atmosphere, amine **1** (0.11 g, 0.67 mmol) was dissolved in MeOH (15 mL). 4-Fluorophenyl-3-(trifluoromethyl)phenyl isothiocyanate (0.22 g, 1.0 mmol) was added to the flask and vigorous stirring of the homogenous mixture was continued at room temperature for 15 h. MeOH was removed under reduced pressure and the crude compound was purified via silica gel column chromatography using a DCM/MeOH solvent mixture (gradient from 100:0 to 95:5). Fractions containing the desired product were combined and concentrated under vacuum to provide brown oil of **11** (0.14 g, 54%). R_f 0.31 (DCM/MeOH, 90:10); $[\alpha]_D^{20}$= +4.4 (*c* 0.20, MeOH); IR (cast film) 3298, 3067, 2927, 1707, 1628, 1545, 1507, 1436, 1327, 1269, 1235, 1166 cm^{-1}; ^1H NMR (400 MHz, CD_3OD): δ 7.80 (dd, *J* = 6.5, 2.8 Hz, 1H), 7.65 (dt, *J* = 7.4, 3.4 Hz, 1H), 7.28 (t, *J* = 9.6 Hz, 1H), 4.17 (t, *J* = 5.9 Hz, 1H), 3.94 (dd, *J* = 8.4, 3.3 Hz, 1H), 3.91 (dt, *J* = 6.2, 2.1 Hz, 1H), 3.80 (dd, *J* = 12.0, 3.5 Hz, 1H), 3.77 – 3.74 (m, 1H), 3.72 (d, *J* = 2.9 Hz, 1H), 3.62 (d, *J* = 4 Hz, 1H), 3.60 (d, *J* = 5 Hz, 1H); ^{13}C NMR (176 MHz, CD_3OD): δ 182.0, 156.6 (d, *J* = 252.7 Hz), 135.5, 130.3, 130.1, 122.8, 122.4 (d, *J* = 271.4 Hz), 116.8 (d, *J* = 23.6 Hz), 84.5, 83.6, 76.2, 63.0, 62.4, 61.6; HRMS (ESI) calcd $C_{14}H_{16}F_4N_2O_4SNa$ $[M+Na]^+$ 407.0659; found 407.0659.

General Procedure to synthesize (12), (13), (14) and (15):

A flask, maintained under N_2 atmosphere was charged with amine **1** (0.13 g, 1.2 mmol) and freshly distilled DMF (20 mL). At room temperature, $NaHCO_3$ (0.35 g, 4.1 mol) was added to the reaction mixture, followed by the addition of the isocyanate derivative (0.16 g, 1.2 mmol of benzyl isocyanate for **12**; 0.16 g, 1.2 mmol of 4-fluorophenyl isocyanate for **13**; 0.24 g, 1.2 mmol of 4-fluorophenyl-3-(trifluoromethyl)phenyl isocyanate for **14;** 0.21 g, 1.2 mmol of 4-fluorophenyl-3-nitrophenyl isocyanate for **15**). The mixture was left to stir for 16 h before solids were filtered off and the filtrate was removed under reduced pressure. The resultant crude product was purified by subjecting to silica gel column chromatography eluted with a DCM/MeOH solvent mixture (gradient from 100:0 to 94:6 for **12**; 100:0 to 92:8 for **13**; 100:0 92:8 for **14;**

100:0 to 93:7 for **15**). Fractions containing the desired product were combined and concentrated under a vacuum to yield the pure compound.

3-deoxy-3-[N-(1-(benzyl)urea)amino]-2,5-anhydro-D-mannitol (12)

White sticky solid (0.20 g, 86%). R_f 0.45 (DCM/MeOH, 90:10); $[\alpha]_D^{20}$= +7.00 (*c* 0.10, MeOH); IR (cast film) 3329, 2923, 1648, 1567, 1453, 1315, 1056, 830, 701 cm^{-1}; ^1H NMR (600 MHz, CD_3OD): δ 7.33 – 7.26 (m, 4H), 7.24 – 7.20 (m, 1H), 4.32 (d, *J* = 1.9 Hz, 2H), 4.03 – 3.95 (m, 2H), 3.82 (tt, *J* = 4.9, 2.9 Hz, 1H), 3.77 (ddd, *J* = 7.7, 5.4, 3.3 Hz, 1H), 3.73 (dd, *J* = 12.0, 3.0 Hz, 1H), 3.70 (dd, *J* = 12.0, 3.4 Hz, 1H), 3.65 – 3.62 (m, 1H), 3.62 – 3.59 (m, 1H); ^{13}C NMR (176 MHz, CD_3OD): δ 159.6, 139.6, 128.0, 126.8, 126.6, 83.5, 82.6, 75.9, 62.2, 61.6, 58.7, 43.3; HRMS (ESI) calcd for $C_{14}H_{21}N_2O_5$ $[M+H]^+$ 297.1445; found 297.1445.

3-deoxy-3-[N-(1-(4-fluorophenyl)urea)amino]-2,5-anhydro-D-mannitol (13)

White sticky solid (0.16 g, 66%). R_f 0.25 (DCM/MeOH, 90:10); $[\alpha]_D^{20}$= +7.87 (*c* 0.32, MeOH); IR (cast film) 3322, 2924, 2855, 1677, 1614, 1564, 1510, 1460, 1407, 1310, 1216, 1156 cm^{-1}; ^1H NMR (700 MHz, D_2O): δ 7.29 (dd, *J* = 8.9, 4.9 Hz, 2H), 7.13 (t, *J* = 8.9 Hz, 2H), 4.17 (t, *J* = 7.8 Hz, 1H), 4.15 (t, *J* = 7.3 Hz, 1H), 3.96 (ddd, *J* = 7.3, 5.0, 2.9 Hz, 1H), 3.93 (ddd, *J* = 8.2, 5.4, 2.9 Hz, 1H), 3.83 – 3.81 (m, 1H), 3.81 – 3.78 (m, 1H), 3.72 (dd, *J* = 5.3, 2.7 Hz, 1H), 3.70 (dd, *J* = 5.4, 2.7 Hz, 1H); ^{13}C NMR (176 MHz, CD_3OD): δ 160.6, 158.7 (d, *J* = 171.6 Hz), 136.8, 122.2 (d, *J* = 7.8 Hz), 116.1 (d, *J* = 22.7 Hz), 85.1, 84.1, 77.3, 63.7, 63.0, 60.0; HRMS (ESI) calcd for $C_{13}H_{17}FN_2O_5Na$ $[M+Na]^+$ 323.1014; found 323.1013.

3-deoxy-3-[N-(1-(4-fluorophenyl-3-(trifluoromethyl)phenyl)urea)amino]-2,5-anhydro-D-mannitol (14)

Clear liquid (0.18 g, 61%). R_f 0.26 (DCM/MeOH, 90:10); $[\alpha]_D^{20}$= +13.44 (*c* 0.18, MeOH); IR (cast film) 3323, 2940, 2879, 1678, 1629, 1611, 1568, 1505, 1428, 1331, 1255, 1226, 1135cm^{-1}; ^1H NMR (700 MHz, CD_3OD): δ 7.80 (dd, *J* = 6.3, 2.8 Hz, 1H), 7.56 (ddd, *J* = 9.1, 4.2, 2.9 Hz, 1H), 7.21 (t, *J* = 9.6 Hz, 1H), 4.10 – 4.08 (m, 1H), 4.08 – 4.06 (m, 1H), 3.88 – 3.85 (m, 1H), 3.85 – 3.83 (m, 1H), 3.77 – 3.75 (m, 1H), 3.75 – 3.72 (m, 1H), 3.67 (dd, *J* = 12.0, 5.6 Hz, 1H), 3.64 (dd, *J* = 11.9, 4.6 Hz, 1H); ^{13}C NMR (176 MHz, CD_3OD): δ 157.8, 156.1 (d, *J* = 249.4 Hz), 137.6, 125.4 (d, *J* = 7.8 Hz),

124.0 (d, J = 271.2 Hz), 118.8 (dd, J = 32.7, 13.2 Hz), 118.2, 118.1, 85.1, 84.1, 77.2, 63.7, 63.0, 59.9; HRMS (ESI) calcd for $C_{14}H_{15}F_4N_2O_5$ $[M-H]^-$ 367.0923; found 367.0918.

3-deoxy-3-[N-(1-(4-fluorophenyl-3-nitrophenyl)urea)amino]-2,5-anhydro-D-mannitol (15)

Yellowish white sticky solid (0.15 g, 55%). R_f 0.25 (DCM/MeOH, 90:10); $[\alpha]_D^{20}$= +11.13 (*c* 0.23, MeOH); IR (cast film) 3326, 3072, 2933, 1686, 1608, 1564, 1540, 1501, 1406, 1351, 1221 cm^{-1}; ^1H NMR (600 MHz, CD_3OD): δ 8.26 (dd, J = 6.6, 2.8 Hz, 1H), 7.62 (ddd, J = 9.1, 3.8, 2.8 Hz, 1H), 7.30 (dd, J = 10.8, 9.1 Hz, 1H), 4.11 – 4.08 (m, 1H), 4.06 (d, J = 6.6 Hz, 1H), 3.86 (td, J = 4.1, 3.3, 1.6 Hz, 1H), 3.85 – 3.82 (m, 1H), 3.77 – 3.74 (m, 1H), 3.74 – 3.71 (m, 1H), 3.67 (dd, J = 12.0, 5.6 Hz, 1H), 3.63 (dd, J = 12.0, 4.6 Hz, 1H); ^{13}C NMR (176 MHz, CD_3OD): δ 157.5, 151.6 (d, J_{C-F} = 257.5 Hz), 138.1 (d, J = 85.0 Hz), 137.9, 126.5, 119.3 (d, J = 22.1 Hz), 116.2, 85.1, 84.1, 77.2, 63.7, 63.1, 59.9; HRMS (ESI) calcd for $C_{13}H_{16}FN_3O_7Na$ $[M+Na]^+$ 368.0864; found 368.0864.

4.4.2. In vitro cell experiments

Instruments

A Cytation5 BioTek fluorescence plate reader was used to measure the 6-NBDF fluorescence in EMT6 cells.

Buffer solutions

Glucose-free Krebs–Ringer buffer solution (120 mM NaCl, 25 mM $NaHCO_3$, 4 mM KCl, 1.2mM KH_2PO_4, 2.5 mM $MgSO_4$, 70 μM $CaCl_2$, pH 7.4) was used for the studies with EMT6 cells. Cold phosphate-buffered saline (PBS) (137 mM NaCl, 2.7mM KCl, 10 mM Na_2HPO_4, 2 mM KH_2PO_4) was used to wash the extracellular probes.

Cell culture

Murine EMT6 mammary gland tumor cells were grown in a humidified 5% CO_2 incubator at 37°C, in Gibco DMEM/F-12 media supplemented with 15 mM HEPES, l-

glutamine,10% fetal bovine serum (GIBCO 12483; Gibco, Gaithersburg, MD) and 1% penicillin/streptomycin with media renewal every 2 to 3 days.

Concentration-dependent uptake of 6-NBDF into EMT6 cells

EMT6 cells were allowed to reach confluence in 12-well cell culture plates with media renewal every 2 days. 1 hour before conducting the uptake study, the media was removed and the plates were washed twice with glucose–free Krebs–Ringer buffer solution, after which, 1 mL of Krebs–Ringer buffer solution was added to each well. The plates were incubated at 37 °C for 1 hour under this glucose-free condition. After 1 hour of incubation, Krebs–Ringer buffer was removed from each well, and 500 µL of Krebs–Ringer buffer containing different concentrations of 6-NBDF (10^{-4} -10^{-1}-9×10^{-1}-1 M) was incubated within each well for a specific period (30 minutes) in a CO_2 incubator at 37 °C. After incubation, the media was aspirated and each well was rinsed with 1 mL ice-cold PBS buffer (1×3), where the plates were stirred for 3 min on a rotating rocker after each wash. After rinsing, 1 mL of PBS buffer was added to each well and fluorescence count was measured via a fluorescence plate reader. The net fluorescence value corresponding to a specific well was calculated by subtracting the background fluorescence value (auto-fluorescence of a well with EMT6 cells and PBS buffer was referred to as background fluorescence).

Time-dependent uptake of 6-NBDF into EMT6 cells

EMT6 cells were allowed to reach confluence in 12-well cell culture plates with media renewal every 2 days. 1 hour before conducting the uptake study, the media was removed and the plates were washed twice with glucose–free Krebs–Ringer buffer solution, after which, 1 mL of Krebs–Ringer buffer solution was added to each well. The plates were incubated at 37 °C for 1 hour under this glucose-free condition. After 1 hour of incubation, Krebs–Ringer buffer was removed from each well, and 500 µL of Krebs–Ringer buffer containing 350 µM of 6-NBDF was incubated within each well for different periods (0- 10- 20- 30- 45- 60- 90- 120 minutes) in a CO_2 incubator at 37 °C. After incubation, the media was aspirated and each well was rinsed with 1 mL ice-cold PBS buffer (1×3), where the plates were stirred for 3 min on a rotating rocker after each wash. After rinsing, 1 mL of PBS buffer was added to each well and fluorescence

count was measured via a fluorescence plate reader. The net fluorescence value corresponding to a specific well was calculated by subtracting the background fluorescence value (auto-fluorescence of a well with EMT6 cells and PBS buffer was referred to as background fluorescence).

General procedure for in vitro inhibition of 6-NBDF uptake into EMT6 cells:
EMT6 cells were allowed to reach confluence in 12-well cell culture plates with media renewal every 2 days. 1 hour before conducting the uptake study, the media was removed and the plates were washed twice with glucose–free Krebs–Ringer buffer solution, after which, 1 mL of Krebs–Ringer buffer solution was added to each well. The plates were incubated at 37 °C for 1 hour under this glucose-free condition. After 1 hour incubation, Krebs–Ringer buffer was removed from each well and 500 μL of glucose-free Krebs-Ringer buffer was added within each well for 1 hour, containing 350 μM of 6-NBDF and increasing concentrations of the 2,5-AM derivatives **2-15** (10^{-5}-10^{-3} M) or fructose (10^{-7}-10^{-3} M) or cytochalasin B **(IV)** (10^{-7}-10^{-5} M) or quercetin **(V)** (10^{-7}-10^{-5} M) or MSNBA **(VI)** (10^{-7}-10^{-4} M) and no compound at all for comparison (blank, 100% uptake). After incubation, the media was aspirated and each well was rinsed with 1 mL ice-cold PBS buffer (1×3), where the plates were stirred for 3 min on a rotating rocker after each wash. After rinsing, 1 mL of PBS buffer was added into each well and fluorescence count was measured via fluorescence plate reader. Net fluorescence value corresponding to a specific well was calculated after subtracting the background fluorescence value (auto-fluorescence of a well with EMT6 cells and PBS buffer was referred as background fluorescence). Competitive inhibition assays were carried out three times using different batches of cells. Graphs were constructed using GraphPad Prism 5.0 (GraphPad Software, San Diego, CA, U.S.A.) and half-maximum inhibition concentrations (IC_{50}) were determined from the concentration-inhibition curves through graphical analysis.

4.5. References

1. Dashty, M. A quick look at biochemistry: Carbohydrate metabolism. *Clin. Biochem.* **2013**, *46*, 1339–1352.

2. Navale, A. M.; Paranjape, A. N. Glucose transporters: physiological and pathological roles. *Biophys. Rev.* **2016**, *8*, 5–9.

3. Manolescu, A. R., Witkowska, K., Kinnaird, A., Cessford, T. & Cheeseman, C. Facilitated Hexose Transporters: New Perspectives on Form and Function. *Physiology* **2007**, *22*, 234–240.

4. Wood, I. S.; Trayhurn, P. Glucose transporters (GLUT and SGLT): expanded families of sugar transport proteins. *Br. J. Nutr.* **2003**, *89*, 3–9.

5. Poulsen, S. B.; Fenton, R. A.; Rieg, T. Sodium-glucose cotransport. *Curr. Opin. Nephrol. Hypertens.* **2015**, ***24***, 463–469.

6. Thorens, B.; Mueckler, M. Glucose transporters in the 21st Century. *Am. J. Physiol. Endocrinol. Metab.* **2010**, *298*, E141-5.

7. Mueckler, M.; Thorens, B. The SLC2 (GLUT) family of membrane transporters. *Mol. Aspects Med.* **2013**, *34*, 121–138.

8. Kasahara, M.; Hinkle, P. C. Reconstitution and purification of the D-glucose transporter from human erythrocytes. *J. Biol. Chem.* **1977**, *252*, 7384–7390.

9. Simpson, I. A.; Vannucci, S. J.; Maher, F. Glucose transporters in mammalian brain. *Biochem. Soc. Trans.* **1994**, *22*, 671–675.

10. Huang, S.; Czech, M. P. The GLUT4 glucose transporter. *Cell Metab.* **2007**, *5*, 237-252.

11. Douard, V.; Ferraris, R. P. Regulation of the fructose transporter GLUT5 in health and disease. *Am. J. Physiol. Endocrinol. Metab.* **2008**, *295*, E227–E237.

12. Uldry, M.; Thorens, B. The SLC2 family of facilitated hexose and polyol transporters. *Pflugers Arch.* **2004**, *447*, 480–489.

13. Long, W.; Cheeseman, C. Structure of, and functional insight into the GLUT family of membrane transporters. *Cell Health Cytoskelet.* **2015**, *7*, 167–183.

14. Deng, D.; Yan, N. GLUT, SGLT, and SWEET: Structural and mechanistic investigations of the glucose transporters. *Protein Sci.* **2016**, *25*, 546–558.

15. Holman, G. D. Structure, function and regulation of mammalian glucose transporters of the SLC2 family. *Pflügers Arch.* **2020**, *472*, 1155–1175.

16. McQuade, D. T.; Plutschack, M. B.; Seeberger, P. H. Passive fructose transporters

in disease: a molecular overview of their structural specificity. *Org. Biomol. Chem.* **2013**, *11*, 4909–4920.

17. Kouidhi, S.; Berrhouma, R.; Rouissi, K.; Jarboui, S.; Clerget-Froidevaux, M.; Seugnet, I.; Bchir, F.; Demeneix, B.; Guissouma, H.; Elgaaied, A. Human subcutaneous adipose tissue Glut 4 mRNA expression in obesity and type 2 diabetes. *Acta Diabetol.* **2013**, *50*, 227–232.

18. Camps, M.; Castelló, A.; Muñoz, P.; Monfar, M.; Testar, X.; Palacín, M.; Zorzano, A. Effect of diabetes and fasting on GLUT-4 (muscle/fat) glucose-transporter expression in insulin-sensitive tissues. Heterogeneous response in heart,red and white muscle. *Biochem. J.* **1992**, *282***,** 765–772.

19. Shepherd, P. R.; Kahn, B. B. Glucose transporters and insulin action implications for insulin resistance and diabetes mellitus. *N. Engl. J. Med.* **1999**, *341*, 248–257.

20. Douard, V.; Ferraris, R. P. The role of fructose transporters in diseases linked to excessive fructose intake. *J. Physiol.* **2013**, *591*, 401–414.

21. Smith, T. A. Facilitative glucose transporter expression in human cancer tissue. *Br. J. Biomed. Sci.* **1999**, *56*, 285–292.

22. Adekola, K.; Rosen, S. T.; Shanmugam, M. Glucose transporters in cancer metabolism. *Curr. Opin. Oncol.* **2012**, *24*, 650–654.

23. Zamora-León, S. P.; Golde, D. W.; Concha, I., I., Rivas, C., I., Delgado-López, F.; Baselga, J.; Nualart, F.; Vera, J. C. Expression of the fructose transporter GLUT5 in human breast cancer. *Proc. Natl. Acad. Sci.* **1996**, *93*, 1847-1852.

24. Godoy, A.; Ulloa, V.; Rodríguez, F.; Reinicke, K.; Yañez, A.; García, M.; Medina, R.; Carrasco, M.; Barberis, S.; Castro, T.; Martínez, F.; Koch, X.; Vera, J.; Poblete, M.; Figueroa, C.; Peruzzo, B.; Pérez, F.; Nualart, F. Differential subcellular distribution of glucose transporters GLUT1-6 and GLUT9 in human cancer: ultrastructural localization of GLUT1 and GLUT5 in breast tumor tissues. *J. Cell. Physiol.* **2006**, *207*, 614–627.

25. Villaamil, V. M.; Gallego, G. A.; Rubira, L.V.; Campelo, R. G.; Valladares-Ayerbes, M.; Pulido, E. G.; Bolós, M. V.; Caínzos, I. S.; Antón Aparicio, L. Fructose transporter Glut5 expression in clear renal cell carcinoma. *Oncol. Rep.* **2011**, *25*, 315–

323.

26. Weng, Y.; Fan, X.; Bai, Y.; Wang, S.; Huang, H.; Yang, H.; Zhu, J.; Zhang, F. SLC2A5 promotes lung adenocarcinoma cell growth and metastasis by enhancing fructose utilization. *Cell Death Discov.* **2018**, *4*, 38.

27. Yan, N. Structural advances for the major facilitator superfamily (MFS) transporters. *Trends Biochem. Sci.* **2013**, *38*, 151–159.

28. Madej, M. G.; Sun, L.; Yan, N.; Kaback, H. R. Functional architecture of MFS D-glucose transporters. *Proc. Natl. Acad. Sci. U. S. A.* **2014**, *111*, E719-27.

29. Nomura, N.; Verdon, G.; Kang, H. J.; Shimamura, T.; Nomura, Y.; Sonoda, Y.; Hussien, S. A.; Qureshi, A. A.; Coincon, M.; Sato, Y.; Abe, H.; Nakada-Nakura, Y.; Hino, T.; Arakawa, T.; Kusano-Arai, O.; Iwanari, H.; Murata, T.; Kobayashi, T.; Hamakubo, T.; Ka, D. Structure and mechanism of the mammalian fructose transporter GLUT5. *Nature* **2015**, *526*, 397–401.

30. Deng, D.; Xu, C.; Sun, P.; Wu, J.; Yan, C.; Hu, M.; Yan, N. Crystal structure of the human glucose transporter GLUT1. *Nature* **2014**, *510*, 121–125.

31. Soueidan, O. M.; Scully, T. W.; Kaur, J.; Panigrahi, R.; Belovodskiy, A.; Do, V.; Matier, C. D.; Lemieux, M. J.; Wuest, F.; Cheeseman, C.; West, F. G. Fluorescent Hexose Conjugates Establish Stringent Stereochemical Requirement by GLUT5 for Recognition and Transport of Monosaccharides. *ACS Chem. Biol.* **2017**, *12*, 1087–1094.

32. Tatibouët, A.; Yang, J.; Morin, C.; Holman, G. D. Synthesis and evaluation of fructose analogues as inhibitors of the D-fructose transporter GLUT5. *Bioorg. Med. Chem.* **2000**, *8*, 1825–1833.

33. Tanasova, M.; Fedie, J. R. Molecular Tools for Facilitative Carbohydrate Transporters (Gluts). *Chembiochem* **2017**, *18*, 1774–1788.

34. Yang, J.; Dowden, J.; Tatibouët, A.; Hatanaka, Y.; Holman, G. D. Development of high-affinity ligands and photoaffinity labels for the D-fructose transporter GLUT5. *Biochem. J.* **2002**, *367*, 533–539.

35. Trayner, B. J.; Grant, T. N.; West, F. G.; Cheeseman, C. I. Synthesis and characterization of 6-deoxy-6-fluoro-D-fructose as a potential compound for imaging

breast cancer with PET. *Bioorg. Med. Chem.* **2009**, *17*, 5488–5495.

36. Levi, J.; Cheng, Z.; Gheysens, O.; Patel, M.; Chan, C.T.; Wang, Y.; Fluorescent fructose derivatives for imaging breast cancer cells. *Bioconjug. Chem.* **2007**, ***18***, 628–634.

37. Wuest, M.; Trayner, B. J.; Grant, T. N.; Jans, H.; Mercer, J. R.; Murray, D.; West, F. G.; McEwan, A. J. B.; Wuest, F.; Cheeseman, C. I. Radiopharmacological evaluation of 6-deoxy-6-[18F]fluoro-d-fructose as a radiotracer for PET imaging of GLUT5 in breast cancer. *Nucl. Med. Biol.* **2011**, *38*, 461–475.

38. Kumar Kondapi, V. P.; Soueidan, O. M.; Cheeseman, C. I.; West, F. G. Tunable GLUT–Hexose Binding and Transport via Modulation of Hexose C-3 Hydrogen-Bonding Capabilities. *Chem. - A Eur. J.* **2017**, *23*, 8073–8081.

39. Rana, N.; Aziz, M.A.; Oraby, A.K.; Wuest, M.; Dufour, J.; Abouzid, K.A.; Wuest, F.; West, F.G. Towards Selective Binding to the GLUT5 Transporter: Synthesis, Molecular Dynamics and In Vitro Evaluation of Novel C-3 Modified 2, 5-Anhydro-D-mannitol Analogs. *Pharmaceutics*, **2022,** *14*, 828.

40. George Thompson, A. M.; Ursu, O.; Babkin, P.; Iancu, C. V.; Whang, A.; Oprea, T. I.; Choe, J. Y. Discovery of a Specific Inhibitor of Human GLUT5 by Virtual Screening and in Vitro Transport Evaluation. *Sci. Rep.* **2016**, *6*, 1–9.

41. Kapoor, K.; Finer-Moore, J. S.; Pedersen, B. P.; Caboni, L.; Waight, A.; Hillig, R. C.; Bringmann, P.; Heisler, I.; Müller, T.; Siebeneicher, H.; Stroud, R. M. Mechanism of Inhibition of Human Glucose Transporter GLUT1 Is Conserved between Cytochalasin B and Phenylalanine Amides. *Proc. Natl. Acad. Sci.* **2016**, *113*, 4711–4716.

42. Strobel, P.; Allard, C.; Perez-Acle, T.; Calderon, R.; Aldunate, R.; Leighton, F. Myricetin, Quercetin and Catechin-Gallate Inhibit Glucose Uptake in Isolated Rat Adipocytes. *Biochem. J.* **2005**, *386*, 471–478.

43. Wuest, M.; Hamann, I.; Bouvet, V.; Glubrecht, D.; Marshall, A.; Trayner, B.; Soueidan, O. M.; Krys, D.; Wagner, M.; Cheeseman, C.; West, F.; Wuest, F. Molecular imaging of GLUT1 and GLUT5 in breast cancer: a multitracer positron emission tomography imaging study in mice. *Mol. Pharmacol.* **2018**, *93*, 79-89.

44. Tripp, J.; Essl, C.; Iancu, C.V.; Boles, E.; Choe, J.Y.; Oreb, M.. Establishing a yeast-based screening system for discovery of human GLUT5 inhibitors and activators. *Sci. Rep.*, **2017**, *7*, 1-9.

Chapter 5

Future directions

5.1. Identification of GLUT5 inhibitors through high throughput screening (HTS)

As mentioned in Chapter 1, abnormal expression of GLUT5 is associated with a number of disease states, especially cancer. Since these transporters are required for the internalization of important nutrients and metabolic fuels such as glucose and fructose, their inhibition could effectively starve cells of their necessary nutrients. As a result, there is a growing interest in finding potential inhibitors of various GLUTs[1,2,3] and various HTS methods have been reported to identify inhibitors from a known library of substrates.[4] Due to aberrant fructose metabolism and its correlation with several cancers, we have proposed that selective inhibitors of GLUT5 could be of significant therapeutic value. We envision that fluorescent probes developed by our group (6-NBDF and 3-NBDAM, Figure 5.1)[5] that selectively target GLUT5 can be developed in a straightforward approach for high throughput screening to identify new promising hits in the search to develop them as GLUT5 inhibitors.

Figure 5.1. Reported GLUT5 probes

Figure 5.2 represents the small number of GLUT5 inhibitors reported to date that have shown low IC_{50} values with poor selectivity among various other transporters.[6] Inhibition of fructose uptake will have therapeutic relevance in the treatment of various cancers and diseases. We are currently working with 6-NBDF as a fluorescent probe and in collaboration with the Centre for High Throughput Chemical

Biology (HTCB) at Simon Fraser University (SFU), and we are hoping to develop a scalable assay that can be used in conjunction with a library of ca. 10,000 natural product extracts and 30,000 drugs like compounds.

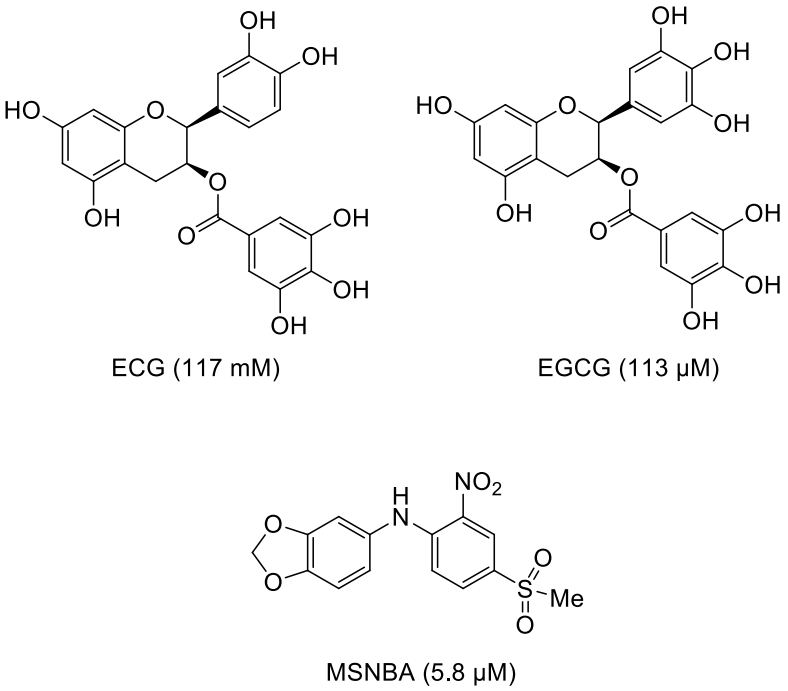

Figure 5.2. Reported GLUT5 inhibitors

Figure 5.3 represents the general scheme for carrying out HTS studies in collaboration with SFU. The first step involves optimization experiments to render the assay reliable, scalable, and subject to automation.

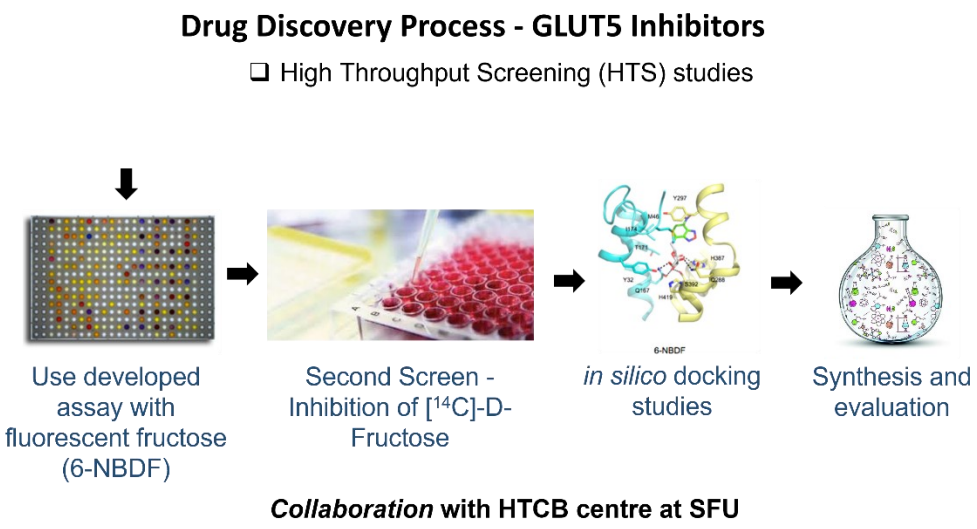

Figure 5.3. General scheme for the development of GLUT5 inhibitors

For initial assays, I used 96-well and 384-well plates to optimize the confluency and concentration dependent inhibition of 6-NBDF against D-fructose and potent 2,5-AM derivatives. Figure 5.4 represents the sample layout of 96-well plate displaying different parameters used for initial optimization. However, due to subsequent manual washing of the plate, a great reduction in confluency (from 100% to 40%) was observed.

	1	2	3	4	5	6	7	8	9	10	11	12		
A	PBS	PBS	PBS	PBS	PBS	PBS	PBS	PBS	PBS	PBS	PBS	PBS		
B	NC	NC	6 MSNBA	6 MSNBA	350	2.5	450	4.5	6 MSNBA	6 MSNBA	NC	NC	NC	PBS + Cells + 0.25 mM 6-NBDF
C	NC	NC	20 MSNBA	20 MSNBA	350	2.5	450	4.5	20 MSNBA	20 MSNBA	NC	NC	Fructose	Concentrations as indicated (in mM)
D	2.5	NC	30 MSNBA	30 MSNBA	350	2.5	450	4.5	30 MSNBA	30 MSNBA	NC	4.5	Mannitol	Concentrations as indicated (in mM)
E	2.5	NC	6 MSNBA	6 MSNBA	350	2.5	450	4.5	6 MSNBA	6 MSNBA	NC	4.5	MSNBA	Concentrations as indicated (in uM)
F	350	NC	20 MSNBA	20 MSNBA	350	2.5	450	4.5	20 MSNBA	20 MSNBA	NC	450		
G	350	NC	30 MSNBA	30 MSNBA	350	2.5	450	4.5	30 MSNBA	30 MSNBA	NC	450		
H	PBS	PBS	PBS	PBS	PBS	PBS	PBS	PBS	PBS	PBS	PBS	PBS		

Figure 5.4. Sample format for 96-well plate for optimization

Therefore, HTCB staff recommended using their automated plate washer at their facility to generate reliable data. In addition, the facility at HTCB is more adept to generate granular data from individual cells using high content microscopy rather than bulk data obtained from a plate reader. After optimization and identification of hits from the first screen, a secondary screen involves validating hits by performing a radioactive assay employing [^{14}C]-D-fructose, a commercially available radioactive

form of the natural substrate for GLUT5. The next step involves a variety of docking studies to evaluate the interactions of identified hits with the published 3-dimensional structure of GLUT5. In these studies, compounds will be allowed to blindly dock with GLUT5 in its outward open conformation using Auto Dock as previously reported.[5]

In this experiment, we will be mostly focusing on the inhibitors that actively block the passage leading to the central core of the protein. Compounds in that subset will be modified in silico and docked with protein in order to identify optimal structures for GLUT5 binding interactions. Analogs/hits predicted to have greater binding or PK properties will be synthesized and screened for their inhibitory potency, and this process will be iterated through the design and synthesis of focused compound libraries until a suitable preclinical candidate is identified. This part of the project focuses on developing a scalable assay for HTS to identify GLUT5 inhibitors, designing, and generation of the novel drug like structures based upon hits from HTS with a potential therapeutic value in the treatment of cancer.

5.2. NIR dye conjugated fructose probes

Fluorescent dyes constructed from small organic molecules and functioning in the near infrared region (NIR) are of great interest in chemical biology.[7] NIR fluorescent probes offer multiple advantages including minimal autofluorescence from biological samples, low phototoxicity, high signal to noise ratio, reduced light scattering, high tissue penetration, and inexpensive laser diode excitation. There are several classes of dyes that are readily available such as cyanines, pthalocyanines, and squarines.[7] However, aggregate formation and aqueous insolubility are issues encountered with squarine and pthalocyanine dyes in biological systems. With cyanine dyes, high molar absorptivity, good photostability, and strong fluorescence are observed making them excellent NIR dyes. Nonetheless, great efforts have been applied to improve the photochemical and photophysical properties of NIR dyes like addition of hydrophilic groups (sulfonate, carboxylate, etc.) to improve aqueous solubility, increase in stearic to reduce aggregation, and addition of charged functional groups.[7] As a result, the development of fluorescent probes aiding in the visualization of tumors can be of great interest to the biomedical imaging community. Therefore, in this project,

fructose/mannitol conjugated NIR dyes can be developed for studying the trafficking of tagged sugar in tumor cells selectively via GLUT5 pathway. The development of new and improved fluorescent probes would be a significant step-in real-time imaging with fundamental and translational applications. Figure 5.5 represents the fluorescent probes that can be developed categorized according to available fluorescent dyes.

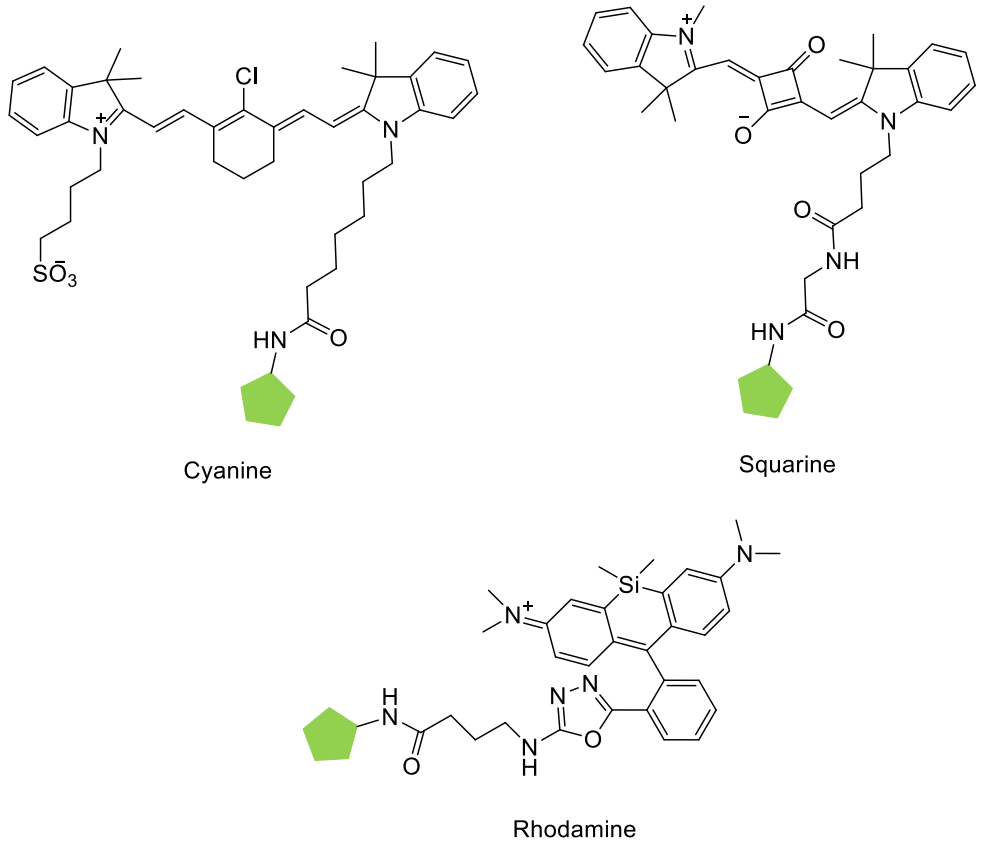

Figure 5.5. Potential NIR dye-fructose/mannitol conjugates

Consequently, there is high demand for fructose based NIR dye tracer for drug delivery research. It is worth exploring the influence of NIR fluorescent dye conjugate of fructose/mannitol on the cellular uptake through hexose transporters. In addition to tumor imaging, NIR dyes can also be utilized as theranostic (therapeutic and diagnostic) agents for photothermal therapy (PTT) and photodynamic therapy (PDT).

PTT (Figure 5.6) is a noninvasive approach that destroys tumor cells by generating heat within a tumor by absorption of specific light in the NIR region.[8] In the

case of PDT (Figure 5.7), photosensitizers and light irradiation is applied to induce oxidation reactions with biomacromolecules generating radicals and ion species to destroy tumor tissues.[8] Therefore, after examining the accumulation of developed fluorescent probes in the tumor, the same probe will guide laser treatment to destroy the tumor cells in cancer areas. Yuan and coworkers have reported a review focusing on the progress and application of NIR dyes along with the limitations offered by both mentioned therapies.[8] Such dyes could be used to form hexose conjugates to guide the probe selectively at tumor cite followed by using that probe for fluorescence guided PTT/PDT.

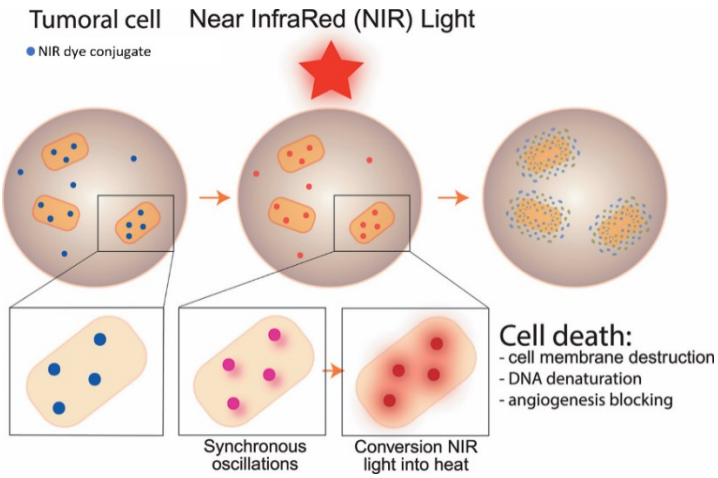

Figure 5.6. Photothermal therapy (Figure copied with permission from Pinto et al.[8])

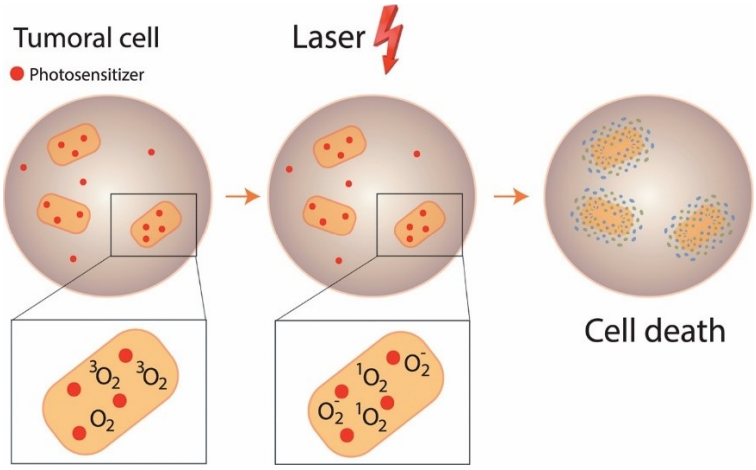

Figure 5.7. Photodynamic therapy (Figure copied with permission from Pinto et al.[8])

5.3. Influence of molecular charge on fructose-based imaging probe

Due to unique substrate preference and overexpression of GLUTs in various diseases and cancer, imaging agents targeting this biomarker have gained special attention in the past few decades.[9,10,11] Several studies have reported the impact of molecular charge and its potential influence on cellular uptake. Park and coworkers reported the influence of the overall charge of glucose probes (Figure 5.8) on GLUT-specific cellular uptake and it was reported that positively charged glucose bioprobe (GB2-Cy3) displayed GLUT dependent uptake as compared to its negatively charged and zwitterionic analogs.[12] In 2018, Jo and coworkers also reported two NIR-based glucose tracers having similar photophysical properties but different charges on the overall fluorochrome glycoconjugates (Figure 5.8). It was observed that tracer (Glc-SiR-COOH) with net charge = 0 displayed GLUT-mediated cellular uptake behavior and demonstrated its potential usage in monitoring the effect of anticancer agents in live cells.[13]

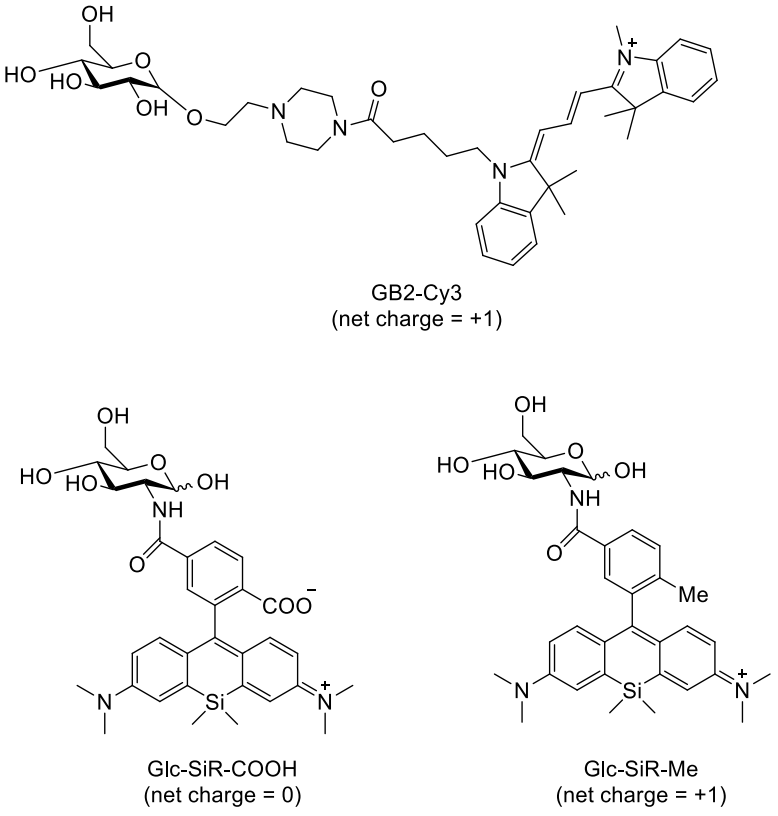

Figure 5.8. Examples of glucose probes with different overall charge

A similar strategy can be used to study the effect of molecular charge on GLUT5 machinery by incorporating charged moieties into fructose or mannitol-based probes. However, the tolerability of GLUT5's binding pocket for bulky IR dyes is still under study. In Chapter 3, we observed GLUT5 dependent uptake of fluorescein conjugated 2,5-AM derivative with net charge =0.

Figures 5.9 and 5.10 depict different conjugates that can be developed (with fluorophores either directly conjugated or having a linker in between) to study the influence of the charge effect.[12,13] The goal of this project is to gain mechanistic understanding of GLUT5 specific uptake and would provide a valuable tool for monitoring cancer and metabolic diseases. Such probes could also aid in the development of high content screening system in drug discovery.

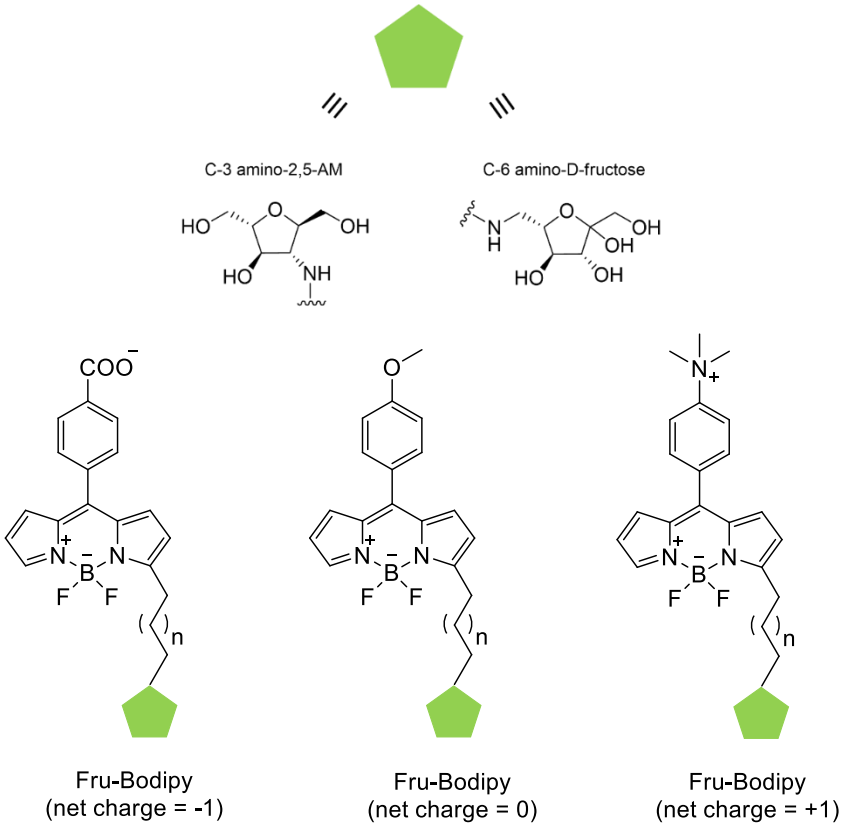

Figure 5.9. Potential fructose/mannitol "BODIPY" based probes with different overall charge

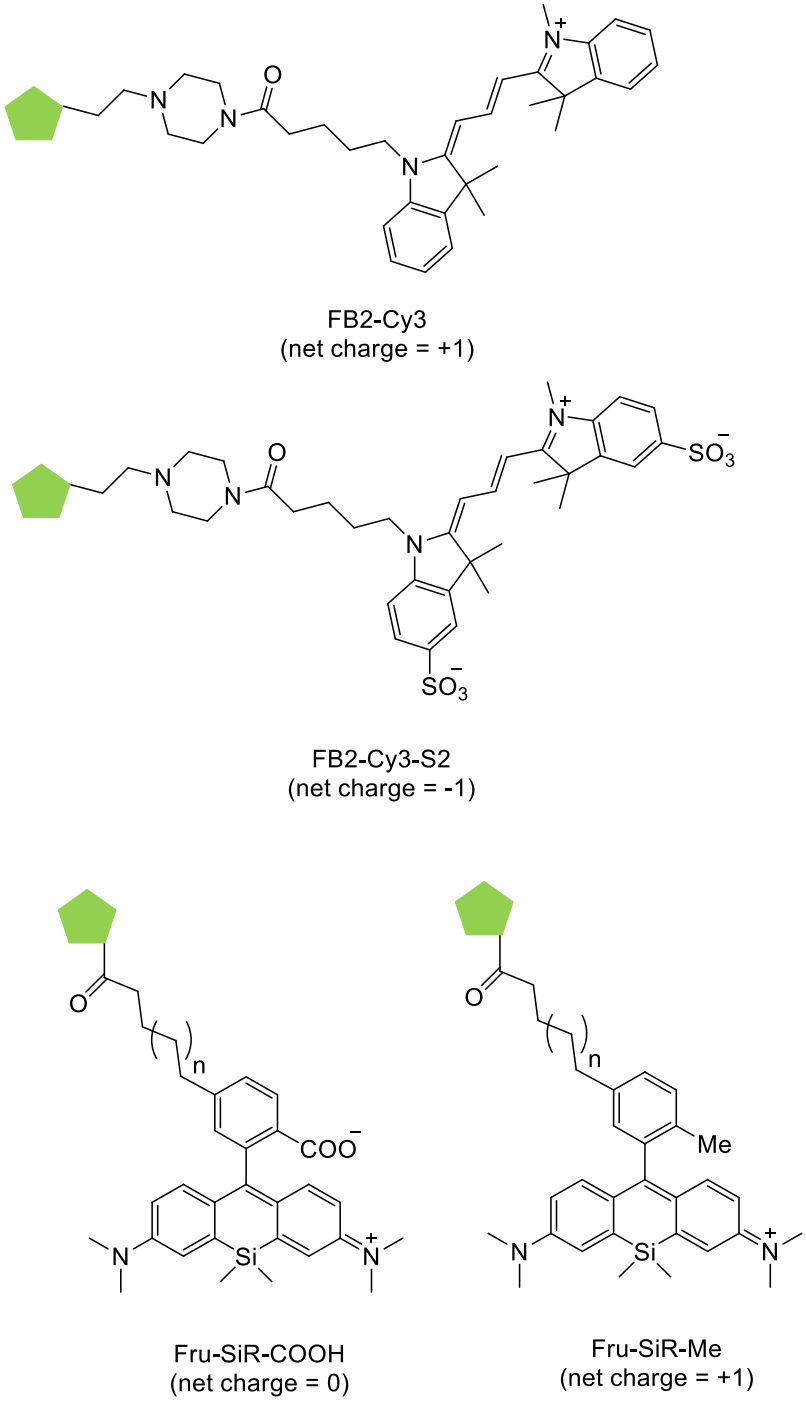

Figure 5.10. Potential fructose/mannitol Cy5- and Si-Rhodamine based probes with different overall charge

5.4. Dual probe conjugates

In recent years, the combination of different imaging methods and developing such probes with multiple functionalities has been getting more attention and significantly advanced in the field of precision medicine and monitoring treatment responses.[14-16] Noninvasive cancer imaging is an essential tool for accurate diagnosis in precision medicine.[17] PET is one of the most widely used and sensitive technique for detecting physiological and metabolic processes. This technique can be combined with fluorescence imaging (FI) allowing longitudinal imaging to ensure maximum removal of the tumor.

The development of dual probes would provide synergistic capabilities for both modalities eliminating the need of developing two different imaging modalities with different biodistribution profiles. In such studies, the tumor would be first located through PET followed by using fluorescence guided surgical resection of the tumor. PET is a high sensitivity imaging method generating images with unlimited tissue penetration depth whereas FI offers its particular application for in situ detection of tumor margins in real time (not limited by the short half-life displayed by PET radionuclides) while minimizing damage to healthy tissue.[18] In a recent review, several PET/FI probes have been reported demonstrating different platforms and vectors on which dual probes can be developed. A similar strategy can be used for the development of fructose/2,5-AM derived dual probe for improved detection of GLUT5.[16] So far, no dual probes for the detection of GLUT5 as a biomarker have been reported. Yuen and coworkers have recently reported dual functionality glucose derivative (2-FBDG), and tested its uptake against the gold standard, 2-[^{18}F]-FDG for transport through GLUT1 (Figure 5.11).[16] They also reported other dual probes with different scaffolds (diarylpyrazoline/diarylpyrazole and benzoxadiazole fluorophores) displaying the potential methods for developing dual PET/FI imaging agents for GLUT5. However, the low excitation/emission wavelength range of the above-mentioned probes provides a disadvantage for their usage in vivo experiments. To overcome this limitation, fructose/2,5-AM can be conjugated to dyes with longer emission wavelength providing the tolerance of GLUT5 to bulky, non-polar, sterically hindered conjugates is well examined and understood.

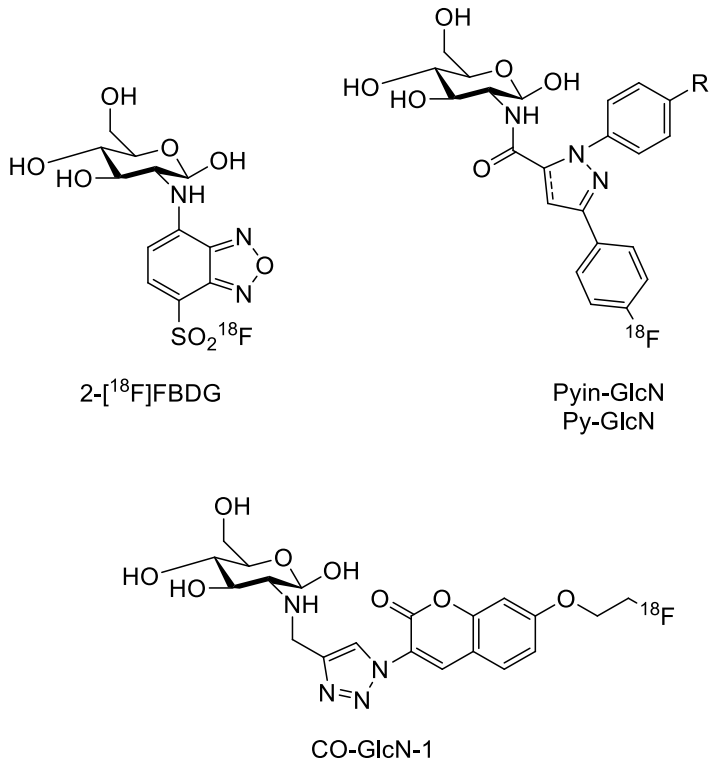

Figure 5.11. Reported glucose conjugate dual probes

Figure 5.12 represents the examples of dual probe conjugates that can be developed to examine GLUT5 mediated uptake and its application in the detection of the tumor. Such probes can be labeled with different radionuclides other than ^{18}F as such as ^{64}Cu, ^{68}Ga, ^{89}Zr, ^{124}I, etc. Radionuclides are selected based on the desired biological half-life of the radiotracer. In this study, ^{11}C, ^{18}F, and ^{68}Ga are appropriate choices for labeling of small molecules as these radionuclides will decay and will be quickly washed out from the body.

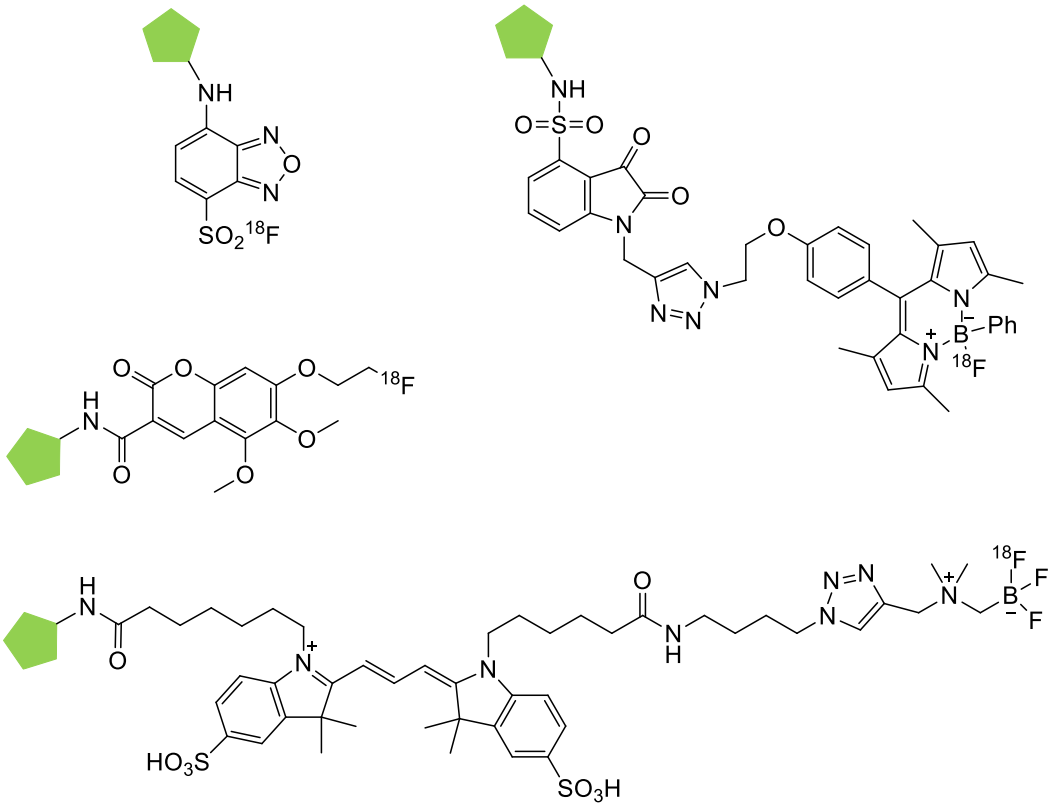

Figure 5.12. Potential fructose/mannitol conjugate dual probes

5.5. Evaluating other scaffolds toward GLUT5 binding

Holman and coworkers reported 2,5-AM as a high affinity GLUT5 ligand.[19] In D-fructose, the ring oxygen and several of the hydroxyl groups are reported to play a critical role in binding interactions with the GLUT5 binding pocket allowing for their smooth passage.[20] These results allow us to explore other structures that resemble the scaffold of 2,5-AM. As represented in Scheme 5.1., 2,5-dihydroxymethyl-3,4-dihydroxy pyrrole (DMDP)[21] and dihydroxymethyl-3,4-dihydroxy thiophene (DMDT)[22], two structures are proposed having same stereochemistry mimicking 2,5-AM. Evaluation of both the scaffolds against 2,5-AM and D-fructose would give more insight into understanding the binding mechanism with GLUT5.

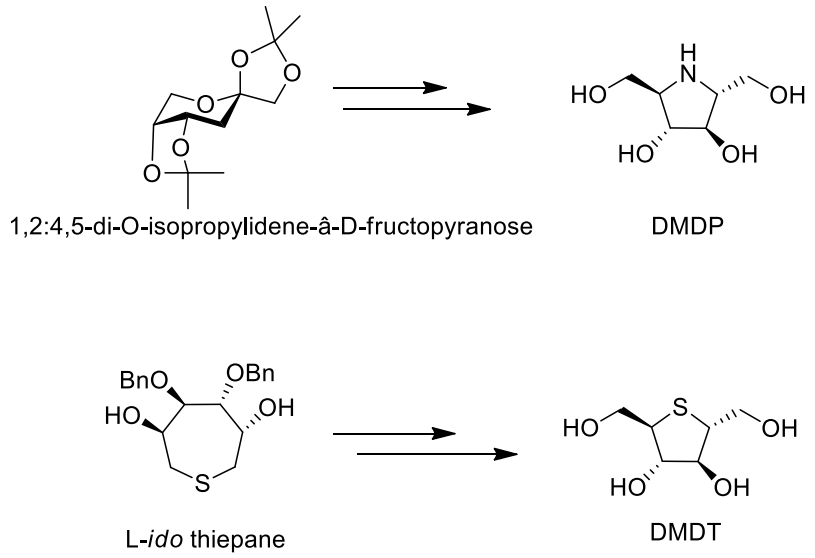

Scheme 5.1. Synthesis of aza- and thio- sugar from respective starting materials

The development of radiolabeled and fluorophore labeled DMDP and DMDT may yield novel scaffolds to target GLUT5. DMDP is expected to exist as an ammonium salt at physiological pH due to basic secondary amine functionality. Labeling of DMDP (Figure 5.13) could be obtained at ring nitrogen by having an electron withdrawing linker (amide, sulfonamide, electron deficient aniline) to keep ring nitrogen unprotonated at physiological pH. In the case of DMDT (Figure 5.13), the sulfur atom is generally considered a weak hydrogen bonding acceptor due to its low electronegativity. In addition, the inductively withdrawing effect of primary and secondary hydroxyl groups would overall result in making it a weak hydrogen bond acceptor as compared to DMDP and 2,5-AM. In addition, ring sulfur cannot be labeled due to its bivalency, DMDT can only be labeled at the same positions as in 2,5-AM. Although, such experiments should be conducted after evaluating the affinity of both DMDP/DMDT towards GLUT5.

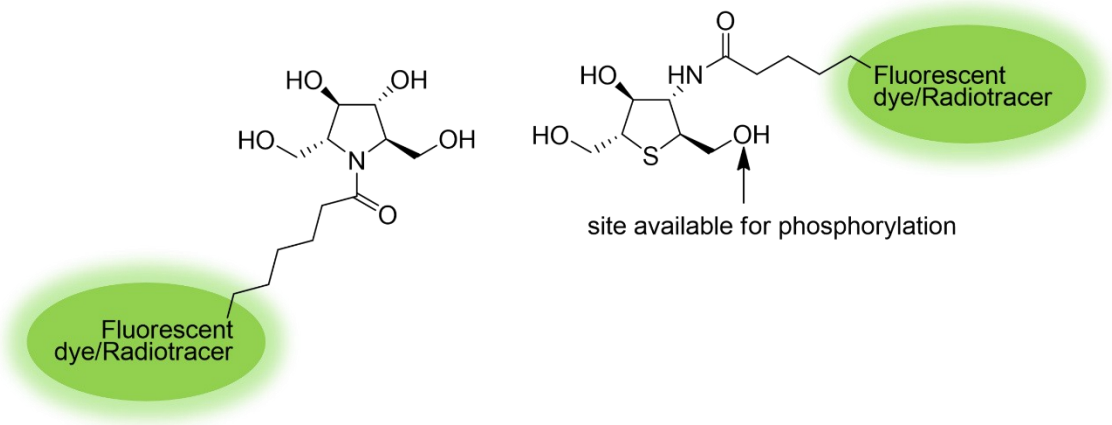

Figure 5.13. Potential tracers with aza- and thio- sugars

5.6. Targeting other diseases showing overexpression of GLUT5 and development of small molecule drug conjugates

5.6.1. Overexpression of GLUT5 in other diseases

As mentioned in chapter 1, high GLUT5 expression and abnormal fructose metabolism are associated with the number of diseases and cancer such as diabetes, NASH (NAFLD), lung adenocarcinoma, and gout.[23,24,25] Because of this association, there is a significant potential for developing and using reported fructose/mannitol-based probes for early detection before progression to severe form of any disease. Similarly, evaluation of the known and currently in development of GLUT5 inhibitors could also be beneficial for the treatment of such diseases.

5.6.2. Small molecule drug conjugates (SMDCs)

SMDCs are a promising approach for targeted therapy as it involves small molecules (Figure 5.14) as the targeted ligand attached to a potent cytotoxic agent via a cleavable linker. The release of this cytotoxic agent selectively in the tumor microenvironment would result in enhancing the therapeutic potential of anticancer drugs.[26] Ghosh and coworkers have reported a review discussing SMDC design, spacer, linker, targeting ligand, and therapeutic payloads along with SMDCs used in clinics.[26]

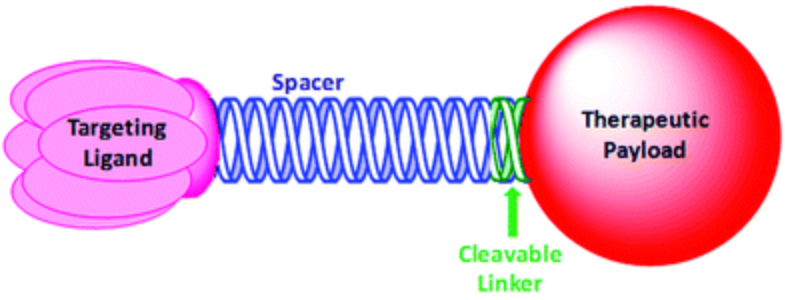

Figure 5.14. General representation of small molecule drug conjugates (Figure copied with permission from Patel et al.[26])

Tanasova et al. recently reported chlorambucil (CLB) 2,5-AM conjugate (Figure 5.15) and reported moderate inhibition in comparison to just chlorambucil drug.[27] Such observations were rationalized due to enhanced hydrophilicity of conjugates affecting the selective uptake via GLUT5. Therefore, it is important to first evaluate the hydrophobicity and affinity of any conjugates to be developed. However, the presence of long and hydrophilic linker, conjugate of a small cytotoxic agent can eliminate the limitation of insoluble and impermeable conjugates.

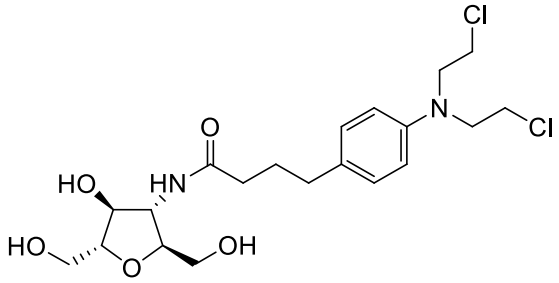

Figure 5.15. Reported mannitol-based drug conjugate

Figure 5.16 represents the potential mannitol-mitomycin drug conjugates (containing spacer and linker) that can be developed to selectively deliver cytotoxic payloads to GLUT5 expressing cancers. Anticancer drugs or therapeutic payloads generally act by inhibiting the cellular functions (such as cytokinesis, replication of DNA, and synthesis of proteins or metabolic mechanisms (such as sugar transport, and glycolysis).[26] Therefore, the development of fructose/mannitol-based drug conjugates

targeting fructose transporters can be of great significance for delivering the anticancer drug selectively to the targeted cells limiting the exposure to healthy cells.

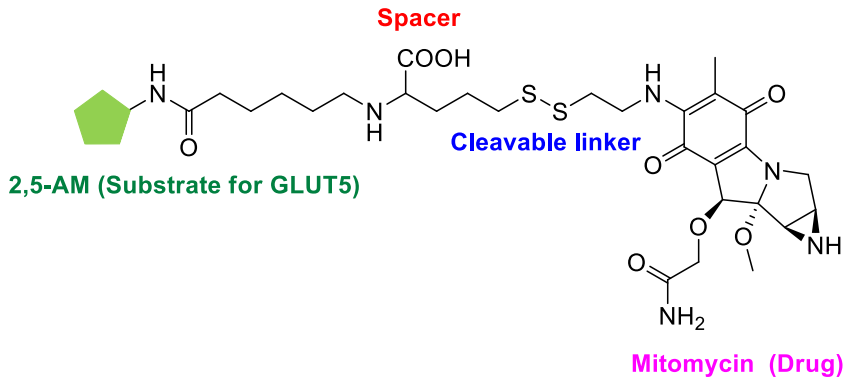

Figure 5.16. Potential fructose/mannitol-based mitomycin drug conjugates

SMDCs can also be modified to identify the overexpressed receptors in the compromised cells through imaging by associating the same substrate/ligand to a tracer (radionuclides, NIR dyes) allowing inspection of deeply buried tumor tissue for optical tumor resection during surgery.

5.7. Fructose directed labeling of GLUT5 transporter with fluorescent tag in live cells

This method involves a selective and noninvasive approach to study the function and localization of native GLUT5. This strategy overcomes the requirement of genetic modification of receptors. By taking advantage of fructose as the preferred substrate for GLUT5, a fluorophore can be linked to fructose through a linker as demonstrated in Figures 5.17 and 5.18.[28] In this strategy, an amino group of lysine (from amino acid residues present on the receptor) would react with an electrophilic region of the linker leading to the dissociation of the fructose moiety and thus causing the labeling of the protein. Kellam and coworkers recently reported the same approach to label GPCR by designing a fluorescent antagonist and observed irreversible fluorescent labeling in presence of an unlabeled antagonist (even at high concentration).[28] This approach could also be used to visualize receptor trafficking without affecting the binding site of the

receptor and to study the signaling in endogenously and clinically relevant systems (Figure 5.18).

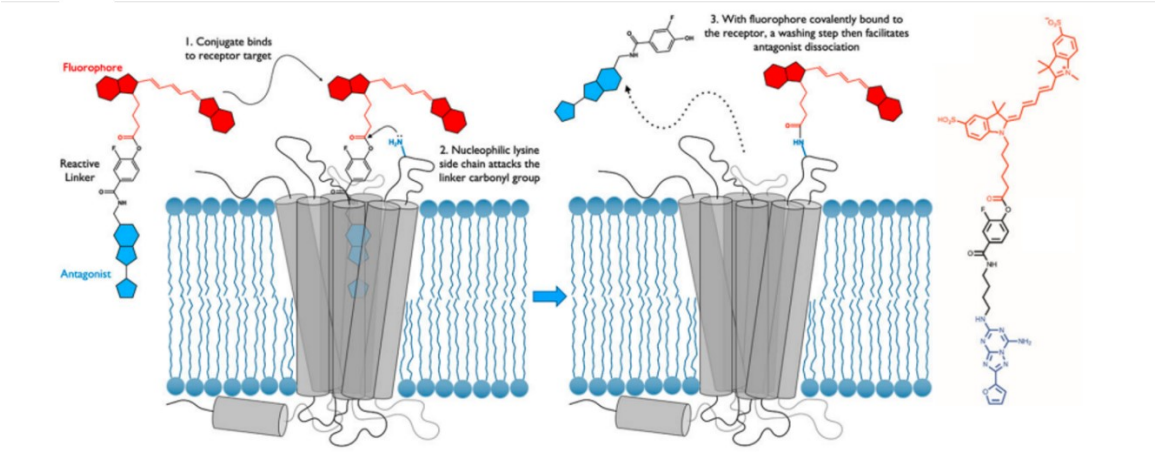

Figure 5.17. Schematic representation of covalently labeled GPCR (Figure copied with permission from Stoddart et al.[28])

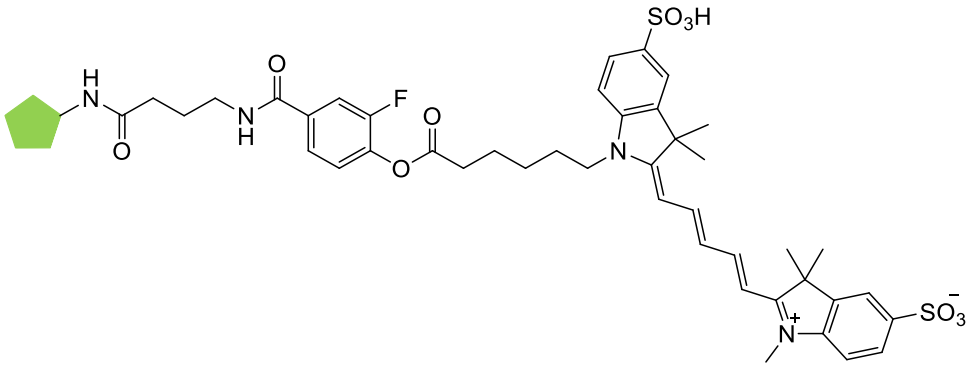

Figure 5.18. Potential fructose-fluorophore conjugate for labeling of GLUT5

5.8. Mechanistic insight into the activation mechanism of GLUT5 and its spatial distribution

There are several studies discussing the uptake of fructose via GLUT5 and its association with diseases. However, molecular mechanisms of its transport and activation along with GLUT5's distribution pattern on the cell membrane remain unknown. In 2018, Wang and coworkers performed super resolution imaging to investigate the assembly of GLUT1 and reported the activation of GLUT1 which

induced the sporadic distribution of GLUT1 in order to facilitate the transport of glucose (Figure 5.19).[29] They also observed the influence of lipid rafts on the cluster formation ability of transporter. A similar approach could be used to understand and study the activation and distribution of GLUT5 by labeling the transporter with anti-GLUT5 antibodies.[29] Such experiments might provide crucial information on the regulatory factors, clustering features, and the relationship between GLUT5 activation and distribution.

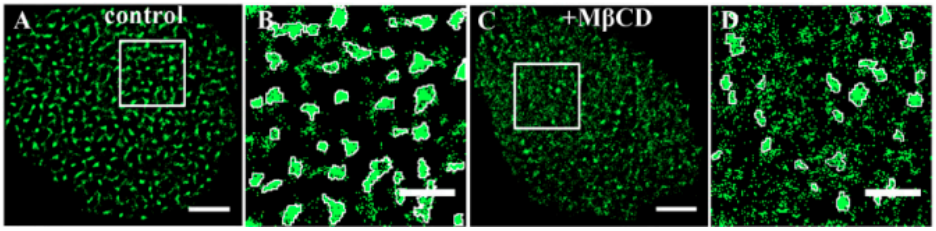

Figure 5.19. Super resolution images of changes in GLUT1 cluster on control (A), MβCD (cyclodextrin) treated (C), and the corresponding magnified images with clusters circled in white (B and D) (Figure copied with permission from Yan et al.[29])

5.9. Conclusion

Due to the strong correlation of the number of disease states with abnormal expression of GLUT5, this transporter protein has become an intriguing target to be explored for the development of therapeutic and diagnostic probes. This chapter describes the exciting directions that could be taken in the area of GLUT5 targeting small molecules. In addition, it would be enlightening to know the mechanism of transport through GLUT5 and changes in distribution pattern on the surface with alterations in their dynamic environment.

5.10. References

1. Ecker, G. F.; Clausen, R. P.; Sitte, H. H. Wiley-VCH: Weinheim.; Transporters as Drug Targets., **2017**.

2. Colas, C.; Ung, P. M. U.; Schlessinger, A. SLC Transporters: Structure, Function, and Drug Discovery. *Med. Chem. Commun.* **2016**, *7*, 1069–1081.

3. Lin, L.; Yee, S. W.; Kim, R. B.; Giacomini, K. M. SLC Transporters as TherapeuticTargets: Emerging Opportunities. *Nat. Rev. Drug Discov.* **2015**, *14*, 543–560.

4. Schmidl, S.; Iancu, C. V.; Choe, J. Y.; Oreb, M. Ligand Screening Systems for Human Glucose Transporters as Tools in Drug Discovery. *Front. Chem.* 2018, *6*, 183.

5. Soueidan, O.-M.; Scully, T. W.; Kaur, J.; Panigrahi, R.; Belovodskiy, A.; Do, V.; Matier, C. D.; Lemieux, M. J.; Wuest, F.; Cheeseman, C.; West, F. G. Fluorescent Hexose Conjugates Establish Stringent Stereochemical Requirement by Glut5 forRecognition and Transport of Monosaccharides. *ACS Chem. Biol.* **2017**, *12*, 1087–1094.; Kondapi, V. P. K. .; Soueidan, O.-M.; Cheeseman, C. I.; West, F. G. Tunable GLUTHexose Binding and Transport via Modulation of Hexose C-3 Hydrogen-Bonding Capabilities. *Chem. Eur. J.* **2017**, *23*, 8073–8081.

6. Slavic, K.; Derbyshire, E. T.; Naftalin, R. J.; Krishna, S.; Staines, H. M. Comparison of effects of green tea catechins on apicomplexan hexose transporters and mammalian orthologues. *Mol. Biochem. Parasitol.* **2009,** *168*, 113–116; Thompson, S. M. G.; Ursu, O.; Babkin, P.; Iancu, C. V.; Whant, A.; Oprea, T. I.; Choe, J. Discovery of a specific inhibitor of human GLUT5 by virtual screening and in vitro transport evaluation. *Sci. Rep.* **2016,** *6*, 24240; Huard, K.; Ahn, K.; Amor, P.; Beebe, D. A.; Borzilleri, K. A.; Chrunyk, B. A.; Coffey, S. B.; Cong, Y.; Conn, E. L.; Culp, J. S.; Dowling, M. S.; Gorgolione, M. F.; Gutierrez, J. A.; Knafels, J. D.; Lachapelle, E. A.; Pandit, J.; Parris, K. D.; Perez, S.; Pfefferkorn, J. A.; Price, D. A.; Raymer, B.; Ross, T. T.; Shavnya, A.; Smith, A. C.; Subashi, T. A.; Tesz, G. J.; Thuma, B. A.; Tu, M.; Weaver, J. D.; Weng, Y.; Withka, J. M.; Xing, G.; Magee, T. V. Discovery of fragment-derived small molecules for in vivo inhibition of ketohexokinase (KHK). *J. Med. Chem.* **2017,** *60*, 7835–7849; Tripp, J.; Essl, C.; Iancu, C.V.; Boles, E.; Choe, J.Y.; Oreb, M.. Establishing a yeast-based screening system for discovery of human GLUT5 inhibitors and activators. *Sci. Rep.*, **2017**, *7*, 1-9.

7. Escobedo, J. O.; Rusin, O.; Lim, S.; Strongin, R. M. NIR Dyes for BioimagingApplications. *Curr. Opin. Chem. Biol.* **2010**, *14*, 64–70.

8. Yuan, A.; Wu, J.; Tang, X.; Zhao, L.; Xu, F.; Hu, Y. Application of Near-InfraredDyes for Tumor Imaging, Photothermal, and Photodynamic Therapies. *J. Pharm. Sci.* 2013, *102*, 6–28; Pinto, A.; Pocard, M.; Photodynamic therapy and photothermaltherapy for the treatment of peritoneal metastasis: a systematic review. *Pleura and peritoneum*, **2018**, *3*(4).

9. Choi, H. S.; Nasr, K.; Alyabyev, S.; Feith, D.; Lee, J. H.; Kim, S. H.; Ashitate, Y.; Hyun, H.; Patonay, G.; Strekowski, L.; Henary, M. Synthesis and in Vivo Fate of Zwitterionic Near-infrared Fluorophores. *Angew. Chem. Int. Ed.* **2011**, *50*, 6258–6263.

10. Choi, H. S.; Gibbs, S. L.; Lee, J. H.; Kim, S. H.; Ashitate, Y.; Liu, F.; Hyun, H.; Park, G.; Xie, Y.; Bae, S.; Henary, M. Targeted Zwitterionic Near-Infrared Fluorophores for Improved Optical Imaging. *Nat. Biotechnol.* **2013**, *31*, 148–153.

11. Kim, E.; Yang, K. S.; Giedt, R. J.; Weissleder, R. Red Si–Rhodamine Drug Conjugates Enable Imaging in GFP Cells. *Chem. Comm.* **2014**, *50*, 4504–4507.

12. Park, J.; Um, J. J.; Jo, A.; Lee, J.; Jung, D. W.; Williams, D. R.; Park, S. B. Impact of Molecular Charge on GLUT-Specific Cellular Uptake of Glucose Bioprobes and in Vivo Application of the Glucose Bioprobe, GB2-Cy3. *Chem. Comm.* **2014**, *50*, 9251–9254.

13. Jo, A.; Sung, J.; Lee, S.; Nam, H.; Lee, H. W.; Park, J.; Kim, H. M.; Kim, E.; Park, S. B. Near-IR Fluorescent Tracer for Glucose-Uptake Monitoring in Live Cells. *Bioconj. Chem.* 2018, *29*, 3394–3401.; Gomez, A.M.; Lopez, J.C. Bringing Color to Sugars: The Chemical Assembly of Carbohydrates to BODIPY Dyes. *Chem. Rec.* **2021**, *21*, 3112-3130.

14. An, F. F.; Chan, M.; Kommidi, H.; Ting, R. Dual PET and Near-Infrared Fluorescence Imaging Probes as Tools for Imaging in Oncology. *AJR. Am. J. Roentgenol.* **2016**, *207*, 266.

15. Klenner, M. A.; Pascali, G.; Massi, M.; Fraser, B. H. Fluorine-18 Radiolabelling and Photophysical Characteristics of Multimodal PET–Fluorescence Molecular Probes. *Chemistry–A Eur. J.* **2021**, *27*, 861–876.

16. Thorp-Greenwood, F. L.; Coogan, M. P. Multimodal Radio-(PET/SPECT) and Fluorescence Imaging Agents Based on Metallo-Radioisotopes: Current Applications and Prospects for Development of New Agents. *Dalton Trans.* **2011**, *40*, 6129–6143.
17. Hussain, T.; Nguyen, Q. T. Molecular Imaging for Cancer Diagnosis and Surgery *Adv. Drug Del. Rev.* **2014**, *66*, 90–100.
18. Yuen, R.; Wagner, M.; Richter, S.; Dufour, J.; Wuest, M.; West, F. G.; Wuest, F. Design, Synthesis, and Evaluation of Positron Emission Tomography/Fluorescence Dual Imaging Probes for Targeting Facilitated Glucose Transporter 1 (GLUT1). *Org. Biomol. Chem.* **2021**, *19*, 3241–3254.
19. Barnett, J. E.; Holman, G. D.; Munday, K. A. Structural Requirements for Binding to the Sugar-Transport System of the Human Erythrocyte. *Biochem. J.* **1973**, *131*,211–221.
20. Girniene, J.; Tatibouët, A.; Sackus, A.; Yang, J.; Holman, G. D.; Rollin, P. Inhibition of the D-Fructose Transporter Protein GLUT5 by Fused-Ring Glycol-1,3-Oxazolidin-2-Thiones and Oxazolidin-2-Ones. *Carbohydrate Res.* **2003**, *338*, 711–719.
21. García-Moreno, M. I.; Aguilar, M.; Ortiz Mellet, C.; García Fernández, J. M. Intramolecular Benzyl Protection Delivery: A Practical Synthesis of DMDP and DGDP from D-Fructose. *Org. Lett.* **2006**, *8*, 297–299.
22. Le Merrer, Y.; Fuzier, M.; Dosbaa, I.; Foglietti, M. J.; Depezay, J. C. Synthesis of Thiosugars as Weak Inhibitors of Glycosidases. *Tetrahedron* **1997**, *53*, 16731–16746.
23. Godoy, A.; Ulloa, V.; Rodríguez, F.; Reinicke, K.; Yañez, A. J.; García, M. D. L. A.; Medina, R. A.; Carrasco, M.; Barberis, S.; Castro, T.; Martínez, F.; Koch, X.; Vera, J. C.; Poblete, M. T.; Figueroa, C. D.; Peruzzo, B.; Nualart, F. Differential Subcellular Distribution of Glucose Transporters GLUT1-6 and GLUT9 in Human Cancer: Ultrastructural Localization of GLUT1 and GLUT5 in Breast Tumor Tissues. *J. Cell Physiol* . **2005**, *207*, 614–627.
24. Jegatheesan, P.; Bandt, J. P. D. Fructose and NAFLD: The Multifaceted Aspects of Fructose Metabolism. *Nutrients* **2017**, *9*, 1–13.

25. McQuade, D. T., Plutschack, M. B. & Seeberger, P. H.; McQuade, D. T.,Plutschack, M. B. & Seeberger, P. H.; McQuade, D. T., Plutschack, M. B. & Seeberger, P. H. Passive Fructose Transporters in Disease: A Molecular Overview of Their Structural Specificity. *Org. Biomol. Chem.* **2013**, *11*, 4909–4920.

26. Patel, T.K.; Adhikari, N.; Amin, S.A.; Biswas, S.; Jha, T.; Ghosh, B. Small molecule drug conjugates (SMDCs): an emerging strategy for anticancer drug design and discovery. *New J. Chem.*, **2021**, *45*, 5291-5321.

27. Nahrjou, N.; Ghosh, A.; Tanasova, M. Targeting of GLUT5 for Transporter-Mediated Drug-Delivery Is Contingent upon Substrate Hydrophilicity. *Int. J. Mol.Sci.* **2021**, *22*, 5073.

28. Stoddart, L. A.; Kindon, N. D.; Otun, O.; Harwood, C. R.; Patera, F.; Veprintsev, D. B.; Woolard, J.; Briddon, S. J.; Franks, H. A.; Hill, S. J.; Kellam, B. Ligand-Directed Covalent Labelling of a GPCR with a Fluorescent Tag in Live Cells.*Commun. Biol.* **2020**, *3*, 1–9.

29. Yan, Q.; Lu, Y.; Zhou, L.; Chen, J.; Xu, H.; Cai, M.; Shi, Y.; Xiong, W.; Jiang, J., Xiong, W., Gao, J. and Wang, H.; Gao, J.; Wang, H. Mechanistic Insights into GLUT1 Activation and Clustering Revealed by Super-Resolution Imaging. *PNAS* **2018,** *115*, 7033–7038.

Compiled References

Chapter1

1. Dashty, M. A Quick Look at Biochemistry: Carbohydrate Metabolism.*Clin.Biochem.* **2013**, *46*, 1339–1352.

2. Kahn, B. B. Facilitative Glucose Transporters: Regulatory Mechanisms and Dysregulation in Diabetes. *J. Clin. Invest.* **1992**, *89*, 1367–1374.

3. Joost, H.-G.; Wandel, S.; Schürmann, A. Structure-Function Relationship of Glucosetransporters Catalyzing Facilitated Diffusion. *Exp. Clin. Endocrinol.* **1994**, *102*, 434–438.

4. Gould, G. W.; Holman, G. D. The Glucose Transporter Family: Structure, Function and Tissue-Specific Expression. *Biochem. J.* **1993**, *295*, 329–341.

5. Kahn, B. B.; Sheperd, P. R. Glucose Transporters and Insulin Action: Implications for Insulin Resistance and Diabetes Mellitus. *N. Engl. J. Med.* **1999**, *341*, 248– 257.

6. Kaiser, N.; Leibowitz, G.; Nesher, R. Glucotoxicity and Beta-Cell Failure in Type 2 Diabetes Mellitus. *J. Pediatr. Endocrinol. Metab.* **2003**, *16*, 5–22.

7. Scheepers, A.; Joost, H.-G.; Schu¨rmann, A. The Glucose Transporter Families SGLT and GLUT: Molecular Basis of Normal and Aberrant Function. *J. Parenter. Enter. Nutr.* **2004**, *28*, 364–371.

8. Thorens, B.; Mueckler, M. Glucose Transporters in the 21st Century. *Am. J. Physiol. Endocrino.l Metab.* **2010**, *298*, E141–E145; Bryant, N.J.; Govers, R.; James, D.E. Regulated transport of the glucose transporter GLUT4. *Nat. Rev.Mol.* **2002,** *3*, 267-277.

9. Manolescu, A. R.; Witkowska, K.; Kinnaird, A.; Cessford, T.; Cheeseman, C. Facilitated Hexose Transporters: New Perspectives on Form and Function. *Physiology* **2007**, *22*, 234–240.

10. McQuade, D. T., Plutschack, M. B. & Seeberger, P. H. Passive Fructose Transporters in Disease: A Molecular Overview of Their Structural Specificity. *Org. Biomol. Chem.* **2013**, *11*, 4909–4920.

11. Mueckler, M.; Thorens, B. The SLC2 (GLUT) Family of Membrane Transporters. *Mol. Asp. Med.* **2013**, *34*.

12. Long, W.; Cheeseman, C. I. Structure and Functional Insights into GLUT Family of Membrane Transporters. *Cell Health Cytoskelet.* **2015**, *7*, 167–183.

13. Deng, D.; Yan, N. GLUT, SGLT, and SWEET: Structural and Mechanistic Investigation of the Glucose Transporters. *Protein Sci.* **2016**, *25*, 546–558.

14. Mueckler, M.; Caruso, C.; Baldwin, S. A.; Panico, M.; Blench, I.; Morris, H. R.; Allard, W. J.; Lienhard, G. E.; Lodish, H. F. Sequence and Structure of a Human Glucose Transporter. *Science* **1985**, *229*, 941–945.

15. Deng, D.; Xu, C.; Sun, P.; Wu, J.; Yan, C.; Hu, M.; Yan, N. Crystal Structure of the Human Glucose Transporter GLUT1. *Nature* **2014**, *510*, 121–125.

16. Joost, H.-G.; Thorens, B. The Extended GLUT-Family of Sugar/Polyol Transport Facilitators: Nomenclature, Sequence Characteristics, and Potential Function of Its Novel Members. *Mol. Membr. Biol*. **2001**, *18*, 247–256.

17. Joost, H.-G.; Bell, G. I.; Best, J. D.; Birnbaum, M. J.; Charron, M. J.; Chen, Y. T.; Doege, H.; James, D. E.; Lodish, H. F.; Moley, K. H.; Moley, J. F.; Mueckler, M.; Rogers, S.; Schurmann, A.; Seino, S.; Thorens, B. Nomenclature of the 53 GLUT/SLC2A Family of Sugar/Poloyl Transport Facilitators. *Am. J. Physiol. Endocrinol. Metab.* **2002**, *282*, E974–E976.

18.Wood, S.; Trayhurn, P. Glucose Transporters (GLUT and SGLT): Expanded Families of Sugar Transport Proteins. *Br. J. Nutr.* **2003**, *89*, 3–9.

19. Simpson, I. A.; Cushman, S. W. Hormonal Regulation of Mammalian Glucose Transport. *Annu. Rev. Biochem.* **1986**, *55*, 1059–1089.

20. Bryant, N. J.; Govers, R.; James, D. E. Regulated Transport of the Glucose Transporter GLUT4. *Nat. Rev. Mol. Cell Biol.* **2002**, *2*, 267–277.

21. Rumsey, S. C.; Darnwala, R.; Al-Hasani, H.; Zarnowski, M. J.; Simpson, I. A.; Levine, M. Dehydroascorbic Acid Transport by GLUT4 in Xenopus Oocytes and Isolated Rat Adipocytes. *J. Biol. Chem.* **2000**, *275*, 28246–28253.

22. Uldry, M.; Ibberson, M.; Horisberger, J.-D.; Chatton, J.-Y.; Riederer, B. M.; Thorens, B. Identification of a Mammalian H_-Myo-Inositol Symporter Expressed Predominantly in the Brain. *EMBO J.* **2001**, 4467–4477.

23. Kasahara, M.; Hinkle, P. C. Recognition and Purification of D-Glucose Transporter from Human Erythrocytes. *J. Biol. Chem.* **1977**, *252*, 7380–7390.

24. Morgello, S.; Uson, R. R.; Schwartz, E. J.; Haber, R. The Human Blood-Brain Barrier Glucose Transporter (GLUT1) Is a Glucose Transporter of Gray Matter Astrocytes. *Glia.* **1995**, *14*, 43–54.

25. Kumagai, K. A. Glucose Transport in Brain and Retina: Implications in the Management and Complications of Diabetes. *Diabetes Metab Res Rev* **1999**, *15*, 261–273.

26. Postic, C.; Burcelin, R.; Rencurel, F.; Pegorier, J.-P.; Loizeau, M.; Girard, J.; Leturque, A. Evidence for a Transient Inhibitory Effect of Insulin on GLUT2 Expression in the Liver: Studies in Vivo and in Vitro. *Biochem. J.* **1993**, *293*, 119–124.

27. Pang, K.; Mukonoweshuro, C.; Wong, G. G. Beta Cells Arise from Glucose Transporter 2 (GLUT2)-Expressing Epithelial Cells of the Developing Rat Pancreas. *Proc. Natl. Acad. Sci. USA* **1994**, *91*, 9559–9563.

28. Maher, F.; Davies-Hill, T. M.; Lysko, P. G.; Henneberry, R. C.; Simpson, I. A. Expression of Two Glucose Transporters, GLUT1 and GLUT3, in Cultured Cerebellar Neurons: Evidence for Neuron-Specific Expression of GLUT3. *Mol. Cell Neurosci.* **1991**, *2*, 351–360.

29. Haung, S.; Czech, P. The GLUT4 Glucose Transporter. *Cell. Metab.* **2007**, *5*, 237–252.

30. Band, E. B.; Depaoli, A. M.; Davidson, N. O.; Bell, C. I.; Burant, C. F. Sequence, Tissue Distribution, and Functional Characterization of the Rat Fructose Transporter GLUT5. *Am. J. Physiol. Gastrointest. Liver Physiol.* **1993**, *264*, G1169-1176.

31. Zhao, F.-Q.; Keating, A. F. Functional Properties and Genomics of Glucose Transporters. *Curr. Genomics* **2007**, *8*, 113–129.

32. Cheeseman, C. GLUT7: A New Intestinal Facilitated Hexose Transport. *Am J. Physiol. Endocrinol. Metab.* **2008**, *295*, E238 E241.

33. Preitner, F.; Bonny, O.; Laverriere, A.; Rotman, S.; Firsov, D.; Costa, A. D.; Metref, S.; Thorens, B. GLUT9 Is a Major Regulator of Urate Homostasis and Its Genetic

Inactivation Induces Hyperuricosuria and Urate Nephropathy. *Proc. Natl.Acad. Sci. USA* **2009**, *106*, 15501–15506.

34. Deng, D.; Xu, C.; Sun, P.; Yan, C.; Ke, M.; Jiang, X.; Xiong, L.; Ren, W.; Hirata, K.; Yamamoto, M.; Fan, S.; Yan, N. Molecular Basis of Ligand Recognition and Transport by Glucose Transporters. *Nature* **2015**, *526*, 391–396.

35. Seatter, M. J.; De La Rue, S. A.; Porter, L. M.; Gould, G. W. QLS Motif in Transmembrane Helix VII of the Glucose Transporter Family Interacts with the C-1 Position of D-Glucose and Is Involved in Substrate Selection at the Exofacial Binding Site. *Biochemistry* **1998**, *37*, 1322–1326.

36. Olson, A. L.; Pessin, J. E. Structure, Function, and Regulation of the Mammalian Facilitative Glucose Transporter Gene Family. *Annu. Rev. Nutr.* **1996**, *16*, 235–256.

37. Mueckler, M.; Weng, W.; Kruse, M. Glutamine 161 of GLUT1 Glucose Transporter Is Critical for Transport Activity and Exofacial Ligand Binding. *J. Biol. Chem.* **1994**, *269*, 20533–20538.

38. Long, W.; Panwar, P.; Witkowska, K.; Wong, K.; O'Neill, D.; Chen, X.-Z.; Lemieux, M. J.; Cheeseman‡, C. I. Critical Roles of Two Hydrophobic Residues within Human Glucose Transporter 9 (HSLC2A9) in Substrate Selectivity and Urate Transport. *J. Biol. Chem.* **2015**, *290*, 15292–15303.

39. Neame, K. D.; Richards, T. G. *Elementary Kinetics of Membrane Carrier Transport.*, Ist.; London, UK: *Blackwell Scientific Publications*;, 1972.

40. Fisher, R. B.; Parsons, D. S. Glucose Movements across the Wall of the Rat Small Intestine. *J. Physiol.* **1953**, *119*, 210–223.

41. Widdas, W. Inability of Diffusion to Account for Placental Glucose Transfer in the Sheep and Consideration of the Kinetics of a Possible Carrier Transfer. *J. Physiol.* **1952**, *118*, 23–39; Augustin, R; Mayoux, E. Mammalian sugar transporters. In *Glucose homeostasis*. IntechOpen, **2014.**

42. Naftalin, R. J. Alternating Carrier Models of Asymmetric Glucose Transport Violate the Energy Conservation Laws. *Biophys. J.* **2008**, *95*, 4300=4314.

43. Vollers, S. S.; Carruthers, A. Sequence Determinants of GLUT1-Mediated Accelerated-Exchange Transport: Analysis by Homology-Scanning Mutagenesis. *J. Biol. Chem.* **2012**, *287*, 42533–42544.

44. Anthony Carruthers. Will the Original Glucose Transporter Isoform Please Stand Up! *Am. J. Physiol. Endocrinol. Metab.* **2009**, *297*, E836–E848.

45. Nomura, N.; Verdon, G.; Kang, H. J.; Shimamura, T.; Nomura, Y.; Sonoda, Y.; Hussien, S. A.; Qureshi, A. A.; Coincon, M.; Sato, Y.; Abe, H.; Nakada-Nakura, Y.; Hino, T.; Arakawa, T.; Kusano-Arai, O.; Iwanari, H.; Murata, T.; Kobayashi, T.; Hamakubo, T.; Kasahara, M.; Iwata, S.; Drew, D. Structure and Mechanism of Mammalian Fructose Transporter GLUT5. *Nature.* **2015**, *526*, 397–401.

46. Gallagher, B. M.; Fowler, J. S.; Gutterson, N. I.; MacGregor, R. R.; Wan, C.-N.; Wolf, A. P. Metabolic Trapping as a Principle of Radiopharmaceutical Design: Some Factors Responsible for the Biodistribution of [18F]-2-Deoxy-2-Fluoro-D-Glucose. *J. Nucl. Med.* **1978**, *19*, 1154–1161.

47. Angyal, S. J. The Composition and Conformation of Sugars in Solution. *Angew. Chem. Int. Ed. Engl.* **1969**, *8*, 157–166.

48. Tajmir-Riahi, H. A. Carbohydrate Complexes with Alkaline Earth Metal Ions. Interactions of D-Glucono-1,5-Lacton with the Mg (II), Ca (II), Sr (II) and Ba (II)Cations in the Crystalline Solid and Aqueous Solution. *J. Inorg. Chem.* **1990**, *39*,33–37.

49. Kahlenberg, A.; Urman, B.; Dolansky, D. Preferential Uptake of D-Glucose by Isolated Human Erythrocyte Membranes. *Biochemistry* **1971**, *10*, 3154–3162.

50. Barnett, J. E.; Holman, G. D.; Munday, K. A. Structural Requirements for Binding to the Sugar-Transport System of the Human Erythrocyte. *Biochem. J.* **1973**, *131*, 211–221.

51. Kahlenberg, A.; Dolansky, D. Structural Requirements of D-Glucose for Its Binding to Isolated Human Erythrocyte Membranes. *Can. J. Biochem.* **1972**, *50*, 638–643.

52. Rees, W. D.; Holman, G. D. Hydrogen Bonding Requirements for the Insulin-Sensitive Sugar Transport System of Rat Adipocytes. *Biochim. Biophys. Acta Biomembr.* **1981**, *646*, 251–260.

53. Gatley, S. J. Labeled Glucose Analogs in the Genomic Era. *J. Nucl. Med.* **2003**, *44*, 1082–1086.

54. Tatibouet, A.; Yang, J.; Morin, C.; Holman, G. D. Synthesis and Evaluation of Fructose Analogues as Inhibitors of the D-Fructose Transporter GLUT5. *Bioorg. Med. Chem.* **2000**, *8*, 1825–1833.

55. Trayner, B. J.; Grant, T. N.; West, F. G.; Cheeseman, C. I. Synthesis and Characterization of 6-Deoxy-6-Fluoro-D-Fructose as a Potential Compound for Imaging Breast Cancer with PET. *Bioorg. Med. Chem.* **2009**, *17*, 5488–5495.; Girniene, J.; Tatibouët, A.; Sackus, A.; Yang, J.; Holman, G. D.; Rollin, P. Inhibition of the D-Fructose Transporter Protein GLUT5 by Fused-Ring Glycol-1,3-Oxazolidin-2-Thiones and Oxazolidin-2-Ones. *Carbohydr. Res.* **2003**, *338*, 711–719.

56. Yang, J.; Dowden, J.; Tatibouet, A.; Hatanaka, Y.; Holman, G. D. Development of High Affinity Ligands and Photoaffinity Labels for the D Fructose Transporter GLUT5. *Biochem. J.* **2002**, *367*, 533–539.

57. Yang, J.; Tatibou[t, A.; Hatanaka, Y.; Holman, G. D. Fructose Analogues with Enhanced Affinity for GLUT5. *Diabetes* **2001**, *50*, A277–A277.

58. Kondapi, V. P. K. .; Soueidan, O.-M.; Cheeseman, C. I.; West, F. G. Tunable GLUT–Hexose Binding and Transport via Modulation of Hexose C-3 Hydrogen-Bonding Capabilities. *Chem. Eur. J.* **2017**, *23*, 8073–8081.

59. Xu, X. D.; Shao, S. X.; Jiang, H. P.; Cao, Y. W.; Wang, Y. H.; Yang, X. C.; Wang, Y. L.; Wang, X. S.; Niu, H. T. Warburg Effect or Reverse Warburg Effect? A Review of Cancer Metabolism. Oncology Research and Treatment. *Oncol. Res. Treat.* **38**, 117–122.

60. Nakagawa, T.; Lanaspa, M. A.; Millan, I. S.; Fini, M.; Rivard, C. J.; Sanchez-Lozada, L. G.; Andres-Hernando, A.; Tolan, D. R.; Johnson, R. J. Fructose Contributes to the Warburg Effect for Cancer Growth. *Cancer Metab.* **2020**, *8*, 1–12.

61. Lassen, U.; Daugaard, G.; Eigtved, A.; Damgaard, K.; Friberg, L. 18F-FDG Whole Body Positron Emission Tomography (PET) in Patients with Unknown Primary Tumours (UPT). *Eur. J. Cancer* **1993**, 1076–1082.

62. Nakagawa, T.; Johnson, R. J.; Andres-Hernando, A.; Roncal-Jimenez, C.; Sanchez-Lozada, L. G.; Tolan, D. R.; Lanaspa, M. A. Fructose Production and Metabolism in the Kidney. *J. Am. Soc. Nephrol.* **2020**, *31*, 898–906.

63. Aparicio, L. M.; Villaamil, V. M.; Calvo, M. B.; Rubira, L. V.; Rois, J. M.; Valladares-Ayerbes, M.; Campelo, R. G.; Bolós, M. V.; Pulido, E. G. Glucose Transporter Expression and the Potential Role of Fructose in Renal Cell Carcinoma: A Correlation with Pathological Parameters. *Mol. Med. Rep.* **2010**, *3*, 575–580.

64. Zamora-León, S. P.; Golde, D. W.; Concha, I. I.; Rivas, C. I.; Delgado-López, F.; Baselga, J.; Nualart, F.; Vera, J. C. Expression of the Fructose Transporter GLUT5 in Human Breast Cancer. *Proc. Natl. Acad. Sci. USA* **1996**, *93*, 1847–1842.

65. Godoy, A.; Ulloa, V.; Rodríguez, F.; Reinicke, K.; Yañez, A. J.; García, M. D. L. A.; Medina, R. A.; Carrasco, M.; Barberis, S.; Castro, T.; Martínez, F.; Koch, X.; Vera, J. C.; Poblete, M. T.; Figueroa, C. D.; Peruzzo, B.; Nualart, F. Differential Subcellular Distribution of Glucose Transporters GLUT1-6 and GLUT9 in Human Cancer: Ultrastructural Localization of GLUT1 and GLUT5 in Breast Tumor Tissues. *J. Cell Physiol.* **2005**, *207*, 614–627.

66. Jegatheesan, P.; Bandt, J. P. D. Fructose and NAFLD: The Multifaceted Aspects of Fructose Metabolism. *Nutrients* **2017**, *9*, 1–13.

67. DiNicolantonio, J.; Subramonian, A. M.; O'Keefe, J. H. Added Fructose as a Principal Driver of Non-Alcoholic Fatty Liver Disease: A Public Health Crisis. *Open Heart* **2017**, *4*, 1–6.

68. Villaamil, V. M.; Gallego, G. A.; Rubira, L. V.; Campelo, R. G.; Valladares-Ayerbes, M.; Pulido, E. G.; Bolós, M. V.; Caínzos, I. S.; Villaamil, V. M. Fructose Transporter GLUT5 Expression in Clear Renal Cell Carcinoma. *Oncol. Rep.* **2011**, *25*, 315–323.

69. Weng, Y.; Zhu, J.; Chen, Z.; Fu, J.; Zhang, F. Fructose Fuels Lung Adenocarcinoma through GLUT5. *Cell Death Dis.* **2018**, *9*, 1–4.

70. Fan, X.; Liu, H.; Liu, M.; Wang, Y.; Qiu, L.; Cui, Y. Increased Utilization of Fructose Has a Positive Effect on the Development of Breast Cancer. *Peer J.* **2017**, *5*, 1–15.

71. Hamann, I.; Krys, D.; Glubrecht, D.; Bouvet, V.; Marshall, A.; Vos, L.; Mackey, J. R.; Wuest, M.; Wuest, F. Expression and Function of Hexose Transporters GLUT1, GLUT2, and GLUT5 in Breast Cancer-Effects of Hypoxia. *FASEB J.* **2018**, *32*, 5104–5118.

72. James, M. L.; Gambhir, S. S. A Molecular Imaging Primer: Modalities, Imaging Agents, and Applications. *Physiol. Rev.* **2012**, *92*, 897–965.

73. Wang, D. S.; Dake, M. D.; Park, J. M.; Kuo, M. D. Molecular Imaging: A Primer for Interventionalists and Images. *J. Vasc. Interv. Radiol.* **2006**, *17*, 1405–1423.

74. Pysz, M. A.; Gambhir, S. S.; Willmann, M. D. Molecular Imaging: Current Status and Emerging Strategies. *Clin. Radiol.* **2010**, *65*, 500–516.

75. Gambhir, S. S. Molecular Imaging of Cancer with Positron Emission Tomography. *Nat. Rev. Cancer* **2002**, *2*, 683–693.

76. Imam, S. K. Review of Positron Emission Tomography Tracers for Imaging of Tumor Hypoxia. *Cancer Biother. Radiopharm.* **2010**, *25*, 365–374.

77. Muehllehner, G.; Karp, J. S. Positron Emission Tomography. *Phys. Med. Biol.* **2006**, *51*, R117–R137.

78. Couturier, O.; Luxen, A.; Chatal, J. F.; Vuillez, J. P.; Rigo, P.; Hustinx, R. Fluorinated Tracers for Imaging Cancer with Positron Emission Tomography. *Eur J. Nucl. Med. Mol. Imaging* **2004**, *31*, 1182–1206.

79. Zanzonico, P. Positron Emission Tomography: A Review of Basic Principles, Scanner Design and Performance, and Current Systems. *Semin. Nucl. Med*. **2004**, *34*, 87–111.

80. Wood, K. A.; Hoskin, P. J.; Saunders, M. I. Positron Emission Tomography in Oncology: A Review. *Clin. Oncol. R. Coll. Radiol.* **2007**, *19*, 237–255.

81. Pagani, M.; Stone-Elander, S.; Larsson, S. A. Alternative Positron Emission Tomography with Non-Conventional Positron Emitters: Effects of Their Physical

Properties on Image Quality and Potential Clinical Applications. *Eur. J. Nucl. Med.* **1997**, *24*, 1304–1327.

82. Maschauer, S.; Prante, O. Sweetening Pharmaceutical Radiochemistry by 18F Fluoroglycosylation: A Short Review. *Bio. Med. Res. Int.* **2014**, *Article ID 214748*.

83. Wester, H. J. *Pharmaceutical Radiochemistry (I)*; Munich Molecular Imaging Handbook Series; *Scintomics,* 1, 2010.

84. Kilbourn, M. R.; Huizenga, J. R. Fluorine-18 Labeling of Radiopharmaceuticals. *Natl. Acad.* **1994**, *3203*.

85. Rozen, S. Elemental Fluorine as a Legitimate Reagent for Selective Fluorination of Organic Compounds. *Acc. Chem. Res.* **1988**, *21*, 307–312.

86. Ramsden, C. A. *Xenon Difluoride in the Organic Laboratory: A Tale of Substrates, Solvents and Vessels.*; *Arkivoc*, 2013; Vol. 109.

87. Furuya, T.; Kamlet, A. S.; Ritter, T. Catalysis for Fluorination and Trifluoromethylation. *Nature* **2011**, *473*, 470–477.

88. Lal, G. S.; Pez, G. P.; Syvret, R. G. Electrophilic NF Fluorinating Agents. *Chem. Rev*. **1996**, *96*, 1737–1756.

89. Singh, R. P.; Shreeve, J. M. Recent Highlights in Electrophilic Fluorination with 1-Chloromethyl-4-Fluoro-1,4-Diazoniabicyclo[2.2.2]Octane Bis(Tetrafluoroborate). *Acc. Chem. Res.* **2004**, *37*, 31–44.

90. Nyffeler, P. T.; Durón, S. G.; Burkart, M. D.; Vincent, S. P.; Wong, C.-H. Selectfluor: Mechanistic Insight and Applications. *Angew. Chem. Int. Ed.* **2004**, *44*, 192–212.

91. Umemoto, T.; Harasawa, K.; Tomizawa, G.; Kawada, K.; Tomita, K. N-F 19-Fluorine Nuclear Magnetic Resonance of N-Fluoropyridinium Salts. *J. Fluor. Chem.* **1991**, *53*, 369–377.

92. Kiselyov, A. S. Chemistry of N-Fluoropyridinium Salts. *Chem. Soc. Rev.* **2005**, *34*, 1031–1037.

93. Champagne, P. A.; Desroches, J.; Hamel, J. D.; Vandamme, M.; Paquin, J.-F. Monofluorination of Organic Compounds: 10 Years of Innovation. *Chem. Rev.* **2015**, *115*, 9073–9174.

94. Nguyen, T.-H.; Abarbri, M.; Guilloteau, D.; Mavel, S.; Emond, P. Nucleophilic Fluorination of Alkynyliodonium Salts by Alkali Metal Fluorides: Access to Fluorovinylic Compounds. *Tetrahedron* **2011**, *67*, 3434–3439.

95. Kim, D. W.; Jeong, H. J.; Lim, S. T.; Sohn, M. H.; Katzenellenbogen, J. A.; Chi, D. Y. Facile Nucleophilic Fluorination Reactions Using Tert-Alcohols as a Reaction Medium: Significantly Enhanced Reactivity of Alkali Metal Fluorides and Improved Selectivity. *J. Org. Chem.* **2008**, *73*, 957–962.

96. Bouvet, V.; Jans, H. S.; Wuest, M.; Soueidan, O.-M.; Mercer, J.; McEwan, A. J. B.; West, F. G.; Cheeseman, C. I.; Wuest, F. Automated Synthesis and Dosimetry of 6-Deoxy-6-[(18)F]Fluoro-D-Fructose (6-[(18)F]FDF): A Radiotracer for Imaging of GLUT5 in Breast Cancer. *Am. J. Nucl. Med. Mol. Imaging* **2014**, *4*, 248–259.

97. Akiyama, Y.; Hiramatsu, C.; Fukuhara, T.; Hara, S. Selective Introduction of a Fluorine Atom into Carbohydrates and a Nucleoside by Ring-Opening Fluorination Reaction of Epoxides. *J. Fluor. Chem.* **2006**, *127*, 920–923.

98. Soueidan, O.-M.; Trayner, B. J.; Grant, T. N.; Henderson, J. R.; Wuest, F.; West, F. G.; Cheeseman, C. I. New Fluorinated Fructose Analogs as Selective Probes of the Hexose Transporter Protein GLUT5. *Org. Biomol. Chem.* **2015**, *13*, 6511–6521.

99. L'Heureux, A.; Beaulieu, F.; Bennettl, C.; Bill, D. R.; Clayton, S.; LaFlamme, M. M.; Tadayon, S.; Tovell, D.; Couturier, M. Aminodifluorosulfinium Salts: Selective Fluorination Reagents with Enhanced Thermal Stability and Ease of Handling. *J. Org. Chem.* **2010**, *75*, 3401–3411.

100. Ni, C.; Hu, M.; Hu, J. Good Partnership between Sulfur and Fluorine: Sulfur-Based Fluorination and Fluoroalkylation Reagents for Organic Synthesis. *Chem. Rev.* **2015**, *115*, 765–825.

101. Clark, A. E.; Holman, G. D. Exofacial Photolabelling of the Human Erythrocyte Glucose Transporter with an Azitrifluoroethylbenzoyl-Substituted Bismannose. *Biochem. J.* **1990**, *269*, 615–622.

102. Koumanov, F.; YANG, J.; JONES, E. A.; Hatanaka, Y.; Holman, G. D. Cell-Surface Biotinylation of GLUT4 Using Bis-Mannose Photolabels. *Biochem. J.* **1998**, *330*, 1209–1215.

103. Hashimoto, M.; Hatanaka, Y.; Yang, J.; Dhesi, J.; Holman, G. D. Synthesis of Biotinylated Bis(D-Glucose) Derivatives for Glucose Transporter Photoaffinity Labelling. *Carbohydr. Res* **2001**, *331*, 119–127.

104. Zou, C.; Wang, Y.; Shen., Z. 2-NBDG as a Fluorescent Indicator for Direct Glucose Uptake Measurement. *ChemBioChem,* **2005**, *64*, 207–215.

105. Levi, J.; Cheng, Z.; Gheysens, O.; Patel, M.; Chan, C. T.; Wang, Y. B.; Namavari, M.; Gambhir, S. S. Fluorescent Fructose Derivatives for Imaging Breast Cancer Cells. *Bioconj. Chem.* **2007**, *18*, 628–634.

106. Tanasova, M.; Plutschack, M.; Muroski, M. E.; Sturla, S. J.; Strouse, G. F.; McQuade, D. T. Fluorescent THF-based Fructose Analogue Exhibits Fructose-dependent Uptake. *ChemBioChem* **2013**, *14*, 1263–1270.

107. Soueidan, O.-M.; Scully, T. W.; Kaur, J.; Panigrahi, R.; Belovodskiy, A.; Do, V.; Matier, C. D.; Lemieux, M. J.; Wuest, F.; Cheeseman, C.; West, F. G. Fluorescent Hexose Conjugates Establish Stringent Stereochemical Requirement by Glut5 for Recognition and Transport of Monosaccharides. *ACS Chem. Biol.* **2017**, *12*, 1087–1094.

108. Begoyan, V. V.; Weseliński, Ł. J.; Xia, S.; Fedie, J.; Kannan, S.; Ferrier, A.; Rao, S.; Tanasova, M. Multicolor GLUT5-Permeable Fluorescent Probes for Fructose Transport Analysis. *Chem. Comm.* **2018**, *54*, 3855–3858.

109. Ido, T.; Wan, C. N.; Casella, V.; Fowler, J. S.; Wolf, A. P.; Reivich, M.; Kuhl, D. E. Labeled 2-deoxy-D-glucose Analogs. 18F-labeled 2-deoxy-2-fluoro-D-glucose, 2-deoxy-2-fluoro-D-mannose and 14C-2-deoxy-2-fluoro-D-glucose. *J. Label. Compd. Radiopharm.* **1978**, *14*, 175–183.

110. Tanasova, M.; Fedie, J. R. Molecular Tools for Facilitative Carbohydrate Transporters (Gluts). *ChemBioChem* **2017**, *18*, 1774–1788.

111. Kim, J.; Lee, J.; Chang, E.; Kim, S.; Suh, K.; Sul, J.; Song, I.; Kim, Y.; Lee, C. Selective Sentinel Node plus Additional Non-Sentinel Node Biopsy Based on an FDG-PET/CT Scan in Early Breast Cancer Patients: Single Institutional Experience. *World J. Surg.* **2009**, *33*, 943–949.

112. Haradahira, T.; Tanaka, A.; Maeda, M.; Kanazawa, Y.; Ichiya, Y. I.; Masuda, K. Radiosynthesis, Rodent Biodistribution, and Metabolism of 1-Deoxy-1-[18F] Fluoro-D-Fructose. *Nucl. Med. Biol.* **1995**, *22*, 719–725.

113. Wuest, M.; Trayner, B. J.; Grant, T. N.; Jans, H. S.; Mercer, J. R.; Murray, D.; West, F. G.; McEwan, A. J.; Wuest, F.; Cheeseman, C. I. Radiopharmacological Evaluation of 6-Deoxy-6-[18F] Fluoro-D-Fructose as a Radiotracer for PET Imaging of GLUT5 in Breast Cancer. *Nucl. Med. Biol.* **2011**, *38*, 461–475.

114. Niu, B.; Wen, X.; Jia, Z.; Wu, X.; Guo, W.; Sun, H. Synthesis and Preliminary Evaluation of 1-[18F] Fluoro-1-deoxy-2, 5-anhydro-D-mannitol as a PET Radiotracer for Breast Cancer Imaging. *Chin. J. Chem.* **2013**, *3*, 1159–1163.

115. Calvaresi, E. C.; Hergenrother, P. J. Glucose Conjugation for the Specific Targeting and Treatment of Cancer. *Chem. Sci.* **2013**, *4*, 2319–2333.

116. Tanaka, M.; Kataoka, H.; Yano, S.; Ohi, H.; Kawamoto, K.; Shibahara, T.; Mizoshita, T.; Mori, Y.; Tanida, S.; Kamiya, T.; Joh, T. Anti-Cancer Effects of Newly Developed Chemotherapeutic Agent, Glycoconjugated Palladium (II) Complex, against Cisplatin-Resistant Gastric Cancer Cells. *BMC Cancer* **2013**, *13*, 1–9.

117. Patra, M.; Awuah, S. G.; Lippard, S. J. Chemical Approach to Positional Isomers of Glucose–Platinum Conjugates Reveals Specific Cancer Targeting through Glucose-Transporter-Mediated Uptake in Vitro and in Vivo. *J. Am. Chem. Soc.* **2016**, *138*, 12541–12551.

118. Yang, K.; Gao, T.; Bao, Z.; Su, J.; Chen, X. Preparation and Characterization of a Novel Thermosensitive Nanoparticle for Drug Delivery in Combined Hyperthermia and Chemotherapy. *J. Mater. Chem. B* **2013**, *1*, 6442–6448.

119. Li, J.; Ma, F. K.; Dang, Q. F.; Liang, X. G.; Chen, X. G. Glucose-Conjugated Chitosan Nanoparticles for Targeted Drug Delivery and Their Specific Interaction with Tumor Cells. *Front. Mater. Sci.* **2014**, *8*, 363–372.

120. Raffaghello, L.; Lee, C.; Safdie, F. M.; Wei, M.; Madia, F.; Bianchi, G.; Longo, V. D. From the Cover: Reactive Oxygen Species Special Feature: Starvation-Dependent Differential Stress Resistance Protects Normal but Not Cancer Cells against High-Dose Chemotherapy. *Proc. Natl. Acad. Sci. U. S. A.* **2008**, *105*, 8215.

121. Barnett, J. E.; Holman, G. D.; Chalkley, R. A.; Munday, K. A. Evidence for Two Asymmetric Conformational States in the Human Erythrocyte Sugar-Transport System. *Biochem. J.* **1975**, *145*, 417–429.

122. Pinkofsky, H. B.; Rampal, A. L.; Cowden, M. A.; Jung, C. Y. Cytochalasin B Binding Proteins in Human Erythrocyte Membranes. Modulation of Glucose Sensitivity by Site Interaction and Partial Solubilization of Binding Activities. *J. Biol. Chem.* **1978**, *253*, 4930–4937.

123. Kapoor, K.; Finer-Moore, J. S.; Pedersen, B. P.; Caboni, L.; Waight, A.; Hillig, R. C.; Bringmann, P.; Heisler, I.; Müller, T.; Siebeneicher, H.; Stroud, R. M. Mechanism of Inhibition of Human Glucose Transporter GLUT1 Is Conserved between Cytochalasin B and Phenylalanine Amides. *Proc. Natl. Acad. Sci.* **2016**, *113*, 4711–4716.

124. Strobel, P.; Allard, C.; Perez-Acle, T.; Calderon, R.; Aldunate, R.; Leighton, F. Myricetin, Quercetin and Catechin-Gallate Inhibit Glucose Uptake in Isolated Rat Adipocytes. *Biochem. J.* **2005**, *386*, 471–478.

125. Nomura, M.; Takahashi, T.; Nagata, N.; Tsutsumi, K.; Kobayashi, S.; Akiba, T.; Yokogawa, K.; Moritani, S.; Miyamoto, K. I. Inhibitory Mechanisms of Flavonoids on Insulin-Stimulated Glucose Uptake in MC3T3-G2/PA6 Adipose Cells. *Biol. Pharm. Bull.* **2008**, *31*, 1403–1409.

126. Pérez, A.; Ojeda, P.; Ojeda, L.; Salas, M.; Rivas, C. I.; Vera, J. C.; Reyes, A. M. Hexose Transporter GLUT1 Harbors Several Distinct Regulatory Binding Sites for Flavones and Tyrphostins. *Biochemistry* **2011**, *50*, 8834–8845.

127. Siebeneicher, H.; Cleve, A.; Rehwinkel, H.; Neuhaus, R.; Heisler, I.; Müller, T.; Bauser, M.; Buchmann, B. Identification and Optimization of the First Highly Selective GLUT1 Inhibitor BAY-876. *ChemMedChem* **2016**, *11*, 2261–2271.

128. Ung, P. M. U.; Song, W.; Cheng, L.; Zhao, X.; Hu, H.; Chen, L.; Schlessinger. Inhibitor Discovery for the Human GLUT1 from Homology Modeling and Virtual Screening. *ACS Chem. Biol.* **2016**, *11*, 1908–1916.

129. George Thompson, A. M.; Ursu, O.; Babkin, P.; Iancu, C. V.; Whang, A.; Oprea, T. I.; Choe, J. Y. Discovery of a Specific Inhibitor of Human GLUT5 by Virtual Screening and in Vitro Transport Evaluation. *Sci. Rep.* **2016**, *6*, 1–9.

Chapter 2

1. Lin, L.; Yee, S. W.; Kim, R. B.; Giacomini, K. M. SLC transporters as therapeutic targets: emerging opportunities. *Nat. Rev. Drug Discov.* **2015***, 14*, 543–560.

2. Colas, C.; Ung P. M.; Schlessinger, A. SLC transporters: structure, function, and drug discovery. *Med. Chem. Comm.* **2016**, *7*, 1069–1081.

3. Kotsampasakou, E.; Ecker, G. F.; Sitte, H. H.; Mannhold, R.; Buschmann, H.; Clausen, R. P.; Transporters as Drug Targets. Eds **2017**, 271-324.

4. Marger, M. D.; Saier Jr, M. H. A major superfamily of transmembrane facilitators that catalyse uniport, symport and antiport. *Trends Biochem. Sci.* **1993**, *18*, 13–20.

5. Manolescu, A. R.; Witkowska, K.; Kinnaird, A.; Cessford, T.; Cheeseman, C. Facilitated hexose transporters: new perspectives on form and function. *Physiology* **2007**, *22*, 234–240.

6. García-Álvarez, I.; Garrido, L.; Fernández-Mayoralas, A. Studies on the uptake of glucose derivatives by red blood cells. *ChemMedChem* **2007**, *2*, 496–504.

7. McQuade, D. T.; Plutschack, M. B.; Seeberger, P. H. Passive fructose transporters in disease: a molecular overview of their structural specificity. *Org. Biomol. Chem.* **2013**, *11*, 4909–4920.

8. Mueckler, M.; Thorens, B. The SLC2 (GLUT) family of membrane transporters. *Mol. Aspects Med.* **2013***, 34,* 121–138.

9. Tappy, L.; Lê, K. A. Metabolic effects of fructose and the worldwide increase in obesity. *Physiol. Rev.* **2010***, 90,* 23–46.

10. Gaby, A. R. Adverse effects of dietary fructose. *Altern. Med. Rev.* **2005**, *10*, 294-306.

11. Camps, M.; Castelló, A.; Muñoz, P.; Monfar, M.; Testar, X.; Palacín, M.; Zorzano, A. Effect of diabetes and fasting on GLUT-4 (muscle/fat) glucose-transporter expression in insulin-sensitive tissues. Heterogeneous response in heart, red and white

muscle. *Biochem. J.* **1992***, 282*, 765–772.

12. Medina, R. A.; Owen, G. I. Glucose transporters: expression, regulation, and cancer. *Biol. Res.* **2002***, 35*, 9–26.

13. Adekola, K.; Rosen, S. T.; Shanmugam, M. Glucose transporters in cancer metabolism. *Curr. Opin. Oncol.* **2012**, *24*, 650–654.

14. Kostakoglu, L.; Agress Jr. H.; Goldsmith, S. J. Clinical role of FDG PET in evaluation of cancer patients. *RadioGraphics* **2003,** *23*, 315–340.

15. Joost, H. G.; Bell, G. I.; Best, J. D.; Birnbaum, M. J.; Charron, M. J.; Chen, Y. T.; Doege, H.; James, D. E.; Lodish, H. F.; Moley, K. H.; Moley, J. F.; Mueckler, M.; Rogers, S.; Schürmann, A.; Seino, S.; Thorens, B. Nomenclature of the GLUT/SLC2A family of sugar/polyol transport facilitators. *Am. J. Physiol. Metab.* **2002**, *282*, E974–E976.

16. Fan, X.; Liu, H.; Liu, M.; Wang, Y.; Qiu, L.; Cui, Y. Increased utilization of fructose has a positive effect on the development of breast cancer. *PeerJ.* **2007**, *5*, e3804.

17. Douard, V.; Ferraris RP. Regulation of the fructose transporter GLUT5 in health and disease. *Am. J. Physiol. Endocrinol. Metab.* **2008**, *238*, E227-E237; original literature: Kane, S.; Seatter, M. J.; Gould, G. W. Functional studies of human GLUT5:effect of pH on substrate selection and an analysis of substrate interactions. *Biochem. Biophys. Res. Commun.* **1997***, 238*, 503-505; Mate, A.; Barfull, A.; Hermosa, A. M.; Planas, J. M.; Vazquez, C. M. Regulation of D-fructose transporter GLUT5 in the ileum of spontaneously hypertensive rats. *J. Membr. Biol.* 199 (2004), 173-179; Gorovits, N.; Charron, M. J; What we know about facilitative glucose transporters: lessons from cultured cells, animal models, and human studies. *Biochem. Mol. Biol. Educ.* **2008**, *31*, 163-172.

18. Chen, W. L.; Wang, Y. Y.; Zhao, A.; Xia, L.; Xie, G.; Su, M.; Zhao, L.; Liu, J.; Qu, C.; Wei, R.; Rajani, C.; Ni, Y.; Cheng, Z.; Chen, Z.; Chen, S.; Jia, W. Enhanced fructose utilization mediated by SLC2A5 is a unique metabolic feature of acute myeloid leukemia with therapeutic potential. *Cancer Cell* **2016***, 30*, 779–791.

19. Weng, Y.; Zhu, J.; Chen, Z.; Fu, J.; Zhang, F. Fructose fuels lung adenocarcinoma

through GLUT5. *Cell Death Dis.* **2018***, 9*, 1-4.

20. Villaamil, V. M.; Gallego, G. A.; Rubira, L. V.; Campelo, R. G.; Valladares-Ayersbes, M.; Pulido, E. G.; Bolós, M. V.; Caínzos, I. S.; Aparicio, L. M. A. Fructose transporter GLUT5 expression in clear renal cell carcinoma. *Oncol. Rep.* **2011**, *25*, 315–323.

21. Zamora-León, S. P.; Golde, D. W.; Concha, I. I.; Rivas, C. I.; Delgado-López, F.; Baselga, J.; Nualart, F.; Vera, J. C. Expression of the fructose transporter GLUT5 in human breast cancer. *Proc. Natl. Acad. Sci.* **1996**, *93*, 1847–1852.

22. Hamann, I.; Krys, D.; Glubrecht, D.; Bouvet, V.; Marshall, A.; Vos, L.; Mackey, J. R.; Wuest, M.; Wuest, F.; Expression and function of hexose transporters GLUT1, GLUT2, and GLUT5 in breast cancer—effects of hypoxia. *FASEB J.* **2018**, *32*, 5104-5118.

23. Nomura, N.; Verdon, G.; Kang, H. J.; Shimamura, T.; Nomura, Y.; Sonoda, Y.; Hussien, S. A.; Qureshi, A. A.; Coincon, M.; Sato, Y.; Abe, H.; Nakada-Nakura, Y.; Hino, T.; Arakawa, T.; Kusano-Arai, O.; Iwanari, H.; Murata, T.; Kobayashi, T.; Hamakubo, T.; Kasahara, M.; Iwata, S.; Drew, D. Structure and mechanism of the mammalian fructose transporter GLUT5. *Nature* **2015***, 526,* 397–401.

24. Review literature: Tanasova, M.; Fedie, JR. Molecular tools for facilitative carbohydrate transporters (Gluts). *Chembiochem* **2017**, *18*, 1774-1788; original literature: Girniene, J.; Tatibouët, A.; Sackus, A.; Yang, J.; Holman, G. D.; Rollin, P. Inhibition of the D-fructose transporter protein GLUT5 by fused-ring glyco-1, 3-oxazolidin-2-thiones and-oxazolidin-2-ones. *Carbohydr. Res.* **2003**, *338*, 711-719.

25. Barnett, J. E. G.; Holman, G. D.; Munday, K. A. Structural requirements for binding to the sugar-transport system of the human erythrocyte. *Biochem. J.* **1973***, 131*, 211–221.

26. Barnett, J. E.; Holman, G. D.; Chalkley, R. A.; Munday, K. A. Evidence for two asymmetric conformational states in the human erythrocyte sugar-transport system. *Biochem. J.* **1975***, 145*, 417–429.

27. Rees, W. D.; Holman, G. D. Hydrogen bonding requirements for the insulin-sensitive sugar transport system of rat adipocytes. *Biochim. Biophys. Acta- Biomembr.*

1981*, 646*, 251–260.

28. Holman, G. D.; Rees, W. D. Side-specific analogues for the rat adipocyte sugar transport system. *Biochim. Biophys. Acta - Biomembr.* **1982,** *685*, 78–86.

29. Holman, G. D.; Midgley, P. J. W. Synthesis of novel bis (d-mannose) compounds. *Carbohydr. Res.* **1985**, *135*, 337–341.

30. Abbadi, M.; Holman, G. D.; Morin, C.; Rees, W. D.; Yang, J. Synthesis of symmetrical 4, 4′-and 6, 6′-bis (d-glucose)-based probes as tools for the study of d-glucose transport proteins. *Tetrahedron Lett.* **1999,** *40*, 5861–5864.

31. Bouvet, V.; Jans, H. S.; Wuest, M.; Soueidan, O. M.; Mercer, J.; McEwan, A. J. B.; West, F. G.; Cheeseman, C. I.; Wuest, F. Automated synthesis and dosimetry of 6-deoxy-6-[18F] fluoro-D-fructose (6-[18F] FDF): a radiotracer for imaging of GLUT5 in breast cancer. *Am. J. Nucl. Med. Mol. Imaging* **2014***, 4,* 248–259.

32. Soueidan, O. M.; Scully, T. W.; Kaur, J.; Panigrahi, R.; Belovodskiy, A.; Do, V.; Matier, C. D.; Lemieux, M. J.; Wuest, F.; Cheeseman, C. I.; West, F. G. Fluorescent hexose conjugates establish stringent stereochemical requirement by glut5 for recognition and transport of monosaccharides. *ACS Chem. Biol.* **2017***, 12*, **1**087–1094.

33. Wuest, M.; Hamann, I.; Bouvet, V.; Glubrecht, D.; Marshall, A.; Trayner, B.; Soueidan, O. M.; Krys, D.; Wagner, M.; Cheeseman, C.; West, F.; Wuest, F. Molecular imaging of GLUT1 and GLUT5 in breast cancer: a multitracer positron emission tomography imaging study in mice. *Mol. Pharmacol.* **2018**, *93*, 79-89.

34. Tatibouët, A.; Yang, J.; Morin, C.; Holman, G. D. Synthesis, and evaluation of fructose analogues as inhibitors of the D-fructose transporter GLUT5. *Bioorg. Med. Chem.* **2000**, *8*, 1825-1833.

35. Inukai, K.; Katagiri, H.; Takata, K.; Asano, T.; Anai, M.; Ishihara, H.; Nakazaki, M.; Kikuchi, M.; Yazaki, Y.; Oka, Y. Characterization of rat GLUT5 and functional analysis of chimeric proteins of GLUT1 glucose transporter and GLUT5 fructose transporter. *Endocrinology* **1995**, *136*, 4850-4857.

36. Soueidan, O. M.; Trayner, B. J.; Grant, T. N.; Henderson, J. R.; Wuest, F.; West, F. G.; Cheeseman, C. I. New fluorinated fructose analogs as selective probes of the hexose transporter protein GLUT5. *Org. Biomol. Chem.* **2015***, 13*, 6511-6521.

37. Tanasova, M.; Plutschack, M.; Muroski, M. E.; Sturla, S. J.; Strouse, G. F.; McQuade, D. T. Fluorescent THF-based fructose analogue exhibits fructose-dependent uptake. *ChemBioChem.* **2013***, 14,* 1263–1270.

38. Kumar Kondapi, V. P.; Soueidan, O. M.; Cheeseman, C. I.; West, F. G. Tunable GLUT–Hexose Binding and Transport via Modulation of Hexose C-3 Hydrogen-Bonding Capabilities. *Chem. Eur. J.* **2017***, 23,* 8073–8081.

39. For an alternative strategy relying on C-1 modification of 2,5-AM with fluorophores, see: Begoyan, V. V.; Weseliński, Ł. J.; Xia, S.; Fedie, J.; Kannan, S.; Ferrier, A.; Rao, S.; Tanasova, M. Multicolor GLUT5-permeable fluorescent probes for fructose transport analysis. *Chem Commun* **2018**, *54*, 3855-3858.

40. Kumar Kondapi, V. P.; Soueidan, O. M.; Hosseini, S. N.; Jabari, N.; West, F. G. Efficient and Easy Access to Optically Pure Tetrasubstituted Tetrahydrofurans via Stereoselective Opening of C2-Symmetric Epoxide and Aziridine Rings. *Eur. J. Org. Chem.* **2016**, *7*, 1367–1379.

41. Tang, F.; Yang, Y.; Tang, Y.; Tang, S.; Yang, L.; Sun, B.; Jiang, B.; Dong, J.; Liu, H.; Huang, M.; Geng, M.Y.; Huang, W. One-pot N-glycosylation remodeling of IgG with non-natural sialylglycopeptides enables glycosite-specific and dual-payload antibody–drug conjugates. *Org. Biomol. Chem.* **2016***, 14*, 9501–9518.

42. Trayner, B. J.; Grant, T. N.; West, F. G.; Cheeseman, C. I. Synthesis and characterization of 6-deoxy-6-fluoro-D-fructose as a potential compound for imaging breast cancer with PET. *Bioorg. Med. Chem.* **2009**, *17*, 5488-5495.

43. Wuest, M.; Trayner, B. J.; Grant, T. N.; Jans, H. S.; Mercer, J. R.; Murray, D.; West, F. G.; McEwan, A. J. B.; Wuest, F.; Cheeseman, C. I. Radiopharmacological evaluation of 6-deoxy-6-[18F] fluoro-D-fructose as a radiotracer for PET imaging of GLUT5 in breast cancer. *Nucl. Med. Biol.* **2011**, *38*, 461-475.

44. Thompson, A. M. G.; Iancu, C. V.; Nguyen, T. T. H.; Kim, D.; Choe, J. Y. Inhibition of human GLUT1 and GLUT5 by plant carbohydrate products; insights into transport specificity. *Sci Rep.* **2015**, *5*, 1-10.

45. George Thompson, A. M.; Ursu, O.; Babkin, P.; Iancu, C. V.; Whang, A.; Oprea, T. I.; Choe, J. Y. Discovery of a specific inhibitor of human GLUT5 by virtual

screening and in vitro transport evaluation. *Sci. Rep.* **2016**, *6*, 24240.

46. a) Ainsley, J.; Chaturvedi, S. S.; Karabencheva-Christova, T. G.; Tanasova, M.; Christov,C. Z. Integrating molecular probes and molecular dynamics to reveal binding modes of GLUT5 activatory and inhibitory ligands. *Chem Commun* 54 (2018), 9917-9920. b) Ferreira, R. S.; Pons, J.-L.; Labesse, G. Insights into Substrate and Inhibitor Selectivity among Human GLUT Transporters through Comparative Modeling and Molecular Docking, *ACS Omega*, **2019**, *4*, 4748-4760.

47. Tian, C.; Kasavajhala, K.; Belfon, K. A. A.; Raguette, L.; Huang, H.; Migues, A. N.; Bickel, J.; Wang, Y.; Pincay, J.; Wu, Q.; Simmerling, C. ff19SB: Amino-acid-specific protein backbone parameters trained against quantum mechanics energy surfaces in solution. *J. Chem. Theory Comput.* **2019,** *16*, 528-552.

48. Wang, J.; Wang, W.; Kollman, P. A.; Case, D. A. Automatic atom type and bond type perception in molecular mechanical calculations.*J. Mol. Graph. Model.* **2006***,* 25, 247-260.

49. Bai, Q.; Zhang, Y.; Li, X.; Chen, W.; Liu, H.; Yao, X. Computational study on the interaction between CCR5 and HIV-1 entry inhibitor maraviroc: insight from accelerated molecular dynamics simulation and free energy calculation. *Phys. Chem. Chem. Phys.* 16 (2014), 24332-24338.

50. Genheden, S.; Ryde, U. The MM/PBSA and MM/GBSA methods to estimate ligand-binding affinities. *Expert Opin. Drug. Discov.* **2015,** *10*, 449-461.

51. Miller, B. R.; McGee, T. D.; Swails, J. M.; Homeyer, N.; Gohlke, H.; Roitberg, A.E. MMPBSA. py: an efficient program for end-state free energy calculations. *J. Chem. Theory Comput.* **2012**, *8*, 3314-3321.

52. Horton, D.; Philips, K. D. The nitrous acid deamination of glycosides and acetates of 2-amino-2-deoxy-D-glucose. *Carbohydr. Res.* **1973**, *30*, 367–374.

53. Brennauer, A. Acylguanidines as bioisosteric groups in argininamide-type neuropeptide Y Y1 and Y2 receptor antagonists: synthesis, stability and pharmacological activity (Doctoral dissertation) **2006**.

54. Tang, F.; Yang, Y.; Tang, Y.; Tang, S.; Yang, L.; Sun, B.; Jiang, B.; Dong, J.; Liu, H.; Huang, M.; Geng, M. Y.; Huang, W. One-pot N-glycosylation remodeling of IgG

with non-natural sialylglycopeptides enables glycosite-specific and dual-payload antibody–drug conjugates. *Org. Biomol. Chem.* **2016**, *14*, 9501–9518.

55. Gnaccarini, C.; Ben-Tahar, W.; Mulani, A.; Roy, I.; Lubell, W. D.; Pelletier, J. N.; Keillor, J. W. Site-specific protein propargylation using tissue transglutaminase. *Org. Biomol. Chem.* **2012**, *10*, 5258–5265.

56. Shiota, S.; Yamamoto, S.; Shimomura, A.; Ojida, A.; Nishino, T.; Maruyama, T. Quantification of amino groups on solid surfaces using cleavable fluorescent compounds. *Langmuir* **2015**, *31*, 8824–8829.

57. Neumann, K. T.; Lindhardt, A. T.; Bang-Andersen, B.; Skrydstrup, T. *J. Label. Compd.* Synthesis and selective 2H-, 13C-, and 15N-labeling of the Tau protein binder THK-523. *Radiopharm.* **2017**, *60*, 30–35.

58. Halgren, T. A.; Murphy, R. B.; Friesner, R. A.; Beard, H. S.; Frye, L. L.; Pollard, W. T.; Banks, J. L. Glide: a new approach for rapid, accurate docking and scoring. 2.Enrichment factors in database screening. *J. Med. Chem.* 2004, 47, 1750-1759.

59. Jo, S.; Kim, T.; Iyer, V. G.; Im, W. CHARMM-GUI: a web-based graphical user interface for CHARMM. *J. Comput. Chem.* **2008**, *29*, 1859-1865.

60. Roe, D. R.; Cheatham III, T. E. PTRAJ and CPPTRAJ: software for processing and analysis of molecular dynamics trajectory data. *J. Chem. Theory Comput*. **2013**, *9*, 3084-3095.

61. Humphrey, W.; Dalke, A.; Schulten, K. VMD: visual molecular dynamics. *J. Mol. Graph.* **1996**, *14*, 27-38.

Chapter 3

1. Siegel, R. L.; Miller, K. D.; Jemal, A. Cancer Statistics 2017. *CA Cancer J. Clin.* **2017**, *67*, 7–30.

2. DeSantis, C.; Siegel, R.; Bandi, P.; Jemal, A. Breast Cancer Statistics, 2011. *CA Cancer J. Clin.* **2011**, *61*, 409–418.

3. Jameson, J. L.; Longo, D. L. Precision Medicine--Personalized, Problematic, and Promising. *N. Engl. J. Med.* **2015**, *372*, 2229–2234.

4. Buist, D. S.; Porter, P. L.; Lehman, C.; Taplin, S. H.; White, E. Factors Contributing to Mammography Failure in Women Aged 40-49 Years. *J. Natl. Cancer Inst.* **2004**, *96*, 1432–1440.

5. Berlin, L. The Missed Breast Cancer Redux: Time for Educating the Public about the Limitations of Mammography? *AJR Am. J. Roentgenol.* **2001**, *176*, 1131–1134.

6. Koomen, M.; Pissano, E. D.; Kuzmiak, C.; Pavic, D.; McLelland, R. Future Directions in Breast Imaging. *J. Clin. Oncol.* **2005**, *23*, 1674–1677.

7. Lehman, C. D.; Schnall, M. D. Imaging in Breast Cancer: Magnetic Resonance Imaging. *Breast Cancer Res.* **2005**, *7*, 215–219.

8. Benard, F.; Turcotte, E. Imaging in Breast Cancer: Single-Photon Emission Computed Tomography and Positron Emission Tomography. *Breast Cancer Res.* **2005**, *7*, 153–162.

9. Jadvar, H.; Alavi, A.; Gambhir, S. S. 18F-FDG Uptake in Lung, Breast, and Colon Cancers: Molecular Biology Correlates and Disease Characterization. *J. Nucl. Med.* **2009**, *50*, 182–1827.

10. Buerkle, A.; Weber, W. A. Imaging of Tumor Glucose Utilization with Positron Emission Tomography. *Cancer Metastasis Rev.* **2008**, *27*, 545–554.

11. Levi, J.; Cheng, Z.; Gheysens, O.; Patel, M.; Chan, C. T.; Wang, Y. B.; Namavari, M.; Gambhir, S. S. Fluorescent Fructose Derivatives for Imaging Breast Cancer Cells. *Bioconj. Chem.* **2007**, *18*, 628–634.

12. Flier, J. S.; Mueckler, M. M.; Usher, P.; Lodish, H. F. Elevated Levels of Glucose Transport and Transporter Messenger RNA Are Induced by Ras or Src Oncogenes. *Science* **1985**, *235*, 1492–1495.

13.Yamamoto, T.; Seino, Y.; Fukumoto, H.; Koh, G.; Yano, H.; Inagaki, N.; Yamada, Y.; Inoue, K.; Manabe, T.; Imura, H. Over-Expression of Facilitative Glucose Transporter Genes in Human Cancer. *Biophys. Res. Commun.* **1990**, *170*, 223–230. Barbosa, A,M.; Martel, F. Targeting Glucose Transporters for Breast Cancer Therapy: The Effect of Natural and Synthetic Compounds. *Cancers (Basel)* **2020**, *12*, 154

14. Younes, M.; Lechago, L. V. .; Somoano, J. R.; Mosharaf, M.; Lechago, J. Wide Expression of the Human Erythrocyte Glucose Transporter Glut1 in Human Cancers. *Cancer Res. 56* (1996), 1164–1167.

15. Medina, R. A.; Owen, G. I. Glucose Transporters: Expression, Regulation and Cancer. *Biol. Res.* **2002**, *35*, 9–26.

16. Ak, I.; Stokkel, M. P.; Pauwels, E. K. Positron Emission Tomography with 2-[18F]Fluoro-2-Deoxy-D-Glucose in Oncology. Part II. The Clinical Value in Detecting and Staging Primary Tumours. *J. Cancer Res. Clin. Oncol.* **2000**, *126*, 560–574.

17. Weir, L.; Worsley, D.; Bernstein, V. The Value of FDG Positron Emission Tomography in the Management of Patients with Breast Cancer. *Breast J.* **2005**, *11*, 204–209.

18. Santiago, J. F.; Gonen, M.; Yeung, H.; Macapinlac, H.; Larson, S. A. A Retrospective Analysis of the Impact of 18F-FDG PET Scans on Clinical Management of 133 Breast Cancer Patients. *Q J. Nucl. Med. Mol. Imaging* **2006**, *50*, 61–67.

19. Mavi, A.; Urhan, M.; Jian, Q. Y.; Zhuang, H.; Houseni, M.; Cermik, T. F.; Thiruvenkatasamy, D.; Czerniecki, B.; Schnall, M.; Alavi, A. Dual Time Point 18F-FDG PET Imaging Detects Breast Cancer with High Sensitivity and Correlates Well with Histologic Subtypes. *J. Nucl. Med.* **2006**, *47*, 1440–1446.

20. Sundararajan, L.; Linden, H. M.; Link, J. M.; Krohn, K. A.; Mankoff, D. A. 18F-Fluoroestradiol. *Semin. Nucl. Med.* **2007**, *37*, 470–476.

21. Buck, A. K.; Schirrmeister, H.; Mattfeldt, T.; Reske, S. N. Biological Characterisation of Breast Cancer by Means of PET. *Eur J. Nucl. Med. Mol. Imaging* **2004**, *31(Suppl 1)*, S80–S87.

22. Alavi, A.; Zhuang, H. Finding Infection-Help from PET. *Lancet* **2001**, *358*, 1386.

23. Schirmer, M.; Calamia, K. T.; Wenger, M.; Klauser, A.; Salvarani, C.; Moncayo, R. 18F-Fluorodeoxyglucose-Positron Emission Tomography: A New Explorative Perspective. *Exp. Gerontol.* **2003**, *38*, 463–470.

24. Kubota, R.; Kubota, K.; Yamada, S.; Tada, M.; Ido, T.; Tamahashi, N. Microautoradiographic Study for the Differentiation of Intratumoral Macrophages,

Granulation Tissues and Cancer Cells by the Dynamics of Fluorine-18-Fluorodeoxyglucose Uptake. *J. Nucl. Med.* **1994**, *35*, 102–112.

25. Younes, M.; Brown, R. W.; Mody, D. R.; Fernandez, L.; Laucirica, R. GLUT1 Expression in Human Breast Carcinoma: Correlation with Known Prognostic Markers. *Anticancer. Res.* **1995**, *15*, 2895–2898.

26. Ravazoula, P.; Batistatou, A.; Aletra, C.; Ladopoulos, J.; Kourounis, G.; Tzigounis B. Immunohistochemical Expression of Glucose Transporter Glut1 and Cyclin D1 in Breast Carcinomas with Negative Lymph Nodes. *Eur. J. Gynaecol. Oncol.* **2003**, *24*, 544–546.

27. Kuo, S. J.; Wu, Y. C.; Chen, C. P.; Tseng, H. S.; Chen, D. R. Expression of Glucose Transporter-1 in Taiwanese Patients with Breast Carcinoma — a Preliminary Report. *Kaohsiung J. Med. Sci.* **2006**, *22*, 339–345.

28. Wuest, M.; Hamann, I.; Bouvet, V.; Glubrecht, D.; Marshall, A.; Trayner, B. J.; Soueidan, O.-M.; Krys, D.; Wagner, M.; Cheeseman, C. I.; West, F. G.; Wuest, F. Molecular Imaging of GLUT1 and GLUT5 in Breast Cancer: A Multitracer PET Imaging Study in Mice. *Mol. Pharmacol.* **2018**, *93*, 79–89. Mankoff D.A.; Eubank W.B. Current and future use of positron emission tomography (PET) in breast cancer. J. Mammary Gland. Biol. Neoplasia. 2006, *11*, 125-36.

29. Henry, K.E.; Ulaner, G.A.; Lewis, J.S. Clinical Potential of Human Epidermal Growth Factor Receptor 2 and Human Epidermal Growth Factor Receptor 3 Imaging in Breast Cancer. *PET Clin.* **2018**, *13*, 423-435; Ulaner, G.A.; Schuster, D.M. Amino Acid Metabolism as a Target for Breast Cancer Imaging. *PET Clin.* **2018**, *13*, 437-444; Fleming, I. N.; Gilbert, F.J.; Miles, K. A.; Cameron, D. Opportunities for PET to deliver clinical benefit in cancer: breast cancer as a paradigm. *Cancer Imag.* 2010, *10,* 144-52; Wibmer, A. G.; Hricak, H.; Ulaner, G. A.; Weber, W. Trends in oncologic hybrid imaging.Eur. J. Hybrid Imaging. **2018**, *2*, 1.

30. Zamora-León, S. P.; Golde, D. W.; Concha, I. I.; Rivas, C. I.; Delgado-López,F.; Baselga, J.; Nualart, F.; Vera, J. C. Expression of the Fructose Transporter GLUT5 in Human Breast Cancer. *Proc. Natl. Acad. Sci. U.S.A.* **1996**, *93*, 1847–1842.

31. Barron, C. C.; Bilan, P. J.; Tsakiridis, T.; Tsiani, E. Facilitative Glucose Transporters: Implications for Cancer Detection, Prognosis and Treatment. *Metabolism* **2016**, *65*, 124–139. Macheda, M. L.; Rogers, S.; Best, J. D. Molecular and Cellular Regulation of Glucose Transporter (GLUT) Proteins in Cancer. *J. Cell Physiol.* **2005**, *202*, 654–662.

32. Godoy, A.; Ulloa, V.; Rodríguez, F.; Reinicke, K.; Yañez, A. J.; García, M. D. L. A.; Medina, R. A.; Carrasco, M.; Barberis, S.; Castro, T.; Martínez, F.; Koch, X.; Vera, J. C.; Poblete, M. T.; Figueroa, C. D.; Peruzzo, B.; Nualart, F. Differential Subcellular Distribution of Glucose Transporters GLUT1-6 and GLUT9 in Human Cancer: Ultrastructural Localization of GLUT1 and GLUT5 in Breast Tumor Tissues. *J. Cell Physiol.* **2005**, *207*, 614–627.

33. Chan, K. K.; Chan, J. Y.; Chung, K. K.; Fung, K. P. Inhibition of Cell Proliferation in Human Breast Tumor Cells by Antisense Oligonucleotides against Facilitative Glucose Transporter. *J. Cell Biochem.* **2004**, *93*, 1134–1142.

34. Wuest, M.; Trayner, B. J.; Grant, T. N.; Jans, H. S.; Mercer, J. R.; Murray, D.; West, F. G.; McEwan, A. J.; Wuest, F.; Cheeseman, C. I. Radiopharmacological Evaluation of 6-Deoxy-6-[18F] Fluoro-D-Fructose as a Radiotracer for PET Imaging of GLUT5 in Breast Cancer. *Nucl. Med. Biol.* **2011**, *38*, 461–475.

35. Manolescu, A. R.; Witkowska, K.; Kinnaird, A.; Cessford, T.; Cheeseman, C. Facilitated Hexose Transporters: New Perspectives on Form and Function. *Physiology* **2007**, *22*, 234–240.

36. Raushel, F. M.; Cleland, W. W. The Substrate and Anomeric Specificity of Fructokinase. *J. Biol. Chem.* **1973**, *248*, 8174.

37. Raushel, F. M.; Cleland, W. W. Bovine Liver Fructokinase: Purification and Kinetic Properties. *Biochemistry* **1977**, *16*, 2169–2175.

38. Chenault, H. K.; Mandes, R. F.; Hornberger, K. R. Synthetic Utility of Yeast Hexokinase. Substrate Specificity, Cofactor Regeneration, and Product Isolation. *J. Org. Chem.* **1977**, *62*, 331–336.

39. Aloj, L.; Caraco, C.; Jagoda, E.; Eckelman, W. C.; Neumann, R. D. Glut-1 and Hexokinase Expression: Relationship with 2-Fluoro-2-Deoxy-D-Glucose Uptake in A431 and T47D Cells in Culture. *Cancer Res.* **1999**, *59*, 4709–4714.

40. Haradahira, T.; Tanaka, A.; Maeda, M.; Kanazawa, Y.; Ichiya, Y. I.; Masuda, K. Radiosynthesis, Rodent Biodistribution, and Metabolism of 1-Deoxy-1-[18F] Fluoro-D-Fructose. *Nucl. Med. Biol.* **1995**, *22*, 719–725.

41. Trayner, B. J.; Grant, T. N.; West, F. G.; Cheeseman, C. I. Synthesis and Characterization of 6-Deoxy-6-Fluoro-D-Fructose as a Potential Compound for Imaging Breast Cancer with PET. *Bioorg. Med. Chem.* **2009**, *17*, 5488–5495.

42. Wester, H. J. *Pharmaceutical Radiochemistry (I)*; Munich Molecular Imaging Handbook Series; *Scintomics*, 1, 2010.

43. Zancan, P.; Sola-Penna, M.; Furtado, C. M.; Da Silva, D. Differential Expression of Phosphofructokinase-1 Isoforms Correlates with the Glycolytic Efficiency of Breast Cancer Cells. *Mol. Genet. Metab.* **2010**, *100*, 372–378.

44. Kim, J.; Kang, J.; Kang, Y. L.; Woo, J.; Kim, Y.; Huh, J.; Park, J. W. Ketohexokinase-A Acts as a Nuclear Protein Kinase That Mediates Fructose-Induced Metastasis in Breast Cancer. *Nat. Comm.* **2020**, *11*, 1–20.

45. Gowrishankar, G.; Zitzmann-Kolbe, S.; Junutula, A.; Reeves, R.; Levi, J.; Srinivasan, A.; Bruus-Jensen, K.; Cyr, J.; Dinkelborg, L.; Gambhir, S. S. GLUT 5 Is Not Over-Expressed in Breast Cancer Cells and Patient Breast Cancer Tissues. *PLoS One* **2011**, *6*, e26902.

46. Kang, H.; Kim, H.; Lee, S.; Youn, H.; Youn, B. Role of Metabolic Reprogramming in Epithelial–Mesenchymal Transition (EMT). *Int. J. Mol. Sci.* **2019**, *20*, 2042.

47. Yoshioka, K.; Takahashi, H.; Homma, T.; Saito, M.; Oh, K. B.; Nemoto, Y.; Matsuoka, H. A Novel Fluorescent Derivative of Glucose Applicable to the Assessment of Glucose Uptake Activity of Escherichia Coli. *Biochim. Biophys. Acta Biomembr.* **1996**, *1289*, 5–9.

48. Yoshioka, K.; Saito, M.; Oh, K. B.; Nemoto, Y.; Matsuoka, H.; Natsume, M.; Abe, H. Intracellular Fate of 2-NBDG, a Fluorescent Probe for Glucose Uptake Activity, in Escherichia Coli Cells. *Biosci. Biotechnol. Biochem.* **1996**, *60*, 1899–1901.

49. Cheng, Z.; Levi, J.; Xiong, Z.; Gheysens, O.; Keren, S.; Chen, X.; Gambhir, S. S. Near-Infrared Fluorescent Deoxyglucose Analogue for Tumor Optical Imaging in Cell Culture and Living Mice. *Bioconj. Chem.* **2006**, *17*, 662–669.

50. Zhang, M.; Zhang, Z.; Blessington, D.; Li, H.; Busch, T. M.; Madrak, V.; Miles, J.; Chance, B.; Glickson, J. D.; Zheng, G. Pyropheophorbide 2-Deoxyglucosamide: A New Photosensitizer Targeting Glucose Transporters. *Bioconj. Chem.* **2003**, *14*, 709–714.

51. Jo, A.; Sung, J.; Lee, S.; Nam, H.; Lee, H. W.; Park, J.; Kim, H. M.; Kim, E.; Park, S. B. Near-IR Fluorescent Tracer for Glucose-Uptake Monitoring in Live Cells. *Bioconj. Chem.* **2018**, *29*, 3394–3401.

52. Yuen, R.; Wagner, M.; Richter, S.; Dufour, J.; Wuest, M.; West, F. G.; Wuest, F. Design, Synthesis, and Evaluation of Positron Emission Tomography/Fluorescence Dual Imaging Probes for Targeting Facilitated Glucose Transporter 1 (GLUT1). *Org. Biomol. Chem.* **2021**, *19*, 3241–3254.

53. Tanasova, M.; Plutschack, M.; Muroski, M. E.; Sturla, S. J.; Strouse, G. F.; McQuade, D. T. Fluorescent THF-based Fructose Analogue Exhibits Fructose-dependent Uptake. *ChemBioChem* **2013**, *14*, 1263–1270.

54. Soueidan, O.-M.; Scully, T. W.; Kaur, J.; Panigrahi, R.; Belovodskiy, A.; Do, V.; Matier, C. D.; Lemieux, M. J.; Wuest, F.; Cheeseman, C.; West, F. G. Fluorescent Hexose Conjugates Establish Stringent Stereochemical Requirement by Glut5 for Recognition and Transport of Monosaccharides. *ACS Chem. Biol.* **2017**, *12*, 1087–1094.

55. Kondapi, V. P. K. .; Soueidan, O.-M.; Cheeseman, C. I.; West, F. G. Tunable GLUT–Hexose Binding and Transport via Modulation of Hexose C-3 Hydrogen-Bonding Capabilities. *Chem. Eur. J.* **2017**, *23*, 8073–8081.

56. Begoyan, V.V.; Weseliński, Ł.J.; Xia, S.; Fedie, J.; Kannan, S.; Ferrier, A.; Rao, S.; Tanasova, M. 2018. Multicolor GLUT5-permeable fluorescent probes for fructose transport analysis. *Chem. Comm.*, **2018,** *54*, 3855-3858.

57. Gnaccarini, C.; Ben-Tahar, W.; Mulani, A.; Roy, I.; Lubell, W. D.; Pelletier, J. N.; Keillor, J. W. Site-specific protein propargylation using tissue transglutaminase. *Org.*

Biomol. Chem. **2012**, *10*, 5258–5265.

58. Shiota, S.; Yamamoto, S.; Shimomura, A.; Ojida, A.; Nishino, T.; Maruyama, T. Quantification of amino groups on solid surfaces using cleavable fluorescent compounds. *Langmuir* **2015**, *31*, 8824–8829.

Chapter 4

1. Dashty, M. A quick look at biochemistry: Carbohydrate metabolism. *Clin. Biochem.* **2013**, *46*, 1339–1352.

2. Navale, A. M.; Paranjape, A. N. Glucose transporters: physiological and pathological roles. *Biophys. Rev.* **2016**, *8*, 5–9.

3. Manolescu, A. R., Witkowska, K., Kinnaird, A., Cessford, T. & Cheeseman, C. Facilitated Hexose Transporters: New Perspectives on Form and Function. *Physiology* **2007**, *22*, 234–240.

4. Wood, I. S.; Trayhurn, P. Glucose transporters (GLUT and SGLT): expanded families of sugar transport proteins. *Br. J. Nutr.* **2003**, *89*, 3–9.

5. Poulsen, S. B.; Fenton, R. A.; Rieg, T. Sodium-glucose cotransport. *Curr. Opin. Nephrol. Hypertens.* **2015**, ***24***, 463–469.

6. Thorens, B.; Mueckler, M. Glucose transporters in the 21st Century. *Am. J. Physiol. Endocrinol. Metab.* **2010**, *298*, E141-5.

7. Mueckler, M.; Thorens, B. The SLC2 (GLUT) family of membrane transporters. *Mol. Aspects Med.* **2013**, *34*, 121–138.

8. Kasahara, M.; Hinkle, P. C. Reconstitution and purification of the D-glucose transporter from human erythrocytes. *J. Biol. Chem.* **1977**, *252*, 7384–7390.

9. Simpson, I. A.; Vannucci, S. J.; Maher, F. Glucose transporters in mammalian brain. *Biochem. Soc. Trans.* **1994**, *22*, 671–675.

10. Huang, S.; Czech, M. P. The GLUT4 glucose transporter. *Cell Metab.* **2007**, *5*, 237-252.

11. Douard, V.; Ferraris, R. P. Regulation of the fructose transporter GLUT5 in health and disease. *Am. J. Physiol. Endocrinol. Metab.* **2008**, *295*, E227–E237.

12. Uldry, M.; Thorens, B. The SLC2 family of facilitated hexose and polyol

transporters. *Pflugers Arch.* **2004**, *447*, 480–489.

13. Long, W.; Cheeseman, C. Structure of, and functional insight into the GLUT family of membrane transporters. *Cell Health Cytoskelet.* **2015**, *7*, 167–183.

14. Deng, D.; Yan, N. GLUT, SGLT, and SWEET: Structural and mechanistic investigations of the glucose transporters. *Protein Sci.* **2016**, *25*, 546–558.

15. Holman, G. D. Structure, function and regulation of mammalian glucose transporters of the SLC2 family. *Pflügers Arch.* **2020**, *472*, 1155–1175.

16. McQuade, D. T.; Plutschack, M. B.; Seeberger, P. H. Passive fructose transporters in disease: a molecular overview of their structural specificity. *Org. Biomol. Chem.* **2013**, *11*, 4909–4920.

17. Kouidhi, S.; Berrhouma, R.; Rouissi, K.; Jarboui, S.; Clerget-Froidevaux, M.; Seugnet, I.; Bchir, F.; Demeneix, B.; Guissouma, H.; Elgaaied, A. Human subcutaneous adipose tissue Glut 4 mRNA expression in obesity and type 2 diabetes. *Acta Diabetol.* **2013**, *50*, 227–232.

18. Camps, M.; Castelló, A.; Muñoz, P.; Monfar, M.; Testar, X.; Palacín, M.; Zorzano, A. Effect of diabetes and fasting on GLUT-4 (muscle/fat) glucose-transporter expression in insulin-sensitive tissues. Heterogeneous response in heart,red and white muscle. *Biochem. J.* **1992**, *282***,** 765–772.

19. Shepherd, P. R.; Kahn, B. B. Glucose transporters and insulin action implications for insulin resistance and diabetes mellitus. *N. Engl. J. Med.* **1999**, *341*, 248–257.

20. Douard, V.; Ferraris, R. P. The role of fructose transporters in diseases linked to excessive fructose intake. *J. Physiol.* **2013**, *591*, 401–414.

21. Smith, T. A. Facilitative glucose transporter expression in human cancer tissue. *Br. J. Biomed. Sci.* **1999**, *56*, 285–292.

22. Adekola, K.; Rosen, S. T.; Shanmugam, M. Glucose transporters in cancer metabolism. *Curr. Opin. Oncol.* **2012**, *24*, 650–654.

23. Zamora-León, S. P.; Golde, D. W.; Concha, I., I., Rivas, C., I., Delgado-López, F.; Baselga, J.; Nualart, F.; Vera, J. C. Expression of the fructose transporter GLUT5 in human breast cancer. *Proc. Natl. Acad. Sci.* **1996**, *93*, 1847-1852.

24. Godoy, A.; Ulloa, V.; Rodríguez, F.; Reinicke, K.; Yañez, A.; García, M.; Medina,

R.; Carrasco, M.; Barberis, S.; Castro, T.; Martínez, F.; Koch, X.; Vera, J.; Poblete, M.; Figueroa, C.; Peruzzo, B.; Pérez, F.; Nualart, F. Differential subcellular distribution of glucose transporters GLUT1-6 and GLUT9 in human cancer: ultrastructural localization of GLUT1 and GLUT5 in breast tumor tissues. *J. Cell. Physiol.* **2006**, *207*, 614–627.

25. Villaamil, V. M.; Gallego, G. A.; Rubira, L.V.; Campelo, R. G.; Valladares-Ayerbes, M.; Pulido, E. G.; Bolós, M. V.; Caínzos, I. S.; Antón Aparicio, L. Fructose transporter Glut5 expression in clear renal cell carcinoma. *Oncol. Rep.* **2011**, *25*, 315–323.

26. Weng, Y.; Fan, X.; Bai, Y.; Wang, S.; Huang, H.; Yang, H.; Zhu, J.; Zhang, F. SLC2A5 promotes lung adenocarcinoma cell growth and metastasis by enhancing fructose utilization. *Cell Death Discov.* **2018**, *4*, 38.

27. Yan, N. Structural advances for the major facilitator superfamily (MFS) transporters. *Trends Biochem. Sci.* **2013**, *38*, 151–159.

28. Madej, M. G.; Sun, L.; Yan, N.; Kaback, H. R. Functional architecture of MFS D-glucose transporters. *Proc. Natl. Acad. Sci. U. S. A.* **2014**, *111*, E719-27.

29. Nomura, N.; Verdon, G.; Kang, H. J.; Shimamura, T.; Nomura, Y.; Sonoda, Y.; Hussien, S. A.; Qureshi, A. A.; Coincon, M.; Sato, Y.; Abe, H.; Nakada-Nakura, Y.; Hino, T.; Arakawa, T.; Kusano-Arai, O.; Iwanari, H.; Murata, T.; Kobayashi, T.; Hamakubo, T.; Ka, D. Structure and mechanism of the mammalian fructose transporter GLUT5. *Nature* **2015**, *526*, 397–401.

30. Deng, D.; Xu, C.; Sun, P.; Wu, J.; Yan, C.; Hu, M.; Yan, N. Crystal structure of the human glucose transporter GLUT1. *Nature* **2014**, *510*, 121–125.

31. Soueidan, O. M.; Scully, T. W.; Kaur, J.; Panigrahi, R.; Belovodskiy, A.; Do, V.; Matier, C. D.; Lemieux, M. J.; Wuest, F.; Cheeseman, C.; West, F. G. Fluorescent Hexose Conjugates Establish Stringent Stereochemical Requirement by GLUT5 for Recognition and Transport of Monosaccharides. *ACS Chem. Biol.* **2017**, *12*, 1087–1094.

32. Tatibouët, A.; Yang, J.; Morin, C.; Holman, G. D. Synthesis and evaluation of fructose analogues as inhibitors of the D-fructose transporter GLUT5. *Bioorg. Med.*

Chem. **2000**, *8*, 1825–1833.

33. Tanasova, M.; Fedie, J. R. Molecular Tools for Facilitative Carbohydrate Transporters (Gluts). *Chembiochem* **2017**, *18*, 1774–1788.

34. Yang, J.; Dowden, J.; Tatibouët, A.; Hatanaka, Y.; Holman, G. D. Development of high-affinity ligands and photoaffinity labels for the D-fructose transporter GLUT5. *Biochem. J.* **2002**, *367*, 533–539.

35. Trayner, B. J.; Grant, T. N.; West, F. G.; Cheeseman, C. I. Synthesis and characterization of 6-deoxy-6-fluoro-D-fructose as a potential compound for imaging breast cancer with PET. *Bioorg. Med. Chem.* **2009**, *17*, 5488–5495.

36. Levi, J.; Cheng, Z.; Gheysens, O.; Patel, M.; Chan, C.T.; Wang, Y.; Fluorescent fructose derivatives for imaging breast cancer cells. *Bioconjug. Chem.* **2007**, ***18***, 628–634.

37. Wuest, M.; Trayner, B. J.; Grant, T. N.; Jans, H.; Mercer, J. R.; Murray, D.; West, F. G.; McEwan, A. J. B.; Wuest, F.; Cheeseman, C. I. Radiopharmacological evaluation of 6-deoxy-6-[18F]fluoro-d-fructose as a radiotracer for PET imaging of GLUT5 in breast cancer. *Nucl. Med. Biol.* **2011**, *38*, 461–475.

38. Kumar Kondapi, V. P.; Soueidan, O. M.; Cheeseman, C. I.; West, F. G. Tunable GLUT–Hexose Binding and Transport via Modulation of Hexose C-3 Hydrogen-Bonding Capabilities. *Chem. - A Eur. J.* **2017**, *23*, 8073–8081.

39. Rana, N.; Aziz, M.A.; Oraby, A.K.; Wuest, M.; Dufour, J.; Abouzid, K.A.; Wuest, F.; West, F.G. Towards Selective Binding to the GLUT5 Transporter: Synthesis, Molecular Dynamics and In Vitro Evaluation of Novel C-3 Modified 2, 5-Anhydro-D-mannitol Analogs. *Pharmaceutics*, **2022,** *14*, 828.

40. George Thompson, A. M.; Ursu, O.; Babkin, P.; Iancu, C. V.; Whang, A.; Oprea, T. I.; Choe, J. Y. Discovery of a Specific Inhibitor of Human GLUT5 by Virtual Screening and in Vitro Transport Evaluation. *Sci. Rep.* **2016**, *6*, 1–9.

41. Kapoor, K.; Finer-Moore, J. S.; Pedersen, B. P.; Caboni, L.; Waight, A.; Hillig, R. C.; Bringmann, P.; Heisler, I.; Müller, T.; Siebeneicher, H.; Stroud, R. M. Mechanism of Inhibition of Human Glucose Transporter GLUT1 Is Conserved between Cytochalasin B and Phenylalanine Amides. *Proc. Natl. Acad. Sci.* **2016**, *113*, 4711–4716.

42. Strobel, P.; Allard, C.; Perez-Acle, T.; Calderon, R.; Aldunate, R.; Leighton, F. Myricetin, Quercetin and Catechin-Gallate Inhibit Glucose Uptake in Isolated Rat Adipocytes. *Biochem. J.* **2005**, *386*, 471–478.

43. Wuest, M.; Hamann, I.; Bouvet, V.; Glubrecht, D.; Marshall, A.; Trayner, B.; Soueidan, O. M.; Krys, D.; Wagner, M.; Cheeseman, C.; West, F.; Wuest, F. Molecular imaging of GLUT1 and GLUT5 in breast cancer: a multitracer positron emission tomography imaging study in mice. *Mol. Pharmacol.* **2018**, *93*, 79-89.

44. Tripp, J.; Essl, C.; Iancu, C.V.; Boles, E.; Choe, J.Y.; Oreb, M.. Establishing a yeast-based screening system for discovery of human GLUT5 inhibitors and activators. *Sci. Rep.*, **2017**, *7*, 1-9.

Chapter 5

1. Ecker, G. F.; Clausen, R. P.; Sitte, H. H. Wiley-VCH: Weinheim.; Transporters as Drug Targets., **2017**.

2. Colas, C.; Ung, P. M. U.; Schlessinger, A. SLC Transporters: Structure, Function, and Drug Discovery. *Med. Chem. Commun.* **2016**, *7*, 1069–1081.

3. Lin, L.; Yee, S. W.; Kim, R. B.; Giacomini, K. M. SLC Transporters as TherapeuticTargets: Emerging Opportunities. *Nat. Rev. Drug Discov.* **2015**, *14*, 543–560.

4. Schmidl, S.; Iancu, C. V.; Choe, J. Y.; Oreb, M. Ligand Screening Systems for Human Glucose Transporters as Tools in Drug Discovery. *Front. Chem.* 2018, *6*, 183.

5. Soueidan, O.-M.; Scully, T. W.; Kaur, J.; Panigrahi, R.; Belovodskiy, A.; Do, V.; Matier, C. D.; Lemieux, M. J.; Wuest, F.; Cheeseman, C.; West, F. G. Fluorescent Hexose Conjugates Establish Stringent Stereochemical Requirement by Glut5 forRecognition and Transport of Monosaccharides. *ACS Chem. Biol.* **2017**, *12*, 1087–1094.; Kondapi, V. P. K. .; Soueidan, O.-M.; Cheeseman, C. I.; West, F. G. Tunable GLUTHexose Binding and Transport via Modulation of Hexose C-3 Hydrogen-Bonding Capabilities. *Chem. Eur. J.* **2017**, *23*, 8073–8081.

6. Slavic, K.; Derbyshire, E. T.; Naftalin, R. J.; Krishna, S.; Staines, H. M. Comparison of effects of green tea catechins on apicomplexan hexose transporters and mammalian

orthologues. *Mol. Biochem. Parasitol.* **2009,** *168*, 113–116; Thompson, S. M. G.; Ursu, O.; Babkin, P.; Iancu, C. V.; Whant, A.; Oprea, T. I.; Choe, J. Discovery of a specific inhibitor of human GLUT5 by virtual screening and in vitro transport evaluation. *Sci. Rep.* **2016,** *6*, 24240; Huard, K.; Ahn, K.; Amor, P.; Beebe, D. A.; Borzilleri, K. A.; Chrunyk, B. A.; Coffey, S. B.; Cong, Y.; Conn, E. L.; Culp, J. S.; Dowling, M. S.; Gorgolione, M. F.; Gutierrez, J. A.; Knafels, J. D.; Lachapelle, E. A.; Pandit, J.; Parris, K. D.; Perez, S.; Pfefferkorn, J. A.; Price, D. A.; Raymer, B.; Ross, T. T.; Shavnya, A.; Smith, A. C.; Subashi, T. A.; Tesz, G. J.; Thuma, B. A.; Tu, M.; Weaver, J. D.; Weng, Y.; Withka, J. M.; Xing, G.; Magee, T. V. Discovery of fragment-derived small molecules for in vivo inhibition of ketohexokinase (KHK). *J. Med. Chem.* **2017,** *60*, 7835–7849; Tripp, J.; Essl, C.; Iancu, C.V.; Boles, E.; Choe, J.Y.; Oreb, M.. Establishing a yeast-based screening system for discovery of human GLUT5 inhibitors and activators. *Sci. Rep.*, **2017**, *7*, 1-9.

7. Escobedo, J. O.; Rusin, O.; Lim, S.; Strongin, R. M. NIR Dyes for BioimagingApplications. *Curr. Opin. Chem. Biol.* **2010**, *14*, 64–70.

8. Yuan, A.; Wu, J.; Tang, X.; Zhao, L.; Xu, F.; Hu, Y. Application of Near-InfraredDyes for Tumor Imaging, Photothermal, and Photodynamic Therapies. *J. Pharm. Sci.* 2013, *102*, 6–28; Pinto, A.; Pocard, M.; Photodynamic therapy and photothermaltherapy for the treatment of peritoneal metastasis: a systematic review. *Pleura and peritoneum*, **2018**, *3*(4).

9. Choi, H. S.; Nasr, K.; Alyabyev, S.; Feith, D.; Lee, J. H.; Kim, S. H.; Ashitate, Y.; Hyun, H.; Patonay, G.; Strekowski, L.; Henary, M. Synthesis and in Vivo Fate of Zwitterionic Near-infrared Fluorophores. *Angew. Chem. Int. Ed.* **2011**, *50*, 6258–6263.

10. Choi, H. S.; Gibbs, S. L.; Lee, J. H.; Kim, S. H.; Ashitate, Y.; Liu, F.; Hyun, H.; Park, G.; Xie, Y.; Bae, S.; Henary, M. Targeted Zwitterionic Near-Infrared Fluorophores for Improved Optical Imaging. *Nat. Biotechnol.* **2013**, *31*, 148–153.

11. Kim, E.; Yang, K. S.; Giedt, R. J.; Weissleder, R. Red Si–Rhodamine Drug Conjugates Enable Imaging in GFP Cells. *Chem. Comm.* **2014**, *50*, 4504–4507.

12. Park, J.; Um, J. J.; Jo, A.; Lee, J.; Jung, D. W.; Williams, D. R.; Park, S. B. Impact of Molecular Charge on GLUT-Specific Cellular Uptake of Glucose Bioprobes and in

Vivo Application of the Glucose Bioprobe, GB2-Cy3. *Chem. Comm.* **2014**, *50*, 9251–9254.

13. Jo, A.; Sung, J.; Lee, S.; Nam, H.; Lee, H. W.; Park, J.; Kim, H. M.; Kim, E.; Park, S. B. Near-IR Fluorescent Tracer for Glucose-Uptake Monitoring in Live Cells. *Bioconj. Chem.* 2018, *29*, 3394–3401.; Gomez, A.M.; Lopez, J.C. Bringing Color to Sugars: The Chemical Assembly of Carbohydrates to BODIPY Dyes. *Chem. Rec.* **2021**, *21*, 3112-3130.

14. An, F. F.; Chan, M.; Kommidi, H.; Ting, R. Dual PET and Near-Infrared Fluorescence Imaging Probes as Tools for Imaging in Oncology. *AJR. Am. J. Roentgenol.* **2016**, *207*, 266.

15. Klenner, M. A.; Pascali, G.; Massi, M.; Fraser, B. H. Fluorine-18 Radiolabelling and Photophysical Characteristics of Multimodal PET–Fluorescence Molecular Probes. *Chemistry–A Eur. J.* **2021**, *27*, 861–876.

16. Thorp-Greenwood, F. L.; Coogan, M. P. Multimodal Radio-(PET/SPECT) and Fluorescence Imaging Agents Based on Metallo-Radioisotopes: Current Applications and Prospects for Development of New Agents. *Dalton Trans.* **2011**, *40*, 6129–6143.

17. Hussain, T.; Nguyen, Q. T. Molecular Imaging for Cancer Diagnosis and Surgery *Adv. Drug Del. Rev.* **2014**, *66*, 90–100.

18. Yuen, R.; Wagner, M.; Richter, S.; Dufour, J.; Wuest, M.; West, F. G.; Wuest, F. Design, Synthesis, and Evaluation of Positron Emission Tomography/Fluorescence Dual Imaging Probes for Targeting Facilitated Glucose Transporter 1 (GLUT1). *Org. Biomol. Chem.* **2021**, *19*, 3241–3254.

19. Barnett, J. E.; Holman, G. D.; Munday, K. A. Structural Requirements for Binding to the Sugar-Transport System of the Human Erythrocyte. *Biochem. J.* **1973**, *131*,211–221.

20. Girniene, J.; Tatibouët, A.; Sackus, A.; Yang, J.; Holman, G. D.; Rollin, P. Inhibition of the D-Fructose Transporter Protein GLUT5 by Fused-Ring Glycol-1,3-Oxazolidin-2-Thiones and Oxazolidin-2-Ones. *Carbohydrate Res.* **2003**, *338*, 711–719.

21. García-Moreno, M. I.; Aguilar, M.; Ortiz Mellet, C.; García Fernández, J. M. Intramolecular Benzyl Protection Delivery: A Practical Synthesis of DMDP and DGDP from D-Fructose. *Org. Lett.* **2006**, *8*, 297–299.

22. Le Merrer, Y.; Fuzier, M.; Dosbaa, I.; Foglietti, M. J.; Depezay, J. C. Synthesis of Thiosugars as Weak Inhibitors of Glycosidases. *Tetrahedron* **1997**, *53*, 16731–16746.

23. Godoy, A.; Ulloa, V.; Rodríguez, F.; Reinicke, K.; Yañez, A. J.; García, M. D. L. A.; Medina, R. A.; Carrasco, M.; Barberis, S.; Castro, T.; Martínez, F.; Koch, X.; Vera, J. C.; Poblete, M. T.; Figueroa, C. D.; Peruzzo, B.; Nualart, F. Differential Subcellular Distribution of Glucose Transporters GLUT1-6 and GLUT9 in Human Cancer: Ultrastructural Localization of GLUT1 and GLUT5 in Breast Tumor Tissues. *J. Cell Physiol* . **2005**, *207*, 614–627.

24. Jegatheesan, P.; Bandt, J. P. D. Fructose and NAFLD: The Multifaceted Aspects of Fructose Metabolism. *Nutrients* **2017**, *9*, 1–13.

25. McQuade, D. T., Plutschack, M. B. & Seeberger, P. H.; McQuade, D. T.,Plutschack, M. B. & Seeberger, P. H.; McQuade, D. T., Plutschack, M. B. & Seeberger, P. H. Passive Fructose Transporters in Disease: A Molecular Overview of Their Structural Specificity. *Org. Biomol. Chem.* **2013**, *11*, 4909–4920.

26. Patel, T.K.; Adhikari, N.; Amin, S.A.; Biswas, S.; Jha, T.; Ghosh, B. Small molecule drug conjugates (SMDCs): an emerging strategy for anticancer drug design and discovery. *New J. Chem.*, **2021**, *45*, 5291-5321.

27. Nahrjou, N.; Ghosh, A.; Tanasova, M. Targeting of GLUT5 for Transporter-Mediated Drug-Delivery Is Contingent upon Substrate Hydrophilicity. *Int. J. Mol.Sci.* **2021**, *22*, 5073.

28. Stoddart, L. A.; Kindon, N. D.; Otun, O.; Harwood, C. R.; Patera, F.; Veprintsev, D. B.; Woolard, J.; Briddon, S. J.; Franks, H. A.; Hill, S. J.; Kellam, B. Ligand-Directed Covalent Labelling of a GPCR with a Fluorescent Tag in Live Cells.*Commun. Biol.* **2020**, *3*, 1–9.

29. Yan, Q.; Lu, Y.; Zhou, L.; Chen, J.; Xu, H.; Cai, M.; Shi, Y.; Xiong, W.; Jiang, J., Xiong, W., Gao, J. and Wang, H.; Gao, J.; Wang, H. Mechanistic Insights into GLUT1

Activation and Clustering Revealed by Super-Resolution Imaging. *PNAS* **2018,** *115*, 7033–7038.

Appendix I: NMR spectra

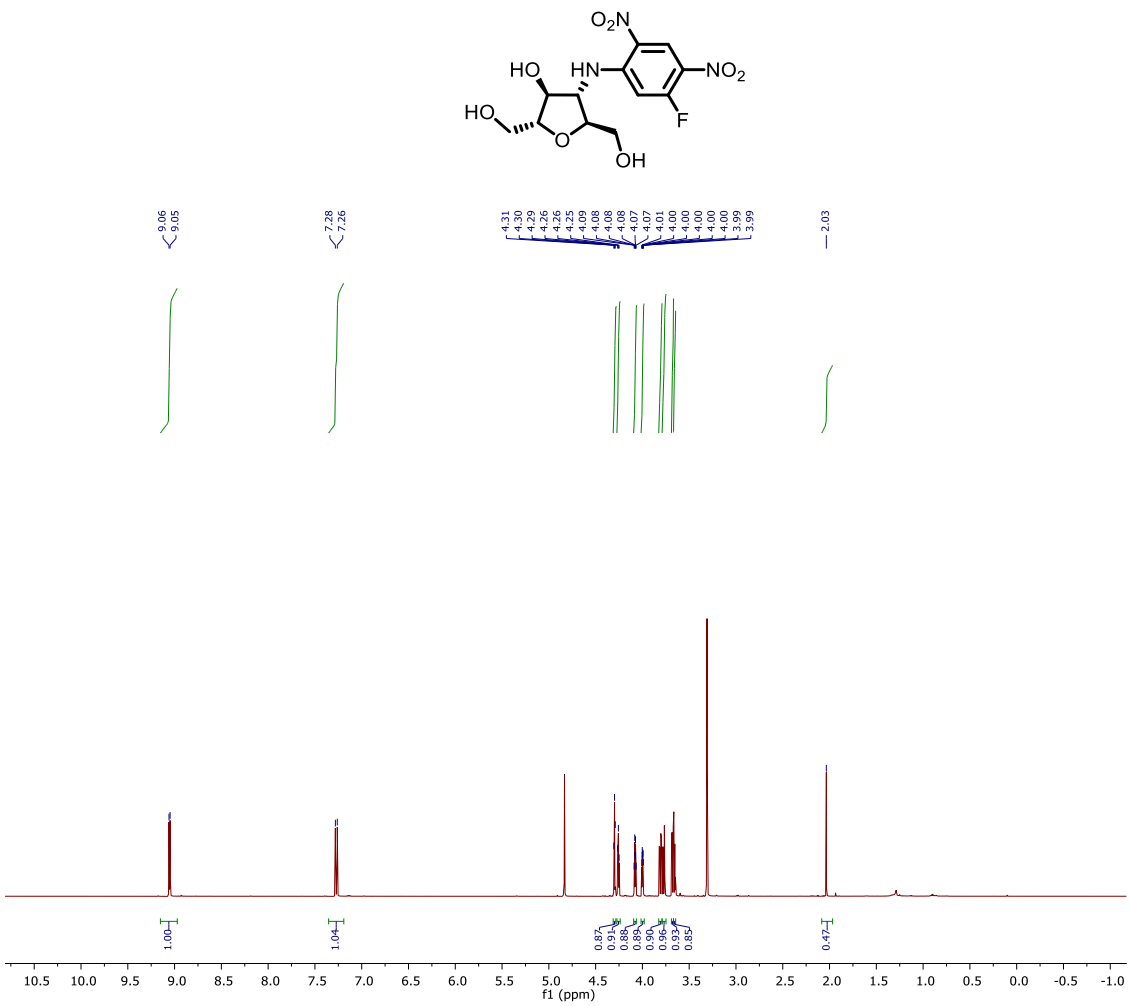
O2N
HO
HN
NO2
F
HO
O
OH
9.06
9.05
7.28
7.26
4.31
4.30
4.29
4.26
4.25
4.09
4.08
4.08
4.08
4.07
4.07
4.01
4.00
4.00
4.00
4.00
4.00
3.99
3.99
2.03
1.00
1.04
0.87
0.91
0.88
0.89
0.90
0.96
0.93
0.85
0.47
10.5
10.0
9.5
9.0
8.5
8.0
7.5
7.0
6.5
6.0
5.5
5.0
4.5
4.0
3.5
3.0
2.5
2.0
1.5
1.0
0.5
0.0
-0.5
-1.0
f1 (ppm)

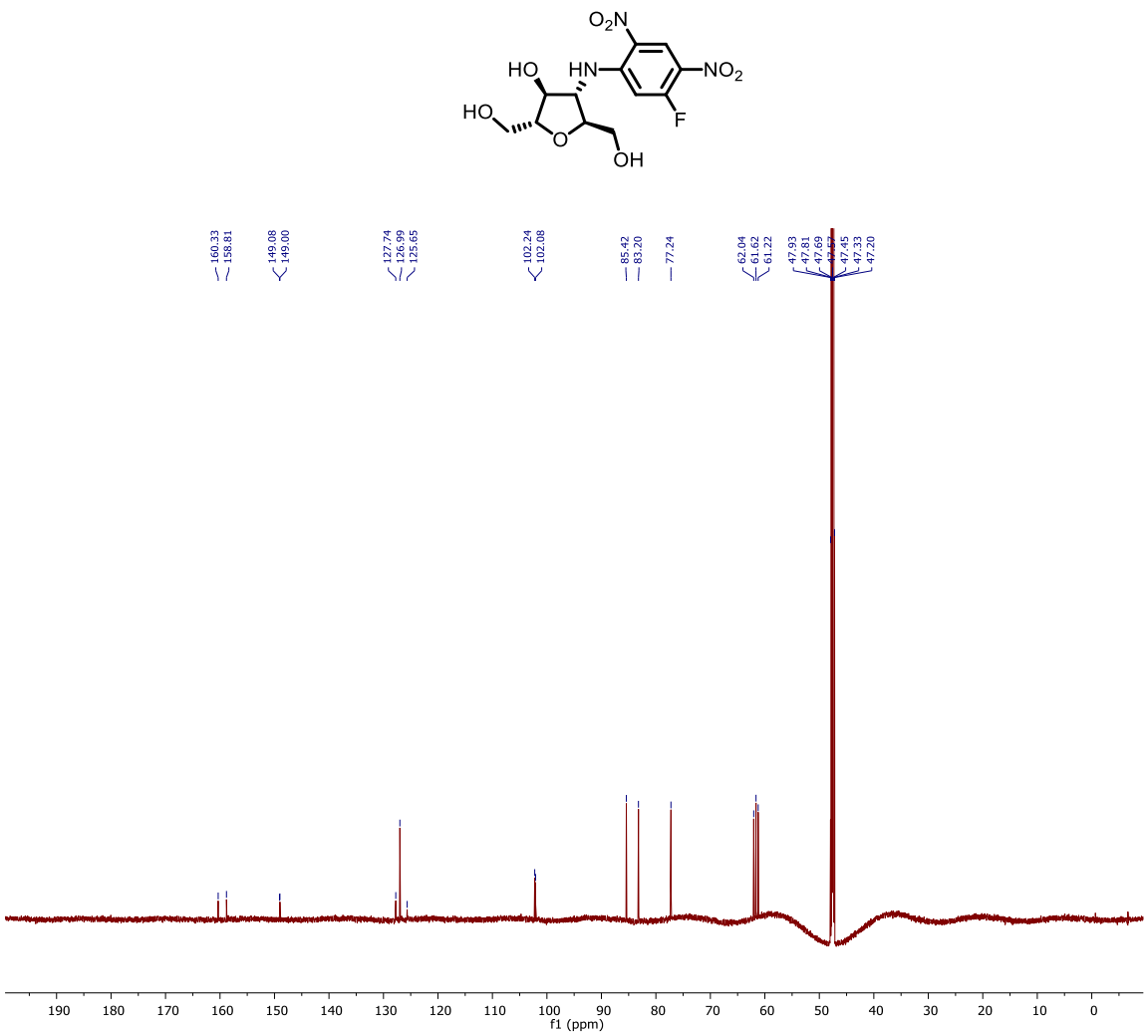
O2N
HO
HN
NO2
HO
F
O
OH
160.33
158.81
149.08
149.00
127.74
126.99
125.65
102.24
102.08
85.42
83.20
77.24
62.04
61.62
61.22
47.93
47.81
47.69
47.57
47.45
47.33
47.20
190
180
170
160
150
140
130
120
110
100
90
80
70
60
50
40
30
20
10
0
f1 (ppm)

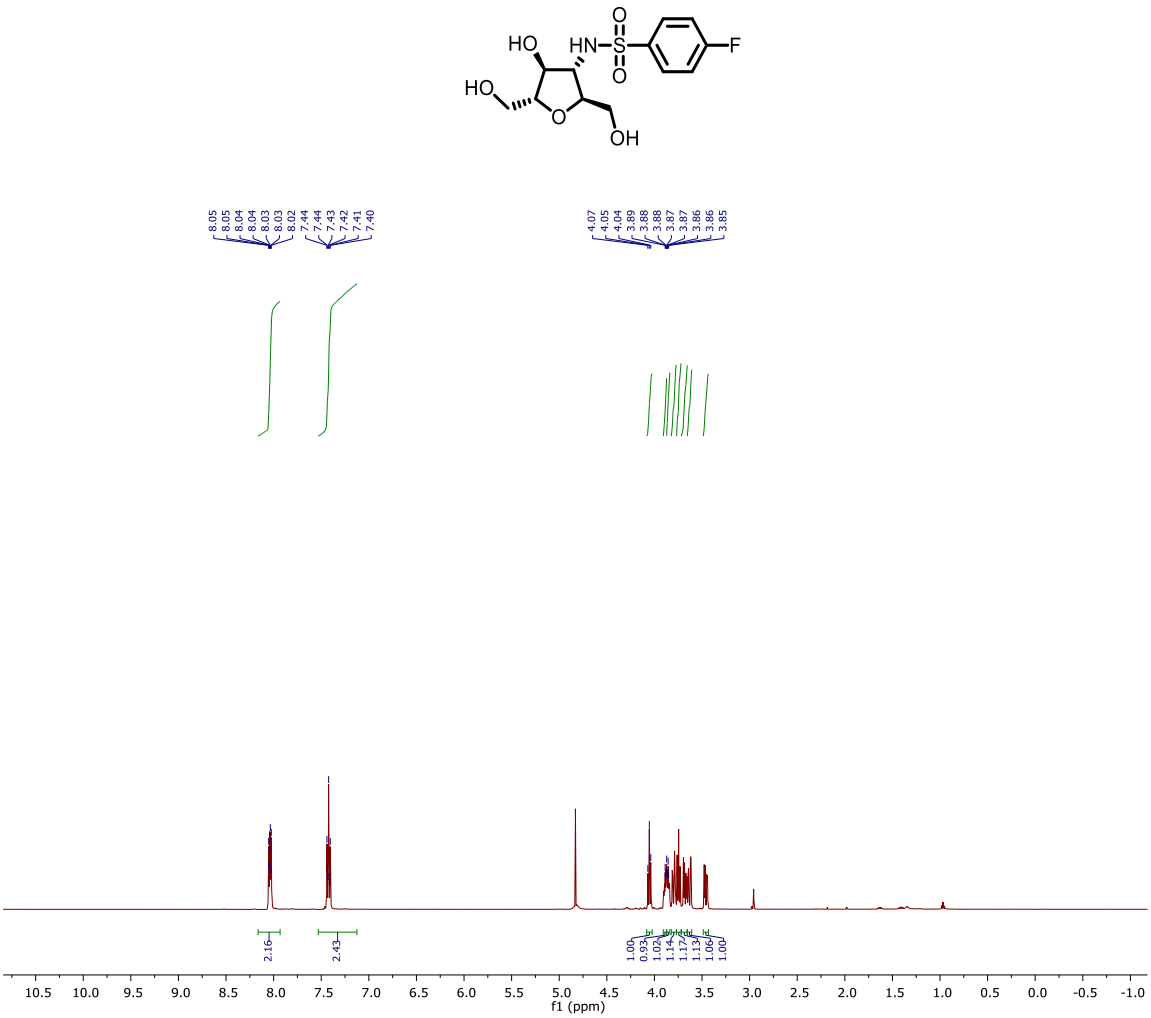
HO
HN
S
O
O
F
HO
O
OH
8.05
8.05
8.04
8.04
8.03
8.03
8.02
7.44
7.44
7.43
7.43
7.42
7.41
7.40
4.07
4.05
4.04
3.89
3.88
3.88
3.87
3.87
3.86
3.86
3.85
2.16
2.43
1.00
0.93
1.02
1.14
1.17
1.13
1.06
1.00
10.5
10.0
9.5
9.0
8.5
8.0
7.5
7.0
6.5
6.0
5.5
5.0
4.5
4.0
3.5
3.0
2.5
2.0
1.5
1.0
0.5
0.0
-0.5
-1.0
f1 (ppm)

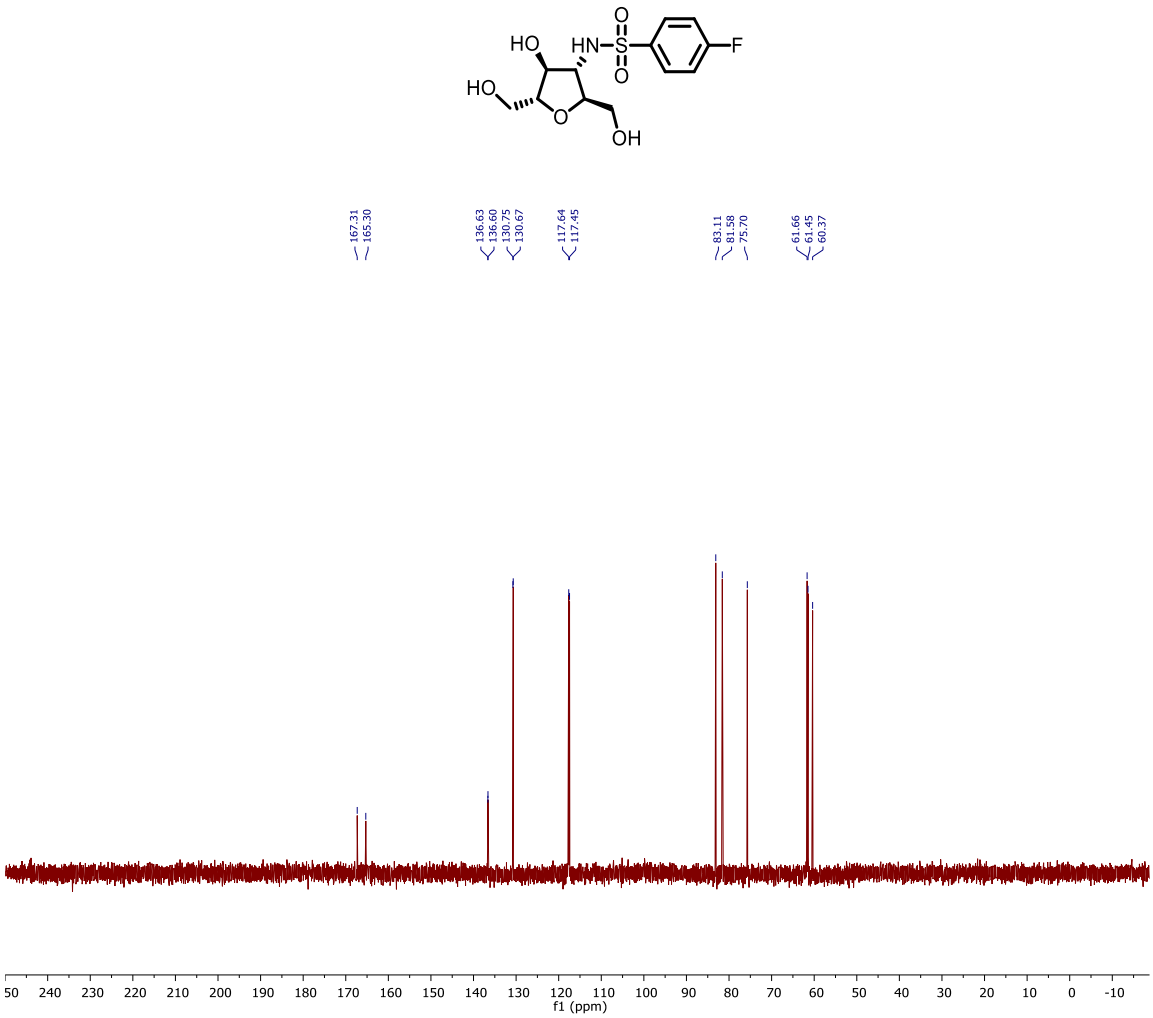
HO
HN
S
O
O
F
HO
O
OH
167.31
165.30
136.63
136.60
130.75
130.67
117.64
117.45
83.11
81.58
75.70
61.66
61.45
60.37
50 240 230 220 210 200 190 180 170 160 150 140 130 120 110 100 90 80 70 60 50 40 30 20 10 0 -10
f1 (ppm)

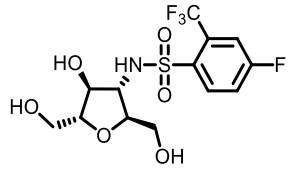
F3C
O
HO
HN
S
F
O
HO
O
OH

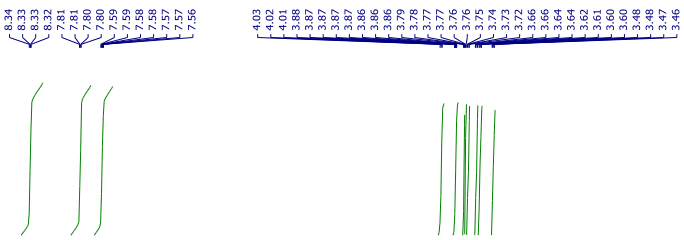
8.34
8.33
8.33
8.32
7.81
7.81
7.80
7.80
7.59
7.59
7.58
7.58
7.57
7.57
7.56
4.03
4.02
4.01
3.88
3.87
3.87
3.87
3.86
3.86
3.86
3.79
3.78
3.77
3.77
3.76
3.76
3.75
3.74
3.73
3.72
3.66
3.66
3.64
3.64
3.62
3.61
3.60
3.60
3.48
3.48
3.47
3.46

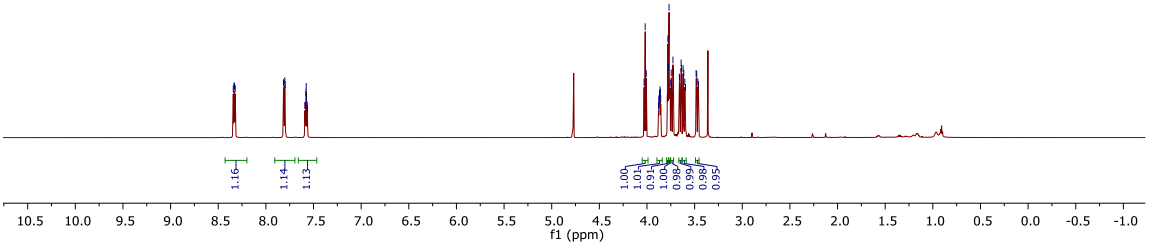
1.16
1.14
1.13
1.00
1.01
0.91
1.00
0.98
0.99
0.98
0.95
10.5
10.0
9.5
9.0
8.5
8.0
7.5
7.0
6.5
6.0
5.5
5.0
4.5
4.0
3.5
3.0
2.5
2.0
1.5
1.0
0.5
0.0
-0.5
-1.0
f1 (ppm)

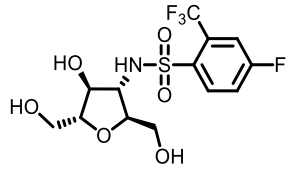
F3C
O
HO
HN
S
F
O
HO
O
OH

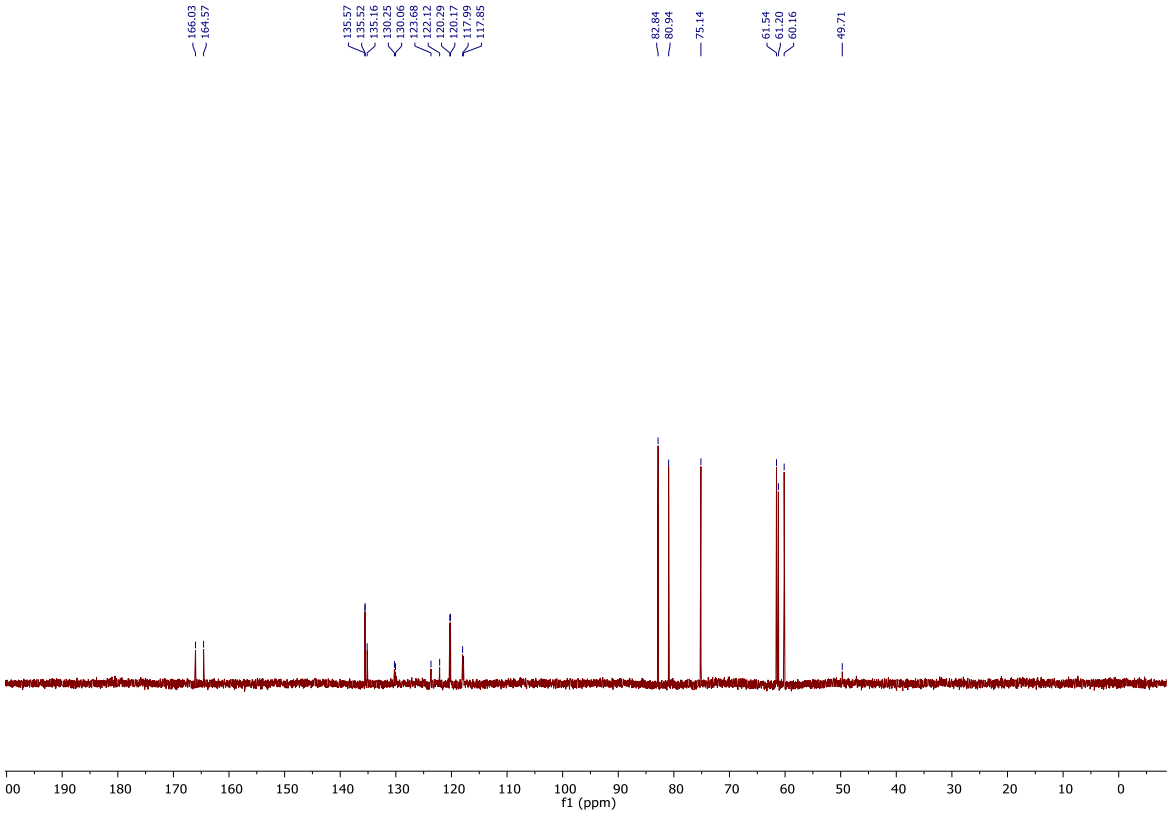
166.03
164.57
135.57
135.52
135.16
130.25
130.06
123.68
122.12
120.29
120.17
117.99
117.85
82.84
80.94
75.14
61.54
61.20
60.16
49.71
00 190 180 170 160 150 140 130 120 110 100 90 80 70 60 50 40 30 20 10 0
f1 (ppm)

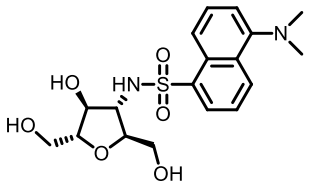
HO
HN
S
O
O
N
HO
O
OH

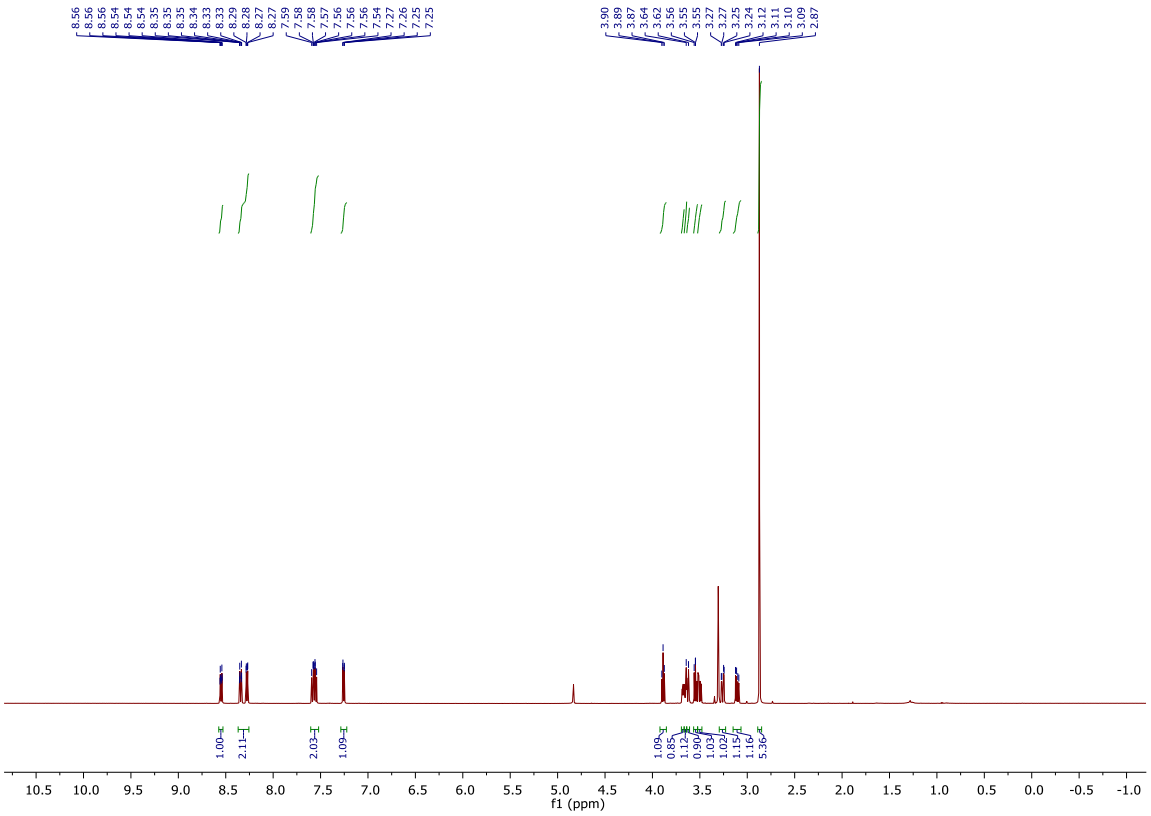
8.56
8.56
8.56
8.54
8.54
8.54
8.35
8.35
8.35
8.34
8.33
8.29
8.28
8.27
8.27
7.59
7.58
7.58
7.57
7.56
7.56
7.56
7.54
7.54
7.27
7.26
7.25
7.25
3.90
3.89
3.87
3.64
3.62
3.56
3.55
3.55
3.27
3.27
3.25
3.24
3.12
3.11
3.10
3.09
2.87
1.00
2.11
2.03
1.09
1.09
0.85
1.12
0.96
1.03
1.02
1.15
1.16
5.36
10.5
10.0
9.5
9.0
8.5
8.0
7.5
7.0
6.5
6.0
5.5
5.0
4.5
4.0
3.5
3.0
2.5
2.0
1.5
1.0
0.5
0.0
-0.5
-1.0
f1 (ppm)

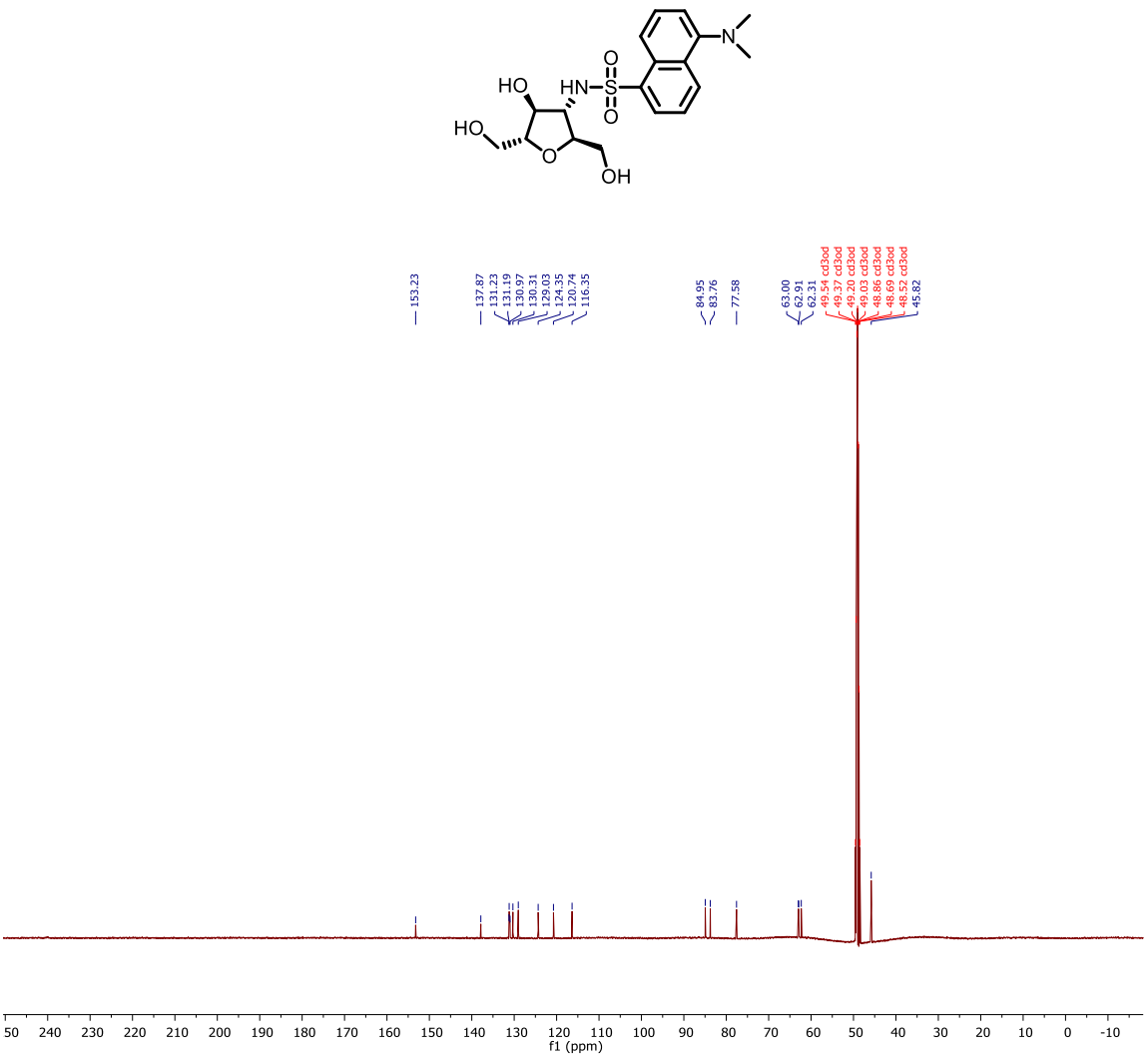
HO
HN
O
S
O
N
HO
O
OH
153.23
137.87
131.23
131.19
130.97
130.31
129.03
124.35
120.74
116.35
84.95
83.76
77.58
63.00
62.91
62.31
49.54 cd3od
49.37 cd3od
49.20 cd3od
49.03 cd3od
48.86 cd3od
48.69 cd3od
48.52 cd3od
45.82
50 240 230 220 210 200 190 180 170 160 150 140 130 120 110 100 90 80 70 60 50 40 30 20 10 0 -10
f1 (ppm)

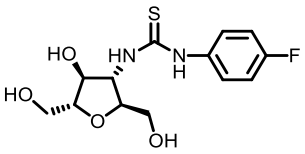
S
HO
HN
N
H
F
HO
O
OH

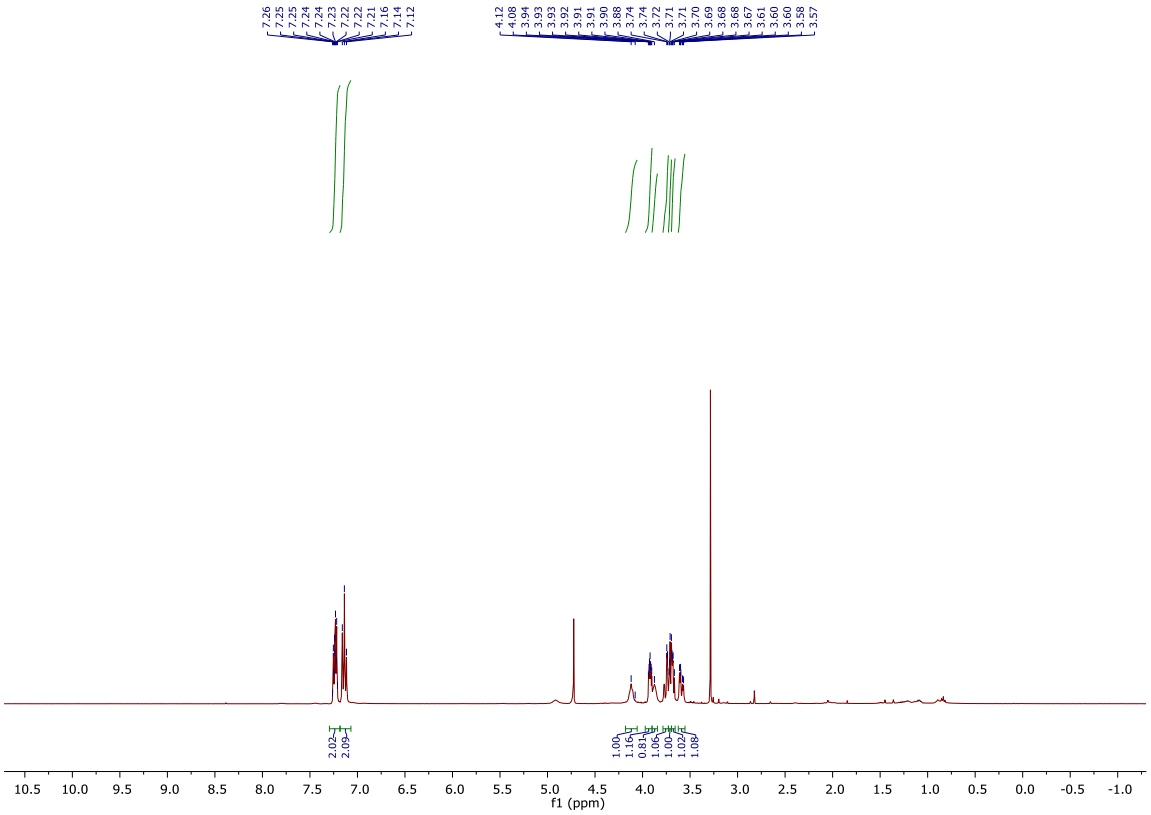
7.26
7.25
7.25
7.24
7.24
7.23
7.22
7.22
7.21
7.16
7.14
7.12
4.12
4.08
3.94
3.93
3.93
3.92
3.91
3.91
3.90
3.88
3.74
3.74
3.72
3.72
3.71
3.71
3.70
3.69
3.68
3.68
3.67
3.61
3.60
3.60
3.58
3.57
2.02
2.09
1.00
1.16
0.84
1.06
1.00
1.02
1.08
10.5
10.0
9.5
9.0
8.5
8.0
7.5
7.0
6.5
6.0
5.5
5.0
4.5
4.0
3.5
3.0
2.5
2.0
1.5
1.0
0.5
0.0
-0.5
-1.0
f1 (ppm)

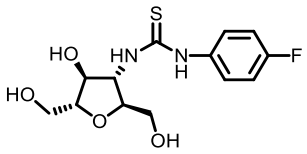
S
HO
HN
N
H
F
HO
O
OH

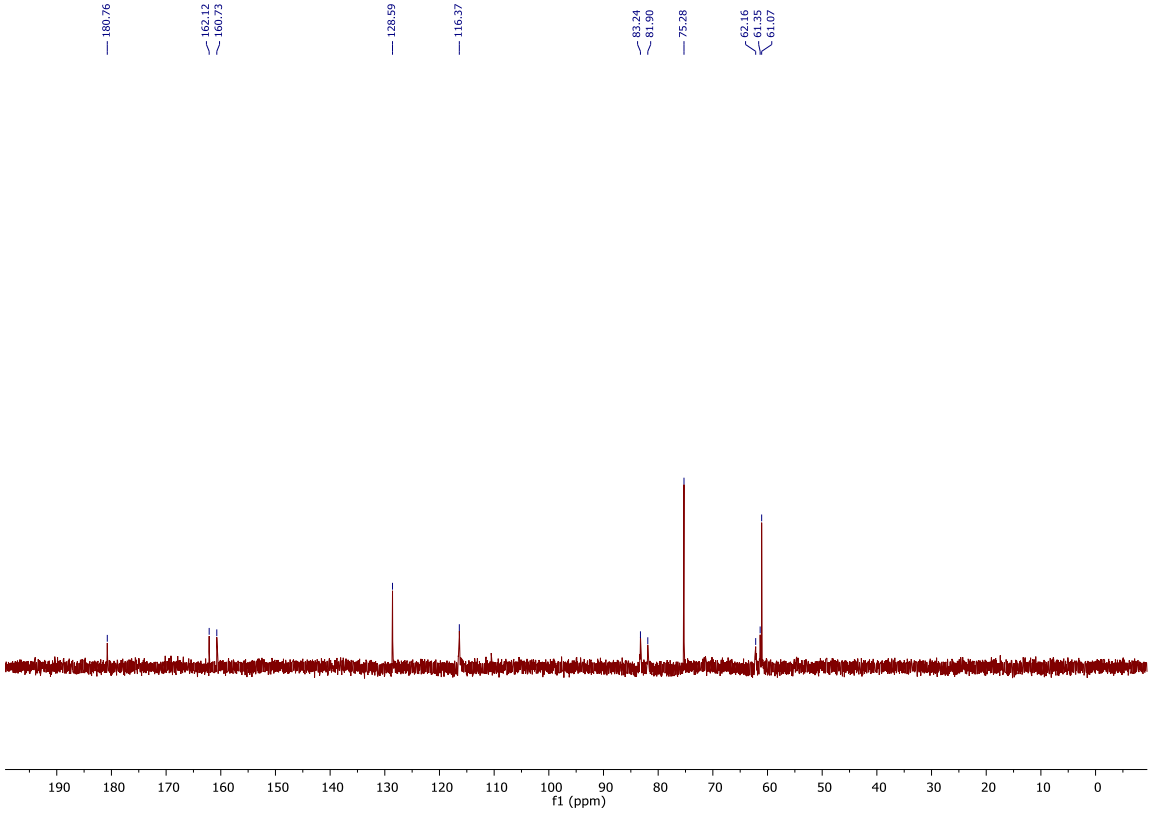
180.76
162.12
160.73
128.59
116.37
83.24
81.90
75.28
62.16
61.35
61.07
190
180
170
160
150
140
130
120
110
100
90
80
70
60
50
40
30
20
10
0
f1 (ppm)

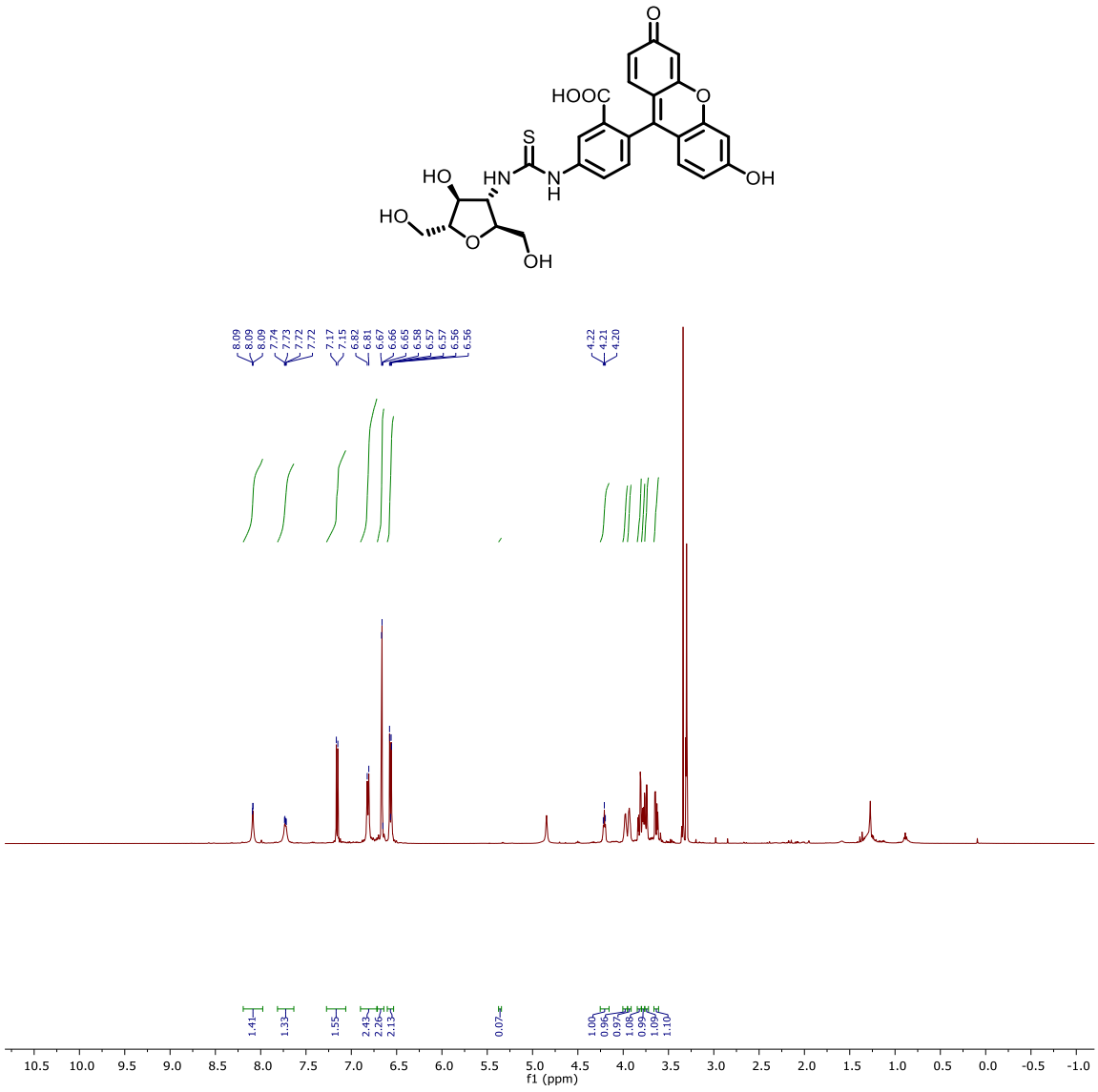
O
HOOC
O
S
HO
HN
N
H
OH
HO
O
OH
8.09
8.09
8.09
7.74
7.73
7.72
7.72
7.17
7.15
6.82
6.81
6.67
6.66
6.65
6.58
6.57
6.57
6.56
6.56
4.22
4.21
4.20
1.41
1.33
1.55
2.43
2.26
2.13
0.07
1.00
0.96
0.97
1.08
0.99
1.09
1.10
10.5 10.0 9.5 9.0 8.5 8.0 7.5 7.0 6.5 6.0 5.5 5.0 4.5 4.0 3.5 3.0 2.5 2.0 1.5 1.0 0.5 0.0 -0.5 -1.0
f1 (ppm)

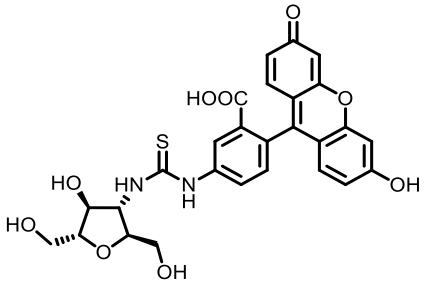
O
HOOC
O
S
HO
HN
N
H
OH
HO
O
OH

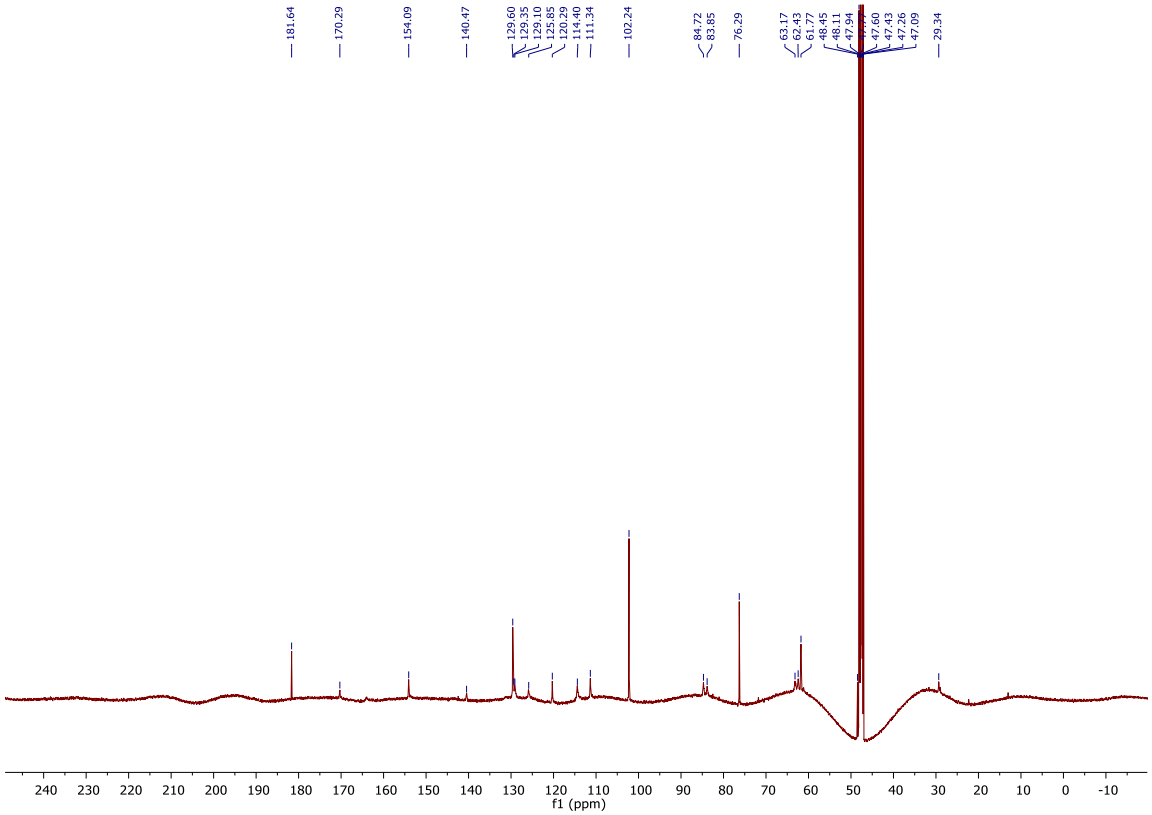
181.64
170.29
154.09
140.47
129.60
129.35
129.10
125.85
120.29
114.40
111.34
102.24
84.72
83.85
76.29
63.17
62.43
61.77
48.45
48.11
47.94
47.77
47.60
47.43
47.26
47.09
29.34
240 230 220 210 200 190 180 170 160 150 140 130 120 110 100 90 80 70 60 50 40 30 20 10 0 -10
f1 (ppm)

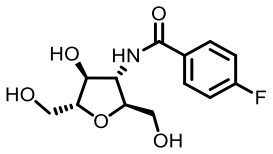
O
HO
HN
HO
F
O
OH

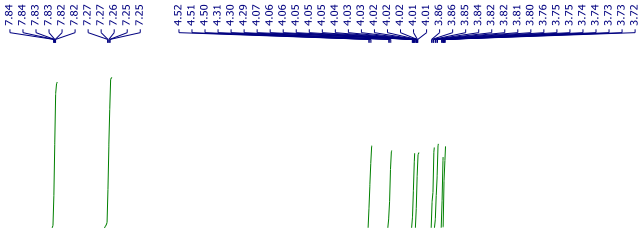
7.84
7.84
7.83
7.83
7.82
7.82
7.27
7.27
7.26
7.25
7.25
4.52
4.51
4.50
4.31
4.30
4.29
4.07
4.06
4.06
4.05
4.05
4.05
4.04
4.03
4.03
4.02
4.02
4.02
4.01
4.01
3.86
3.86
3.85
3.84
3.82
3.82
3.81
3.80
3.76
3.75
3.75
3.74
3.74
3.73
3.73
3.72

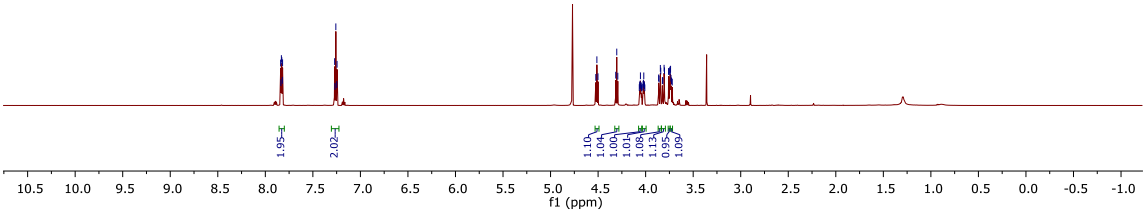
1.95
2.02
1.10
1.04
1.00
1.01
1.08
1.13
0.95
1.09
10.5
10.0
9.5
9.0
8.5
8.0
7.5
7.0
6.5
6.0
5.5
5.0
4.5
4.0
3.5
3.0
2.5
2.0
1.5
1.0
0.5
0.0
-0.5
-1.0
f1 (ppm)

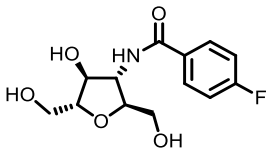
O
HO
HN
HO
F
O
OH


171.23
166.41
164.99
130.61
130.56
130.52
116.59
116.46
83.41
81.65
75.41
63.34
62.33
61.76
58.08

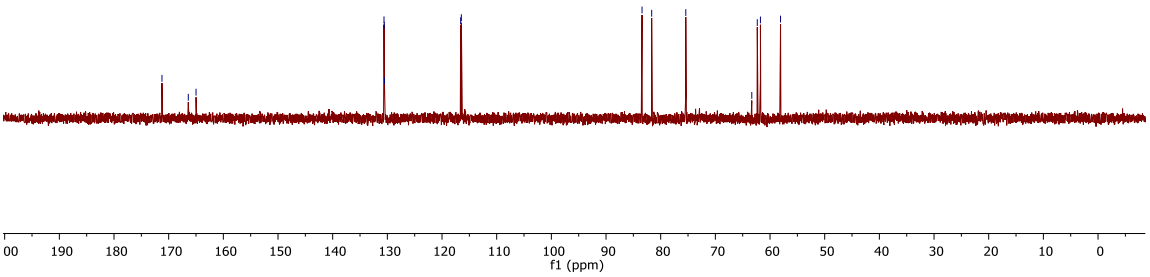
00 190 180 170 160 150 140 130 120 110 100 90 80 70 60 50 40 30 20 10 0
f1 (ppm)

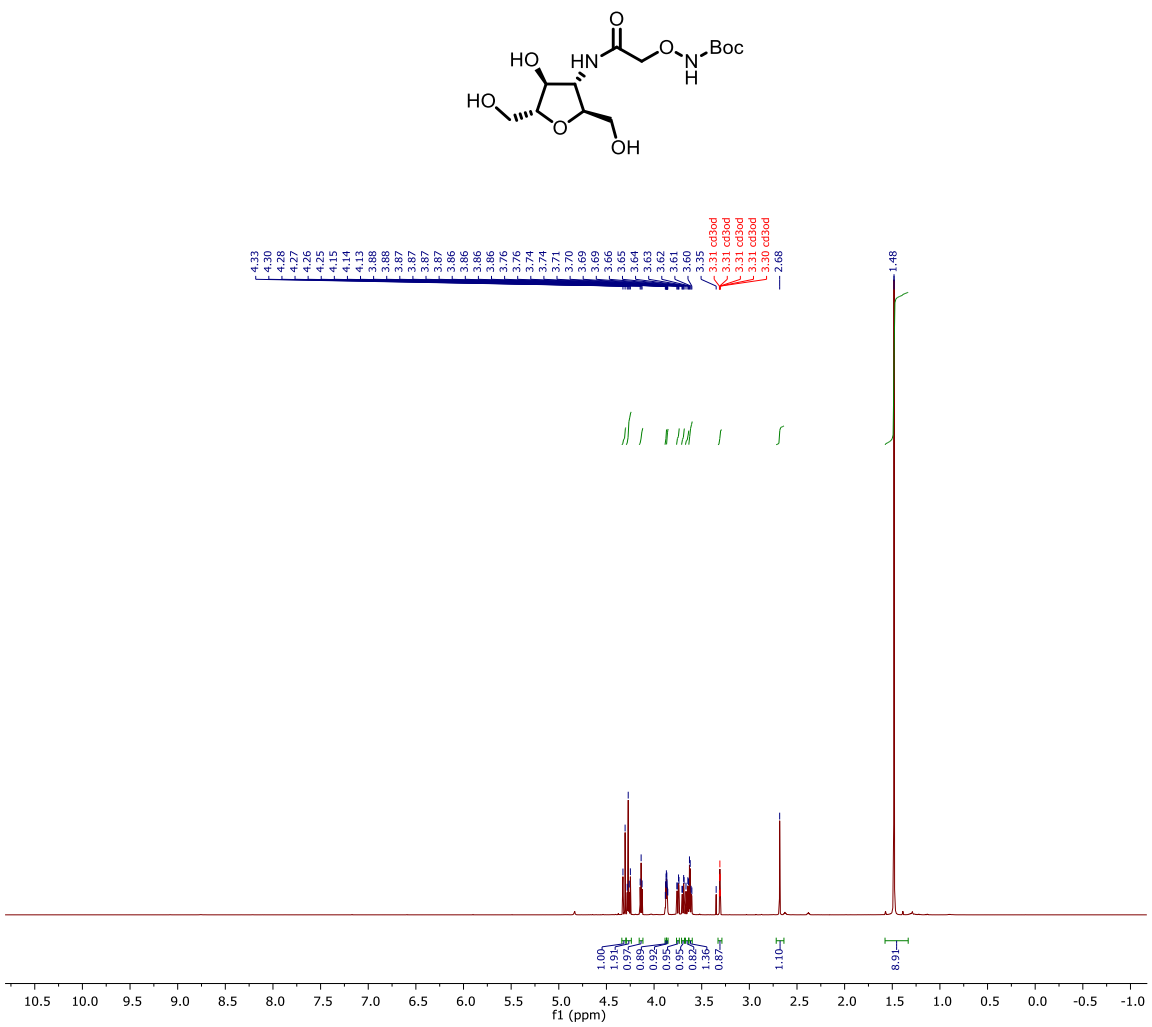
HO
HN
O
O
N
H
Boc
HO
O
OH
f1 (ppm)

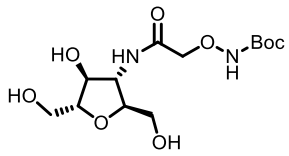
O
HO
HN
O
N
Boc
H
HO
O
OH

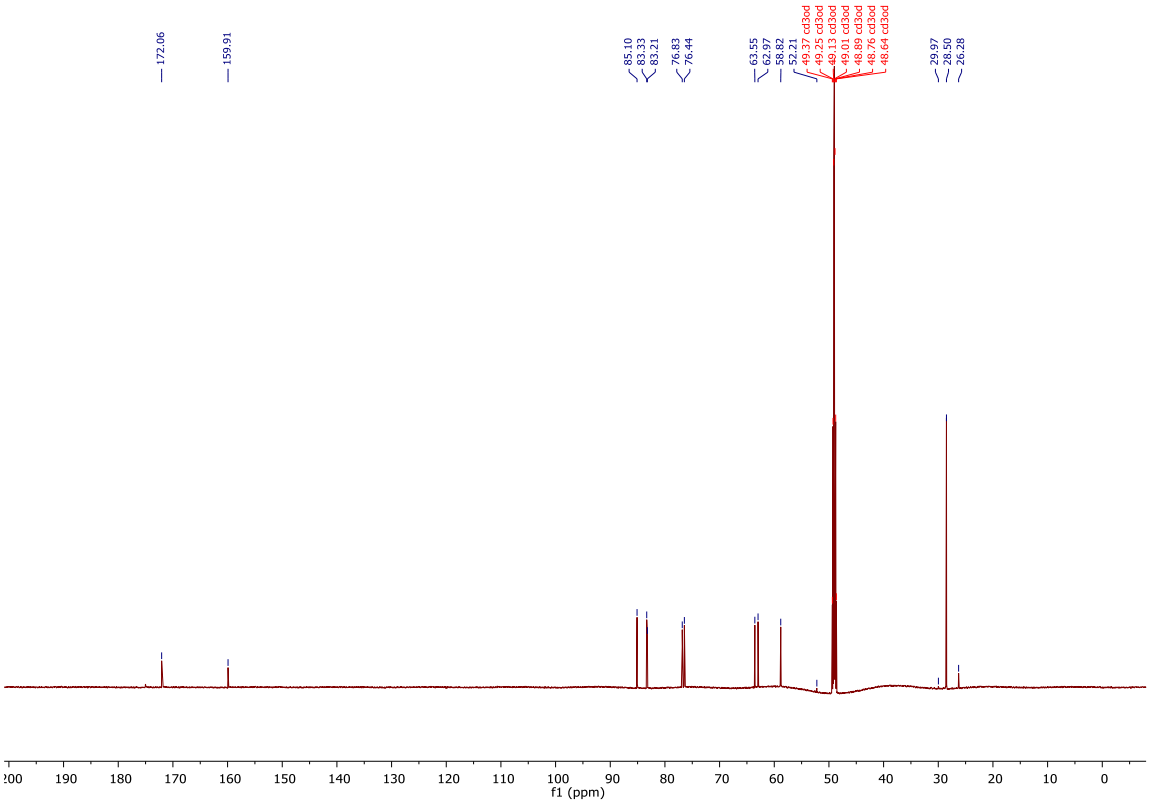
172.06
159.91
85.10
83.33
83.21
76.83
76.44
63.55
62.97
58.82
52.21
49.37 cd3od
49.25 cd3od
49.13 cd3od
49.01 cd3od
48.89 cd3od
48.76 cd3od
48.64 cd3od
29.97
28.50
26.28
200 190 180 170 160 150 140 130 120 110 100 90 80 70 60 50 40 30 20 10 0
f1 (ppm)

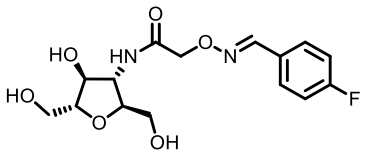
O
HO
HN
O
N
F
HO
O
OH

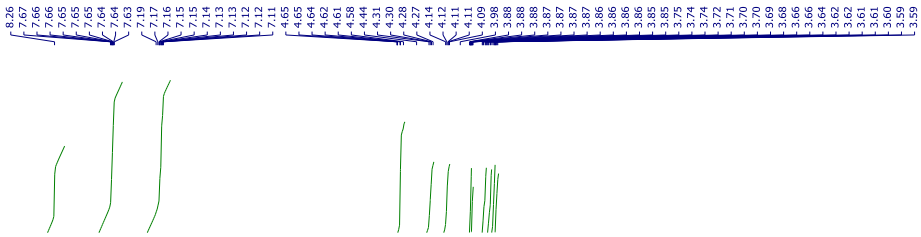
8.26
7.67
7.66
7.66
7.65
7.65
7.65
7.64
7.64
7.63
7.19
7.17
7.16
7.15
7.15
7.14
7.13
7.13
7.12
7.12
7.11
4.65
4.65
4.64
4.62
4.61
4.58
4.44
4.31
4.30
4.28
4.27
4.14
4.12
4.11
4.11
4.09
3.98
3.88
3.88
3.87
3.87
3.87
3.86
3.86
3.86
3.86
3.85
3.85
3.75
3.74
3.74
3.72
3.71
3.70
3.70
3.69
3.68
3.66
3.66
3.64
3.62
3.62
3.61
3.61
3.60
3.59
3.59

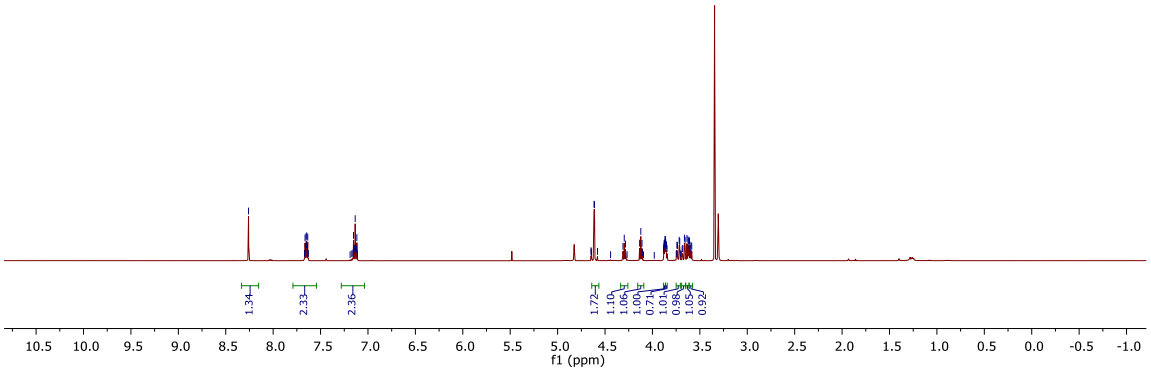
1.34
2.33
2.36
1.72
1.10
1.06
1.00
0.74
1.01
0.98
1.05
0.92
10.5
10.0
9.5
9.0
8.5
8.0
7.5
7.0
6.5
6.0
5.5
5.0
4.5
4.0
3.5
3.0
2.5
2.0
1.5
1.0
0.5
0.0
-0.5
-1.0
f1 (ppm)

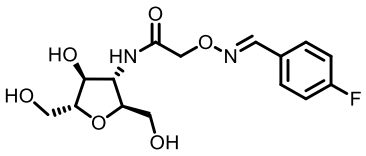
O
HO
HN
O
N
F
HO
O
OH

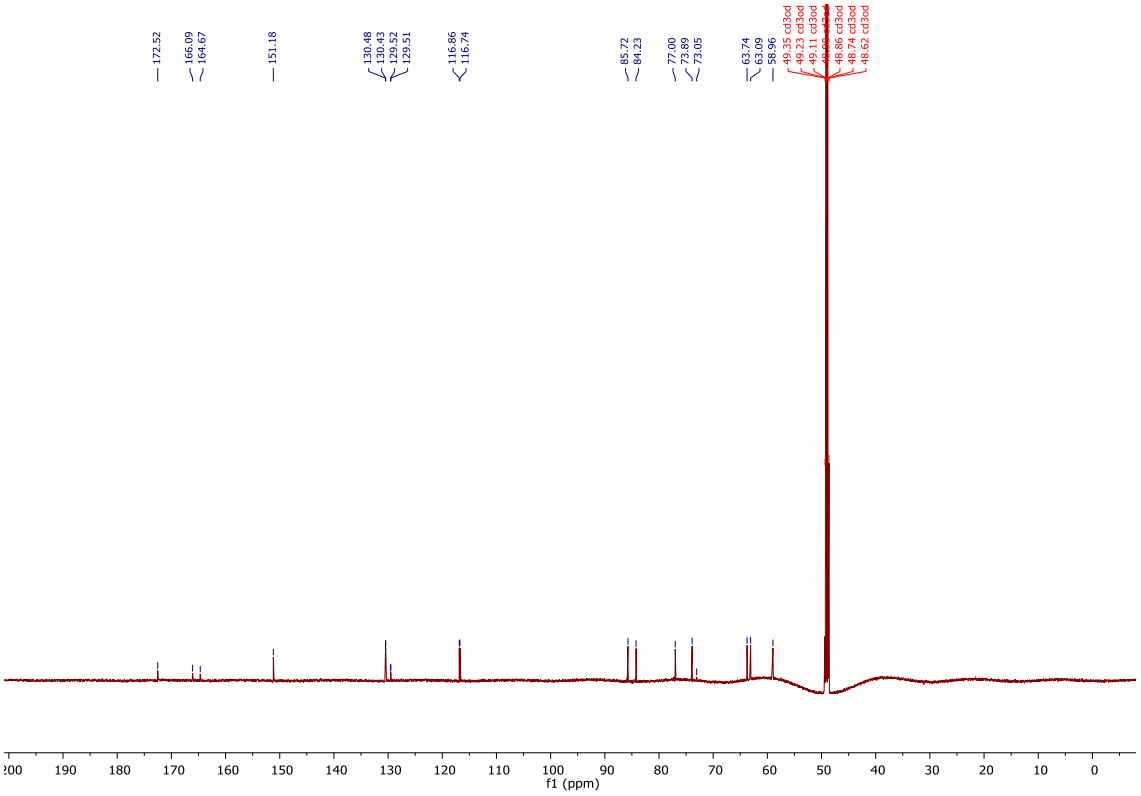
172.52
166.09
164.67
151.18
130.48
130.43
129.52
129.51
116.86
116.74
85.72
84.23
77.00
73.89
73.05
63.74
63.09
58.96
49.35 cd3od
49.23 cd3od
49.11 cd3od
48.86 cd3od
48.74 cd3od
48.62 cd3od
200
190
180
170
160
150
140
130
120
110
100
90
80
70
60
50
40
30
20
10
0
f1 (ppm)

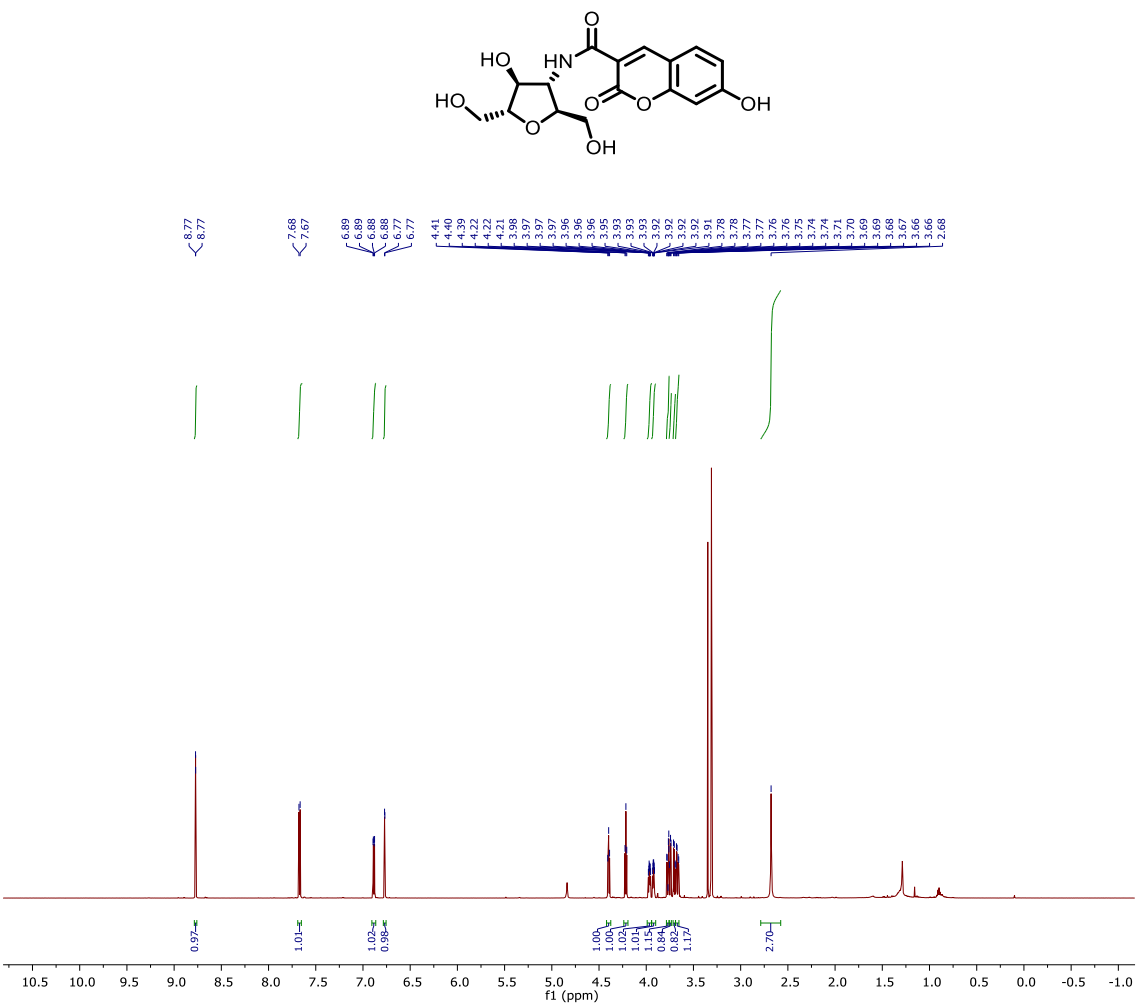
HO
HN
O
HO
O
O
O
OH
OH
8.77
8.77
7.68
7.67
6.89
6.89
6.88
6.88
6.77
6.77
4.41
4.40
4.39
4.22
4.22
4.21
3.98
3.97
3.97
3.96
3.96
3.96
3.95
3.93
3.93
3.92
3.92
3.92
3.91
3.78
3.77
3.77
3.76
3.76
3.75
3.74
3.74
3.71
3.70
3.69
3.69
3.68
3.67
3.66
3.66
2.68
0.97
1.01
1.02
0.98
1.00
1.00
1.02
1.01
1.15
0.84
0.82
1.17
2.70
10.5
10.0
9.5
9.0
8.5
8.0
7.5
7.0
6.5
6.0
5.5
5.0
4.5
4.0
3.5
3.0
2.5
2.0
1.5
1.0
0.5
0.0
-0.5
-1.0
f1 (ppm)

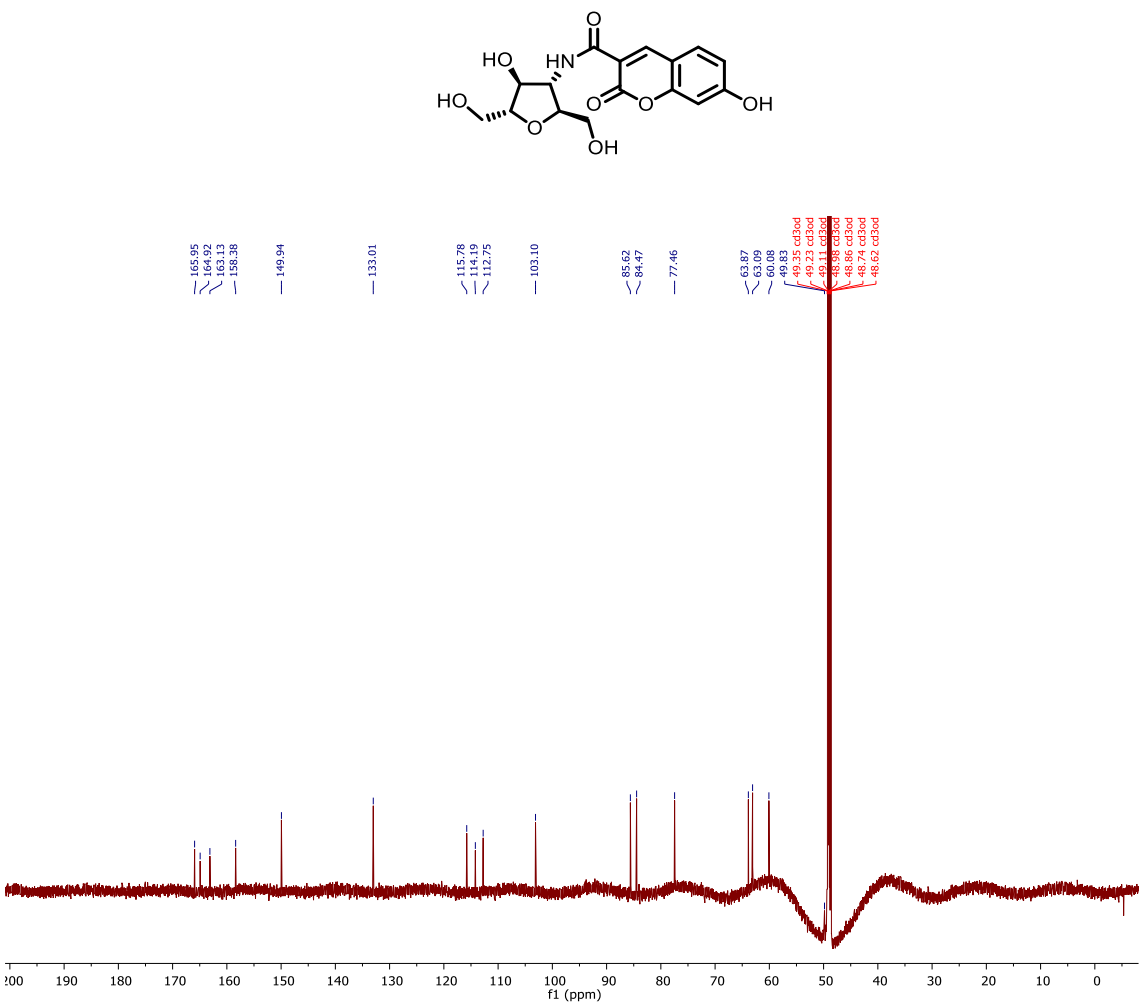
HO
HN
O
HO
O
O
O
OH
OH
165.95
164.92
163.13
158.38
149.94
133.01
115.78
114.19
112.75
103.10
85.62
84.47
77.46
63.87
63.09
60.08
49.83
49.35 cd3od
49.23 cd3od
49.11 cd3od
48.98 cd3od
48.86 cd3od
48.74 cd3od
48.62 cd3od
200
190
180
170
160
150
140
130
120
110
100
90
80
70
60
50
40
30
20
10
0
f1 (ppm)

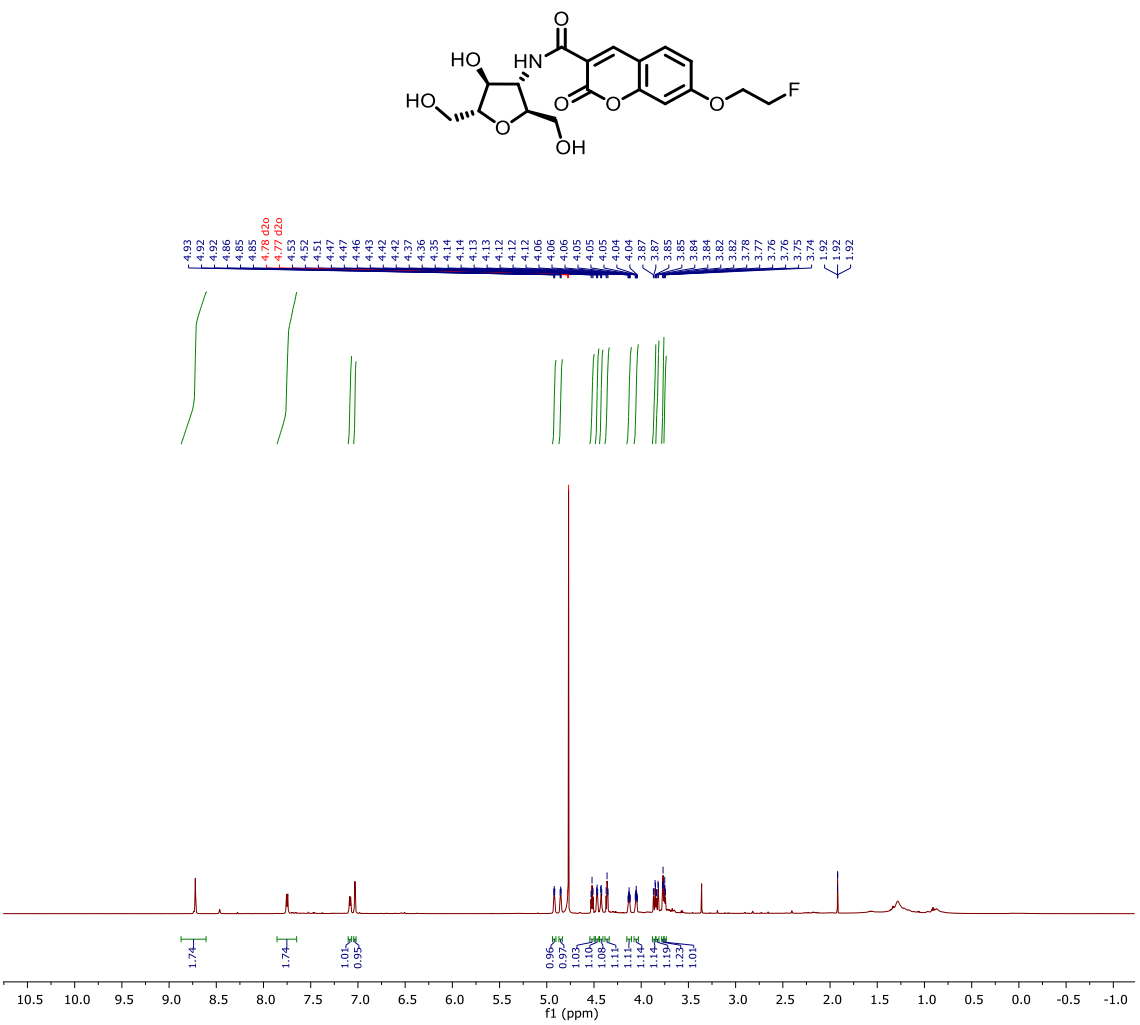
HO
HN
O
HO
O
O
O
O
F
OH
f1 (ppm)

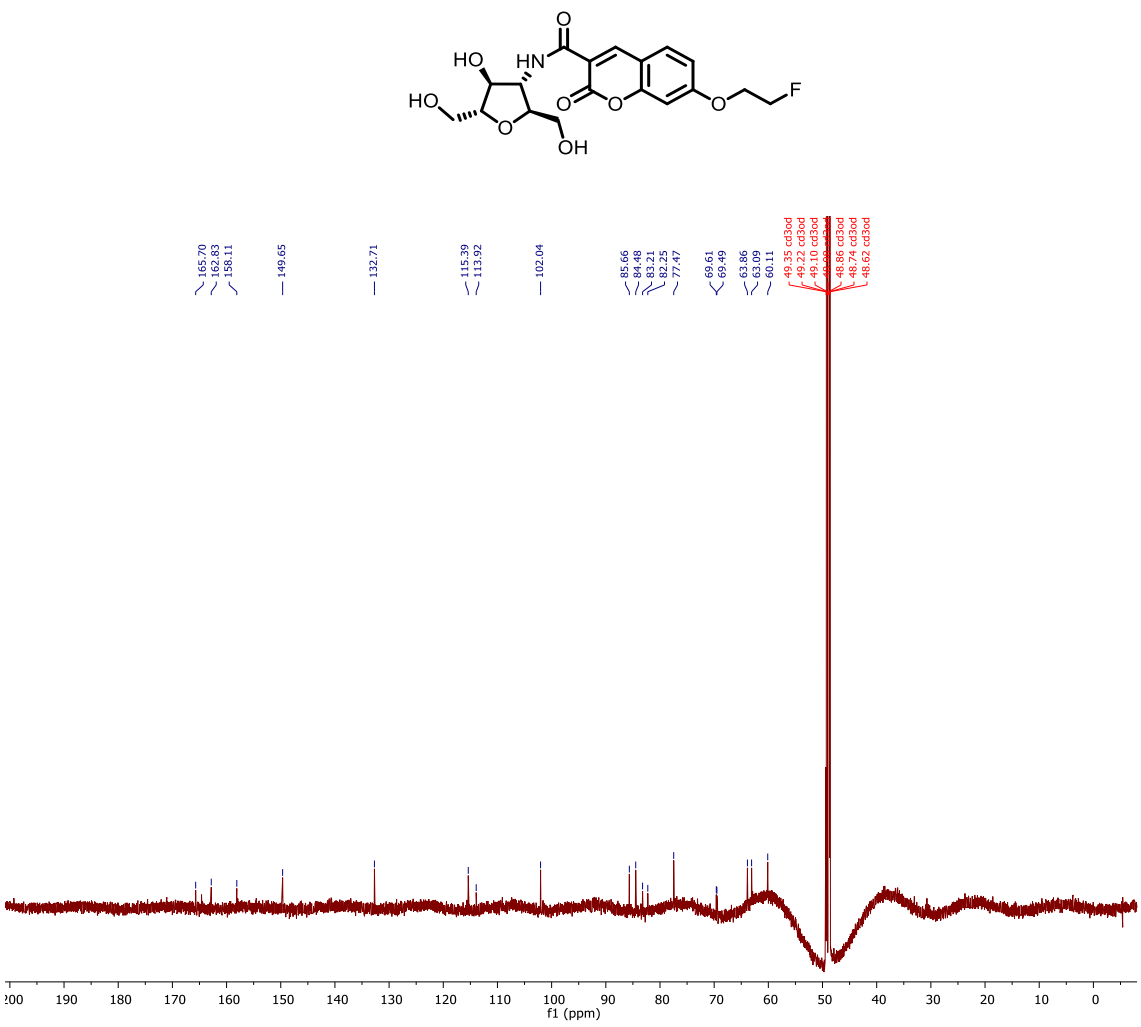
HO
HN
O
HO
O
O
O
O
F
OH
165.70
162.83
158.11
149.65
132.71
115.39
113.92
102.04
85.66
84.48
83.21
82.25
77.47
69.61
69.49
63.86
63.09
60.11
49.35 cd3od
49.22 cd3od
49.10 cd3od
48.86 cd3od
48.74 cd3od
48.62 cd3od
200
190
180
170
160
150
140
130
120
110
100
90
80
70
60
50
40
30
20
10
0
f1 (ppm)

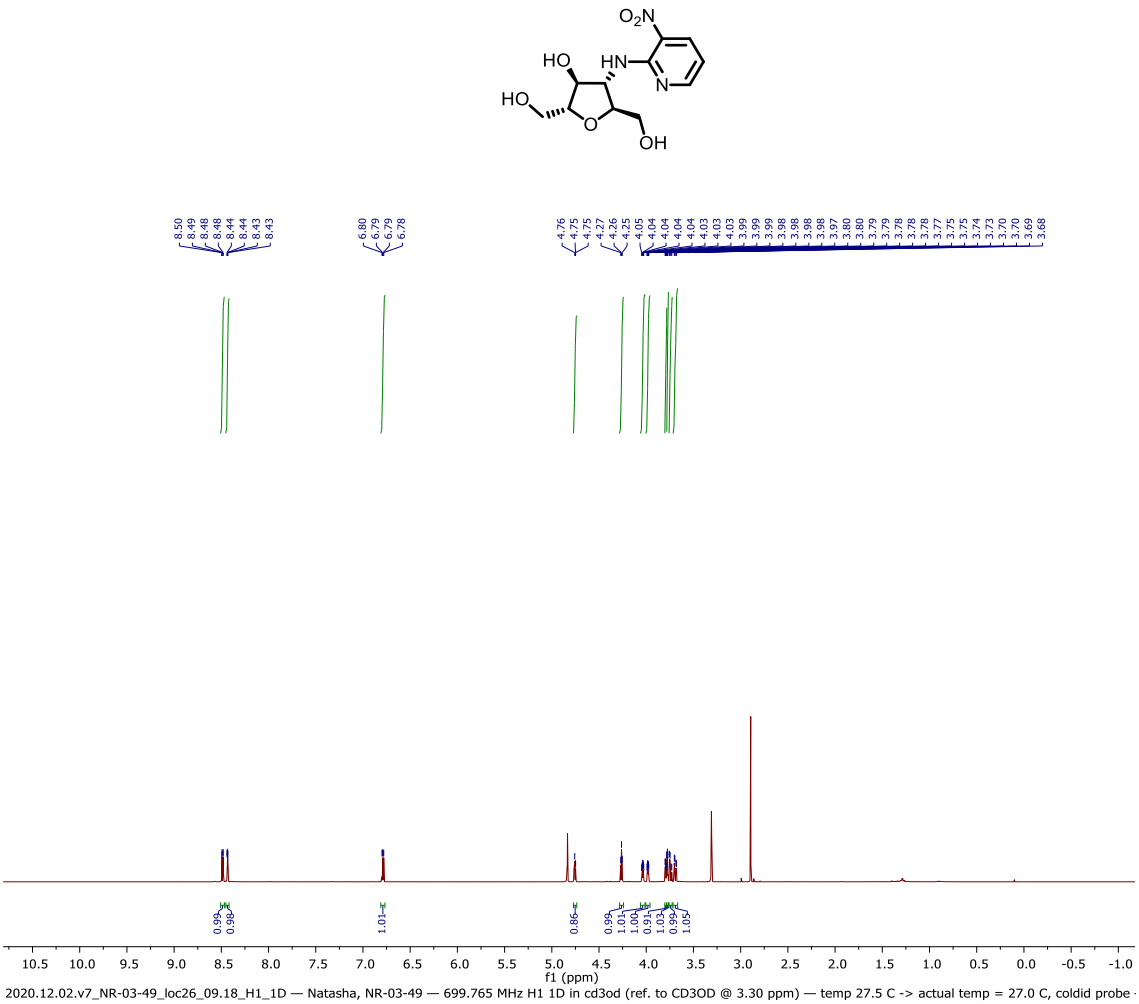
O2N
HO
HN
N
HO
O
OH
8.50 8.49 8.48 8.48 8.44 8.44 8.43 8.43
6.80 6.79 6.79 6.78
4.76 4.75 4.75 4.27 4.26 4.25 4.05 4.04 4.04 4.04 4.03 4.03 3.99 3.99 3.98 3.98 3.98 3.98 3.97 3.80 3.79 3.79 3.78 3.78 3.78 3.77 3.75 3.75 3.74 3.73 3.70 3.70 3.69 3.68
0.99 0.98 1.01 0.86 0.99 1.01 1.00 0.91 1.03 0.99 1.05
10.5 10.0 9.5 9.0 8.5 8.0 7.5 7.0 6.5 6.0 5.5 5.0 4.5 4.0 3.5 3.0 2.5 2.0 1.5 1.0 0.5 0.0 -0.5 -1.0
f1 (ppm)
2020.12.02.v7_NR-03-49_loc26_09.18_H1_1D — Natasha, NR-03-49 — 699.765 MHz H1 1D in cd3od (ref. to CD3OD @ 3.30 ppm) — temp 27.5 C -> actual temp = 27.0 C, coldid probe

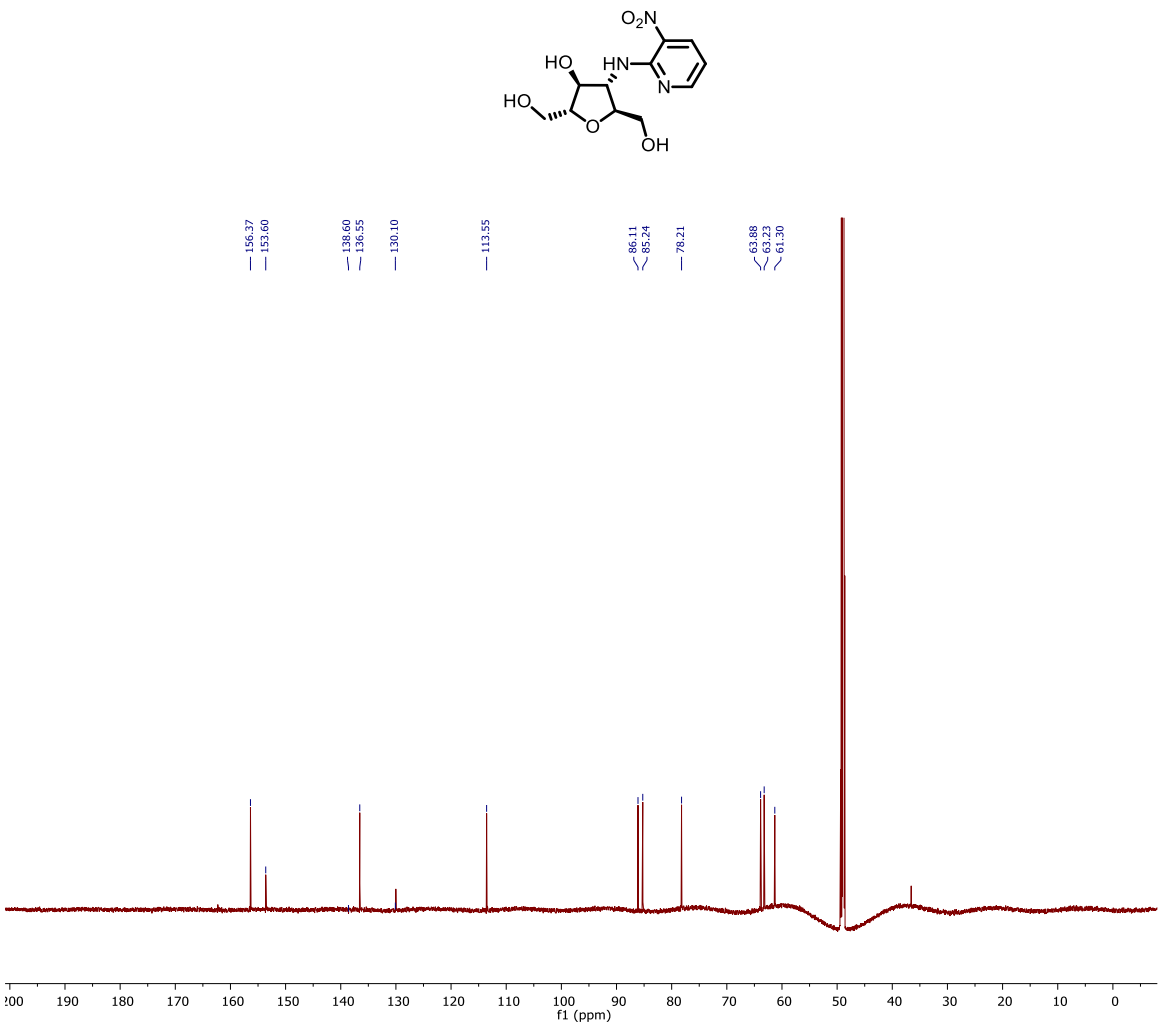
O2N
HO
HN
N
HO
O
OH
156.37
153.60
138.60
136.55
130.10
113.55
86.11
85.24
78.21
63.88
63.23
61.30
200
190
180
170
160
150
140
130
120
110
100
90
80
70
60
50
40
30
20
10
0
f1 (ppm)

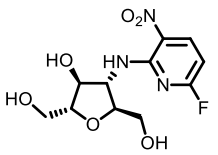
O2N
HO
HN
N
F
HO
O
OH

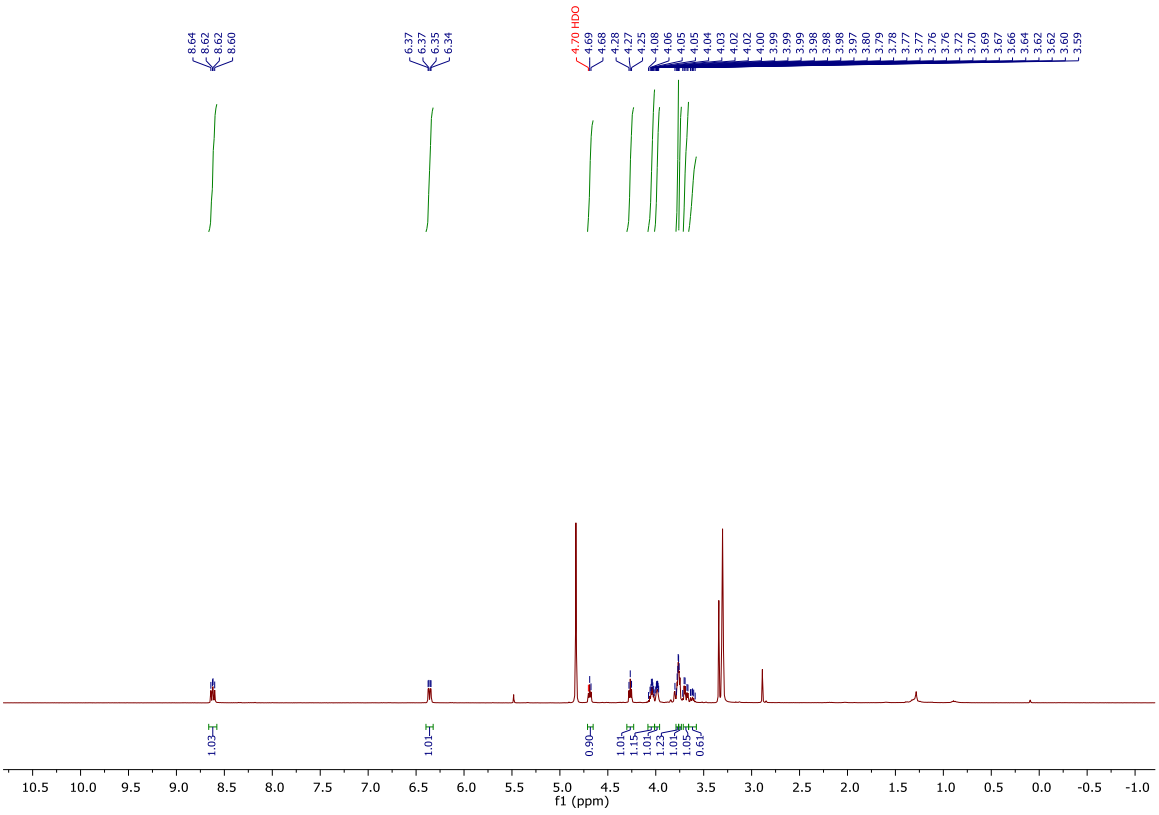
8.64
8.62
8.62
8.60
6.37
6.37
6.35
6.34
4.70 HDO
4.69
4.68
4.28
4.27
4.25
4.08
4.06
4.05
4.05
4.04
4.03
4.02
4.02
4.00
3.99
3.99
3.99
3.98
3.98
3.98
3.97
3.80
3.79
3.78
3.77
3.77
3.77
3.76
3.76
3.72
3.70
3.69
3.67
3.66
3.64
3.62
3.62
3.60
3.59
1.03
1.01
0.90
1.01
1.15
1.01
1.23
1.01
1.05
0.61
10.5
10.0
9.5
9.0
8.5
8.0
7.5
7.0
6.5
6.0
5.5
5.0
4.5
4.0
3.5
3.0
2.5
2.0
1.5
1.0
0.5
0.0
-0.5
-1.0
f1 (ppm)

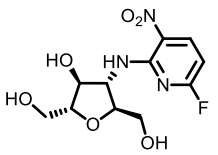
O2N
HO
HN
N
F
HO
O
OH

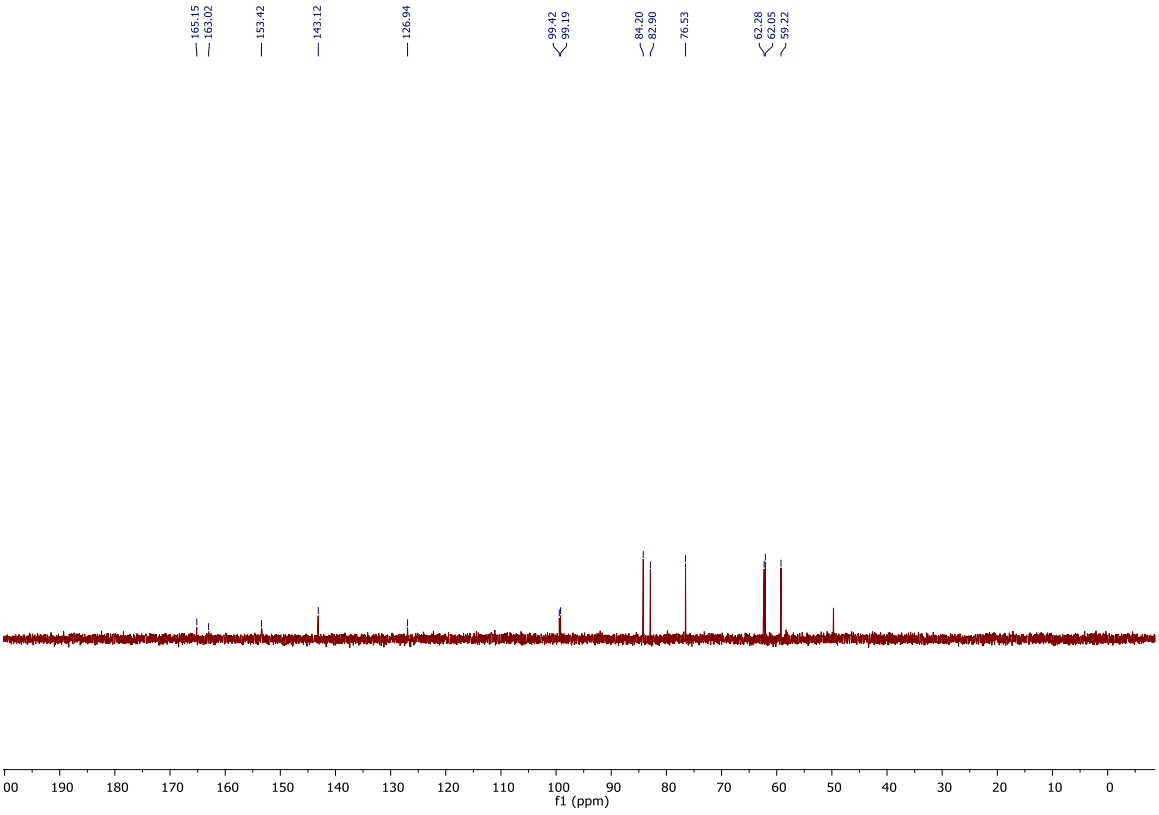
165.15
163.02
153.42
143.12
126.94
99.42
99.19
84.30
82.90
76.53
62.28
62.05
59.22
00 190 180 170 160 150 140 130 120 110 100 90 80 70 60 50 40 30 20 10 0
f1 (ppm)

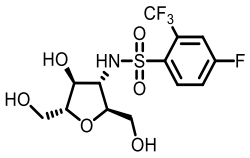
CF3
O
HO
HN
S
F
O
HO
O
OH

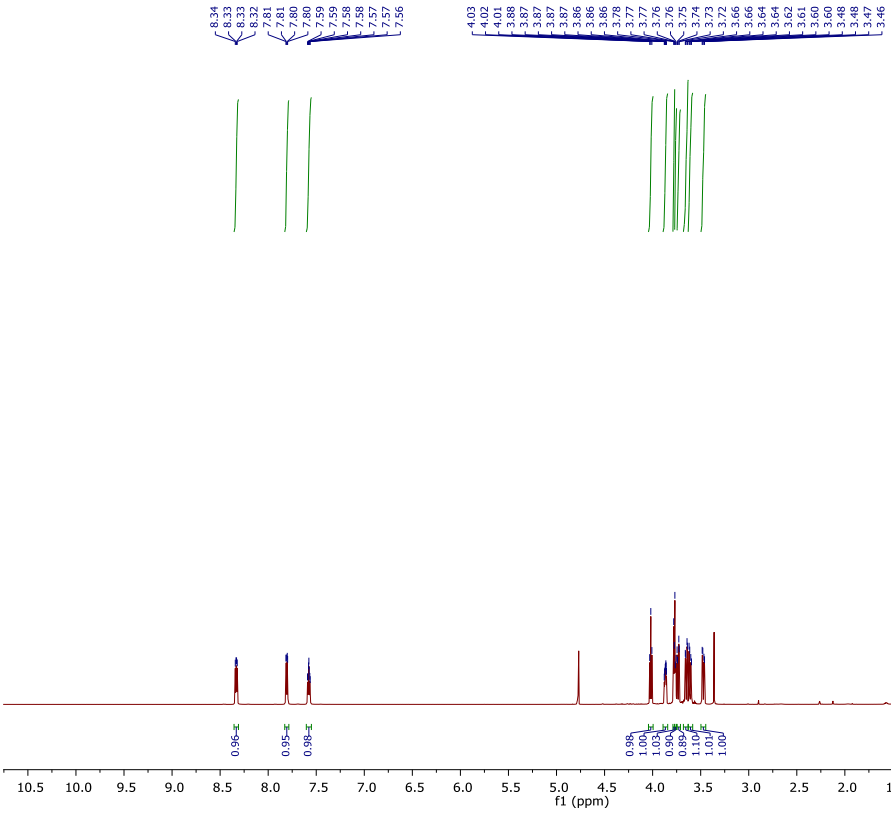
8.34
8.33
8.33
8.32
7.81
7.81
7.80
7.80
7.59
7.59
7.58
7.58
7.57
7.57
7.56
4.03
4.02
4.01
3.88
3.87
3.87
3.87
3.87
3.86
3.86
3.86
3.78
3.77
3.77
3.76
3.76
3.75
3.74
3.73
3.72
3.66
3.66
3.64
3.64
3.62
3.61
3.60
3.60
3.48
3.48
3.47
3.46
0.96
0.95
0.98
0.98
1.00
1.03
0.96
0.89
1.10
1.01
1.00
10.5
10.0
9.5
9.0
8.5
8.0
7.5
7.0
6.5
6.0
5.5
5.0
4.5
4.0
3.5
3.0
2.5
2.0
1.5
1.0
0.5
0.0
-0.5
-1.0
f1 (ppm)

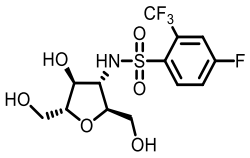
CF3
O
HO
HN
S
F
O
HO
O
OH

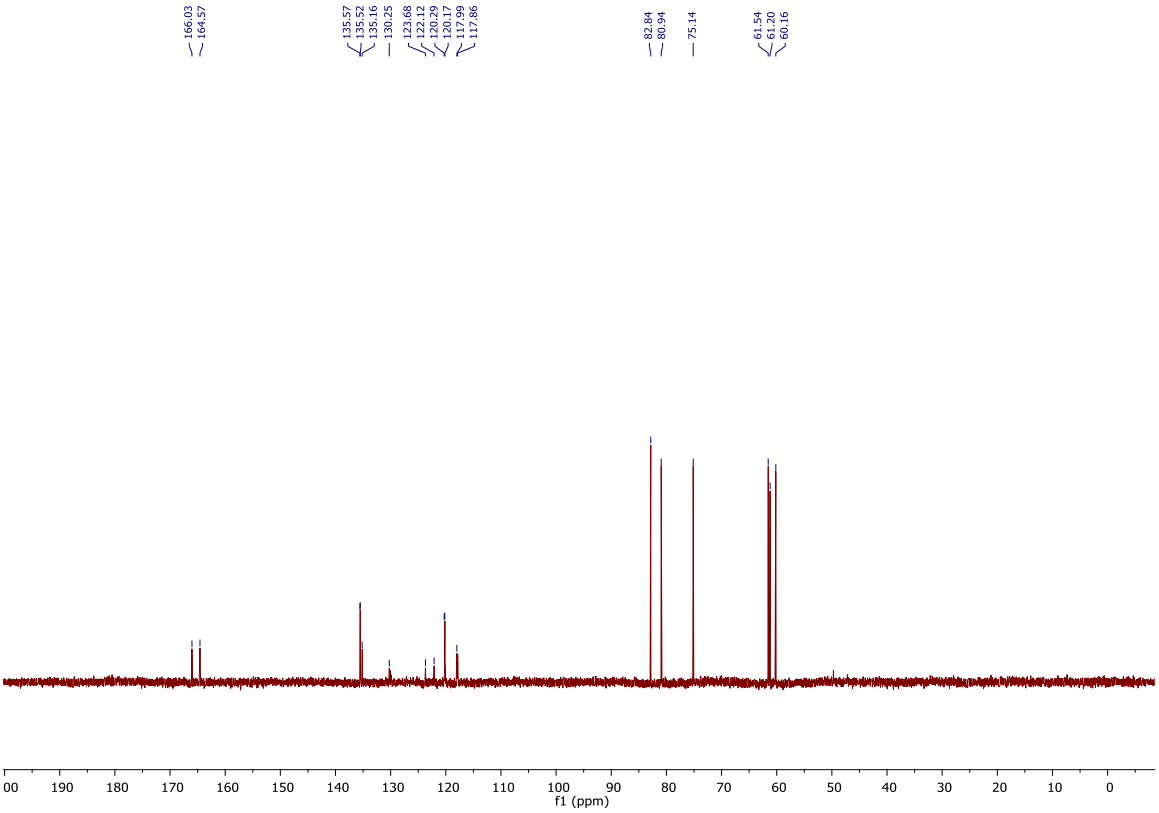
166.03
164.57
135.57
135.52
135.16
130.25
123.68
122.12
120.29
120.17
117.99
117.86
82.84
80.94
75.14
61.54
61.20
60.16
00 190 180 170 160 150 140 130 120 110 100 90 80 70 60 50 40 30 20 10 0
f1 (ppm)

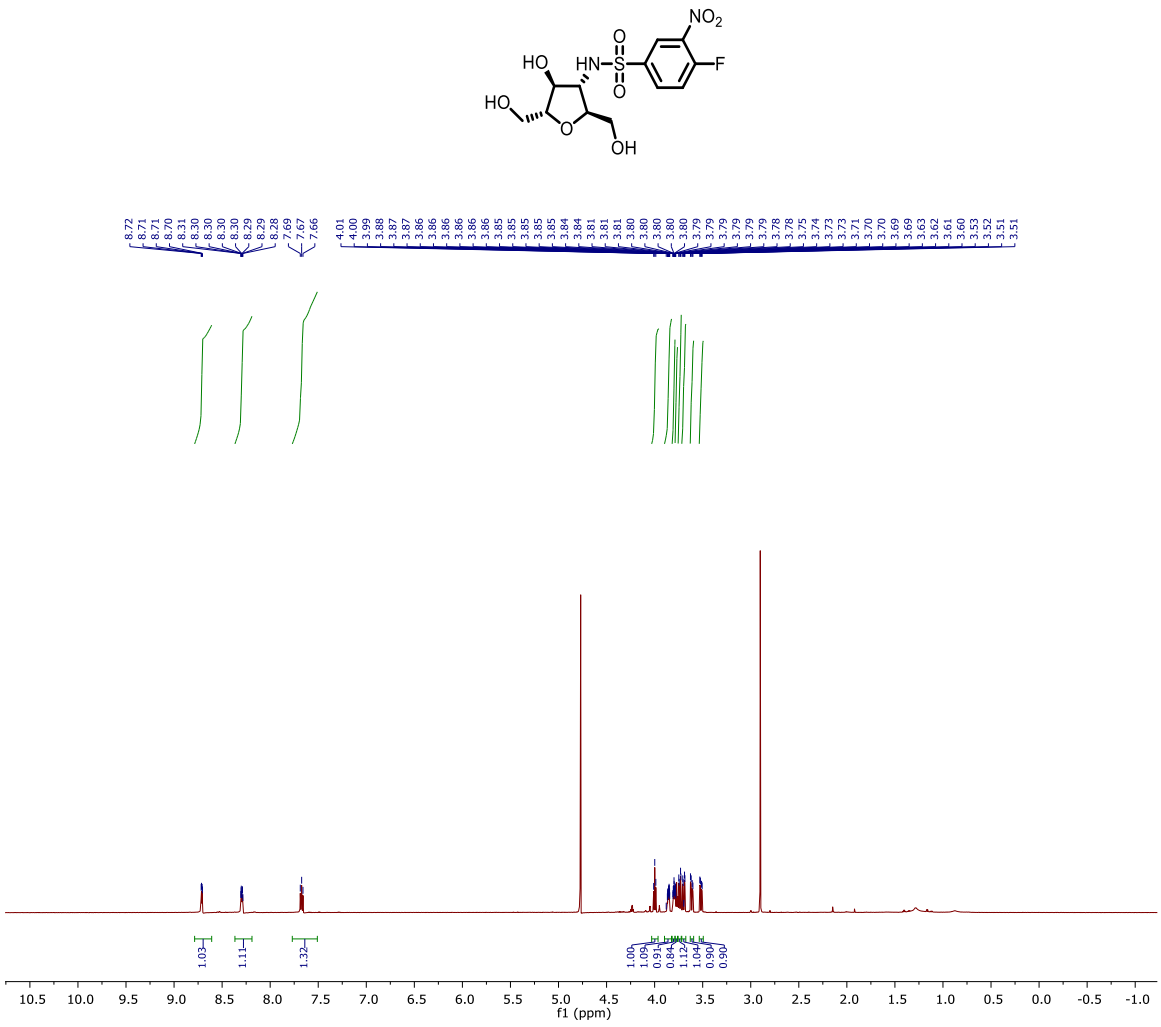
NO2
HO
HN
S
O
O
F
HO
O
OH
8.72 8.71 8.71 8.70 8.31 8.30 8.30 8.30 8.30 8.29 8.28 7.69 7.67 7.66
4.01 4.00 3.99 3.88 3.87 3.87 3.86 3.86 3.86 3.86 3.86 3.85 3.85 3.85 3.85 3.85 3.84 3.84 3.81 3.81 3.80 3.80 3.80 3.80 3.80 3.79 3.79 3.79 3.79 3.79 3.79 3.78 3.78 3.75 3.74 3.73 3.73 3.71 3.70 3.70 3.69 3.69 3.63 3.62 3.61 3.60 3.53 3.52 3.51 3.51
1.03
1.11
1.32
1.00
1.09
0.91
0.84
1.12
1.04
0.90
0.90
10.5 10.0 9.5 9.0 8.5 8.0 7.5 7.0 6.5 6.0 5.5 5.0 4.5 4.0 3.5 3.0 2.5 2.0 1.5 1.0 0.5 0.0 -0.5 -1.0
f1 (ppm)

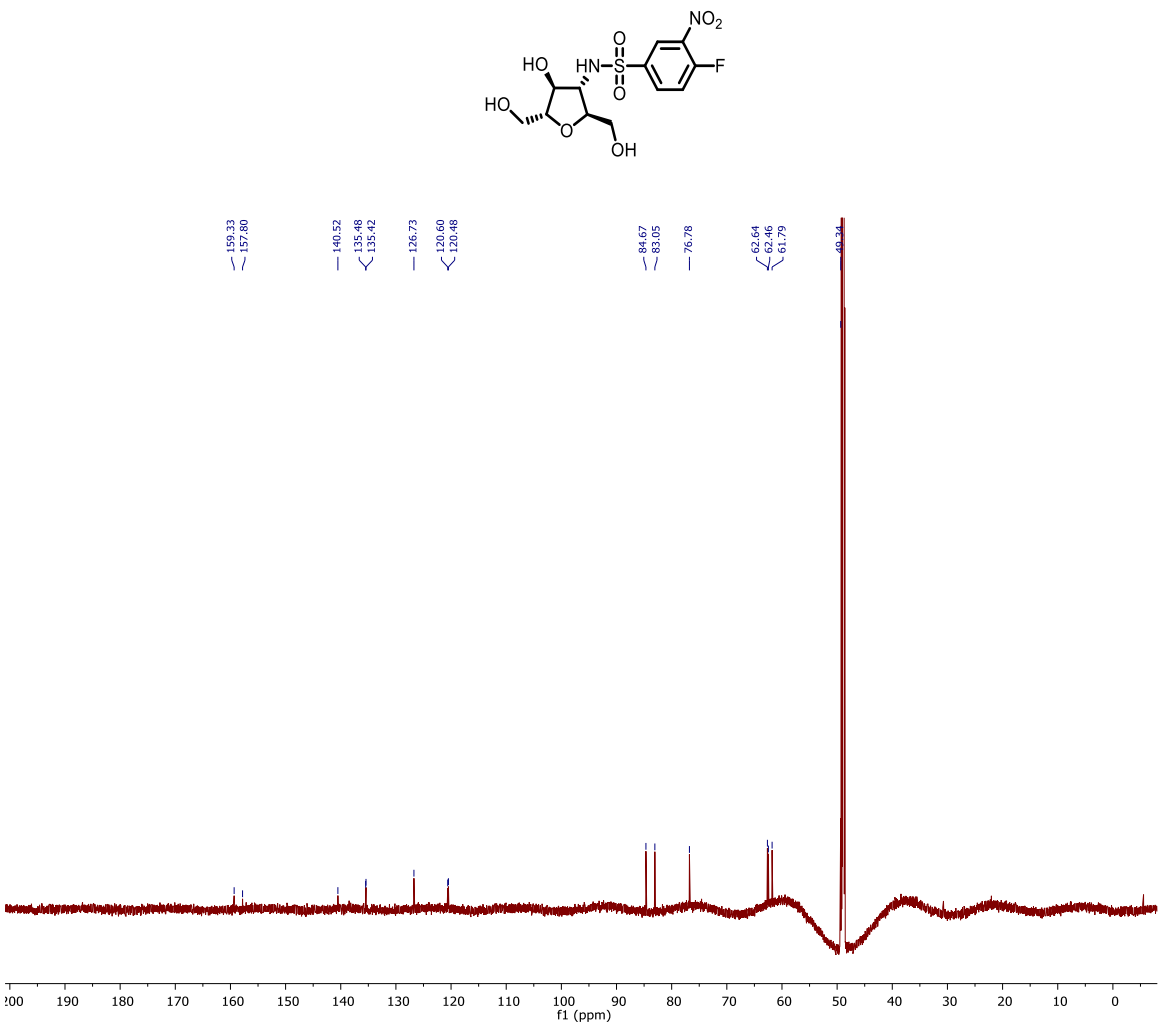
NO2
O
HO
HN
S
O
F
HO
O
OH
159.33
157.80
140.52
135.48
135.42
126.73
120.60
120.48
84.67
83.05
76.78
62.64
62.46
61.79
49.24
200
190
180
170
160
150
140
130
120
110
100
90
80
70
60
50
40
30
20
10
0
f1 (ppm)

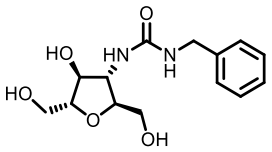
O
HO
HN
N
H
HO
O
OH

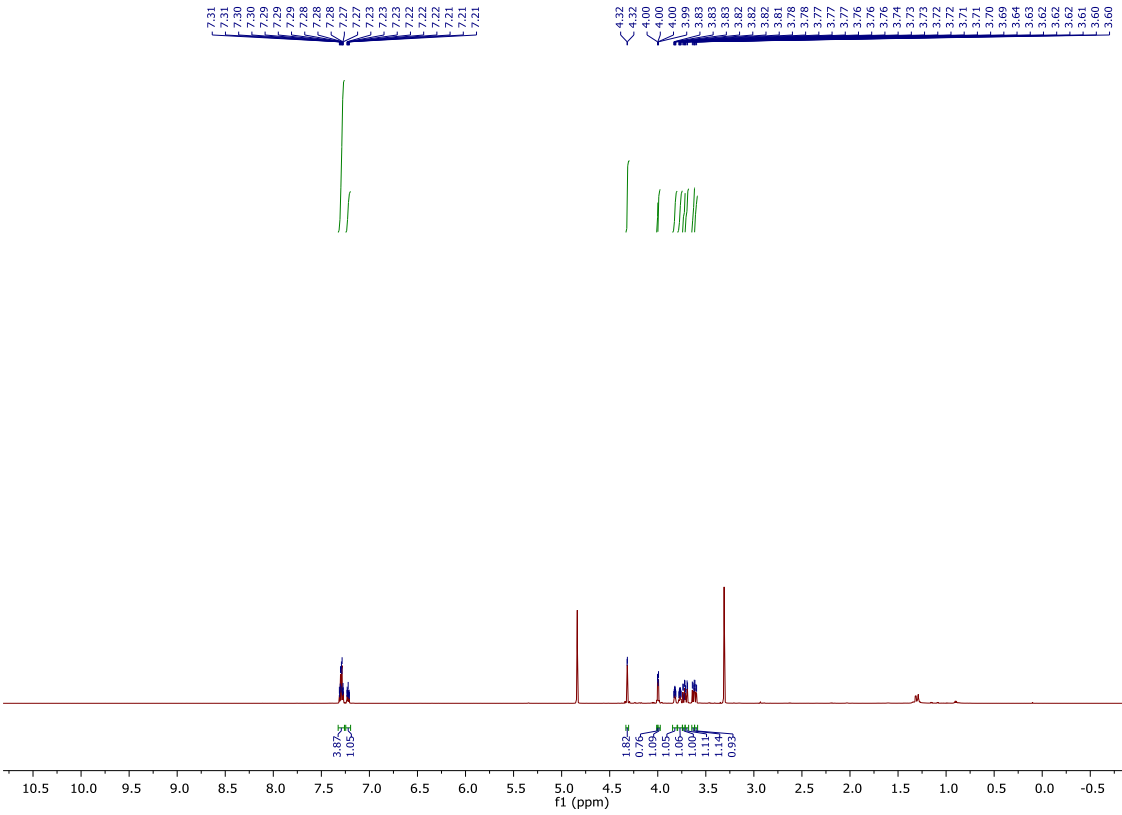
7.31
7.31
7.30
7.30
7.29
7.29
7.29
7.28
7.28
7.28
7.27
7.27
7.23
7.23
7.23
7.22
7.22
7.22
7.21
7.21
7.21
4.32
4.32
4.00
4.00
4.00
3.99
3.83
3.83
3.82
3.82
3.82
3.81
3.78
3.78
3.77
3.77
3.77
3.76
3.76
3.76
3.74
3.73
3.73
3.72
3.72
3.71
3.71
3.70
3.69
3.64
3.63
3.62
3.62
3.61
3.60
3.60
3.87
1.05
1.82
0.76
1.08
1.05
1.05
1.00
1.14
1.14
0.93
10.5
10.0
9.5
9.0
8.5
8.0
7.5
7.0
6.5
6.0
5.5
5.0
4.5
4.0
3.5
3.0
2.5
2.0
1.5
1.0
0.5
0.0
-0.5
-1.0
f1 (ppm)

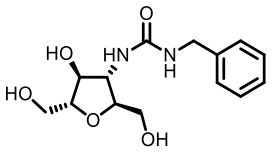
O
HO
HN
N
H
HO
O
OH

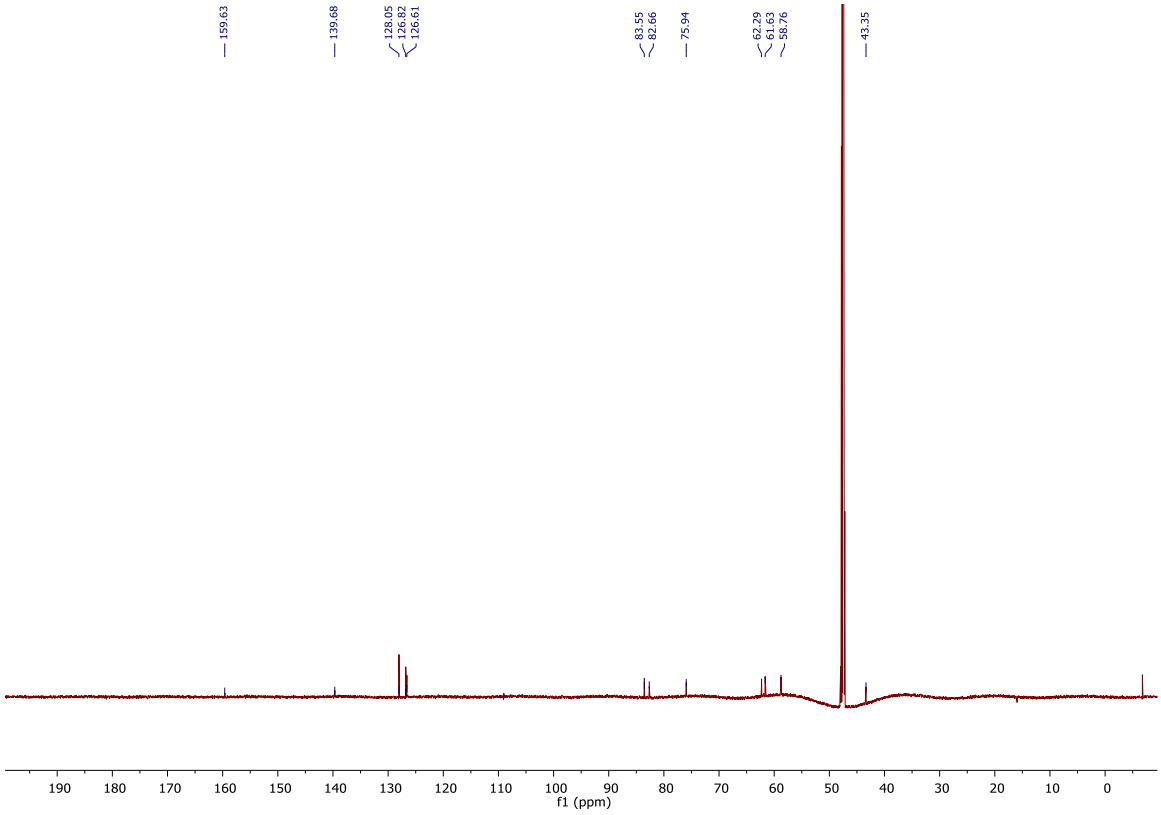
159.63
139.68
128.05
126.82
126.61
83.55
82.66
75.94
62.29
61.63
58.76
43.35
190
180
170
160
150
140
130
120
110
100
90
80
70
60
50
40
30
20
10
0
f1 (ppm)

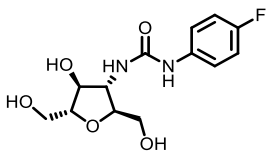
F
O
HO
HN
N
H
HO
O
OH

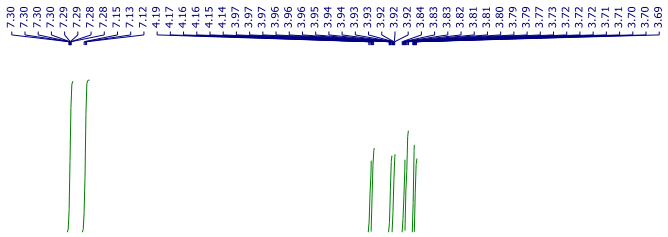
7.30 7.30 7.30 7.30 7.29 7.29 7.28 7.28 7.15 7.13 7.12
4.19 4.17 4.16 4.16 4.15 4.14 3.97 3.97 3.97 3.96 3.96 3.96 3.95 3.94 3.94 3.93 3.93 3.92 3.92 3.92 3.84 3.83 3.83 3.82 3.81 3.81 3.80 3.79 3.79 3.77 3.73 3.72 3.72 3.72 3.71 3.71 3.70 3.70 3.69

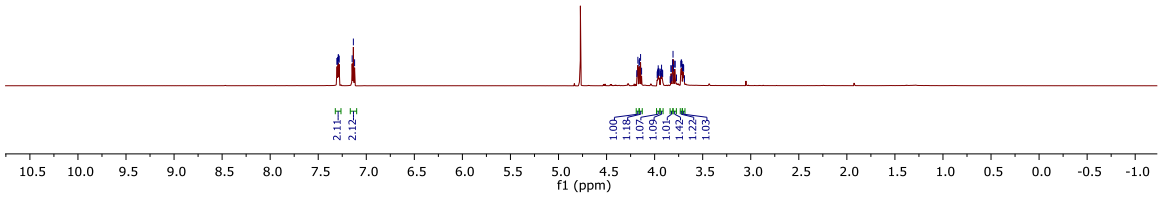
2.11
2.12
1.00
1.18
1.07
1.09
1.01
1.42
1.22
1.03
10.5 10.0 9.5 9.0 8.5 8.0 7.5 7.0 6.5 6.0 5.5 5.0 4.5 4.0 3.5 3.0 2.5 2.0 1.5 1.0 0.5 0.0 -0.5 -1.0
f1 (ppm)

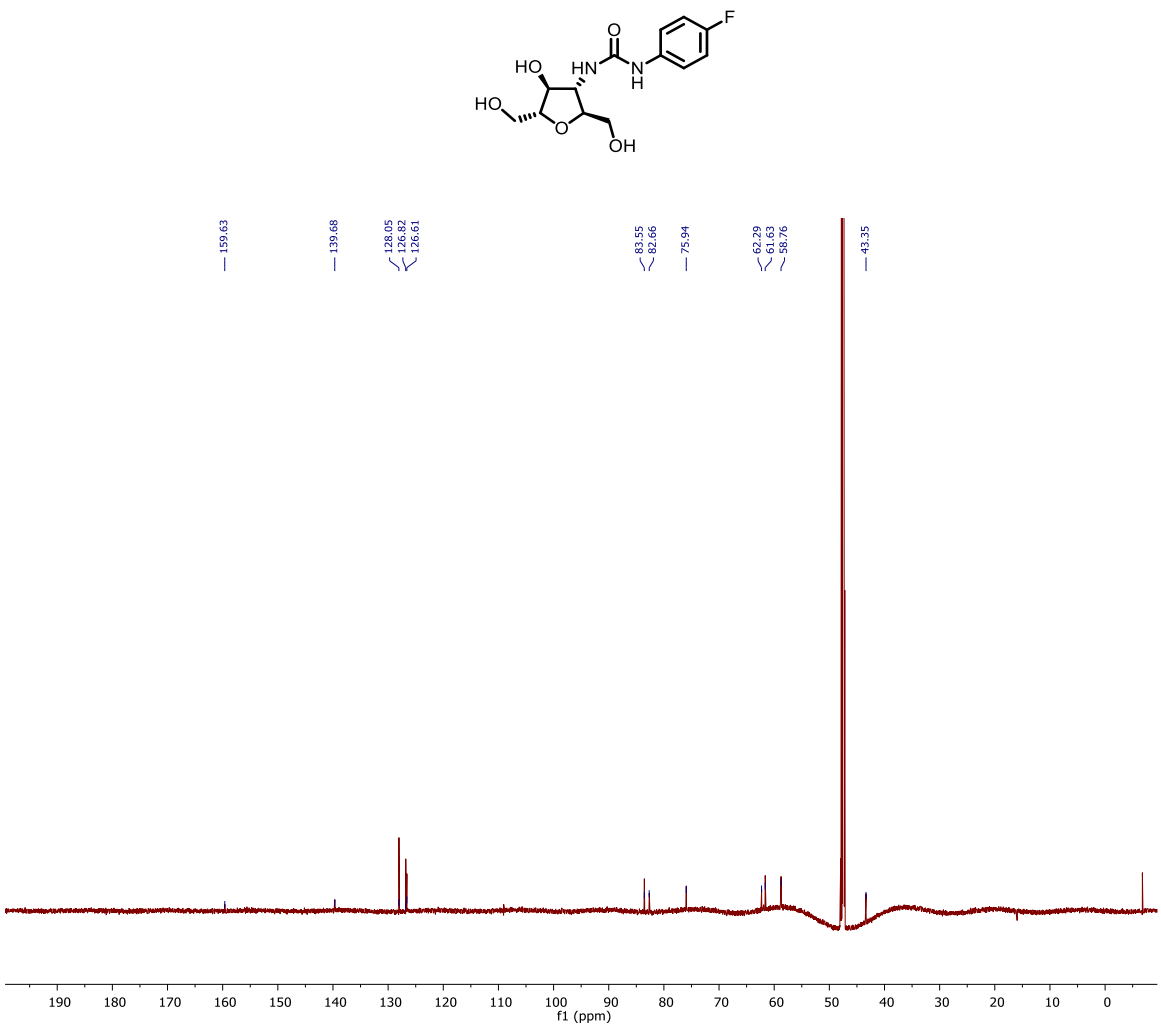
F
O
HO
HN
N
H
HO
O
OH
159.63
139.68
128.05
126.82
126.61
83.55
82.66
75.94
62.29
61.63
58.76
43.35
190
180
170
160
150
140
130
120
110
100
90
80
70
60
50
40
30
20
10
0
f1 (ppm)

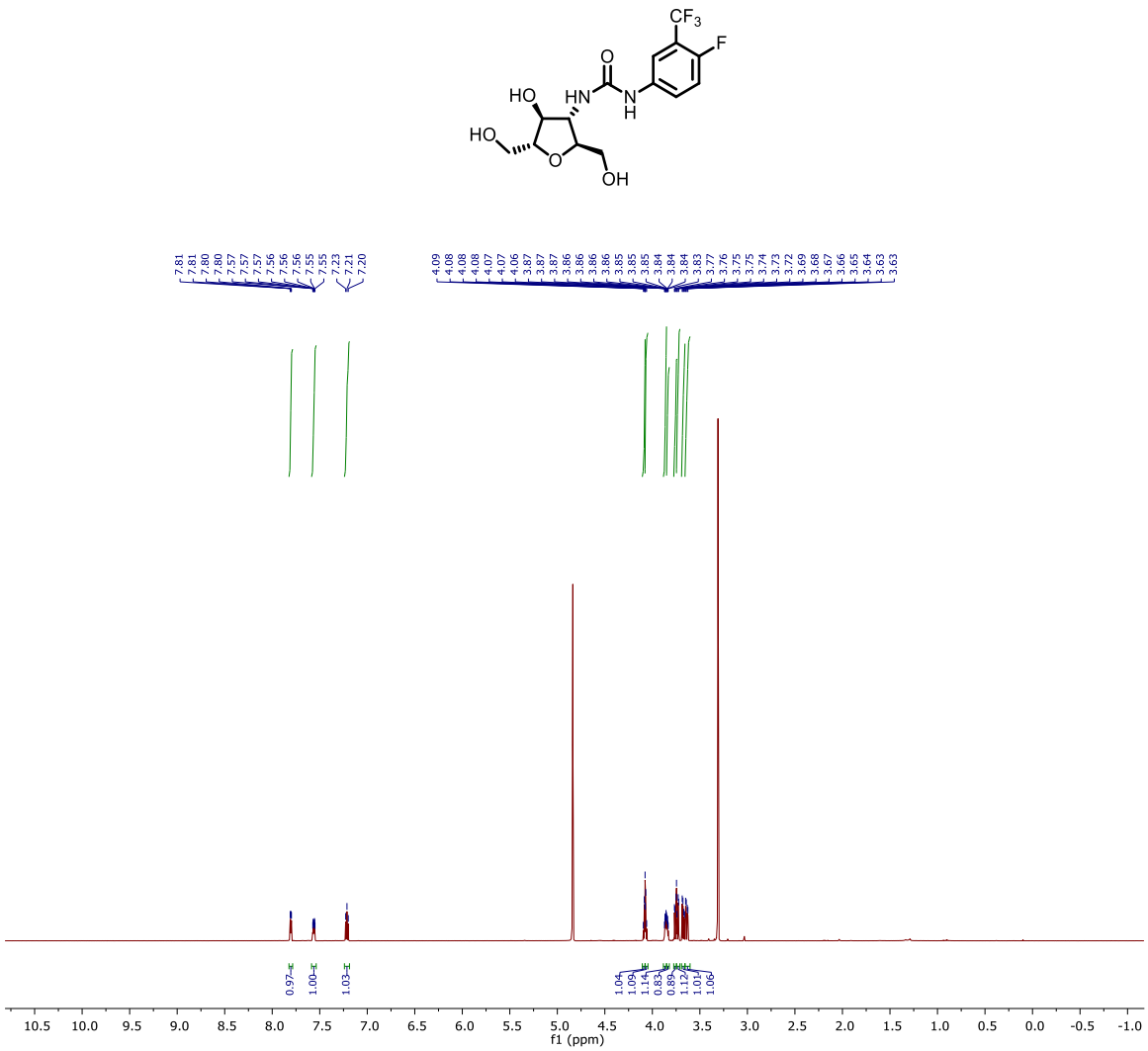
CF3
F
O
HO
HN
N
H
HO
O
OH
7.81
7.81
7.80
7.80
7.57
7.57
7.56
7.56
7.56
7.55
7.55
7.23
7.21
7.20
4.09
4.08
4.08
4.08
4.07
4.07
4.06
3.87
3.87
3.87
3.86
3.86
3.86
3.86
3.85
3.85
3.85
3.84
3.84
3.84
3.84
3.83
3.77
3.76
3.75
3.75
3.74
3.73
3.72
3.69
3.68
3.67
3.66
3.65
3.64
3.63
3.63
0.97
1.00
1.03
1.04
1.09
1.14
0.83
0.89
1.12
1.01
1.06
10.5
10.0
9.5
9.0
8.5
8.0
7.5
7.0
6.5
6.0
5.5
5.0
4.5
4.0
3.5
3.0
2.5
2.0
1.5
1.0
0.5
0.0
-0.5
-1.0
f1 (ppm)

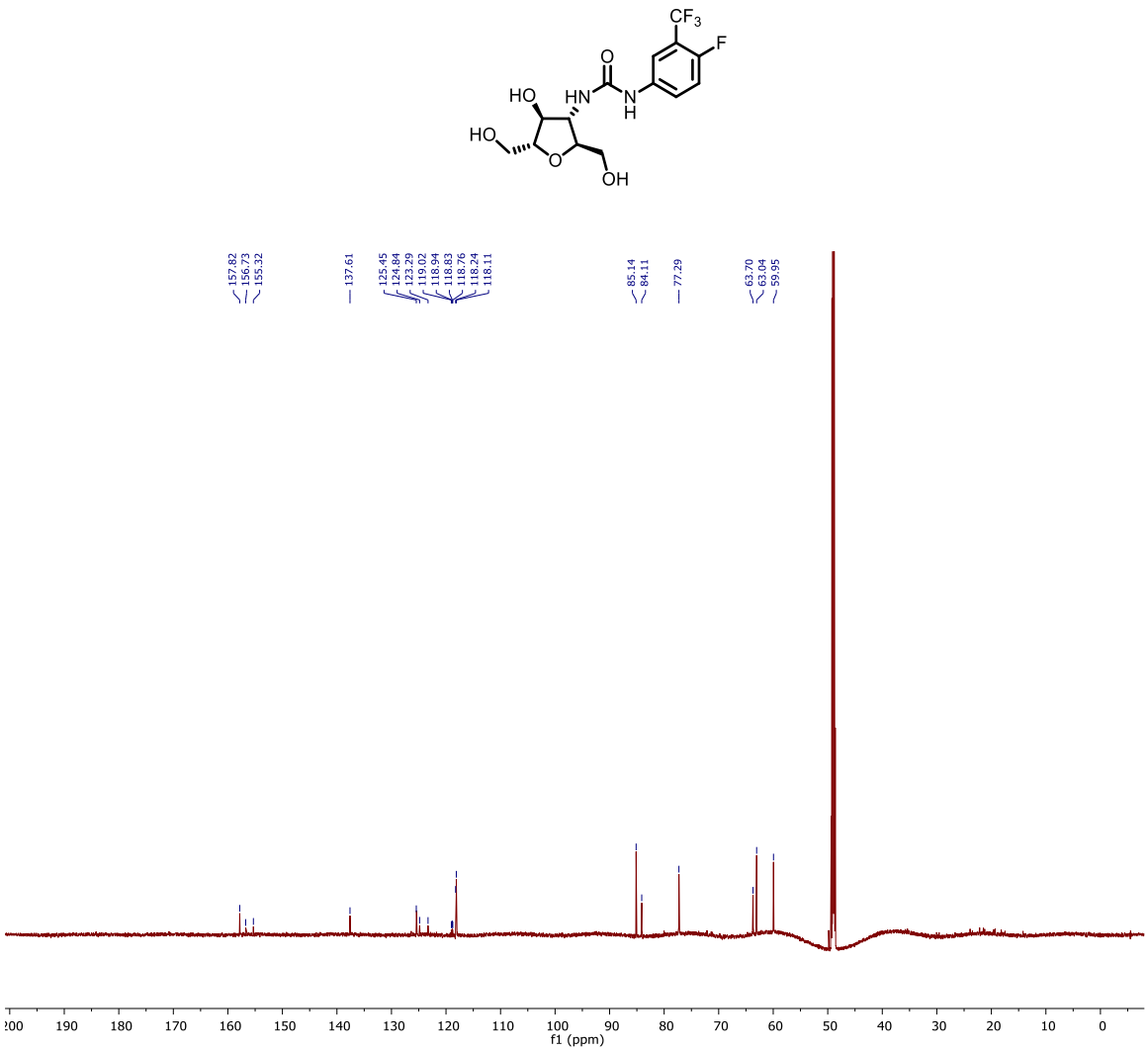
CF3
F
O
HO
HN
N
H
HO
O
OH
157.82
156.73
155.32
137.61
125.45
124.84
123.29
119.02
118.94
118.83
118.76
118.24
118.11
85.14
84.11
77.29
63.70
63.04
59.95
200
190
180
170
160
150
140
130
120
110
100
90
80
70
60
50
40
30
20
10
0
f1 (ppm)

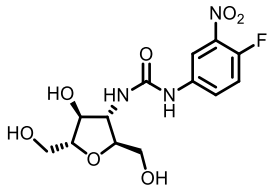
NO2
F
O
HO
HN
N
H
HO
O
OH

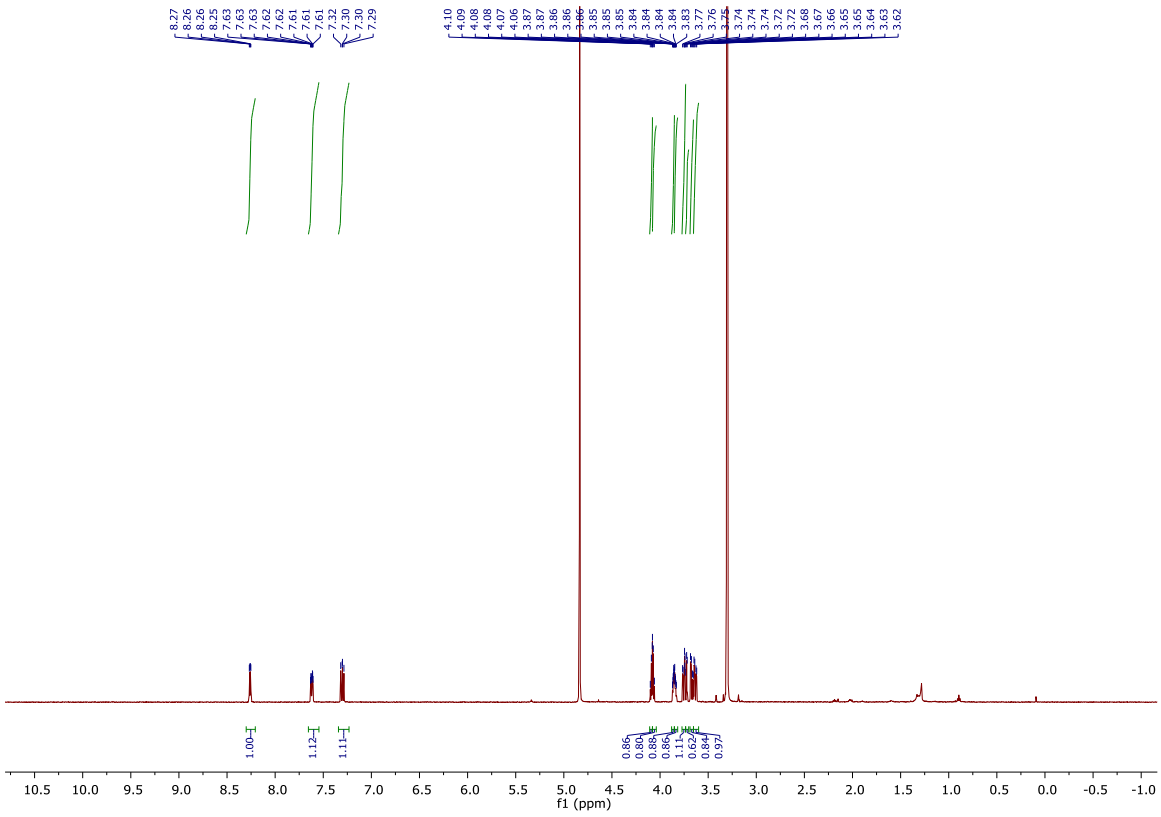
8.27
8.26
8.26
8.25
7.63
7.63
7.62
7.62
7.61
7.61
7.31
7.30
7.30
7.29
4.10
4.09
4.08
4.08
4.07
4.06
3.87
3.87
3.86
3.86
3.86
3.85
3.85
3.85
3.84
3.84
3.84
3.84
3.83
3.77
3.76
3.75
3.74
3.74
3.74
3.72
3.72
3.68
3.67
3.66
3.65
3.65
3.64
3.63
3.62
1.00
1.12
1.11
0.86
0.80
0.88
0.86
1.11
0.62
0.84
0.97
10.5
10.0
9.5
9.0
8.5
8.0
7.5
7.0
6.5
6.0
5.5
5.0
4.5
4.0
3.5
3.0
2.5
2.0
1.5
1.0
0.5
0.0
-0.5
-1.0
f1 (ppm)

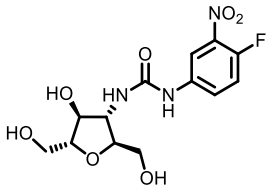
NO2
F
O
HO
HN
N
H
HO
O
OH

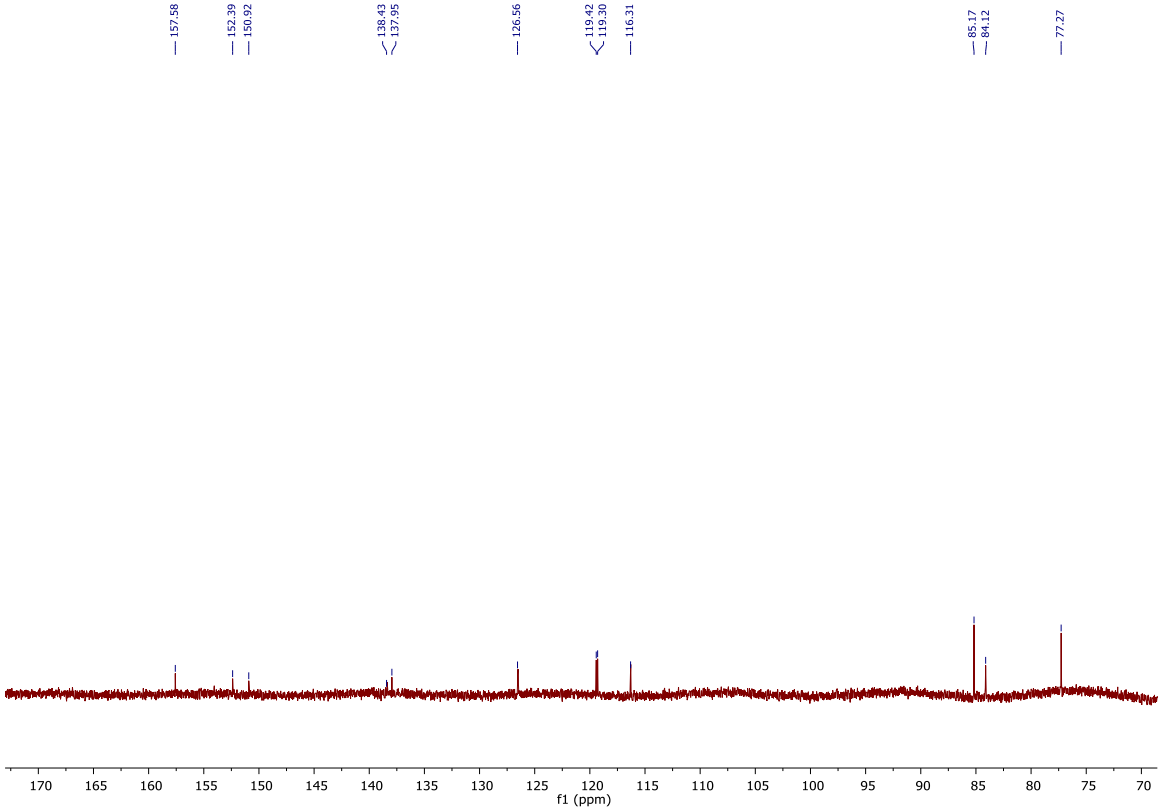
157.58
152.39
150.92
138.43
137.95
126.56
119.42
119.30
116.31
85.17
84.12
77.27
170
165
160
155
150
145
140
135
130
125
120
115
110
105
100
95
90
85
80
75
70
f1 (ppm)

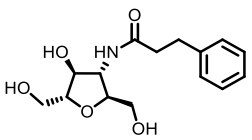
O
HO
HN
HO
O
OH

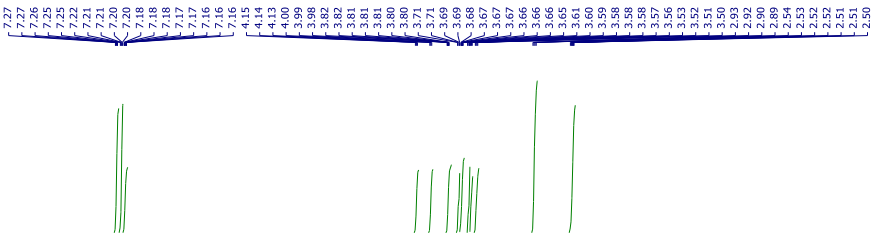

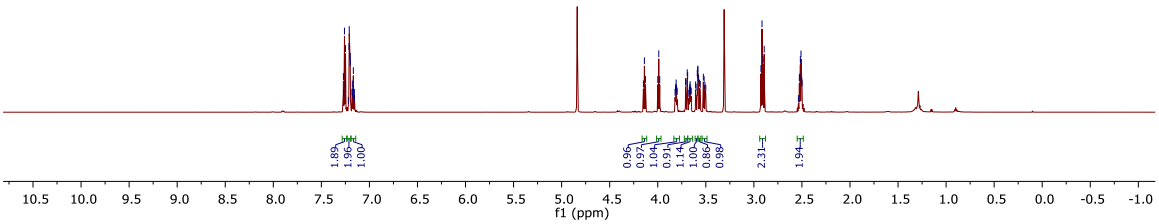
1.89
1.96
1.00
0.96
0.97
1.04
0.94
1.14
1.00
0.86
0.98
2.31
1.94
10.5 10.0 9.5 9.0 8.5 8.0 7.5 7.0 6.5 6.0 5.5 5.0 4.5 4.0 3.5 3.0 2.5 2.0 1.5 1.0 0.5 0.0 -0.5 -1.0
f1 (ppm)

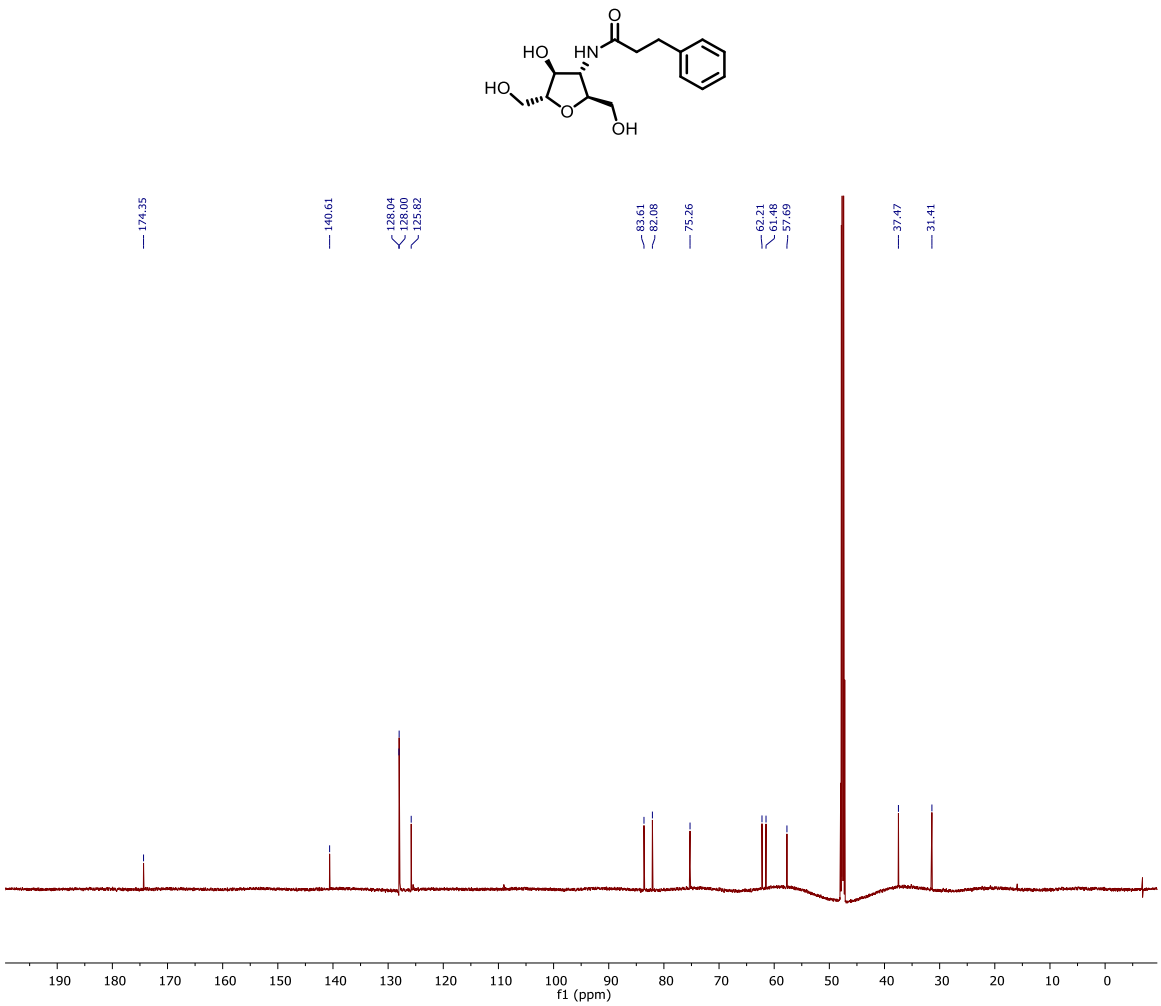
HO
HN
O
HO
O
OH
174.35
140.61
128.04
128.00
125.82
83.61
82.08
75.26
62.21
61.48
57.69
37.47
31.41
190
180
170
160
150
140
130
120
110
100
90
80
70
60
50
40
30
20
10
0
f1 (ppm)

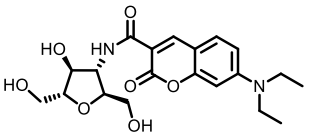
HO
HN
O
HO
O
O
O
N
OH

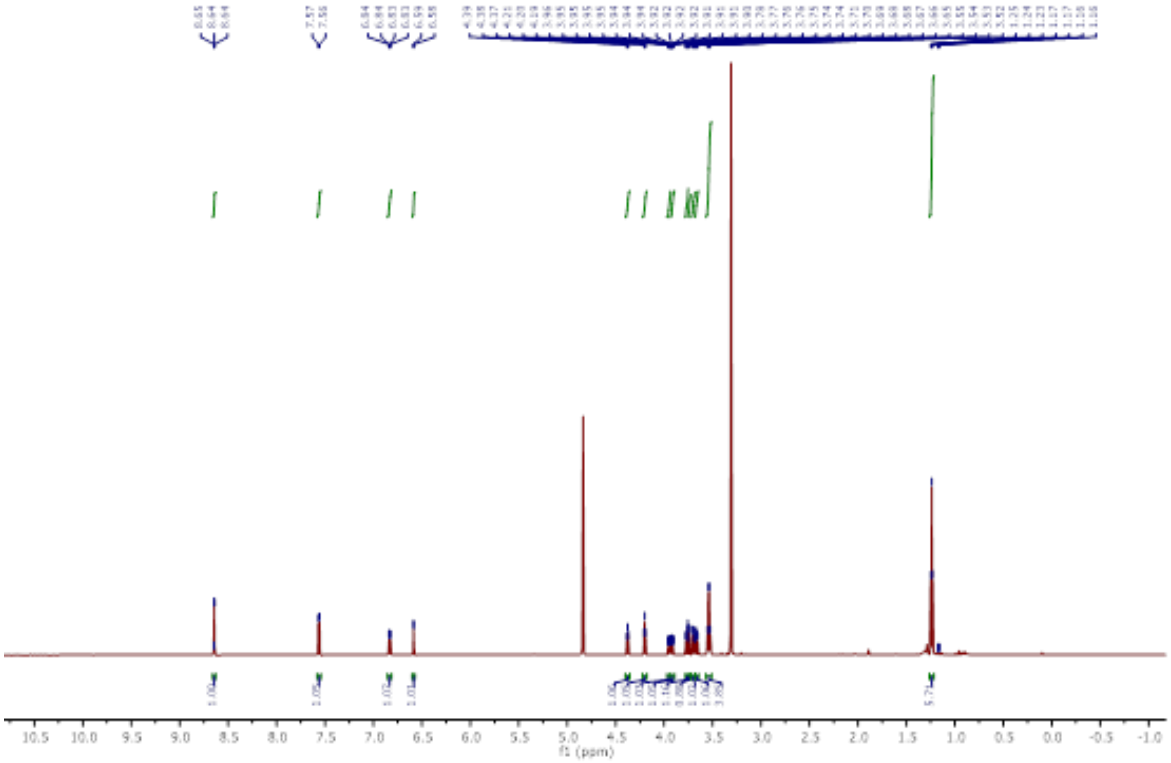
f1 (ppm)

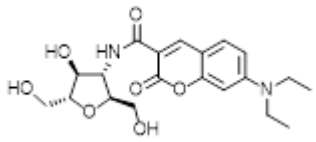
O
HO
HN
HO
O
O
N
OH

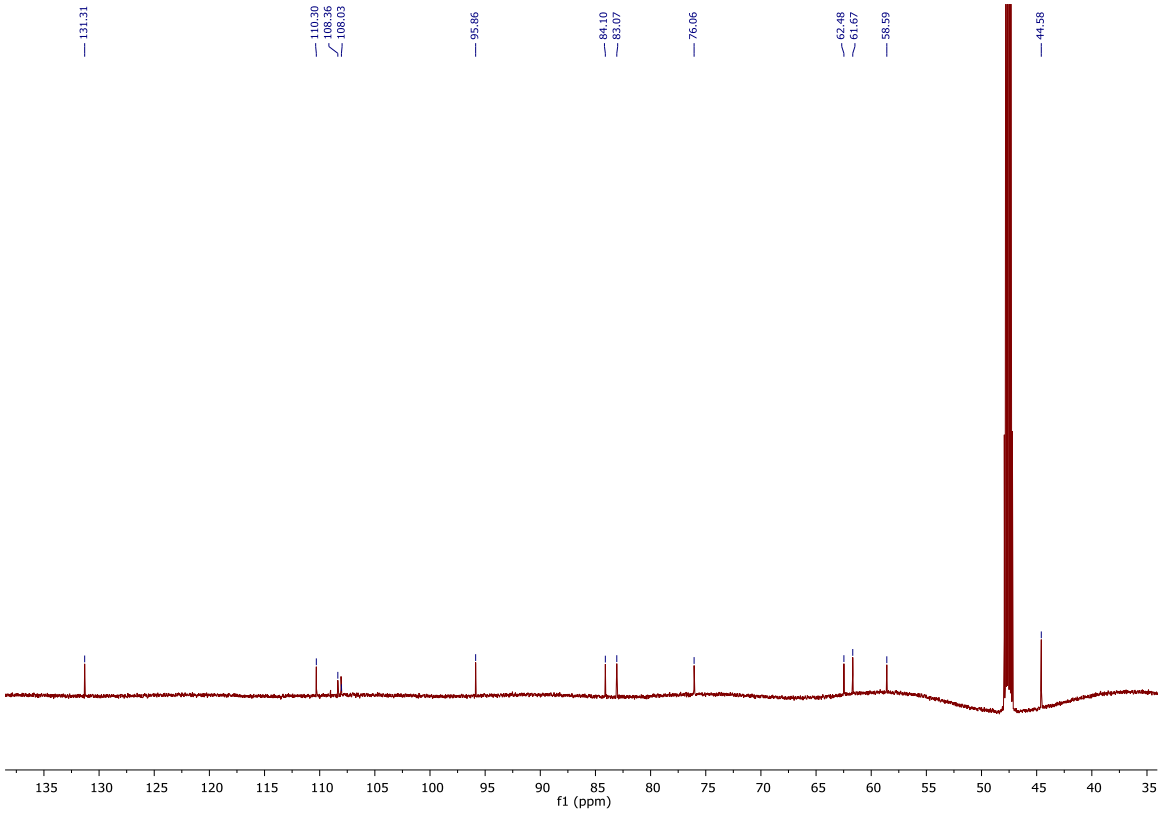
131.31
110.30
108.36
108.03
95.86
84.10
83.07
76.06
62.48
61.67
58.59
44.58
135 130 125 120 115 110 105 100 95 90 85 80 75 70 65 60 55 50 45 40 35
f1 (ppm)